School of Physical Sciences
Department of Applied Physics

Lunar Neutron Energy Spectra from Isotope Abundance Measurements on Cadmium, Samarium and Gadolinium

by

Daphne Gillian Sands

This thesis is presented as part of the requirements for the award of the Degree of Doctor of Philosophy of the Curtin University of Technology

November 1998

School of Physical Sciences
Department of Applied Physics

Lunar Neutron Energy Spectra from Isotope Abundance Measurements on Cadmium, Samarium and Gadolinium

by

Daphne Gillian Sands

This thesis is presented as part of the requirements for the award of the Degree of Doctor of Philosophy of the Curtin University of Technology

November 1998

Abstract

This thesis provides new evidence which contributes to a clearer understanding of the mixing history of the lunar soil, the interactions of cosmic rays with the lunar surface and any temporal and spatial variations in cosmic ray intensity at the lunar surface.

The bombardment of the lunar surface by cosmic rays produces secondary neutrons which are thermalised by the lunar soil. These thermal neutrons are captured by trace elements with large neutron capture cross sections such as cadmium, gadolinium and samarium. Measurements by thermal ionisation mass spectrometry of the changes in the isotopic abundances of cadmium, gadolinium and samarium due to neutron capture are presented in this thesis. Evidence is also presented of the first observations of mass fractionation in cadmium in lunar soils.

Changes have been observed in samples from the Apollo 14, 16 and 17 missions. In $^{114}Cd/^{113}Cd$ changes of 0.3% to 0.5% have been observed in lunar samples 60501,105, 65701,23 and 72161,73, of 0.4% and 0.8% in $^{158}Gd/^{157}Gd$ in samples 14163,848 and 60501,105 and of 0.8%, 1.2% and 0.06% in $^{150}Sm/^{149}Sm$ in samples 14163,848 and 60501,105 and 74220,125 respectively. This is the first time that neutron capture has been detected in cadmium.

Mass fractionation effects of 0.30%, 0.53% and 0.54% per mass unit have been observed in lunar samples 60501,105, 65701,23 and 72161,73, the first cadmium mass fractionation observed in lunar soils. The cause of elemental mass fractionation on the Moon is not yet understood. These new data from cadmium, a volatile element with a large mass range from ^{106}Cd to ^{116}Cd is a valuable contribution to the debate.

Thermal neutrons are captured preferentially at resonance energies of 0.03 eV by ^{155}Gd and ^{157}Gd, at 0.09 eV by ^{149}Sm and at 0.178 eV by ^{113}Cd. A comparison of the changes in $^{114}Cd/^{113}Cd$, $^{156}Gd/^{155}Gd$, $^{158}Gd/^{157}Gd$ and $^{150}Sm/^{149}Sm$ due to neutron capture can therefore indicate the relative energies of the neutrons. Previous work has

compared changes in $^{158}Gd/^{157}Gd$ and $^{150}Sm/^{149}Sm$, this work extends the comparison with the new measurements of the changes in $^{114}Cd/^{113}Cd$. This thesis shows that the intensity of the thermal neutrons peaks at a higher energy than the <0.1 eV assumed by Lingenfelter et al. (1972). The capture rate for gadolinium calculated by Lingenfelter, has been shown to be too high, this thesis shows that if a modified energy spectrum is considered, biased towards higher energies, it will bring the calculated neutron capture rate by gadolinium closer to the measured rates.

The concentrations of cadmium, gadolinium and samarium in nine lunar samples have been measured for the first time by high precision isotope dilution mass spectrometry. Cadmium in 10017,341, 14310,615, 15041,188, 15059,240, 60501,105, 65701,23, 72161,73 and 74220,125 is 10.0±0.2, 1.51±0.02, 32.8±0.6, 34.9±0.3, 112±2, 68.3±0.8, 57.0±0.6 and 300±7 ppb respectively. Gadolinium concentrations of 21±7 ppm in 14163,848, 3.26±0.05 and 5.8±0.3 ppm in 60501,105, and 8.1±0.2 and 8.6±0.1 ppm in 74220,125 are presented. Samarium concentrations of 24.3±0.4 and 29.8±0.5 ppm were found in 14163,848, 2.68±0.04 and 14±2 ppm in 60501,105, and 6.3±0.1 and 6.8±0.1 ppm in 74220,125.

The concentrations of cadmium, gadolinium and samarium in the seven geochemical reference materials BCR-1, BHVO-1, BIR-1, DNC-1, MAG-1, PCC-1 and W-2 are also presented, some measured for the first time by isotope dilution mass spectrometry.

Acknowledgments

There are many people I would like to thank for all their support during six years of experimental work and thesis writing.

My three supervisors have steadily helped and encouraged me through the highs and lows. I am very grateful for Kevin Rosman's perpetual enthusiasm and practical advice, for John De Laeter's thoughtful assessments, and for David Nelson's quick grasp of detail.

Warrick Chisholm has given inestimable support and advice over several years with the mass spectrometer and all the other problems that came along. He was followed more recently by the cheerful and helpful Graeme Burton.

Others who have offered support over the years include Ian Fletcher, Roland Maas, Cliff Smith and Terry Margrain.

Last, but most important, are my family, David especially, but also Evelyn, Robin, Alison and Duncan.

I gratefully acknowledge the provision of nine lunar samples by NASA to John De Laeter, the designated Principal Investigator for these studies, and the assistance of the NASA lunar sample curators.

I have been supported for three years by a Curtin University Postgraduate Research Scholarship and for two years by an Isotope Studies Scholarship.

The A.F.U.W.(WA) Inc Mary Walters Memorial bursary of $1500.00 allowed the purchase of a Pharmacia RediFrac fraction collector, which saved me many hours of beaker changing during the development of the ion exchange chemistry.

I am indebted to you all.

Table of Contents

List of Tables

List of Figures

1. Background

1.1 Aims of this thesis

- To identify neutron capture by the measurement of the isotopic abundances of cadmium, gadolinium and samarium in samples from a number of different sites on the lunar surface; neutron capture in cadmium in lunar samples will be measured for the first time.
- To assess the accuracy of previous measurements of neutron capture in the rare earth elements and to provide new neutron capture data on previously unmeasured samples of lunar soil.
- To integrate the cadmium, gadolinium and samarium isotopic abundance measurements to determine the neutron energy spectrum at the lunar surface.
- To search for isotope fractionation in cadmium.

1.2 Introduction

Both the atmosphere of the Earth and the surface of the Moon are bombarded by cosmic rays. Nuclear reactions produce an avalanche of secondary neutrons which, in the Earth's atmosphere, invariably decay before they reach the surface. However, on the Moon, the reactions take place at the surface, so the secondary neutrons are thermalised by the lunar soil and captured by isotopes which have high neutron capture cross sections at thermal energies. Four of these isotopes are ^{113}Cd, ^{149}Sm, ^{155}Gd and ^{157}Gd.

Neutrons of different energies are preferentially captured by each of these isotopes, ^{113}Cd capture occurs at 0.178 eV which is significantly different from that of ^{149}Sm (0.0973 eV) and of $^{155\text{ and }157}$Gd (0.0268 eV, and 0.0314 eV respectively). A comparison of the changes from terrestrial values of the isotopic ratios ^{114}Cd/^{113}Cd, ^{150}Sm/^{149}Sm, ^{156}Gd/^{155}Gd, and ^{158}Gd/^{157}Gd caused by neutron capture will allow the shape of the neutron energy spectrum to be more accurately defined, in particular at the higher energies where ^{113}Cd capture occurs.

Details of the formation and evolution of the Moon, the depositional and mixing history of the soil and the impact of the cosmic ray flux at the lunar surface are still uncertain despite the increase in research following the Apollo missions, the Clementine orbiter and now the Lunar Prospector.

This thesis presents the first measurements of neutron capture by cadmium in lunar samples, new rare earth neutron capture data from new locations on the Moon, new evidence to determine the thermal neutron energy spectrum, as well as new elemental concentration measurements and the first evidence of cadmium fractionation in lunar surface soils.

1.3 Cosmic rays

1.3.1 Origin

The lunar surface is continuously bombarded by cosmic rays. These include very high energy (GeV) but low flux galactic cosmic rays (GCR), high energy (MeV) and high flux solar cosmic rays (SCR) from solar flares and the lower energy solar wind (eV to keV) (Reedy et al., 1983).

Most of the SCR and the heavier GCR (Z>20) don't penetrate far into the lunar regolith, but leave dense track records in the top few centimetres of the surface of rocks. The high energy, but lighter, GCR penetrate into the surface and induce nuclear reactions.

Cosmic ray particles, which have been measured at the lunar surface and in the Earth's atmosphere, are primarily protons and electrons, with a proton to alpha ratio of 10 to 20 and about 1% heavier nuclei (Reedy et al., 1983).

1.3.2 Effect of the solar cycle on cosmic rays

The intensity of the SCR and GCR flux is modulated by the 11 year solar cycle, during a time of high solar activity almost the total flux of SCR particles reaching the Earth are ejected from the Sun in several major flares. At the same time the GCR are at a minimum as the increased interplanetary magnetic field from the solar plasma deflects the

galactic cosmic ray particles outwards (Reedy et al., 1983 and Figure 1-1).

The GCR and SCR flux can be estimated by observing the concentrations of radioactive and stable nuclides in the lunar soil, the proton flux measured by satellite matches well the radionuclides measured in lunar rocks (Reedy et al., 1983).

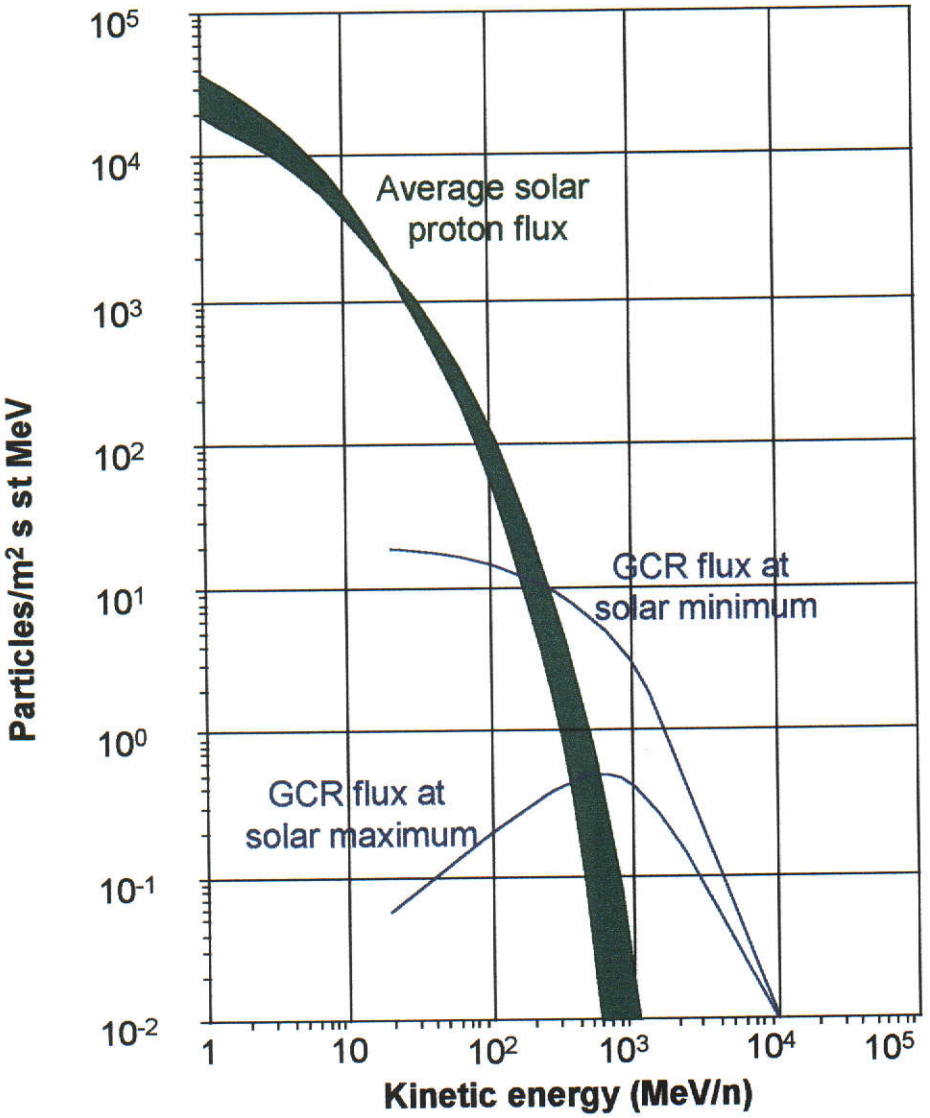

Figure 1-1 The flux of solar protons and galactic cosmic ray protons during solar maxima and minima (adapted from Reedy et al., 1983).

The mean intensities of SCR and GCR are roughly constant, though there may be long periods of high or low solar activity (1645 to 1715 AD,

the Maunder Minimum). The GCR flux has been constant within ±30% for the last 2.5 million years (Tanaka and Inoue, 1979), though there is some evidence that it has been 30% to 50% higher during the last million years (Nishiizumi et al., 1980).

Table 1-1 Summary of the three major types of radiation in the lunar environment (from Heiken et al., 1991).

Type	**Solar Wind**	**Solar Cosmic Rays**	**Galactic Cosmic Rays**
Nuclei energies	0.3-3 keV/nucleon	1 to >100 MeV/n	0.1 to >10 GeV/n
Electron energies	1-100 eV	<0.1 to 1 MeV	0.1 to >10 GeV/n
Fluxes (protons/cm^2 s)	3x10^8	0-10^6	2-4
Electron/proton	1	1	0.02
Proton/alpha	22	60	7
Lunar Penetration Depths			
Proton and alpha	<micrometres	centimetre	metre
Heavier nuclei	<micrometres	millimetres	centimetre

Between 1967-1978 the SCR flux was found to vary more than expected, causing the GCR produced nuclear reactions to vary by 1.5 over the 11 year cycle. This introduces the possibility that variations of a similar magnitude may occur over a longer time span than one solar cycle (Evans et al., 1982).

1.3.3 Galactic Cosmic Rays

GCR are from outside the solar system and are particles accelerated in violent astrophysical events such as supernova, interstellar plasma clouds and shock waves. Though the average energy of these GCR is 1 GeV the range of energies is very large, following the form of $E^{-2.5}$ for the higher energy particles (Walker, 1975 and Figure 1-1). The interplanetary magnetic field from the solar plasma deflects the interstellar particles away from the Sun, so few lower energy particles (<1 GeV/n) are found at 1 AU (Reedy et al., 1983).

1.3.4 Solar Cosmic Rays

Solar flare particles reach the Moon in less than a day, they have energies less than 300 MeV, with most in the range 10 to 100 MeV. While the energy of solar wind particles is roughly constant, the energy of solar flare particles decreases steeply with increasing energy, according to $dN/dE = AE^{-\gamma}$ with $\gamma = 2$ to 4 (Walker, 1975 and Figure 1-1).

Few particles are detected from low solar activity, though there are sometimes more particles in just one solar flare event than in the total GCR flux (Reedy et al., 1983).

1.3.5 Effects of cosmic rays at the lunar surface

The ionised cosmic ray particles interact at the lunar surface in various ways which depend on the energy, charge and mass of the incident particles and the composition and temperature of the targets.

The main interactions are ionisation energy losses, nuclear scattering, and nuclear reactions. The latter result in heavy nuclei tracks, the production of radioactive and stable isotopes, the emission of gamma rays and the generation of secondary particles, especially neutrons, pions, gamma rays and new nuclei, (Reedy and Arnold, 1972).

Typical nuclear reactions are (Reedy and Arnold, 1972):

$^{56}Fe(p,n)^{56}Co$	- (SCR)
$^{24}Mg(n,p2n)^{22}Na$	- (secondary neutrons from GCR)
$^{16}O(n,n'\gamma)^{16}O$	- (inelastic scattering of secondary neutrons with γ-ray emission)

Typical MeV particles will induce nuclear interactions with a mean free path of about 150 g/cm^2 (Walker, 1975), so even the highest energy GCR particle will have interacted before passing through 1000 g/cm^2, which is the thickness of the atmosphere or of 5 m of the lunar soil. Reactions from these high energy particles are constant near the lunar surface then increase to a maximum at about 50 g/cm^2. There are fewer SCR than GCR secondary neutrons by one or two orders of magnitude and below 20 g/cm^2 SCR activity is negligible. At 20 g/cm^2 there are equal numbers

of protons and neutrons (Armstrong and Alsmiller, 1971); below 20 g/cm^2 neutrons dominate.

Secondary neutrons cause further interactions and particle cascades. Below 100 MeV they are dominant as any of the secondary particles which are charged are further slowed by ionisation interactions (Reedy and Arnold, 1972).

GCR reactions from more energetic particles (E>1 MeV) producing one or more nucleons, are called spallogenic nuclides. Reedy and Arnold (1972) developed a method for calculating the production rate P(d) of nuclear reactions made by highly energetic spallation reactions:

$$P(d) = N \int_0^{\infty} dJ/dE\ (E,d)\sigma(E)dE \qquad \text{Equation 1-1}$$

at a depth d

where $\sigma(E)$ is the excitation function for this reaction,

N is the number of target atoms per unit mass and

dJ/dE (E,d) is the differential flux of the strongly interacting particles at that depth.

The secondary high energy neutrons are moderated by the lunar soil, so neutron reactions which depend on the energy of the neutrons will be depth dependent (Walker, 1975). This is shown by the Lunar Neutron Probe Experiment on the Apollo 17 mission (Woolum and Burnett, 1974 and Burnett and Woolum, 1974) and theoretical estimates by Lingenfelter et al. (1972).

1.4 Production of neutrons in the Earth's atmosphere

This and succeeding Sections follow a historical sequence starting with Hess, Canfield and Lingenfelter in 1961.

Neutron production in the Earth's atmosphere has been used as a model for the production of neutrons at the lunar surface. One such model (Hess et al., 1961) considered that the production, slowing down and absorption of neutrons in the atmosphere is in a state of equilibrium, where

gain = loss

knock-on + evaporation reactions = leakage into space + absorption

Fast neutrons, 5 MeV to 1 GeV, with the flux peaking at 10 MeV (Figure 1-2), are produced in "knock-on" reactions made by direct interactions of high energy cosmic rays with the atmosphere (or at the lunar surface). About four times more neutrons are emitted in a process called "nuclear evaporation" as O_2 and N_2, are excited to >8 MeV from collisions with cosmic rays, then drop back to a lower energy and emit neutrons <10 MeV. The neutron flux peaks at about 1 MeV (Figure 1-2). About 64% of the thermalised neutrons are captured by the $^{14}N(n,p)^{14}C$ reaction, so that the thermal spectrum peaks at 0.1 eV and not the expected 0.02 eV (i.e. a 'hardened spectrum').

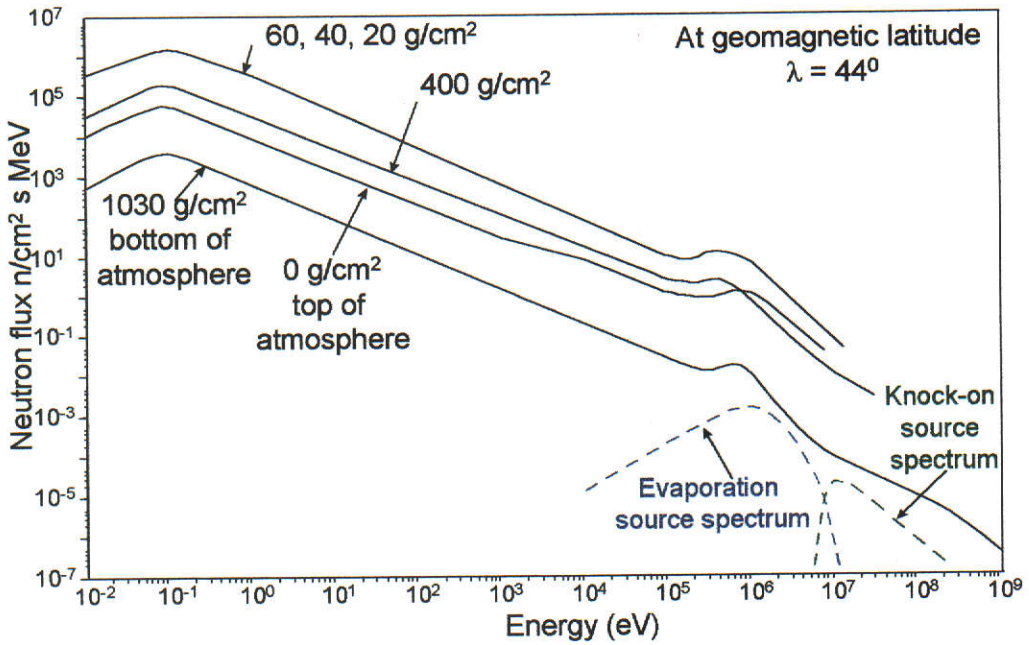

Figure 1-2 The energy of the neutron flux at different depths in the atmosphere for latitude 44°, including the source spectrum for knock-on and evaporation spectra. 400 to 1030 g/cm^2 are experimental data, at 0 g/cm^2 neutrons are lost from leakage from the atmosphere (adapted from Hess et al., 1961).

Hess et al. (1961) developed a diffusion equation for equilibrium neutron flux $\phi(E,r)$, (neutrons/cm^2 s) in the atmosphere, for neutrons with energies less than 10 MeV. An estimate can be made of the neutrons

which lose energy to <10 MeV, so they can be added to the diffusion equation. Hess et al. (1961) uses the multigroup diffusion theory instead of the Boltzmann transport equation. This is valid if these lower energy neutrons, for which the atmosphere is a good moderator, are isotropic and can be represented as a gas with a Maxwell Boltzmann distribution.

$$-\nabla \cdot D(E,r)\nabla\phi(E,r) + \Sigma(E,r)f(E,r) - \int_0^\infty dE'\Sigma(E' \rightarrow E,r)\phi(E',r) = S(E,r)$$

Equation 1-2

where

$\phi(E,r)$ = $n(E,r)v$ = scalar neutron flux

$n(E,r)dE$ = number of neutrons/cm^2 in the energy interval E, E + dE

$\Sigma(E,r)$ = total macroscopic cross section

$\Sigma(E' \rightarrow E,r)$ = macroscopic cross section for scattering from dE' $\rightarrow$ dE

$D(E,r)$ =diffusion coefficient = $1/\{3\Sigma_{tr}(E,r)\}$

$\Sigma_{tr}(E,r)$ = macroscopic transport cross section

$S(E,r)$ = neutron source = number of neutrons/cm^2 s fed into the system

Integrating Equation 1-2 with respect to E, then assuming the atmosphere to be a uniform density (1 g/cm^3) homogenous slab, infinite in two directions, the equation can be restated in mass units (x), where x is the mass of a column of air extending r cm above 1 cm^2 of Earth, by

$$-\frac{d}{dx}D^i(x)\frac{d}{dx}\phi^i(x) + \Sigma^i(x)\phi^i(x) - (sum)_j\,\Sigma^{ij}(x)\phi^j(x) = S^i(x)$$

Equation 1-3

The principle neutron source used in the diffusion calculation was a Maxwellian distribution of the "neutron evaporation" spectrum,

$N(E)\,dE = kEe^{-E/\theta}\,dE$ Equation 1-4

where N(E) is the number of neutrons/second produced in the energy interval dE. The nuclear temperature θ = 1 MeV.

For neutrons with energy greater than 10 MeV an estimate can be made of the numbers losing energy, so these can be added to the low energy evaporation neutrons. The spectrum

$$N(E)\,dE = kE^{-2}\exp(-160\,E^{-2})\,dE \qquad \text{Equation 1-5}$$

fits the high energy neutron "knock-on" spectrum.

52% of these high energy neutrons are degraded to less than 10 MeV, so the source for the diffusion calculation is the neutron evaporation spectrum (E), plus a contribution from the knock-on neutrons of (0.52)xE/4.1 (evaporation/knock-on = 4.1).

The source strength of the neutrons <10 MeV in the atmosphere at latitude 44° is calculated to be 6.2±1.5 neutrons/cm^2 s. This gives an equilibrium neutron flux which agrees with the measured flux to ±25% (source evaporation = 5.0 neutrons/cm^2 s, source knock-on = 1.2 neutrons/cm^2 s).

1.5 Production of neutrons at the lunar surface

Continuing the historical survey Lingenfelter et al. (1961) argued that, with a few modifications, the model of Hess et al. (1961) for the production of atmospheric neutrons could be applied to the lunar surface.

There are more neutrons on the Moon than in the Earth's atmosphere as, with no (or a very small) magnetic field on the Moon, there is a much higher cosmic ray intensity. The neutron flux is likely to be similar to that at the poles of the Earth, about two times the average for the Earth, or 9.2 neutrons/cm^2 s cosmic ray produced neutrons from knock-on and evaporation reactions. Lingenfelter et al. in 1961 estimated that the average atomic mass of the Moon could be similar to that of chondrites, i.e. 24.5, whereas the atomic mass of the Earth's atmosphere is 14.5. The result is an average neutron production cross section for lunar material of 1.3 times that on Earth, so one can estimate a flux of 12 ± 2 neutrons/cm^2 s from evaporation and knock-on reactions (9.6 neutrons/cm^2 s from evaporation and 2.4 neutrons/cm^2 s from knock-on).

Pi mesons, produced in cosmic ray interactions, decay in the Earth's atmosphere with a half-life of 2x10^{-8} s, but in the denser lunar surface

every π^- meson produced from cosmic ray interactions will be captured and will release 4 neutrons (Lingenfelter et al., 1961). Each cosmic ray proton produces one π^- meson. If there are 2 protons/cm^2 s then 8 ± 3 neutrons/cm^2 s will come from (π^-,n) reactions. So the total neutron flux on the lunar surface from evaporation, knock-on and π^- capture is 20 ± 5 neutrons/cm^2 s (Lingenfelter et al., 1961).

Assuming that the energy distribution is the same as in the Earth's atmosphere, then the neutrons from evaporation reactions (9.6 neutrons/cm^2 s), which are all less than 10 MeV, will have the evaporation energy spectrum described by Equation 1-4. Pi meson neutrons (8 neutrons/cm^2 s) also have the same energy spectrum as evaporation neutrons, so 88% of the source for the diffusion equation has this same energy spectrum.

The neutrons from knock-on reactions (2.4 neutrons/cm^2 s), which are all over 10 MeV, will have the energy spectrum given by Equation 1-5.

However, only 52% of the knock-on neutrons are scattered to lower energies (52% x 2.4 = 1.25 neutrons <10 MeV).

So the source for the diffusion equation at the lunar surface is 8 neutrons/cm^2 s from pi mesons, 9.6 neutrons/cm^2 s from evaporation neutrons and 1.25 neutrons/cm^2 s from knock-on neutrons with energy scattered down to less than 10 MeV. This results in 18.8 neutrons/cm^2 s with energies <10 MeV at the surface of the Moon (Lingenfelter et al., 1961).

Lingenfelter et al. (1972) re-calculated the neutron flux on the Moon using a modified flux of 7.1 neutrons/cm^2 s at the poles of the Earth, from evaporation and knock-on reactions, and an atomic number of A = 23 for material at the Moon's surface, based on the Apollo 11 fines composition, which, with the same calculations as above and with the eight pi meson neutrons/cm^2 s, leads to a flux of 16±5 neutrons/cm^2 s with energy < 10 MeV.

Measurement by satellite of the leakage of the neutron flux from the surface of the Moon was initially planned to identify the composition of

the soil (Lingenfelter et al., 1961, Armstrong and Alsmiller, 1971), but was not found to be useful (Lingenfelter et al., 1972). But the calculation of the neutron flux at the lunar surface has proven to be useful in light of the measurements of neutron capture in the lunar regolith (Eugster et al., 1970a, Russ, 1972 and 1973, Russ et al., 1972, and Lugmair et al., 1975). The calculations of flux as a function of depth can be used in conjunction with the measured flux to study the mixing and irradiation history of the lunar surface (Eugster et al., 1970a and Curtis and Wasserburg, 1975).

Neutron capture cross sections calculated for basalt, granite and tektites by Lingenfelter et al. in 1961 did not include the rare earths. Their exclusion allowed the calculated neutron fluences at thermal energies to be above the experimental values (Armstrong and Alsmiller, 1971), because the large cross sections of the rare earth elements (REE) increases the total cross section of the soil, reducing the number of uncaptured source neutrons.

Continued theoretical and experimental research on the production of neutrons in the Sun (Lingenfelter et al., 1965a and b, Lingenfelter and Ramaty, 1967 and Webber and Ormes, 1967), the production of neutrons in the atmosphere (Korff and Mendell, 1967), neutron leakage from the Earth's atmosphere (Lingenfelter, 1963 and Lingenfelter and Flamm, 1964), numerous measurements of neutron flux and energy reviewed (Lockwood, 1973), and the return of samples from the Moon, provided new data for further modification of the models describing neutron production at the lunar surface.

High-energy neutrons produced in acceleration and deceleration in solar flares proved to be an additional source of neutrons in the Earth's atmosphere and at the lunar surface, though their 10^{-3} s half-life at rest, provides some constraints.

An alternative approach based on the Monte Carlo method calculates the trajectories and energy loss of high energy protons with a GCR or SCR energy spectrum and the resulting secondary particles, and gives the production rate and depth dependence of radionuclides and neutrons

on the Moon (Armstrong and Alsmiller, 1971). The discrete ordinates method of calculation (Engle, 1967 from Armstrong and Alsmiller (1971)) is used by Armstrong and Alsmiller (1971) for neutron energies less than 15 MeV, as it is better than the Monte Carlo method for low energy neutrons. Estimated, not calculated, uncertainties are thought to be ±20%, or less.

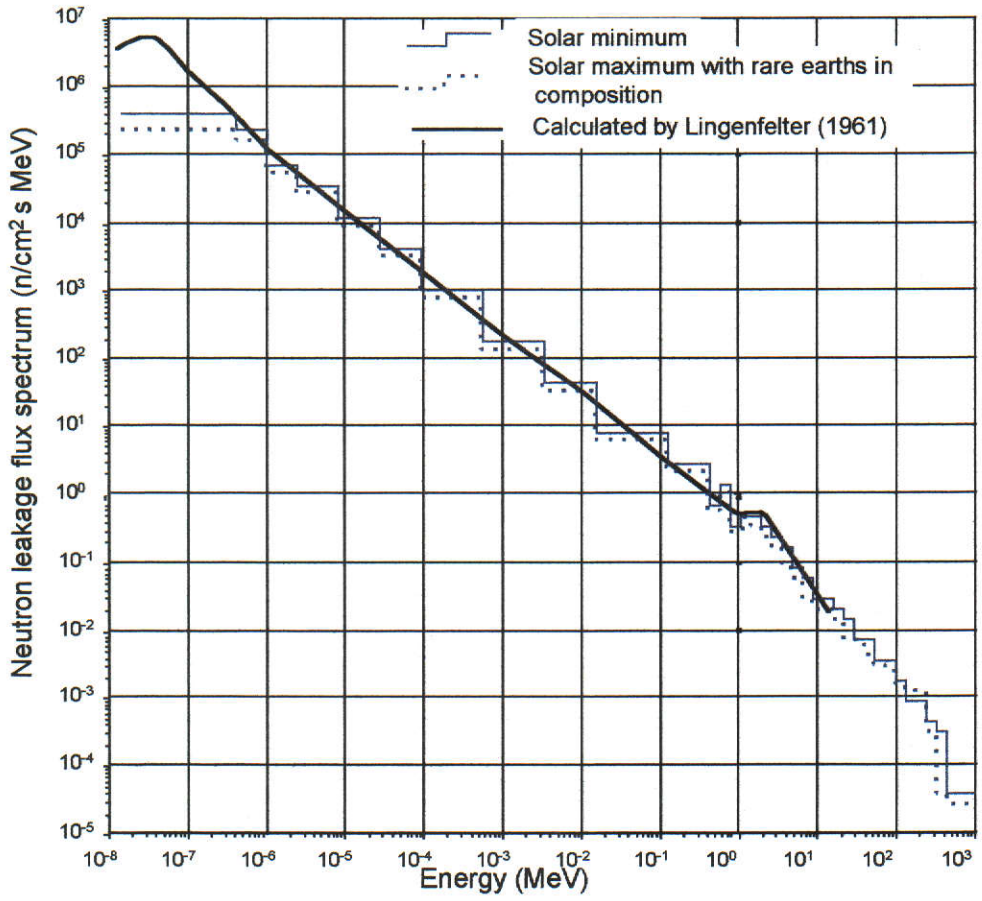

Figure 1-3 Calculation of the leakage of neutron flux induced by galactic proton bombardment on the Moon, compared to that from a basaltic composition (adapted from Armstrong and Alsmiller, 1971).

Calculated neutron leakage from the lunar surface with and without REE, compared to a spectrum using material with a basaltic-type composition (Lingenfelter et al., 1961), show good agreement, except at thermal energies (Figure 1-3). Armstrong and Alsmiller (1971) shows a flat neutron flux spectrum for neutrons with energies less than about 0.6

eV, in comparison the Lingenfelter et al. (1961) spectrum first increases, and then decreases exponentially.

Armstrong and Alsmiller (1971) suggest that the differences could be because Lingenfelter et al. (1961) include hydrogen in the calculations. In comparison Lingenfelter et al. (1972) suggests that the Armstrong and Alsmiller calculations could be based on the lower cosmic ray flux found at lower latitudes on the Earth, or that perhaps the pi meson neutrons produced on the Moon are not included.

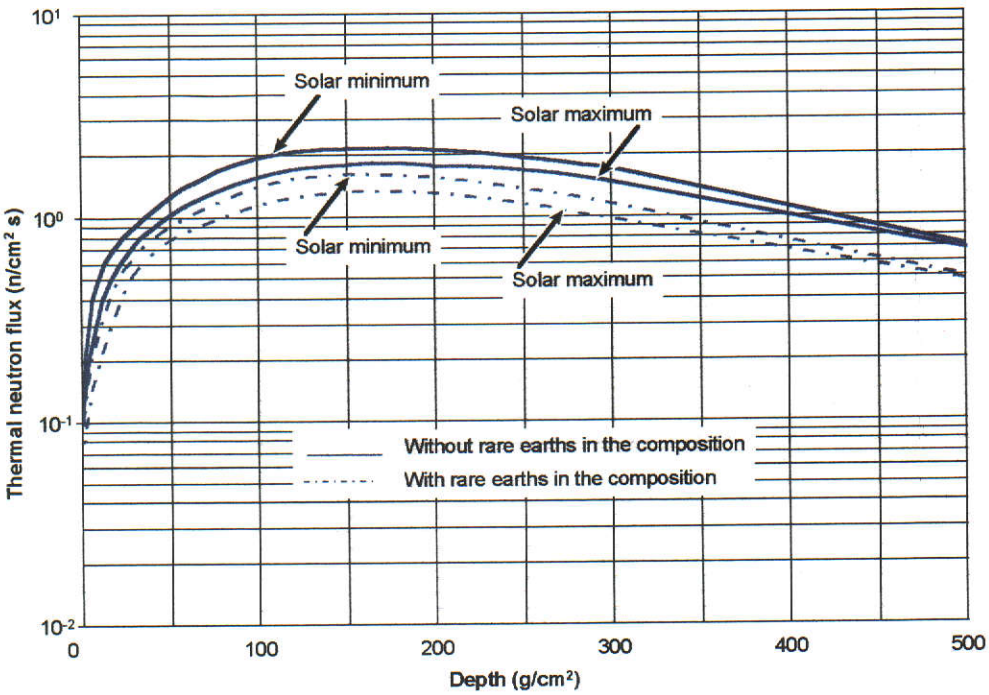

Figure 1-4 Calculation of the thermal neutron flux <0.4 eV versus depth induced by galactic protons at the surface of the Moon (adapted from Armstrong and Alsmiller, 1971).

Armstrong and Alsmiller (1971) calculate the neutron flux to a depth of 500 g/cm^2 for eight energy groups with energies <0.4 eV to >1000 MeV. (the lunar soil is assumed to be of a constant density of 1 g/cm^2 Lingenfelter et al., 1961). This indicates an inverse relationship between the depth of the neutron flux peak and the energy of the neutrons. Neutrons with energy greater than 1000 MeV peak at about 70 g/cm^2, whereas neutrons with energy less than 0.4 eV peak at nearly 200 g/cm^2

(Figure 1-4). The magnitude of the flux is a maximum for neutrons between 100 eV to 0.1 MeV.

The spectrum of thermal neutrons <0.4 eV from a neutron source experiencing both maximum and minimum solar activity shows a reduction of the thermal neutron flux of 30% for a soil composition with REE, compared to one without. The 30% reduction occurs across all energies and at all depths in the soil (Figure 1-4).

An alternative model (Reedy and Arnold, 1972) for calculating nuclear reactions from GCR and ionisation energy loss from SCR at any depth assumes that the source for the reactions is primarily high energy secondary neutrons, produced in knock-on reactions. The flux and spectrum of the neutrons at various depths in a solid body, such as the Moon, was used to calculate the nuclear reactions at that depth.

The production rate for a nuclear reaction is found from Equation 1-1 above. It is assumed that all interacting particles under 100 MeV are secondary neutrons and above 100 MeV are any strongly interacting particle.

Over 100 MeV the energy spectrum of the particles is described by:

$dJ/dE(E,d) = K(\alpha + 100)^{-2.5}$,

where α determines the shape of the spectrum and K is a constant,

while the spectrum for secondary neutrons between 2.5 MeV to 100 MeV:

$dJ/dE(E,d) = K(\alpha + 100)^{-2.5}(M(E) - \{\alpha - 50\}\delta(E))$, where

$\delta(E) = 0.3E^{-1.26} - 0.00091$

$M(E) = 94E^{-1} + 603E^{-2} - 300E^{-3}$.

Reedy and Arnold (1972) use the neutron spectral shape M(E) from Hess (1959), for neutrons 10 MeV to 100 MeV and Tajima (1967) and Mendell & Korff (1963) for 2 MeV to 10 MeV. These references are from Reedy and Arnold (1972).

For the energies 0.5 MeV to 2.5 MeV:

$$dJ/dE(E,d) = K(\alpha + 100)^{-2.5} \cdot (115 - \{\alpha - 50\}0.094)(1.3125 + 0.5E - 0.25E^{2})$$

and for secondary neutrons with energy less than 0.5 MeV Reedy and Arnold (1972) use 1/E, from Lingenfelter et al. (1961).

These calculations (Reedy and Arnold, 1972) show that the flux of high energy particles from cosmic ray interactions decrease with depth, while the flux of low energy particles at first increases, then decrease, with depth.

Table 1-2 Composition of Apollo 11 and Apollo 16 soils fines including three REE, from Armstrong and Alsmiller (1971) and Kornblum et al. (1973).

Element	Weight % Apollo 11 fines	Apollo 16 soil
O	42.07	44.923
Si	20.00	21.064
Al	6.90	14.70
Fe	12.40	4.0
Ca	8.60	11.4
Mg	4.80	3.2
Ti	4.20	0.35
Na	0.40	0.29
K	0.10	0.083
Gd	17 ppm	6 ppm
Sm	14 ppm	5.5 ppm
Dy	20 ppm	7 ppm

Kornblum et al., 1973 also calculated the neutron production rate with depth for neutrons with energies below 15 MeV, using the discrete ordinate method (Engle, 1967, quoted in Kornblum et al., 1973). Measured values of ^{37}Ar from the $^{40}Ca(n,\alpha)^{37}Ar$ reaction in the Apollo 16 drill core to 300 g/cm^2 gave the magnitude of the neutron source, which decreased as $e^{-1.5d/155}$ at large depths. The Lingenfelter et al. (1972) energy spectrum for source neutrons was assumed and three soil compositions; the Apollo 11 soil used by Armstrong and Alsmiller (1971) and Lingenfelter et al. (1972); the Apollo 16 soil with samarium, gadolinium and dysprosium with the Apollo 11 concentrations; and the

Apollo 16 soil with samarium, gadolinium and dysprosium with the Apollo 16 concentrations, were used for the calculations (Table 1-2).

A total neutron production of 26±4 neutrons/cm^2 s, below 15 MeV, was found.

The low energy, <0.4 eV, fluxes are very sensitive to changes in chemical composition. Changing the REE concentrations from the Apollo 11 values to the Apollo 16 values, increased the neutron flux by 50%. Compared to Armstrong and Alsmiller (1971), the Kornblum et al. (1973) neutron flux, especially at higher energies, peaks closer to the surface, caused by differences in the neutron source functions and cross sections used by each.

1.6 Neutron capture

Anomalies in lunar soils from thermal neutron capture in ^{157}Gd and ^{149}Sm, were experimentally verified by Eugster et al. (1970a) and by Russ et al. (1971). Lingenfelter et al. (1972) recalculated the cosmic ray produced neutron flux, the neutron energy spectrum at the lunar surface, and the production rates at depth of various isotopes with high thermal neutron capture cross sections. Soils of four different compositions based on the Apollo 11 fines, and of three soil temperatures, were used. A careful choice of energy groups gave especially good detail from 0.00178 eV to 1 eV, the region of energy resonance for cadmium, gadolinium and samarium.

1.6.1 Composition and cross sections

At thermal energies the major elements have 1/velocity dependent cross sections while the trace elements show strong resonance capture cross sections (Tables 1-3 and 1-4). Cross sections at 0.0253 eV have been calculated by Lingenfelter et al. (1972) using the Breit-Wigner resonance parameters, the macroscopic cross section for elements in the Apollo 11 fines are given in the last column of Table 1-4. The total macroscopic cross section for neutron capture (Σ_{eff}) characterises the total neutron absorption by a material of given composition.

Table 1-3 Resonance at thermal energies (Lingenfelter et al., 1972 and Holden, 1987).

Reaction	Breit-Wigner resonance at thermal energies (eV)	Resonance energy (eV)	Thermal cross-section (barns)
$^{155}Gd(n,\gamma)^{156}Gd$	0.0268	0.0268±0.0002	60,900±500
$^{157}Gd(n,\gamma)^{158}Gd$	0.0314	0.0314±0.0002	254,000±815
$^{149}Sm(n,\gamma)^{150}Sm$	0.0976	0.0973±0.0002	40,140±600
$^{113}Cd(n,\gamma)^{114}Cd$	0.178	0.178±0.002	20,600±400

Table 1-4 Macroscopic cross sections for Apollo 11 fines (1 barn = 10^{-24} cm^2) (Lingenfelter et al., 1972).

Element	Abundance in Apollo 11 fines (10^{24} atoms/g)	Neutron capture cross section at 0.0253 eV	
		Calculated using Breit-Wigner thermal cross sections σ_{eff} (barns)	Macroscopic cross section (cm^2/g)
O	1.58×10^{-2}	$<2\times10^{-4}$	$<3\times10^{-6}$
Si	4.23×10^{-3}	1.6×10^{-1}	6.8×10^{-4}
Al	1.63×10^{-3}	2.3×10^{-1}	3.7×10^{-4}
Fe	1.32×10^{-3}	2.53×10^{0}	3.3×10^{-3}
Ca	1.29×10^{-3}	4.3×10^{-1}	5.5×10^{-4}
Mg	1.19×10^{-3}	6.3×10^{-2}	7.5×10^{-5}
Ti	5.70×10^{-4}	6.1×10^{0}	3.5×10^{-3}
^{155}Gd	9.8×10^{-9}	5.8×10^{4}	5.7×10^{-4}
^{157}Gd	1.03×10^{-6}	2.4×10^{5}	2.4×10^{-3}
^{149}Sm	7.3×10^{-9}	4.08×10^{4}	3.0×10^{-4}
^{113}Cd	2.6×10^{-11}	2.0×10^{4}	5.2×10^{-7}
^{151}Eu	3.4×10^{-9}	7.8×10^{3}	2.6×10^{-5}
^{130}Ba	1.00×10^{-9}	8.8×10^{0}	8.8×10^{-9}
^{79}Br	7.50×10^{-10}	1.14×10^{1}	8.5×10^{-9}
^{81}Br	7.50×10^{-10}	3.2×10^{0}	2.4×10^{-9}
^{186}W	2.30×10^{-10}	4.0×10^{1}	9.2×10^{-9}

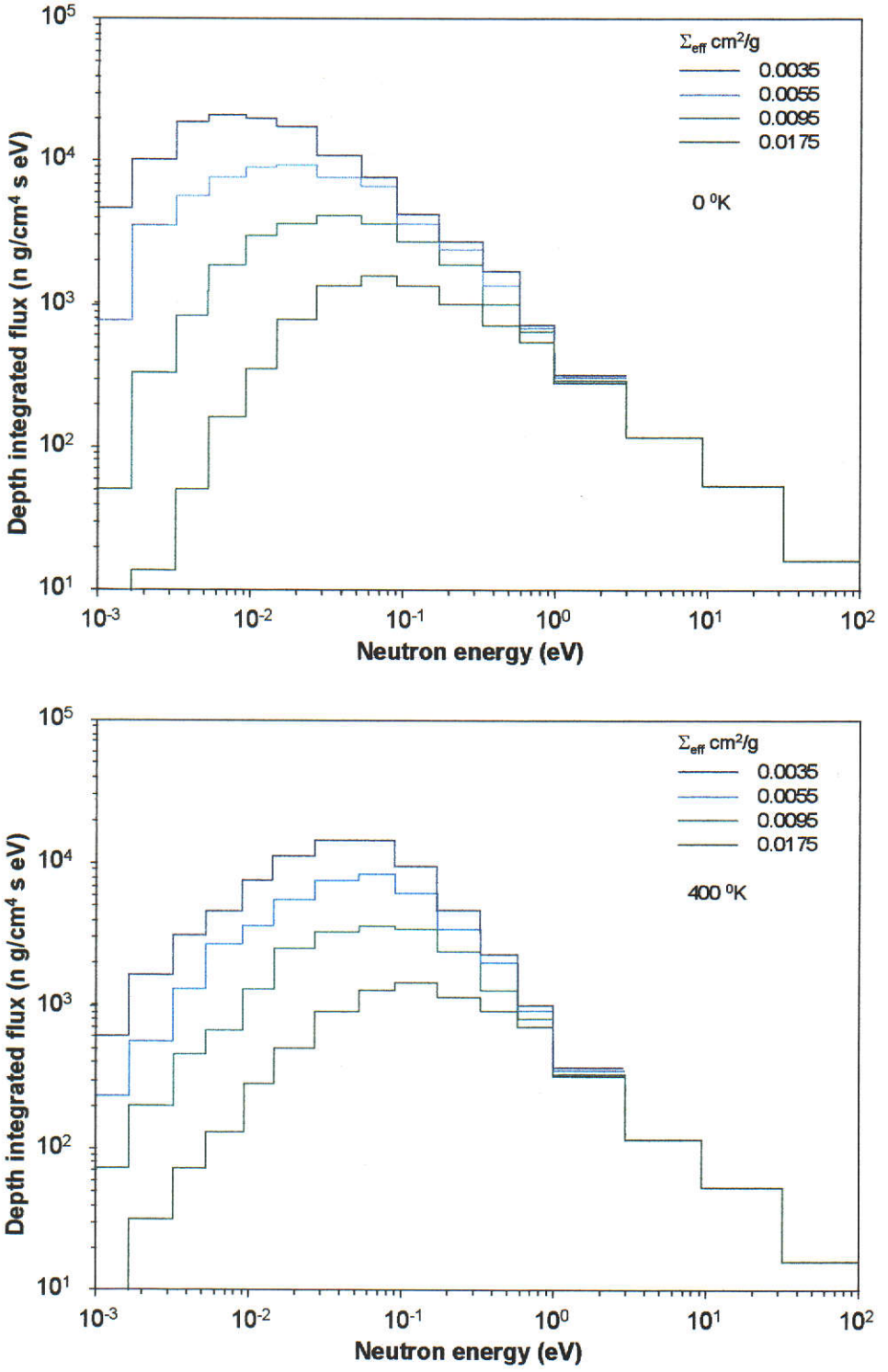

Figure 1-5 Depth integrated neutron flux spectrum at 0 K and 400 K for four soil compositions (adapted from Lingenfelter et al., 1972).

Alternative total macroscopic cross sections, covering the range of compositions of samples from Apollo 11, 12, 14 and 15, were calculated by Lingenfelter et al. (1972) using two times, half and a quarter of the Apollo 11 fines cross section.

When the composition of the soil is changed so that the macroscopic cross section of the major elements increases more thermal neutrons are captured, resulting in a reduction of the magnitude of the peak flux and a hardened thermal neutron energy spectrum, particularly at 400 K (Figure 1-5), so that the capture rate of the trace elements is reduced. Changes in the abundances of individual major elements will have no effect on neutron capture if the *total* cross section does not change.

Table 1-4 shows that the strongly absorbing properties of the Apollo 11 fines is caused mainly by the major elements Ti and Fe which capture most of the thermal neutrons, though ^{157}Gd also has a large macroscopic cross section in this soil. The cross sections for the trace elements shown in Table 1-4 are not the cross sections used to calculate the total macroscopic cross section for the Apollo 11 fines. They must first be modified, as they depend on the total macroscopic cross section of the major elements.

Figure 1-6 shows the effective neutron capture cross sections of some of the trace elements relevant to this work as a function of the total macroscopic cross section of the soil. The Figure contains a combination of data from Lingenfelter et al. (1972) and Curtis and Wasserburg (1975) and shows the effective cross section for gadolinium, samarium, cadmium and europium at 0 ^{0}K, 200 ^{0}K and 400 ^{0}K. To correspond to the Moon's average surface temperature the values of effective cross sections at 200 K are required.

It can be seen in the Figure that cadmium is not sensitive to a change in soil composition, it has an almost constant σ_{eff} at 4.2×10^4 barns from Σ_{eff} 0.48×10^{-2} cm^2/g to 0.925×10^{-2} cm^2/g. There is a very small change in σ_{eff} for samarium in this range, from 5×10^4 barns to 6×10^4 barns, though gadolinium is much more sensitive to soil composition, changing from 1.1×10^5 barns to 8×10^4 barns in the range.

1.6.2 Temperature

A change in temperature of 0 ^{0}K to 400 ^{0}K (the lunar day is 120 ^{0}K to 400 ^{0}K) has little effect on the magnitude of the neutron flux (Figure 1-5),

though ^{155}Gd and ^{157}Gd neutron capture rates (resonant energies 0.0268 eV and 0.0314 eV) drop by 20% with a change in temperature from 0 ^{0}K to 400 ^{0}K. ^{113}Cd (0.178 eV) and ^{149}Sm (0.0976 eV) capture rates increase by 5-15% with the same temperature increase (Lingenfelter et al., 1972).

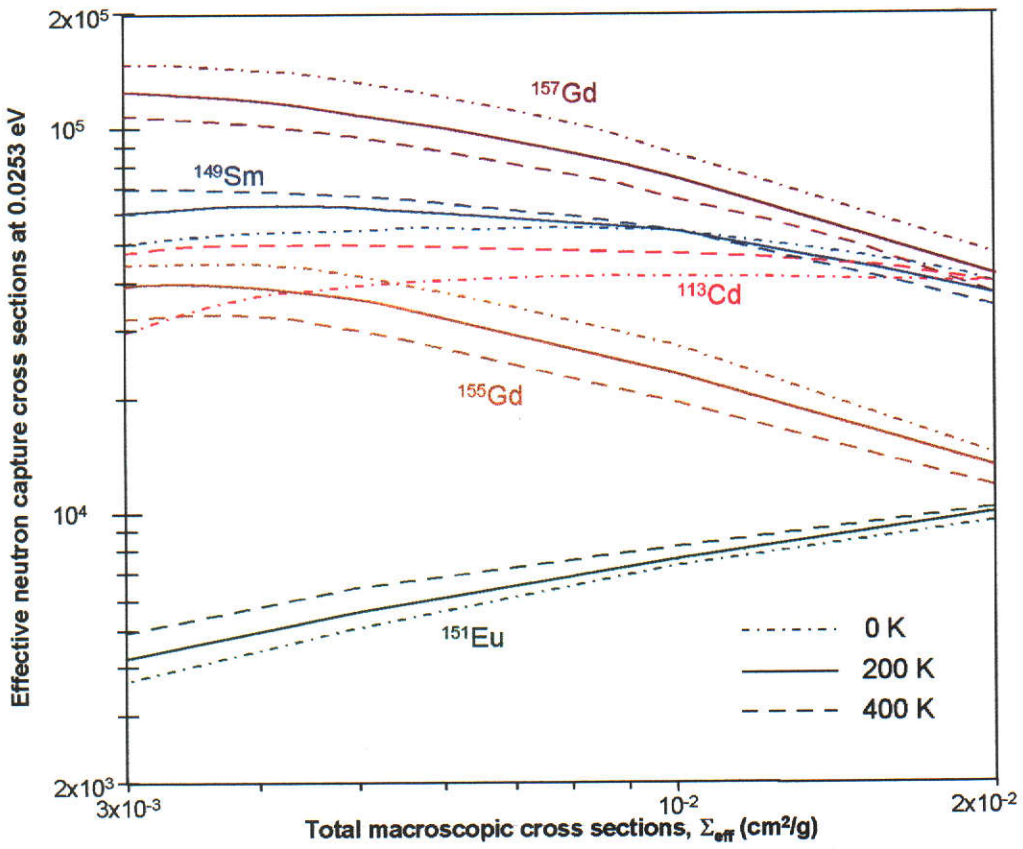

Figure 1-6 Effective neutron capture cross section for 0.0253 eV neutrons as a function of the chemical composition of the soil (adapted from Lingenfelter et al., 1972, and Curtis and Wasserburg, 1975).

1.6.3 Source neutrons and neutron capture rates

The neutron evaporation spectrum for source neutrons, Equation 1-4 above, used by Lingenfelter et al. (1961) for the spectrum of the low energy neutron flux, is modified by Lingenfelter et al. (1972) to

$$S(E,x) = S_o E e^{-E/\theta} e^{-x/\Lambda} \qquad \text{Equation 1-6}$$

where x is the depth in g/cm^2,

Λ = attenuation length in g/cm^2, (165 g/cm^2 measured in the Earth's atmosphere at the poles),

θ = evaporation temperature (1 MeV), and

S_o is normalised to give 1 neutron/s under each cm^2 of lunar surface.

A source of 16±5 neutrons/cm^2 s (<10 MeV) cosmic ray produced neutrons is used for the calculations.

Lingenfelter et al. (1972) compared his exponential profile for the production rate of high energy (MeV) neutrons with the Armstrong and Alsmiller (1971) source profile with the flat neutron production rate near the surface to 165 g/cm^2, followed by an exponential decrease (Figure 1-3). The Armstrong and Alsmiller (1971) neutron source profile results in a 15% increase in the thermal neutron density below 150 g/cm^2 with a lower density near the surface compared to calculations based on the Lingenfelter et al. exponential neutron source (Figure 1-9).

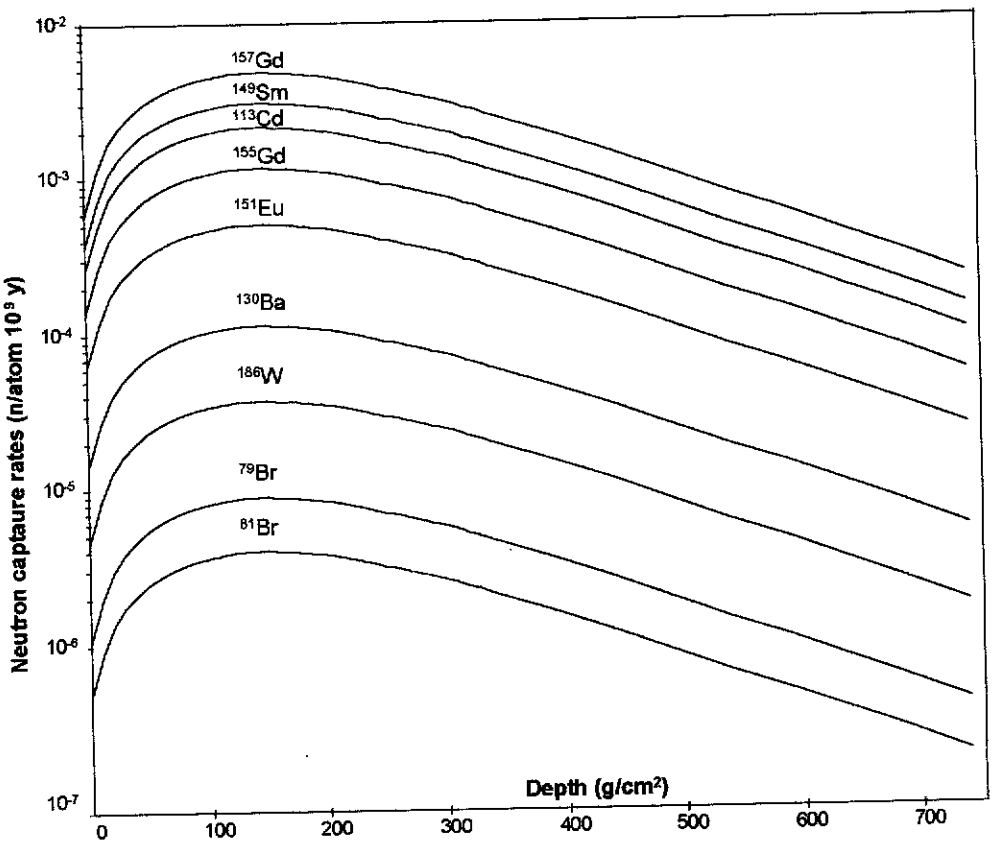

Figure 1-7 Neutron capture rate for trace elements in Apollo 11 fines at 0 ^0K (adapted from Lingenfelter et al. (1972)).

Thermal neutron capture rates for trace elements are shown by Lingenfelter et al. (1972) to be largest for ^{157}Gd, ^{149}Sm, ^{113}Cd and ^{155}Gd

(Figure 1-7) and vary by less than ±5% with depth from 0 g/cm^2 to 750 g/cm^2.

1.6.4 Calculation of the total macroscopic cross section for E<0.18 eV

The procedures to calculate the total macroscopic cross section (Σ_{eff}) for any soil is described in Lingenfelter et al. (1972) and Curtis and Wasserburg (1975):

$\Sigma_{eff} = \Sigma X_i\sigma_i + \Sigma X'_j\sigma'_j$ Equation 1-7,

where X and X' are the number of atoms of element i or j per gram of irradiated material,

σ_i is the neutron capture cross section at 0.0253 eV for major elements with a 1/velocity cross section (Table 1-4).

σ'_j is the effective capture cross section for trace elements at 0.0253 eV for elements with thermal resonance cross sections.

Because the effective capture cross section varies according to the macroscopic cross section of the major elements it must be determined by iteration.

The total cross section of the major elements ($\Sigma X_i\sigma_i$) is used as a first guess at the total macroscopic cross section Σ_{eff}. An estimate is then made of the total cross sections of the trace elements using Σ_{eff} and Figure 1-6. A new value of $\Sigma_{eff} = \Sigma X_i\sigma_i + \Sigma X'_j\sigma'_j$ is calculated. Another estimate of the trace element cross sections is made, using this new value of Σ_{eff} and Figure 1-6, giving another value of $\Sigma_{eff} = \Sigma X_i\sigma_i + \Sigma X'_j\sigma'_j$. The same procedure is repeated until the result converges.

The elements used by Lingenfelter et al. (1972) to calculate Σ_{eff} for the Apollo 11 fines are shown in Table 1-4. He did not include the contribution of the REE in his calculations, but most later calculations, for example by Russ et al. (1972), Russ (1973) and Curtis and Wasserburg (1975, 1977b), include not only the REE contribution, but also additional trace elements.

Table 1-5 Examples of Σ_{eff} calculated for various lunar soils

Sample	Σeff ($x10^{-2}$ cm^2/g)	Reference
Apollo11 fines	1.03	Lingenfelter et al., 1972
10017	1.32	Russ et al., 1971
14148	0.91	Curtis and Wasserburg, 1975
14310	0.75	Lugmair and Marti, 1971
60501	0.48	Curtis and Wasserburg, 1975
72701	0.58	Curtis and Wasserburg, 1975
72161	0.85	Curtis and Wasserburg, 1977b
L-chondrites	0.71	Bogard et al., 1995
H-chondrites	0.92	Bogard et al., 1995
Angrites	0.60	Bogard et al., 1995
Aubrites	0.18	Bogard et al., 1995

Table 1-6 Examples of σ_{eff} for ^{157}Gd, calculated for various lunar soils (Russ et al., 1972)

Sample	σ_{eff} for ^{157}Gd (barns)
Apollo 11	$8.9x10^4$
Apollo 12 and 14	$9.4x10^4$
15221 15231	$1.02x10^5$
15601	$9.7x10^4$
Luna 16	$9.6x10^4$

σ^{155} is found from (0.24)*(σ^{157}) (Eugster et al., 1970b).

Tables 1-5 and 1-6 give examples of calculated total macroscopic cross sections and the effective capture cross sections for gadolinium for various rocks and soils.

Uncertainties for Σ_{eff} from the neutron production rate normalisation is ±30%, and from the uncertain history, ±50% (Lingenfelter et al., 1972).

Neutron fluence was calculated for various meteorites (i.e. Chico and Torino) by Bogard et al., 1995 using a σ_{eff} for ^{149}Sm of $6.4x10^4$ barns. Neutron fluence calculated from measurements of ^{36}Cl, ^{41}Ca and ^{36}Ar found similar values, reinforcing the accuracy of the method used above.

1.6.5 The Apollo 17 Lunar Neutron Probe Experiment (LNPE)

The Apollo 17 Lunar Neutron Probe Experiment (LNPE) provides experimental data on neutron capture rates and depth profiles for mainly low energy neutrons (Woolum and Burnett, 1974, Burnett and Woolum, 1974 and Woolum et al., 1975). A two metre probe (0 to 400 g/cm^2 depth) was placed in the hole provided by the Apollo 17 deep drill core, and exposed for 49 hours at the surface of the Moon (Woolum and Burnett, 1974).

Sixteen ^{235}U targets with mica detectors recorded the fission fragment tracks from ^{235}U low energy neutron induced fission (Figure 1-8).

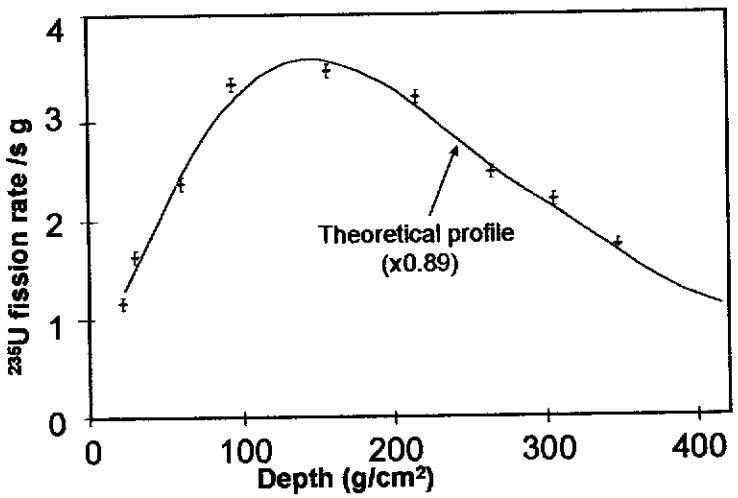

Figure 1-8 The experimental ^{235}U fission rate versus depth compared with the Lingenfelter et al. (1972) theoretical curve, (adapted from Woolum and Burnett, 1974).

A second set of neutron measurements involved twenty three ^{10}B targets placed "essentially continuously" down the probe. The alpha particles produced in the low energy neutron capture reaction $^{10}B(n,\alpha)^7Li$ leave tracks in the cellulose triacetate plastic detectors surrounding the ^{10}B targets. Two sections of the probe at 180 g/cm^2 and 370 g/cm^2 were wrapped in 0.45 mm of cadmium, to absorb neutrons with energies less than 0.5 eV (Woolum et al., 1975).

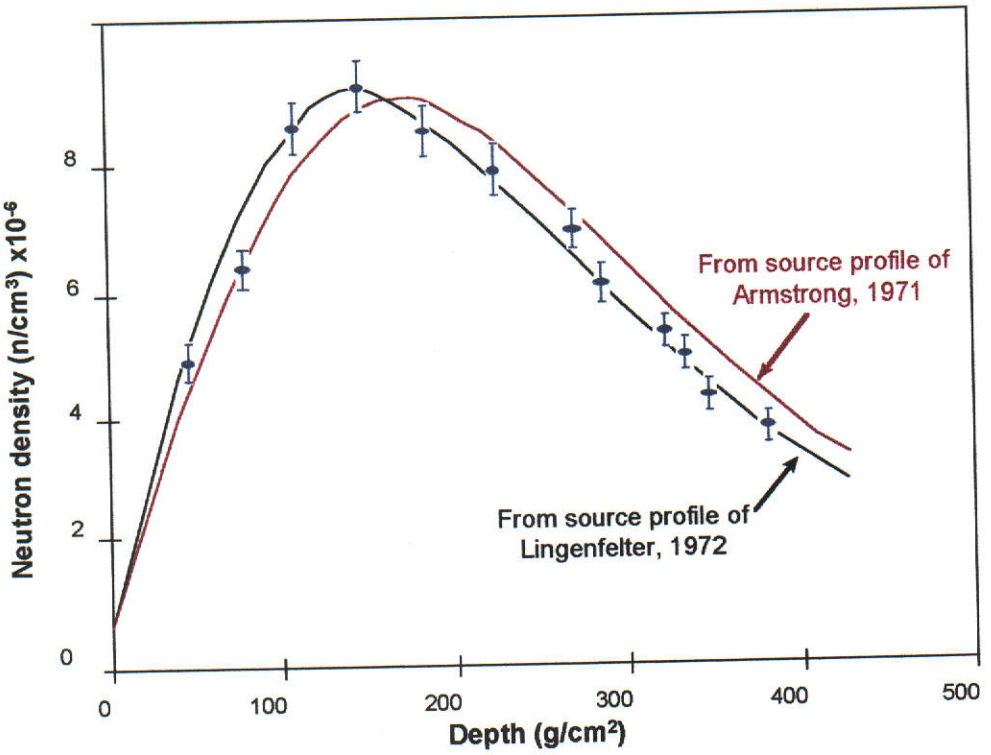

Figure 1-9 A comparison of experimental neutron density profiles from ^{10}B targets compared to theoretical neutron source profiles from Lingenfelter et al. (1972) and Armstrong and Alsmiller (1971) seen in Figure 1-3 (adapted from Woolum et al., 1975).

In both cases the experimental values are in good agreement with the Lingenfelter et al. (1972) theoretical calculations for an Apollo 11 composition at 200 K, with an uncertainty of ±30% (Figures 1-8 and 1-9). The theoretical spectrum (Lingenfelter et al., 1972) is about 11±11% too high compared to the ^{235}U experimental data, though with the uncertainties in the Lingenfelter et al. data of ±30% the agreement is good. The capture rate at 150 g/cm^2 for ^{10}B is 467±74 captures/(g ^{10}B) s compared to the theoretical value of 575 captures/(g ^{10}B) s from Lingenfelter et al. (1972) (Burnett and Woolum, 1974). Thus, the measured track density for $^{10}B(n,\alpha)^7Li$ gives a depth profile in good agreement with Lingenfelter et al. (1972), but 15-20% lower.

Woolum et al. (1975) compared their results with two other theoretical calculations, those of Armstrong and Alsmiller (1971)) and Kornblum et al. (1973), both discussed in Section 1.5 above.

Armstrong and Alsmiller (1971) used a MeV neutron source initially constant, then decreasing exponentially (Figure 1-3). The calculated spectrum of thermal neutrons with energies less than 0.4 eV is too low at shallow depths to 150 g/cm^2 and too high deeper, compared to the measured values (Figure 1-9) (Woolum et al., 1975).

The production rate of ^{37}Ar, from ^{40}Ca interacting with MeV neutrons (Fireman, 1973; Stoenner, 1974; and Kornblum et al., 1973, from Woolum et al., 1975), suggests that the MeV neutrons peak at 30 g/cm^2 or less, closer to the Lingenfelter et al. (1972) MeV neutron source profile (seen in Figure 1-3), rather than that of Armstrong and Alsmiller (1971).

However, the ^{157}Gd neutron capture rate versus depth calculated by Kornblum et al. (1973) peaks too close to the surface compared to LNPE data, so also does not fit as well as the Lingenfelter et al. (1972) profile.

The conclusion of Woolum et al. (1975) is that the ^{157}Gd capture rate is between 0.7 and 0.5 of the rate calculated by Lingenfelter et al. (1972) at all depths and as ^{157}Gd is very sensitive to changes in this low energy spectrum, further work needs to be done. However, the special effects of neutron scattering from the crystalline lattices of materials in the lunar soil are not yet fully understood (Woolum et al., 1975).

Curtis and Wasserburg (1975) suggest that a simpler mixing model could be used for the lunar regolith if the theoretical ^{157}Gd capture rate calculated by Lingenfelter et al. (1972) is three times higher than the actual capture rate.

1.7 Neutron capture measurements

Measurement of the variations in isotopic abundances from neutron capture have provided important information on the history of the lunar regolith, the mechanisms and rates of transport, the deposition on the lunar surface, and the magnitude of the cosmic ray produced neutron fluence. As the changes in isotopic abundance are a direct measure of the exposure of materials to low energy neutron flux over time, changes in ^{157}Gd can resolve a minimum of 100 million years (Curtis and Wasserburg, 1975).

Thermal neutron capture, $^{155}Gd(n,\gamma)^{156}Gd$ and $^{157}Gd(n,\gamma)^{158}Gd$, has been measured in meteorites (Eugster et al., 1970c and Hidaka et al., 1997), and in lunar samples (Eugster et al., 1970b, Lugmair and Marti, 1971, Burnett et al., 1971, Russ et al., 1972, Russ, 1973, Curtis and Wasserburg, 1975 and 1977a and b).

Neutron capture, $^{149}Sm(n,\gamma)^{150}Sm$, has been measured in meteorites (Bogard et al., 1995 and Hidaka et al., 1997) and in lunar samples (Russ et al., 1971 and 1972, Russ, 1973, Curtis and Wasserburg, 1975, 1977a and b).

Neutron capture on cadmium $^{113}Cd(n,\gamma)^{114}Cd$ has not been measured before.

The first measurements of neutron capture on ^{157}Gd in the Norton County Meteorite (Eugster et al., 1970b) allow 0.1% changes in isotopic abundances from neutron capture to be detected. Terrestrial gadolinium exposed to a thermalised neutron flux showed percentage changes in $^{158}Gd/^{157}Gd$ of 2.02±0.03% and 0.20±0.03% for fluxes of $59x10^{15}$ neutrons/cm^2 and $6.1x10^{15}$ neutrons/cm^2 (Table 1-7). The detection rate is now ten times better (Hidaka et al., 1995).

Table 1-7 The change in the isotopic ratios of $^{158}Gd/^{157}Gd$ in terrestrial gadolinium after exposure to thermal neutrons in the Brookhaven Medical Reactor (Eugster et al., 1970b).

Sample	**Neutron fluence 10^{15} n/cm^2**	**$^{158}Gd/^{157}Gd$**	**Change**
Terr	none	1.58670	
GdF_3	59	1.61869	2.02%
GdF_3	6.1	1.58984	0.20%

When $^{156}Gd/^{160}Gd = 0.9361$ is used to normalise data which have experienced neutron capture a false discrimination correction of

$$¼\{^{155}\sigma\psi(^{155}Gd/^{156}Gd)_{terr}\}$$

per mass unit will result, where $^{155}\sigma$ is the neutron capture cross section on ^{155}Gd and ψ is the neutron fluence (Russ, 1974).

Russ (1974) shows that when ^{158}Gd/^{160}Gd is plotted against ^{157}Gd/^{160}Gd, to show the effect of neutron capture a slope of -1 would normally be expected, but as a result of the false discrimination effect, to first order, the ratios will follow a line with slope,

$$\frac{\Delta(158/160)_N}{\Delta(157/160)_N} = -\frac{\{1 - 0.5(^{155}\sigma/^{157}\sigma)(155/156)_T(158/157)_T\}}{\{1 + 0.75(^{155}\sigma/^{157}\sigma)(155/156)_T\}}$$

$$= -\ 0.763 \qquad \text{Equation 1-8}$$

where N is a normalised ratio. An assumption is made that the maximum neutron fluence will be 10^{17} n/cm^2, introducing an uncertainty of 0.04%.

1.8 Neutron fluence from neutron capture measurements

Lingenfelter et al. (1972), Armstrong and Alsmiller (1971) and Kornblum et al. (1973) calculated the total neutron flux (the fluence) with depth, whereas the Lunar Neutron Probe Experiment measured the neutron flux directly (Woolum and Burnett, 1974, Burnett and Woolum, 1974 and Woolum et al., 1975).

Estimates of the total thermal neutron fluence (ψ) at thermal energies are calculated from the observed isotopic measurements and the cross sections for ^{157}Gd or ^{149}Sm and a correction must be made when gadolinium has been normalised to ^{156}Gd/^{160}Gd = 0.9361.

$$\psi = \frac{\left(^{158}/_{157}\right)_N - \left(^{158}/_{157}\right)_T}{^{157}\sigma\left[1+\left(^{158}/_{157}\right)_T\right] + \frac{1}{4}\,^{155}\sigma\left(^{158}/_{157}\right)_T\left(^{155}/_{156}\right)_T} \qquad \text{Equation 1-9}$$

where N is the normalised ratio, T is the true ratio and $^{157}\sigma$ and $^{155}\sigma$ the neutron capture cross section for ^{157}Gd and ^{155}Gd. An assumption made here is that ^{158}Gd/^{157}Gd$_N$ will at the most be 5% greater than ^{158}Gd/^{157}Gd$_T$.

The second term in the denominator is the correction term required because of normalisation to ^{156}Gd/^{160}Gd = 0.9361. Between 96% and

98% of the neutrons with energies less than 0.18 eV are captured by gadolinium in soils with effective cross sections of Σ_{eff} $0.5x10^{-2}$ cm^2/g to $1.0x10^{-2}$ cm^2/g (Russ, 1974). $^{158}Gd/^{157}Gd$ is the most sensitive to changes in the energy of the thermal neutron fluence, compared to $^{150}Sm/^{149}Sm$ and $^{114}Cd/^{113}Cd$.

The neutron fluence for the Norton County meteorite was initially estimated with a calculated thermal cross section of σ^{157} (200 K) = 262,000 barns and $<\sigma^{155}>/<\sigma^{157}> = 0.2386$, assuming a Maxwell Boltzmann distribution (Eugster et al., 1970b). Using the Lingenfelter et al. (1972) calculations for effective cross section (σ_{eff}) for ^{157}Gd, instead of the thermal calculations, Burnett et al. (1971) found fluences 2.5 times higher. Bogard et al. (1995), using the Eugster et al. (1970b) measurements of neutron capture on ^{157}Gd in the Norton County meteorite and the Lingenfelter et al. (1972) method of calculating σ_{eff}, found a neutron fluence of $11x10^{15}$ n/cm^2 in the Norton County meteorite, compared to the Eugster et al. (1970c) value of $6.3x10^{15}$ n/cm^2.

Similarly Lugmair and Marti (1971) using the thermal neutron fluence for samples from Apollo 11, 12 and 14 reported fluences 2 to 4 times too small. The Apollo 16 drill stem shows the largest neutron fluences yet observed, up to $9.9x10^{16}$ n/cm^2 (Russ, 1973). However, after normalisation, the largest fluence found so far is in the Luna 16 sample, a fluence of $4.6x10^{16}$ n/cm^2 (Curtis and Wasserburg, 1975).

In the 1970s the minimum fluence detectable was $3x10^{15}$ neutrons/cm^2, considered at the time the upper limit of the primordial thermal neutron flux (Eugster et al., 1970b). Recent measurements of neutron capture in gadolinium and samarium in meteorites shows a fluence of $9.0x10^{14}$ neutrons/cm^2 (Hidaka et al., 1997). Narrowing the constraints on the primordial thermal neutron fluence gives a hold on the magnitude of the irradiation by moderated secondary neutrons since the solar system was formed. Lowest limits of $2.6x10^{14}$ neutrons/cm^2 and $1.3x10^{14}$ neutrons/cm^2 can be detected in irradiated samarium and gadolinium standards (Hidaka et al., 1995).

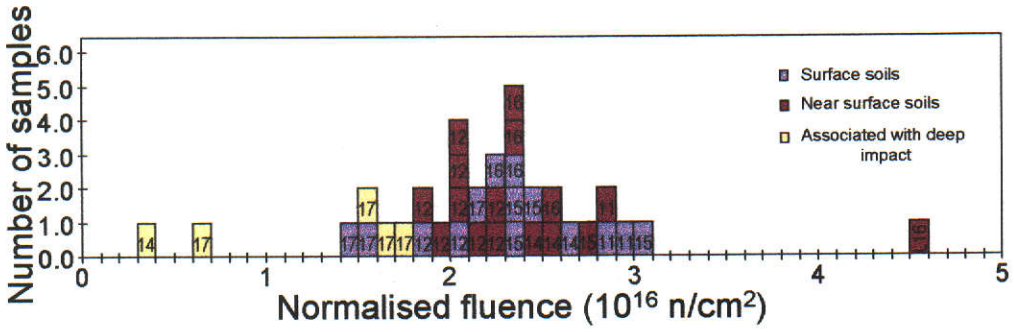

Figure 1-10 Fluences in lunar surface soils standardised to an arbitrary chemical soil composition (Curtis and Wasserburg, 1975).

Samples which come from different areas of the Moon, with different soil compositions, but with the same exposure history, can show a fluence twice as large if they were irradiated in soil of highland composition, compared to soil of basaltic composition. For a true comparison of fluences from different areas on the lunar surface Curtis and Wasserburg (1975) normalised all previously measured fluences to a soil with a standard composition where Σ_{eff} = 9.25x10^{-3} cm^2/g (Figure 1-10).

For these normalised samples the average fluence in the top 100 g/cm^2 of the soil is 2.3x10^{16} g/cm^2, indicating a well mixed surface layer, while samples from between 100 g/cm^2 to 500 g/cm^2 show an average fluence of 3.5x10^{16} n/cm^2. Samples from a lot deeper than the irradiated zone have fluences of less than 10^{16} n/cm^2 (Curtis and Wasserburg, 1975).

1.9 The neutron energy spectrum

A comparison of the magnitude of the changes caused by neutron capture in isotopes with differing resonance energies can describe the energy spectrum of the neutrons. A value ε is defined as the number of neutrons captured per atom of a particular isotope (Russ et al., 1971), where $\varepsilon=\langle\sigma\rangle$(cross section)$\psi$ (fluence). It is related to experimental quantities by:

$$\varepsilon_{Sm} = \frac{\left[\left(^{150}Sm/^{149}Sm\right)_{meas} - \left(^{150}Sm/^{149}Sm\right)_{terr}\right]}{\left[1+\left(^{150}Sm/^{149}Sm\right)_{meas}\right]}$$

Equation 1-8

where the subscripts meas and terr indicate measured and terrestrial values. Then $\varepsilon_{Sm}/\varepsilon_{Gd}$ is equal to the ratio of the average cross sections $<\sigma^{149}>/<\sigma^{157}>$, and is a measure of the neutron energy spectrum at a site. ^{157}Gd and ^{149}Sm have resonance cross sections at 0.0314 eV and 0.0973 eV respectively, so a "hardening" of the neutron energy spectrum will result in an increase in the ratio $\varepsilon_{Sm}/\varepsilon_{Gd}$.

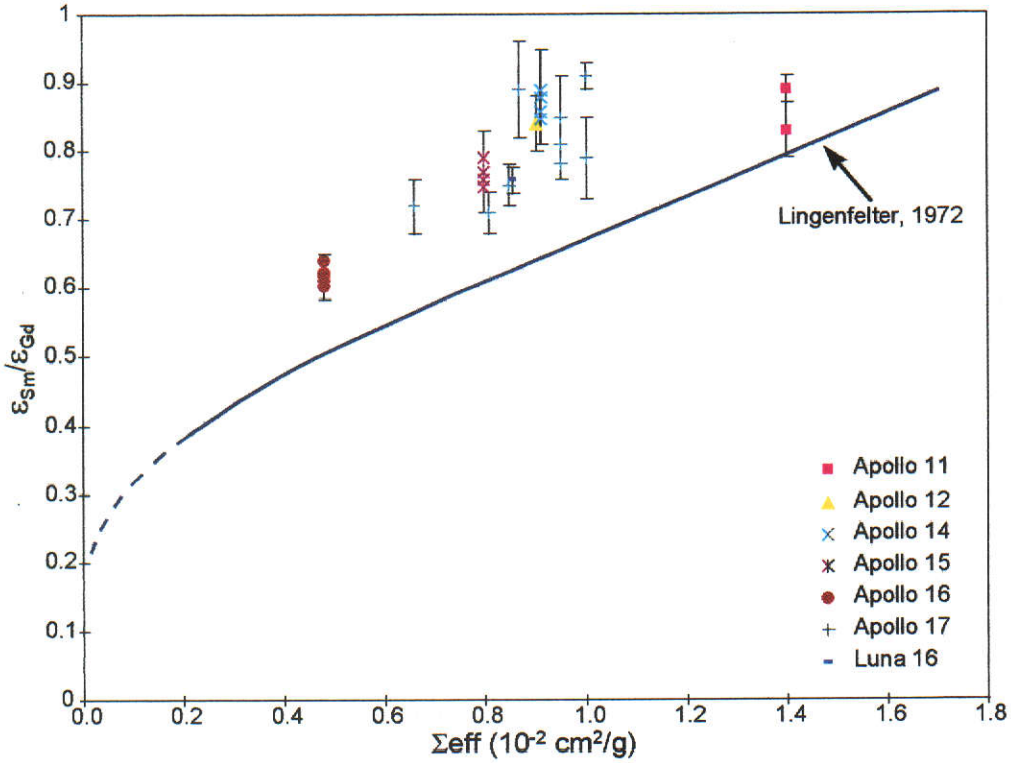

Figure 1-11 Variation of $\varepsilon_{Sm}/\varepsilon_{Gd}$ as a function of the macroscopic cross section Σ_{eff} compared to the Lingenfelter et al. predicted curve (adapted from Russ, 1972, 1973 and Russ et al., 1971, and Curtis and Wasserburg 1975, 1977b).

When $\varepsilon_{Sm}/\varepsilon_{Gd}$ is plotted against the macroscopic cross section Σ_{eff}, the measured values are about 20% greater than those predicted by

Lingenfelter et al. (1972), though still parallel to the predicted curve. This is observed in samples from Apollo 11, 12, 14, 15, 16 and 17 and Luna 16 (Russ et al., 1971 and 1972, Russ, 1972 and 1973, Curtis and Wasserburg, 1975 and 1977b) (Figure 1-11).

The Lunar Neutron Probe Experiment (LNPE) compared the total neutron flux to a depth of 400 g/cm^2 with the flux with energy greater than 0.5 eV at two depths. The ratio of *Total Neutron Density/Neutron Density >0.5 eV* is the same as that predicted by Lingenfelter et al. (1972) at 370 g/cm^2, but at 180 g/cm^2 the measured values are much lower (Table 1-8). This shows a shift in the energy spectrum with depth so that at 180 g/cm^2, near the peak, the Lingenfelter et al. (1972) calculations have too many low energy neutrons, so that the predicted ^{149}Sm and ^{157}Gd capture rates are too high, especially for gadolinium which is very sensitive to changes in the low energy fluence.

Table 1-8 Total Neutron Density/Neutron Density >0.5 eV measured in the Lunar Neutron Probe Experiment, compared to theoretical predictions by Lingenfelter et al. (1972) (Burnett and Woolum, 1974).

Depth g/cm^2	**LNPE Experiment**	**Theory**
180	2.11±0.16	2.7
370	2.9±0.3	2.9

However, from the Apollo 15, 16 and 17 deep drill stems, there is no evidence of a change of energy spectrum with depth (Russ et al., 1972, Russ, 1973 and Curtis and Wasserburg, 1975).

1.10 Mass fractionation in cadmium

Mass fractionation in cadmium has been observed before in meteorites (Rosman and De Laeter, 1976 and Rosman and De Laeter, 1988) but not in lunar samples. Positive fractionation in cadmium of 2.3‰ and 2.7‰ was found in the Brownfield H3 chondrite (Rosman and De Laeter, 1976) and in the Bishunpur LL3 chondrite (Rosman and De

Laeter, 1988), while negative fractionation of 2.1‰ was observed in the Semarkona LL3 chondrite (Rosman and De Laeter, 1988).

Isotopic mass fractionation in lunar soils has been found in oxygen, silicon (reference a), sulfur (b), potassium (c), and small effects seen in calcium (Russell et al., 1978). It has been suggested that the fractionation could be caused by ion sputtering of grain surfaces (d), micro-meteorite impact volatilisation (e) and separation by gravity (f). There is some disagreement as to whether the shift in isotopic ratios follows the Rayleigh distillation process (Humayun and Clayton, 1995; Esat and Williams, 1998). References (a) to (f) are listed in Table 1-9 and were quoted by Humayun and Clayton, 1995.

Table 1-9 References in the previous paragraph, quoted by Humayun and Clayton, 1995.

a	Epstein and Taylor, 1971; Taylor and Epstein, 1973; Clayton et al., 1974
b	Rees and Thode, 1972; Thode and Rees, 1976, 1979
c	Barnes et al., 1973; Garner et al., 1975; Church et al., 1976
d	Haff et al., 1977; Switkowski et al., 1977
e	Clayton et al., 1974; Housley, 1979
f	Haff et al., 1977; Housley, 1979

Cadmium, a volatile element, is likely to be isotopically fractionated in lunar materials. The discovery of fractionation in cadmium may cast a light on the causes of the effect.

An extra dimension on the neutron energy spectrum opens another window onto the mixing history of the lunar regolith and will also help to describe the neutron capture rates in different energy ranges so it is possible to convert the capture rate of one nucleus into another (Burnett and Woolum, 1974).

2. Chemistry

2.1 Introduction

The measurement of very small (ng) samples of cadmium, gadolinium and samarium using thermal ionisation mass spectrometry requires extensive chemical processing to achieve samples which are of sufficient chemical purity. This involves the complete digestion of the samples, followed by separation using ion exchange chemistry. The procedures for the separation and purification of cadmium are quite different from those used for the separation of the REE.

A major difficulty in measuring such small samples is contamination from reagents, resins and apparatus, procedures for minimising such contamination are described below. A particular problem was samarium contamination which was retained in the perfluoralkoxy (PFA) beakers even after extensive cleaning.

The procedures which were initially developed to dissolve and separate seven geochemical reference materials (GRMs) (Sands and Rosman, 1997, attached at Appendix I) for the measurement of the cadmium, gadolinium and samarium concentrations were modified for the measurement of the composition and concentration of the lunar samples.

All the sample processing is done in a laboratory with HEPA filtered air and laminar-flow clean air hoods (Section 2.6).

New, unused, 15 ml and 7.5 ml PFA Teflon beakers with screw top lids (Savillex Corporation, USA) were used for all lunar sample digestions, solution collections and evaporation. Used, but well cleaned, 15 ml and 7.5 ml beakers were used for the GRM samples. All beakers were numbered, dedicated either to composition or concentration measurements and a record kept of the use of each one.

2.2 Cadmium

2.2.1 Introduction

Cadmium is a chalcophile element so preferentially forms sulphides. The chemical behaviour is predictable, contamination during chemical processing is the main problem.

Table 2-1 The main chemical properties of cadmium.

Geochemical classification	Common stable form	Common stable ligands	Solubility
Chalcophile	Metal, sulphide	Cd^{2+}, $CdCl_x^y$	HCl, HNO_3

Table 2-2 Concentrations of cadmium

Levels in lunar samples	Lunar concentration compared to chondrites (Heiken et al., 1991),	Terrestrial abundance (crust)
30 - 500 ng/g 1 - 100 ng/g in rocks	soil/chondrite = ~0.1 rock/chondrites = ~0.01	~150 ng/g

Cd has eight isotopes whose abundances are listed in Table 2-3 and illustrated in Figure 2-1 and an atomic weight of 112.411±0.008 (IUPAC, 1986).

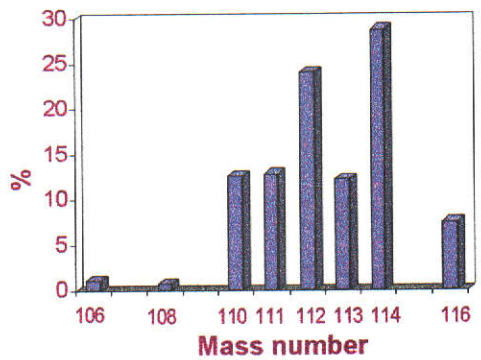

Figure 2-1 The abundances of the cadmium isotopes.

Table 2-3 The abundances of the cadmium isotopes (IUPAC, 1998).

Cadmium isotopes	Abundances (%)
106	1.25±0.02
108	0.89±0.01
110	12.49±0.06
111	12.80±0.04
112	24.13±0.07
113	12.22±0.04
114	28.73±0.14
116	7.49±0.06

Table 2-4 Isotopes isobaric with cadmium (% abundances)

Mass no.	Isobaric isotopes				
	Cd	**Pd**	**Sn**	**In**	**Ag**
102		1.0			
103					
104		11.0			
105		22.2			
106	1.2	27.3			
107					51.8
108	0.9	26.7			
109					48.2
110	12.4	11.8			
111	12.8				
112	24.0		1.0		
113	12.3			4.3	
114	28.8		0.65		
115			0.35	95.7	
116	7.6		14.4		
117			7.6		
118			24.1		
119			8.6		
120			32.8		
121					
122			4.7		
123					
124			5.8		

Isobaric isotopes interfere with cadmium isotope measurements during thermal ionisation mass spectrometry. The main isotopes which fall near

and between the cadmium isotopes are palladium, tin, indium and silver, (Tables 2-4 and 2-5), so the chemistry needs to completely remove these elements from the final cadmium sample.

Table 2-5 Average abundance on Moon of isobaric ions which interfere with cadmium (Heiken et al., 1991)

Pd	0.2 to 200 ng/g
Ag	1 to 100 ng/g
Sn	0.1 to 1 μg/g
In	0.1 to 100 ng/g

2.2.2 A historical review of cadmium separation chemistry

Anion and cation exchange has been successfully used to separate metals since before 1955.

Details of the amount of adsorption on anion exchange resins of each of the elements formed the basis for developing a suitable procedure to extract pure cadmium, with little contamination from palladium, silver, tin and indium. Published graphs included elements complexed in 0 to 12 M HCl (Kraus and Nelson, 1955), in 1M HF and 0 to 12 M HCl together (Nelson et al., 1960), in 0 to 20 M HF (Faris, 1960), and in 0 to 12 M HNO_3 (Buchanan and Faris, 1964).

For cation exchange resins graphs include elements complexed in 0 to 12 M HCl (Nelson et al., 1964), together with tables of equilibrium distribution coefficients (Distribution D_V = concentration held on the resin/concentration in solution) of elements complexed in HCl (Strelow, 1960) and in HNO_3 and H_2SO_4 (Strelow et al., 1965).

Table 2-6 Details of the elements removed from the columns at each stage of the cadmium separation procedure used in this work (from the references cited in Section 2.2.2). Elements with isotopes isobaric to cadmium are underlined.

Anion column (1)	Elements fully eluted	Elements partially eluted
⇓ **9 M HCl** **and** **3 M HCl** ⇒ ⇒ ⇒ ⇓ ⇓ ⇓	REE, all alkalis, alkali earths and group III elements, Al III, Ti III&IV, V IV&V, Cr III, Mn II, Fe II, Co II, Ni II, Ge IV, As III, Se IV, Zr IV, Rh III , Ag 1, In III, Te VI, Hf IV, Ta V, Ir III, Pb II, Th IV, U IV	Cr III, Cu II, W VI, Pa V
3 M HF:2 M HCl ⇒ ⇓	Fe III, Cu II, Ga III, Sn IV, Tl I	Cr VI, Rh III&IV, Ag I, In III, Sb III, Pb II
0.1 M HCl ⇒ ⇒ ⇓ ⇓	Fe III, Cu II, Zn II, Ga III, Se IV, Mo VI, Sb V, W VI, Pa V, U VI	Sc III, Ti III, V IV, Cr VI, In III, Sn IV, W VI, Re III, Pb II
1 M HNO_3 ⇒ ⇒	P, Cd II, Ir III ↙	Rh III, Sn IV, Pt IV, Hg II, Tl III, Pb II

↙
↙
⇓

Anion column (2) ⇓	Elements fully eluted	Elements partially eluted
0.1 M HCl⇒ ⇒ ⇒ ⇓	Fe III, Cu II, Zn II, Ga III, Se IV, Mo VI, Sb V, W VI, Pa V, U VI	Sc III, Ti III, V IV, Cr VI, In III, Sn IV, W VI, Re III, Pb II
1 M HNO_3⇒ ⇒	P, Cd II, Ir III ↙	

↙
↙
⇓

Cation column ⇓	Elements fully eluted	Elements partially eluted
0.5 M HCl ⇒ ⇒	Cd II, Sn IV	Pd II retained on column

Early procedures used for cadmium separation included two anion exchange columns where 0.5 M HCl, followed by 4 column volumes of 1 M HNO_3 removed both zinc and cadmium from the first column, and a second anion column where more zinc was removed with 0.01 M HCl, then cadmium with four column volumes of 1 M HNO_3 (Rosman and De

Laeter, 1974a and b). Later modifications included using 0.01 M HCl on the first anion column, instead of on the second, to remove the zinc (Rosman and De Laeter, 1975).

A cation exchange column, added for samples with substantial tin or palladium, was first washed with 0.1 M HCl, then 0.5 M HCl which eluted the cadmium, separating it from the tin and palladium (Rosman and De Laeter, 1978).

2.2.3 Procedures to chemically separate cadmium, developed for this work

The procedures described above have been further modified for this work and are summarised in Tables 2-6 and 2-7 on page 41. Problems with silver contamination on the mass spectrometer have been reduced by initially washing the anion column with 9 M and 3 M HCl. To remove tin more effectively an acid mix of 3 M HF with 2 M HCl was included.

Initially one anion and one cation exchange column were used, for the separation of the GRMs, but for the lunar samples a second anion column allowed larger cuts to be collected, with better purity and increased efficiency. Details of the cadmium chemistry are in Appendix C.

2.2.4 Digestion procedures

A progression of HF, HNO_3, $HClO_4$ and HCl is generally used to digest rock and soil samples. In this work HF, HNO_3 and HCl were used in turn, with a microwave oven to assist the dissolution. Details of the complete procedure are listed in Appendix B.

For concentration measurements of the GRM the tracers enriched in $^{106 \text{ and } 111}Cd$, ^{152}Gd, and ^{147}Sm were added at the start of the digestion process, whereas for the lunar samples the tracers were added to 5% of the sample, at the end of the digestion procedure.

After digestion the sample was separated in a six stage ion exchange process, three for cadmium and four for the REE.

2.2.4.1 Residues

The digestion procedure left a fine carbon residue, of negligible weight compared to the sample, in two of the GRMs (MAG-1 and PCC-1), and some fine chips, again of negligible weight, in several of the lunar samples (detailed in Table 5-7 in Chapter 5, Section 5.3).

2.2.5 Separation of cadmium

Chemical separation of cadmium for the seven GRMs included one anion and one cation column, for the lunar samples two anion and one cation column. The REE and the other matrix elements were eluted from the first anion exchange column in the 9 M HCl and 3 M HCl.

The procedure is summarised in Table 2-7 and described in detail in Appendix C.

2.2.5.1 Anion exchange, first column

A detailed description of the procedures are described in Appendix C, Section 1.

Columns are LDPE transfer pipettes (Samco 202-20S) with force-fitted PE frits. The tip was trimmed close to the frit and the top of the squeeze bulb cut off to form the reservoir. The anion exchange resin Bio-Rad AG1x8, 100 - 200 mesh was washed into the column in Milli-Q water (MQW), to a height of 4 cm, and volume of 1.5 ml (the column's external dimensions are 8 mm x 9 cm). The reservoir above the resin is 6 ml (Figure 2-2).

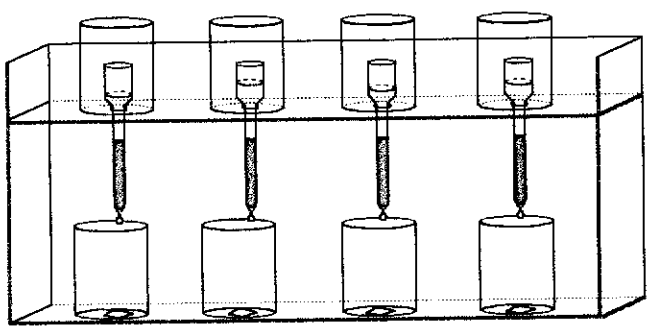

Figure 2-2 The anion/cation exchange columns used for the separation of cadmium.

The resin was first cleaned, to remove rare earths, silver, tin, indium or cadmium, the previously digested sample was added, a small amount at a time, dissolved in <1 ml 9 M HCl. The beaker and inside of the top of the column were rinsed with a further 1 ml 9 M HCl.

Various concentrations and volumes of HCl, HF and HNO_3, detailed in Appendix C, were added to the anion column. The REE and matrix elements were collected from the column during the first stage, evaporated and put aside for the rare earth element separation procedures. The cadmium was washed off in 1 M HNO_3, evaporated to dryness, and passed to the second anion column (one anion column only was used for the GRMs).

2.2.5.2 Anion exchange, second column

A detailed description of the procedures are described in Appendix C, Section 2.

The same type of column was used for the second anion column as for the first, but the resin was washed in to a height of only 1 cm and volume of 0.4 ml. The reservoir above the resin is 7 ml.

The resin was cleaned, then the sample from the first anion column dissolved in ¼ ml 3 M HCl and transferred to the column. The beaker and column were rinsed with a further ¼ ml 3 M HCl. Tin ions were washed off first in 0.1 M HCl, then the cadmium in 1 M HNO_3. The cadmium was evaporated to dryness and passed to the cation column.

2.2.5.3 Cation exchange

A detailed description of the procedures are described in Appendix C, Section 3.

The same type of column was used as for the anion exchange (Figure 2-2). Resin was washed into the column to a height of 3 cm, and volume of 1 ml. The reservoir above the resin is 6.5 ml. The cation exchange resin used is Bio-Rad AG50x8, 200 - 400 mesh.

Table 2-7 Summary of the cadmium and REE separation chemistry (Mass spec is short for mass spectrometry).

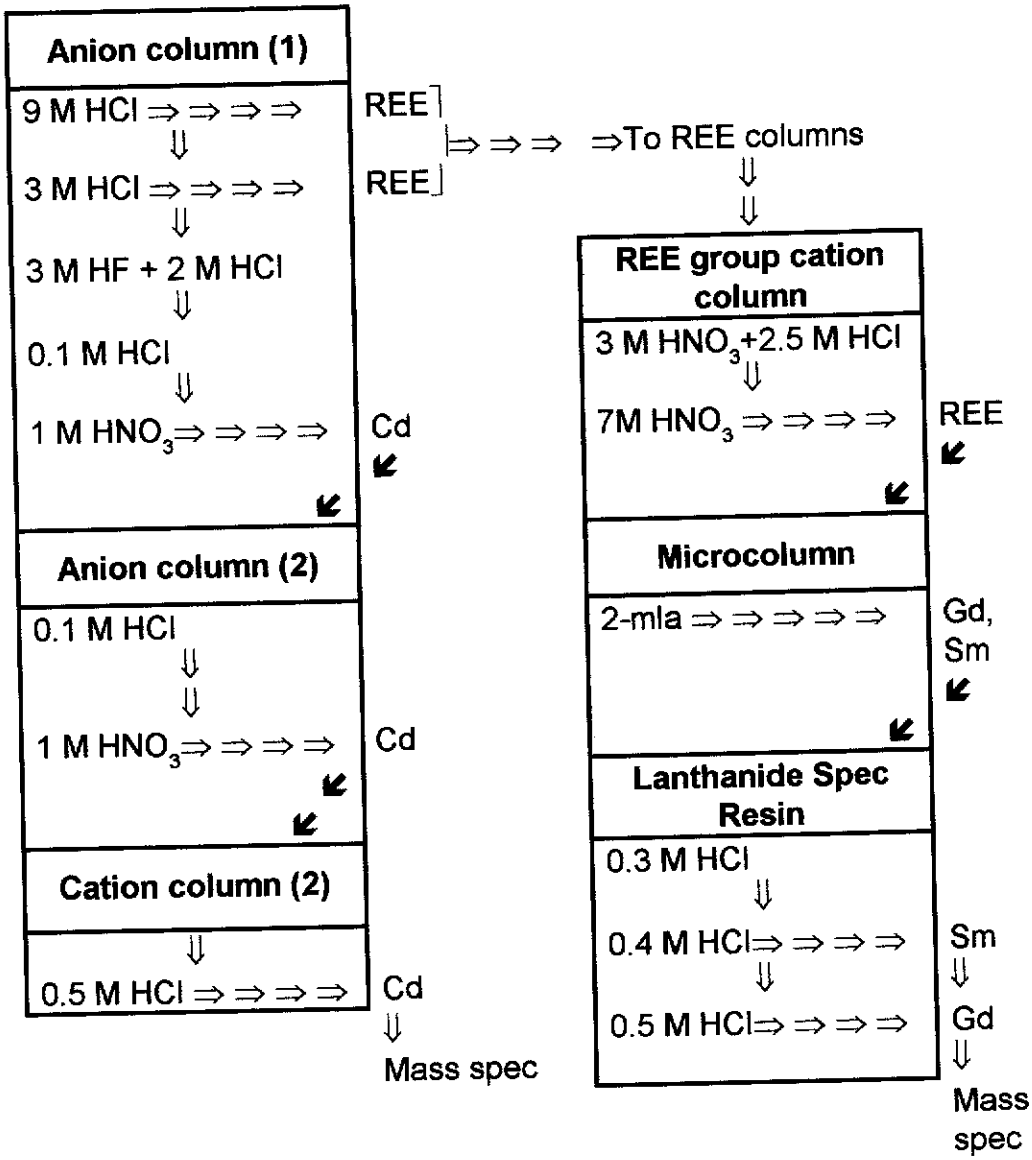

The cation resin was cleaned and the sample from the second anion column was dissolved in 1 ml 0.5 M HCl and transferred to the column. The beaker and column were rinsed with a further 1 ml 0.5 M HCl. Cadmium was eluted immediately with 10 ml 0.5 M HCl. When the cadmium has been collected, 10 μL H_3PO_4 was added, then the sample was evaporated. On evaporation the sample concentrates in the residual H_3PO_4 as it has a higher boiling point than the HCl. This allows the sample to be identified in the beaker after evaporation.

2.2.6 Efficiency

The overall extraction efficiency was 96% for cadmium in the three stage ion exchange process used for the lunar samples, determined by Isotope Dilution Mass Spectrometry (IDMS). The use of the three ion exchange columns allowed larger cuts to be collected than with two columns, with no increase in contamination and with improved efficiency. The two column separation procedure used for the GRMs, yielded 85% efficiency.

Several observations have been made to verify the behaviour of cadmium in anion and cation exchange columns. A Varian Spectra AA-10 Atomic Absorption Spectrometer was used to measure the efficiency of cadmium standards washed from the anion (Tables 2-8 and 2-9) and cation (Table 2-10) columns with various concentrations and acids.

Table 2-8 The elution of cadmium standard from an anion column, measured by an Atomic Absorption Spectrometer (±12%).

Acid added to column	**Observations**
6 ml 3 M HCl	No Cd eluted
12 ml 3 M HF + 2 M HCl	No Cd eluted
24 ml 0.1 M HCl	No Cd eluted
6 ml 1 M HNO_3	1.6 ml No Cd eluted 1.7 ml 75% Cd eluted 1.6 ml 25% Cd eluted

Table 2-8 shows that no cadmium was detected, within uncertainties, when the anion column was washed with 3 M HCl, the acid mix (3 M HF + 2 M HCl) or 0.1 M HCl. Cadmium was washed from the column in 1 M HNO_3. The first 1.6 ml 1 M HNO_3 contained no cadmium, though in the next two cuts cadmium was eluted in proportions of 3 to 1. The final 1.5 ml was not collected at this time, but it was found, during the separation of cadmium from BCR-1, that approximately 0.1% of cadmium was eluted in this stage.

The GRMs were separated with one anion column and just 6 ml 1 M HNO_3 was used to remove the cadmium, so as to avoid collecting tin in a

larger volume of 1M HNO_3. When the second anion column was included for the lunar samples 9-10 ml 1M HNO_3 was used to collect as much cadmium as possible in the first anion column, and any tin was extracted in the second anion column.

More precise measurements on the VG 354 mass spectrometer showed that the loss of cadmium standard from the two anion exchange columns was only 0.3% in the 9 M HCl, 3 M HCl, 0.1 M HCl and acid mix stages (Table 2-9).

Table 2-9 The loss of cadmium standard from the anion exchange columns.

Anion Column (1)	**Cadmium lost**
9 M HCl	0.09%
3 M HCl	
3 M HF:2 M HCl	0.2%
0.1 M HCl	none detected
Anion Column (2)	
0.1 M HCl	0.3%

Table 2-10 The elution of cadmium standard from five cation columns by different concentrations of HCl, measured by an Atomic Absorption Spectrometer (±12%).

6 ml of each acid	**Observations**
0.3 M HCl	56% of Cd eluted
0.4 M HCl	75% of Cd eluted
0.5 M HCl	80% of Cd eluted
0.7 M HCl	82% of Cd eluted
1 M HCl	88% of Cd eluted

Five separate cation columns were used to observe how cadmium standard was washed the columns in 0.3 M to 1 M HCl. 6 ml HCl was used in each case and the concentration of cadmium eluted measured by an Atomic Absorption Spectrometer. It was found that increasing the concentration of HCl from 0.3 M HCl to 1 M HCl increased the proportion of cadmium eluted from 56% to 88% (Table 2-10). To minimise the

elution of tin with the cadmium it was decided to use 0.5 M HCl to wash the cadmium from the cation column.

The results obtained here do not fully correspond to the Distribution Coefficients for cation exchange tabulated in Strelow (1960).

2.3 Gadolinium and samarium

2.3.1 Introduction

The lanthanides, or rare earth elements, have such similar electronic configurations, resulting in very similar chemical properties and compounds, that they are very hard to separate. After lanthanum the energy of the 4f orbital falls below that of the 5d, so electrons are added to the inner shell, so the outer shell is $6s^2$ for all the REE (Table 2-11).

The reduction in radius with increase in atomic number (Figure 2-3) is responsible for the small variations in properties which allow separation with some difficulty. Several properties follow this pattern, basicity and ease of oxidation decrease with decrease in radius, ionisation energy increases.

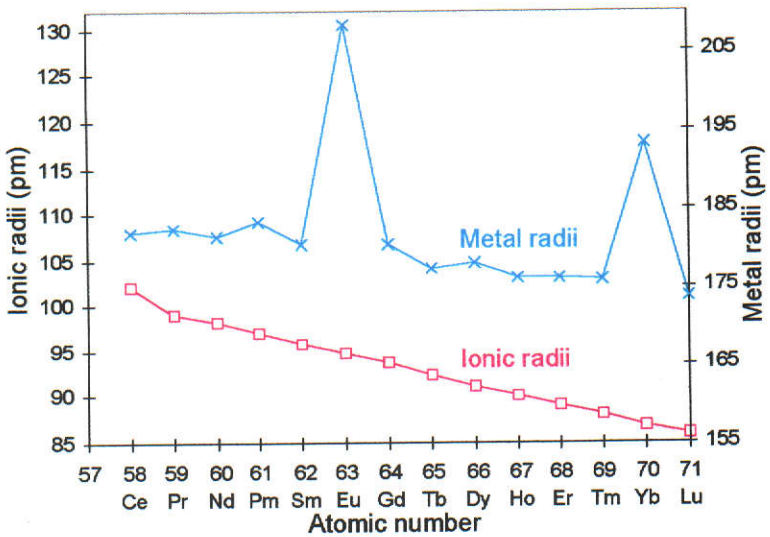

Figure 2-3 Variation of metal and ionic radii of the REE (adapted from Greenwood and Earnshaw, 1984).

Table 2-11 Rare earth chemistry (Moeller, 1963)

Atomic number	Element	Ground state electronic configurations	Observed oxidation states		
			+2	+3	+4
57	Lanthanum	$5d^1 6s^2$		La^{3+}	
58	Cerium	$4f^1 5d^1 6s^2$	$CeCl_2$	Ce^{3+}	Ce^{4+}
59	Praseodymium	$4f^3 .... 6s^2$		Pr^{3+}	PrO_2, Na_2PrF_6
60	Neodymium	$4f^4 .... 6s^2$	NdI_2	Nd^{3+}	Cs_3NdF_7
61	Promethium	$4f^5 .... 6s^2$		Pm^{3+}	
62	Samarium	$4f^6 .... 6s^2$	Sm^{2+}	Sm^{3+}	
63	Europium	$4f^7 .... 6s^2$	Eu^{2+}	Eu^{3+}	
64	Gadolinium	$4f^7 5d^1 6s^2$		Gd^{3+}	
65	Terbium	$4f^9 .... 6s^2$		Tb^{3+}	TbO_2, TbF_4
66	Dysprosium	$4f^{10} ... 6s^2$		Dy^{3+}	Cs_3DyF_7
67	Holmium	$4f^{11} ... 6s^2$		Ho^{3+}	
68	Erbium	$4f^{12} ... 6s^2$		Er^{3+}	
69	Thulium	$4f^{13} ... 6s^2$	TmI_2	Tm^{3+}	
70	Ytterbium	$4f^{14} ... 6s^2$	Yb^{2+}	Yb^{3+}	
71	Lutetium	$4f^{14} 5d^1 6s^2$		Lu^{3+}	

Table 2-12 Geochemistry of the REE samarium and gadolinium (Mason and Moore, 1982).

Element	Geochemical classification	Common stable form	Solvent
Sm	lithophile (silicates)	Sm^{+3} (oxide)	HCl , HNO_3, H_2SO_4
Gd	lithophile (silicates)	Gd^{+3} (oxide)	HCl , HNO_3, H_2SO_4

The rare earths are very reactive metals, reactivity depending on the metallic radius, with Eu the most reactive. Except for Ce, in aqueous solutions the +3 state dominates, thus there is no correlation between electronic states and oxidation states. The rare earths are found with nearly all known anionic species (OH^-, CO_3^{-2}, SO_4^{-2}, $C_2O_4^{-2}$, NO_{-3}), the

compounds turn to oxides when heated. Except for $\{Ln(H_2O)_n\}^{3+}$, there are few complex species.

Table 2-13 Properties of the REE (Greenwood and Earnshaw, 1984), ionisation energy from Moeller (1963), chondrites are adapted by Heiken (1991) from Haskin et al., 1968, Nakamura, 1974, Masuda et al., 1973, Evensen et al., 1978.

		Ionisation energy (eV)	**MP (°C)**	**BP (°C)**	**Concentration in chondrites (ppm)**
	La				0.319 ± 0.012
58	Ce	5.65	804	3470	0.836 ± 0.043
59	Pr	5.42	935	3020	0.113 ± 0.007
60	Nd	5.49	1024	3027	0.602 ± 0.019
61	Pm	5.55			
62	Sm	5.70	1072	1800	0.186 ± 0.005
63	Eu	5.68	826	1439	0.0724 ± 0.0035
64	Gd	6.16	1312	3000	0.259 ± 0.012
65	Tb	5.85	1356	2800	0.0483 ± 0.0022
66	Dy	5.80	1407	2600	0.324 ± 0.013
67	Ho	6.19	1461	2600	0.0725 ± 0.0032
68	Er	6.38	1497	2900	0.21 ± 0.011
69	Tm	6.22	1545	1727	0.0315 ± 0.0013
70	Yb	6.25	824	1427	0.208 ± 0.009
71	Lu	6.41	1652	3327	0.0328 ± 0.0013

The concentration of the REE in the Earth's crust and in three lunar samples of different composition are compared to the REE in chondrites (Table 2-13, Figures 2-4 and 2-5). It can be seen that in KREEP the REE concentration is about ten times higher than in the Earth's crust, in the Apollo 14 basalts the same and in the Highland material about 10 times lower.

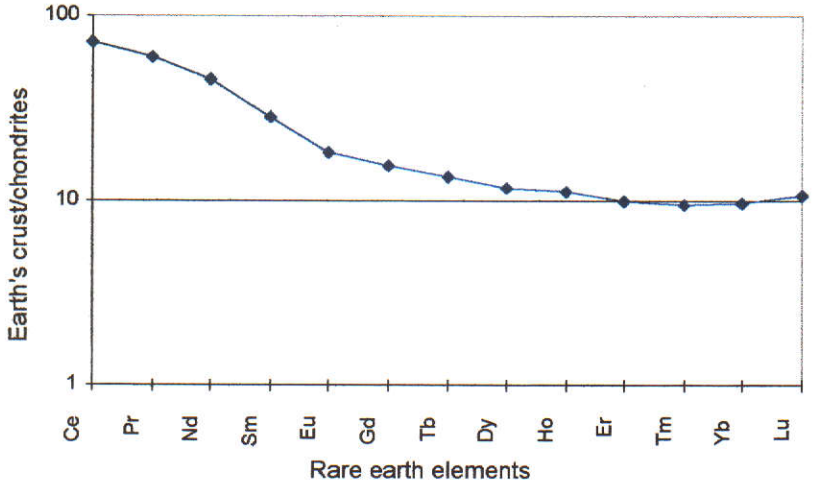

Figure 2-4 Concentration of REE in the Earth's crust (Wedepohl, 1995) compared to REE in chondrites (Heiken et al., 1991).

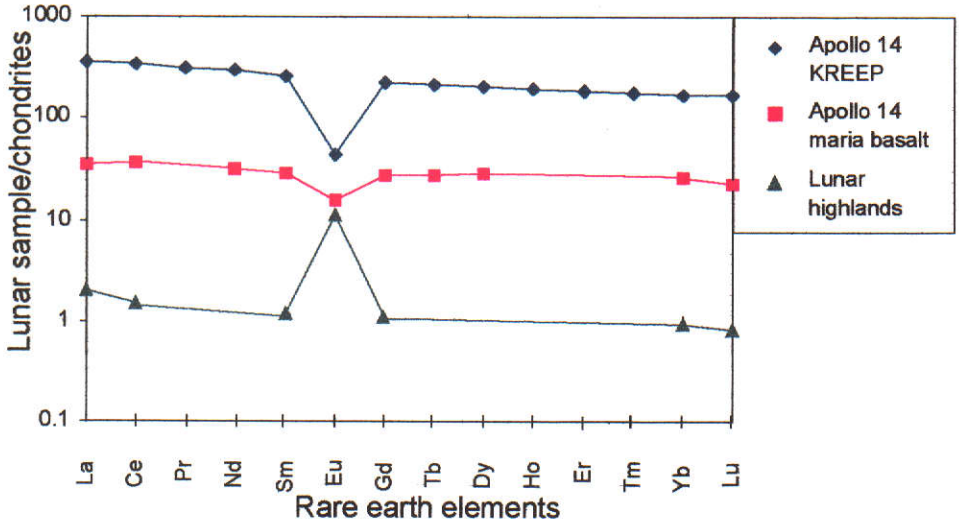

Figure 2-5 Concentration of REE in lunar samples, compared to chondrites. Data from Heiken (1991).

Gadolinium and samarium have mass numbers 157.25±3 and 150.36±3 (Commission of Atomic Weights and Isotopic Abundances, 1986) $_{64}$Gd and $_{62}$Sm have seven isotopes each and the isotopic abundances shown in Table 2-14 and Figure 2-6.

Table 2-14 The abundances of the gadolinium and samarium isotopes (IUPAC, 1998)

Gd isotopes	Abundance (%)	Sm isotopes	Abundance (%)
152	0.2029±0.0004	**144**	3.0734±0.0009
154	2.1809±0.0004	**147**	14.9934±0.0018
155	14.7998±0.0017	**148**	11.2406±0.0015
156	20.4664±0.0006	**149**	13.8189±0.0018
157	15.6518±0.0009	**150**	7.3796±0.0014
158	24.8347±0.0016	**152**	26.7421±0.0066
160	21.8635±0.0007	**154**	22.7520±0.0068

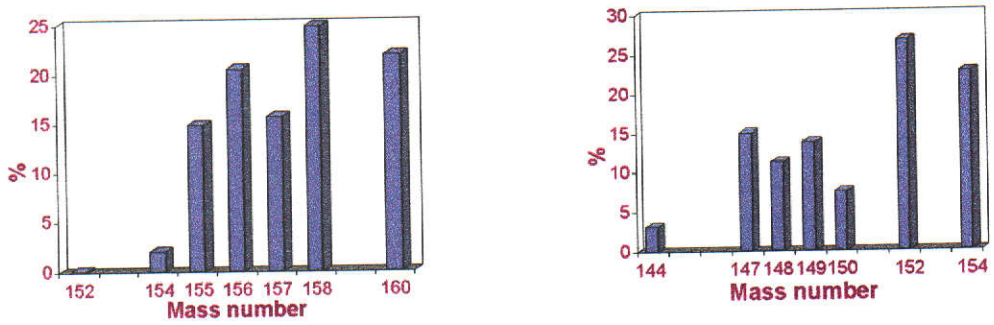

Figure 2-6 The abundances of the gadolinium and samarium isotopes.

Isobaric isotopes which may interfere with gadolinium and samarium isotope measurements during thermal ionisation mass spectrometry are listed in Table 2-15. The chemistry needs to completely remove these elements and not introduce any external contamination during any of the procedures.

Table 2-15 Isobaric isotopes which might interfere with gadolinium or samarium metal (%).

Mass no.	Gd	Sm	SmO	Nd/NdO	CeO	Eu	BaO	BaF	Dy	Other
142				27.1						
143				12.2						
144		3.1		23.9						
145				8.3						
146				17.2			0.10			
147		15.0								
148		11.2		5.7			0.1			
149		13.8						0.10		CsO
150		7.4		5.6			2.4			
151						47.8	6.5	0.1		
152	0.20	26.7			0.19		7.8			
153						52.2	11.2	2.4		
154	2.2	22.8			0.26		71.9	6.5		
155	14.9							7.8		LaO
156	20.6				88.5			11.2	0.06	
157	15.7							71.9		PrO
158	24.7			27.1	11.1				0.10	
159				12.2						Tb
160	21.7		3.1	23.9					2.3	
161				8.3					18.9	
162				17.2					25.5	
163			15.0						24.9	
164			11.2	5.7					28.2	
165			13.8							
166			7.4	5.6						
167										
168			26.7							
169										
170			22.8							

2.3.2 Historical review of the separation chemistry for the rare earth elements

The difficulty of REE separation means that two, or sometimes three, procedures are required, first to separate the rare earths as a group from other elements, and then to separate the individual rare earths from each other. Anion or cation exchange can be used, though anion exchange requires careful control of pH and large elution volumes, so cation

exchange is more commonly used to separate rare earths as a group (Croudace and Marshall, 1991).

2.3.3 Separating the rare earth elements as a group using a cation exchange resin

Resin is normally a copolymer of divinyl benzene and polystyrene with attached quaternary ammonium or sulfonic acid groups (Croudace and Marshall, 1991). Several methods of separation of the rare earth group of elements have been described using Bio-Rad AG 50W-X8 resin, 100-200 mesh resin and various concentrations of HCl and HNO_3 (Eugster et al., 1970b, Lugmair and Marti, 1971, Crock et al., 1984, Crock et al., 1986, Sullivan, 1988 and Croudace and Marshall, 1991).

Graded concentrations of HCl or HNO_3 gives complete recovery of the REE, though the use of HCl results in a tail containing the lighter mass REE (Crock et al., 1984). A combination of graded HCl, followed by graded HNO_3 successfully extracted the REE, with no tail (Crock et al., 1986). An oxalic-nitric acid mixture, used to complex Fe, Ti and Al (Sullivan, 1988), results in their early removal from the column in graded HNO_3, so that they are not removed with the REE. This method uses about 60 ml of acid, in comparison to the over 200 ml used in the earlier procedures.

Croudace and Marshall (1991), with a 15 cm x 1 cm column of resin, used an acid mix of 3 parts 3 M HNO_3 combined with 1 part 2.5 M HCl. 60 ml of the acid mix used as eluent removes all the matrix elements, including Fe, from the column. The rare earths are then eluted with 60 ml 7M HNO_3. A greater column length or reduced acid concentration gives a wider separation between the REE and the matrix elements.

A modification of this last procedure was used in this work.

2.3.4 Separating individual rare earth elements

There are two main procedures for the separation of the individual REE, High Performance Liquid Chromatography (HPLC), which removes the heavy REE off the column first, and di(2-ethylhexyl)orthophosphoric acid (HDEHP), which takes the light REE off first.

2.3.4.1 High Performance Liquid Chromatography (HPLC)

Initially HPLC was used for the separation of organic materials, but its use was extended to the separation of metal ions, (Elchuk and Cassidy, 1979) using strong acid, small particle, styrene divinyl benzene ion exchange resins. The best complexing agent for the REE is methyl lactic acid (also called 2-mla; α-hydroxy-isobutyric acid; or α-HIBA, with the chemical formula $(CH_3)_2C(OH)CO_2H$).

The distribution of the REE between the ion exchange sites on the resin and the mobile phase is determined by the affinity of the REE for the methyl lactic acid. The relative strength of the complexes is determined by the ionic radii of the REE (seen in Figure 2-3), the ions with smaller radii have the highest affinity for methyl lactic acid so the heavier REE remain in the mobile phase and are washed off the column first. The REE are trivalent, but the complexes are less positive, so changing the concentration of the methyl lactic acid affects the distribution of the REE between the resin and the mobile phase. With increased acidity the H+ competes with REE for ion exchange sites so more are in the mobile phase (Sullivan, 1988). So the separation of the peaks is easily controlled, reducing the concentration of the methyl lactic acid spreads the peaks, and increasing acidity puts more into the mobile phase.

The HPLC method for the separation of small samples of the REE is frequently used (Eugster et al., 1970b, Lugmair and Marti, 1971, Fletcher, 1982 and Sullivan, 1988), resulting in good resolution and separation of peaks. The REE are separated with 0.2 M methyl lactic acid at pH 4.10, and at a pressure of 0.14 kg/cm^2 (Eugster et al., 1970b). A lower, or higher pH value has been used (Lugmair and Marti, 1971, Lugmair et al., 1975, Maas and McCulloch, 1990, Hidaka et al., 1995), depending on the equipment, the separation required or the rare earths to be isolated.

2.3.4.2 HDEHP, reverse phase partition

HDEHP is di(2-ethylhexyl)orthophosphoric acid, with the chemical formula ($\{CH_3(CH_2)_3CH(C_2H_5)CH_2O\}_2P(O)OH$). In reverse phase partition the resin can be re-used after regenerating with 6 M HCl, unlike the cation resin used with methyl lactic acid. Various resins (Kel-F, Corvic, Cellulose powder) and various eluting acids are used. Coated resins have been used for some time for the separation of REE (Kiss, 1987, Fidelis and Siekierski, 1965, Sochacka and Siekierski, 1964, Siekierski and Sochacka, 1964, Pierce and Hobbs, 1963, Winchester, 1963, Cerrai and Testa, 1963, Pierce and Peck, 1962a and b, Peppard et al., 1957). Problems can be experienced with air pockets when coating the resin with acetone and HDEHP and the preparation takes some time. The column is conditioned in 0.05 M to 0.1 M HCl before use, and increasing molarity HCl is used to elute the REE from La (0.11 M HCl) to Lu (4.0 M HCl) (Kiss, 1987).

Cerium contamination has been reported, with interference on the mass spectrometer at ^{142}Nd (Maas, no date recorded).

The recently developed Eichrom Lanthanide Specific, 50-100 μm bead size, dedicated to the separation of the REE, requires no special preparation before use. The lighter to heavier rare earths are extracted using increasing concentrations of HCl. Cerium oxide contamination at masses 152, 154, 156 and 158 is a major problem for the measurement of ^{152}Sm, ^{154}Sm and ^{152}Gd, ^{154}Gd, ^{156}Gd and ^{158}Gd (personal observation).

2.3.5 Quantitative detection of the rare earth elements

The indicator Chlorophosphonazo, developed for the photometric determination of uranium (Nemodruk et al., 1961), is very satisfactory for detecting the REE in acid media. A 0.025% aqueous solution, initially a deep pink when metal free, becomes a stable blue-green in the presence of the REE, in a methyl lactic acid or HCl medium. The colour ranges from deep pink through a range of transition shades including dark mauve, deep blue and bluish green (a blank was kept for comparison).

The best sensitivity is for 1 to 2 ppm of gadolinium in an acid medium.

2.4 Separation of the rare earth elements in this work

A detailed description of the chemical procedures used for the separation of the REE is in Appendix D.

After digestion (Section 2.2.4 and Appendix B) the REE in the GRMs were separated in a three stage ion exchange procedure, while four stages were used for the lunar samples. As gadolinium and samarium were measured on the thermal ionisation mass spectrometer it is particularly important to separate them well and to ensure no contamination with interfering ions.

The four ion exchange stages were:

- The REE and the matrix elements were washed from the first anion column, used for cadmium separation (Section 2.2.5.1), with concentrated 9 M and 3 M HCl.
- The group of REE was separated from the matrix elements using a modification of the procedure described by Croudace and Marshall (1991).
- Gadolinium and samarium were separated by HPLC (Eugster et al., 1970b). Problems were experienced with ammonium chloride in the sample (due to HCl in the air from poor ventilation in the laboratory) and with dysprosium interfering with gadolinium. As a result an extra ion exchange procedure was added for the separation of the lunar materials.
- The final separation stage uses an HDEHP style ion exchange with Eichrom Lanspec resin.

The possibility was considered of cutting out the HPLC stage and using only the Lanspec resin this was rejected, however, because of massive cerium oxide contamination in the latter. HPLC was retained as the heavier REE wash off first and the cerium was left on the column, so no cerium was passed on to the Lanspec resin column.

Another advantage of using the two final ion exchange columns is that the lighter REE were extracted first from the Lanspec resin column so the

heavier dysprosium remained on the column and does not interfere with gadolinium.

2.4.1 Anion exchange

Described in Section 2.2.5.1 above in cadmium chemistry and in Appendix C, Section 1.

2.4.2 Cation exchange, group separation

The chemistry is described in detail in Appendix D, Section 2.

A Pharmacia RediFrac fraction collector and the metal indicator Chlorophosphonazo were used in the initial development of these procedures. A mix of elements (listed in Table 2-16) was prepared and used to observe how various matrix elements and the REE were washed from the columns.

Table 2-16 A mix of standards used to test the separation of the REE group from the matrix elements, prepared from powdered standards and from already mixed standards of various concentrations, mixed to the proportions shown (%).

Sn	Mg	Fe	Ti	Ca	Al	Cd	Gd	Pd
3	19	17.5	9	19.5	32	0.02	0.09	0.0004

The small samples and the importance of minimum contamination required a reduction in the volume of resin and acids used in this work compared to those used in Croudace and Marshall (1991).

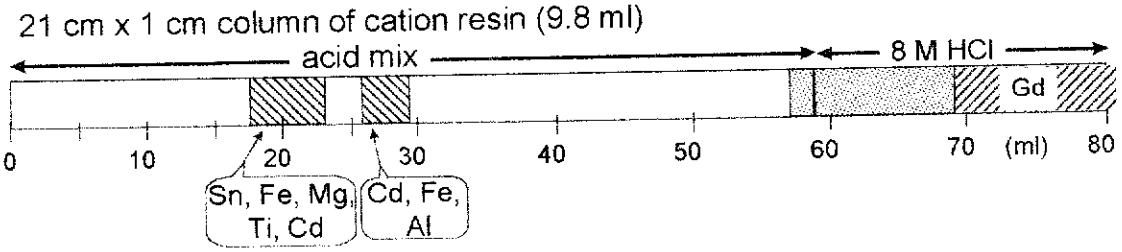

Figure 2-7 In 9.8 ml resin, 60 ml of acid mix wash off the matrix elements, which were well separated from the gadolinium. Gadolinium was partly eluted by 20 ml 8 M HCl. The striped area is of higher concentration than the dots.

Following the resin and acid volumes used by Croudace and Marshall (1991) Figure 2-7 shows that the matrix elements were fully removed in 60 ml of the acid mix (3 parts 3 M HNO_3 combined with 1 part 2.5 M HCl), whereas gadolinium requires nearly 20 ml of 8 M HCl to start moving off the column.

Figure 2-8 shows a reduced volume of 1.37 ml of resin in a 15 cm x 0.5 cm column. The matrix elements were washed off in 9 ml of the acid mix, with a good separation from gadolinium. However, gadolinium was not fully washed off with 20 ml of 8 M HCl.

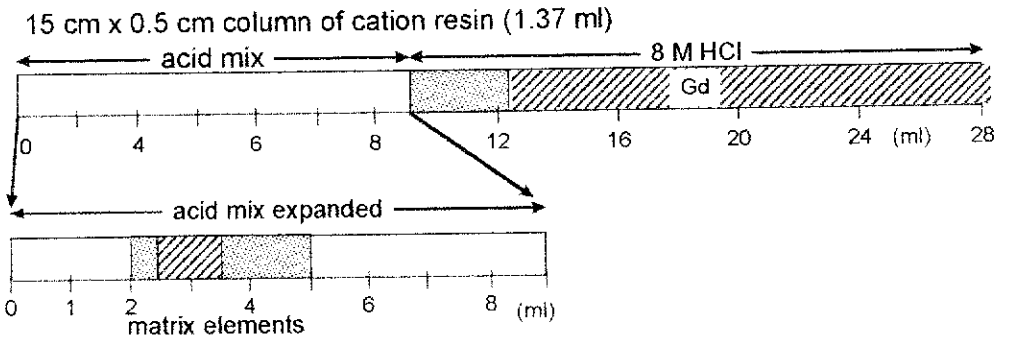

Figure 2-8 In 1.4 ml resin, 9 ml of the acid mix removed the matrix elements, whereas gadolinium was only partially eluted by 20 ml 8 M HCl. The striped area is of higher concentration than the dots.

Figure 2-9 uses the same size column and the same volume of resin and acid mix as in Figure 2-8, gadolinium was removed in only 6 ml of 7 M HNO_3. Samarium is washed off the columns before gadolinium.

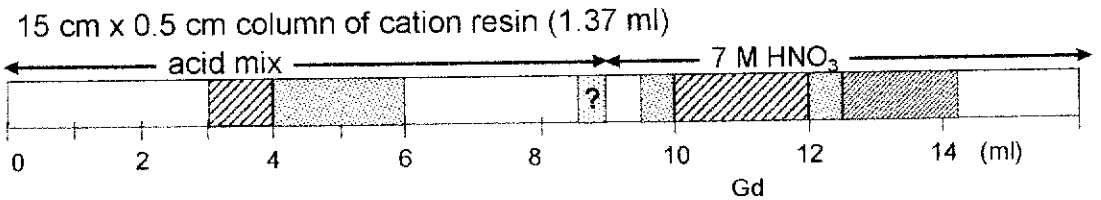

Figure 2-9 In a 15 cm x 0.5 cm column with 1.4 ml resin 9 ml of the acid mix removes the matrix elements then gadolinium was fully eluted by 6 ml 7 M HNO_3. The striped area is of higher concentration than the dots.

The volumes of resin and acids used in this work are about 14% of those used by Croudace and Marshall (1991). Details of the chemistry are in Appendix D, Section 2.

The columns are made from LDPE transfer pipettes of outside diameter of 5 mm and length 16.5 cm, with force fitted PE frits. The tip was trimmed close to the frit and the top of the squeeze bulb cut off to form a 3 ml reservoir. The resin bed from the frit to just below the bed of the reservoir is 15 cm long, with a volume of 1.8 ml (Figure 2-10).

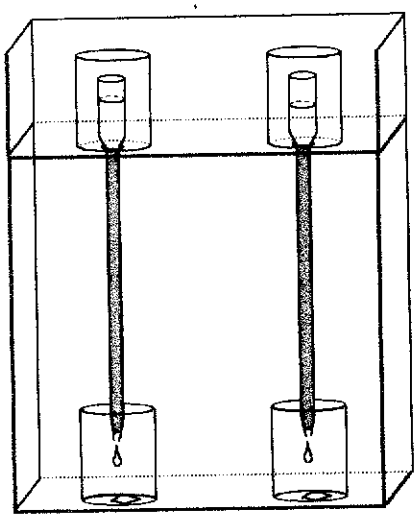

Figure 2-10 The ion exchange columns used for the separation of the rare earth group.

The cation resin Bio-Rad AG50-x8 with 200 - 400 mesh was loaded into a MQW filled column, to the top of the cone. Care has to be taken that there are no bubbles trapped by the resin, a problem with such a thin and relatively long column. After the resin has been cleaned the sample was dissolved in ½ ml of acid mix and transferred to the column. The acid mix and 7 M HNO_3, separate the matrix elements from the REE.

2.4.3 Separation of gadolinium and samarium with HPLC

This procedure is described in detail in Appendix D, Section 3.

The method of separation with HPLC described by Eugster et al. (1970b) and Fletcher (1982) was followed using 0.2 M methyl lactic acid with a pH of 4.3 (pH 4.6 for the GRMs), and with the Bio-Rad AG 50x8

200 - 400 mesh cation exchange resin. The resin was pre-cleaned in bulk, stored in MQW, then again pre-cleaned in the microcolumn, described in Appendix D, Section 3.

Vycor columns 21 cm x 1.9 mm external diameter, with Teflon reservoir and base, were fitted into a frame (Figure 2-11). A 0.5 μm MF-Millipore cellulose acetate membrane filter, 13 mm in diameter, supports the resin, fitted in the Teflon base piece, with the Vycor column fitting tightly on to it.

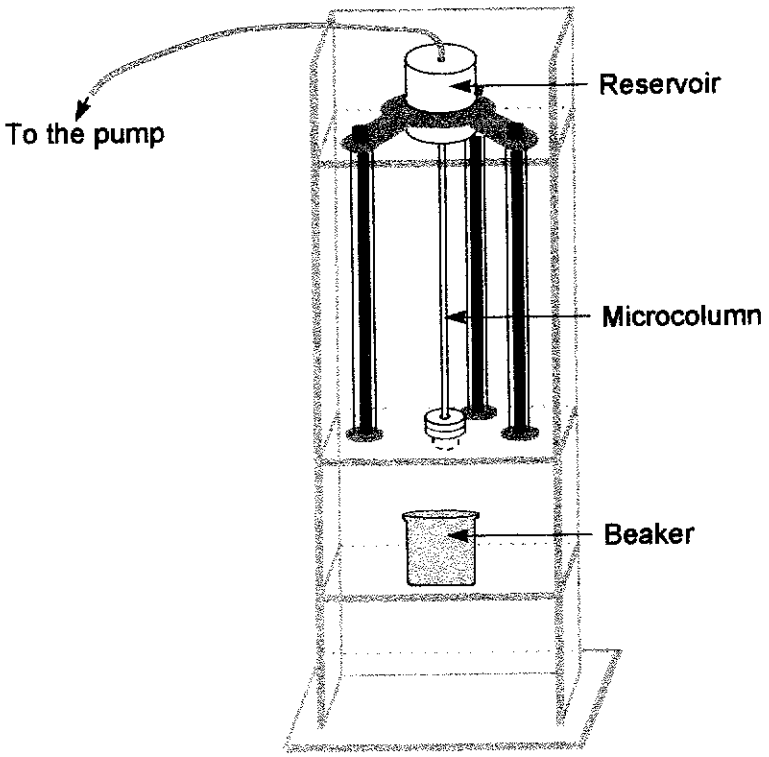

Figure 2-11 The microcolumn used for the separation of gadolinium and samarium by HPLC.

The 15 ml PFA beakers used to collect the eluent were cleaned with concentrated HF just before use to reduce samarium or barium fluoride contamination in the beaker. This procedure also reduces any residual HCl in the beaker, minimising ammonium chloride formation.

The sample was loaded in 10 μL 0.75 M HCl and separated with 12 ml methyl lactic acid. Gadolinium was collected between 1.9 and 3.1 ml and samarium between 4.1 and 8.5 ml (Figure 2-12).

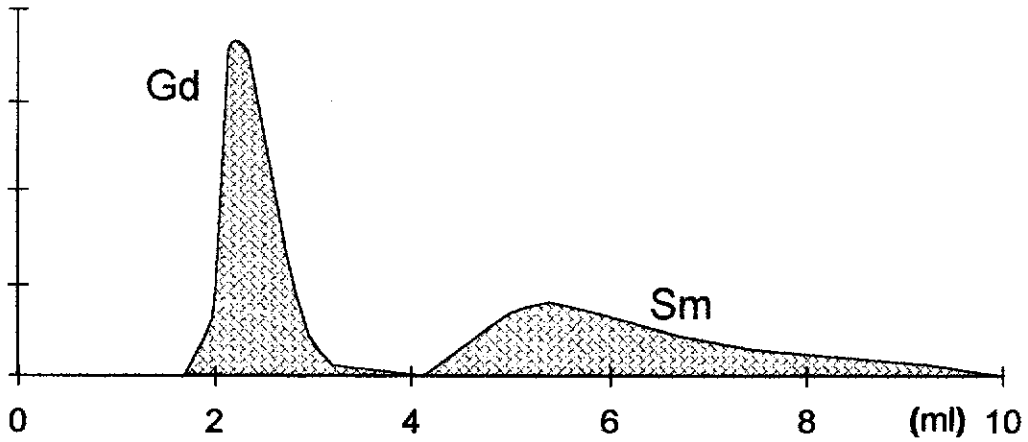

Figure 2-12 The separation of gadolinium and samarium with HPLC

Ammonium chloride often forms when the gadolinium and samarium samples eluted in methyl lactic acid are evaporated. The ammonium chloride was decomposed by adding three drops of concentrated HNO_3 and one drop of concentrated HCl to the sample. The problem has been minimised by delaying cleaning procedures in the laboratory which require HCl until after REE separation. With the lunar samples the Lanspec resin removes any remaining ammonium chloride.

2.4.4 Separation of gadolinium and samarium with Lanspec resin.

Details of this chemistry procedure, used for the separation of the lunar samples only, is in Appendix D, Section 4.

Lanspec Resin (Eichrom Lanthanide Specific Resin, small bead size, 25 g Ln Resin SPS (50-100μm) LN-B025-S from Eichrom Industries Inc.) (Fletcher, 1996 and Horwitz, 1975) was loaded in columns made from LDPE transfer pipettes (Samco 204, 9 cm x 6 mm) with force-fitted PE frits. The top of the squeeze bulb was cut off to form the reservoir. New resin was used each time as samarium contamination was sometimes evident after one use. 0.6 ml of resin was washed into the column in MQW to a height of 3 cm. The reservoir above the resin holds 7 ml.

The samples of gadolinium and samarium collected from the microcolumn were placed on separate Lanspec Resin columns. Samples were dissolved and loaded in 0.3 M HCl and washed off in a progression

of increasingly concentrated HCl. Samarium was washed off in a 0.4 ml cut, whereas gadolinium was collected in a 0.5 ml HCl cut (Figure 2-13). 2 μL H_3PO_4 was added to each sample before evaporation.

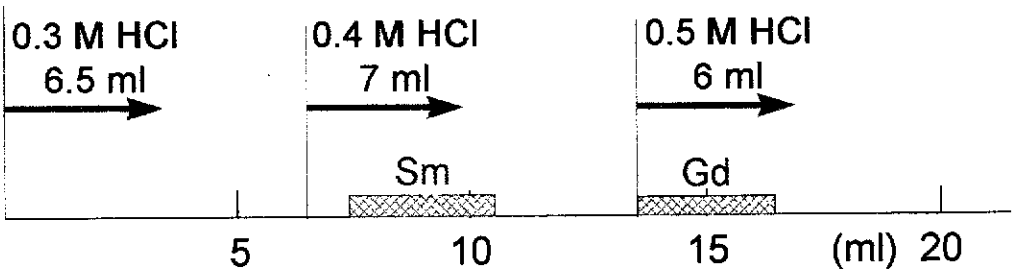

Figure 2-13 The elution of gadolinium and samarium from the Lanspec resin

For the REE samples 2 μL of phosphoric acid was used to concentrate the sample. The H_3PO_4 must be evaporated from the filament when loading the sample for the mass spectrometer, leading to the possibility of gadolinium or samarium oxides forming, so the minimum possible was used.

2.5 Efficiency

The overall extraction efficiency for the two rare earth stages, determined by IDMS using thermal ionisation, was 70% for gadolinium and 78% for samarium.

2.6 Dry weight of GRM samples, the reduction of volatile elements by heating

When the GRM samples are heated they experience a reduction in weight which is different in each sample. To quantify the weight loss the 150 mg to 250 mg samples were placed in open PFA beakers for 24 hours on a hot plate at about 50°C. Later other samples were placed in open PFA beakers in a closed oven, at 110°C for 24 hours. Some were re-weighed immediately they were taken out of the oven, and others were allowed to cool for one hour in a sealed container before re-weighing (summarised in Table 2-17 and Figure 2-14). The PFA beakers lost less than 0.02% weight during heating.

Table 2-17 Percentage loss in weight of GRM samples heated for 24 hours at 110°C in an oven, except for column 2, which was heated to 50°C on a hot plate. Columns 3 to 5 were weighed immediately on removal from the oven, columns 6 and 7 were weighed after one hour.

	50°C on a hot plate (%)	(3) (%)	(4) (%)	(5) (%)	(6) (%)	(7) (%)	Average loss in weight ((6) and (7)) (%)
BCR-1	-2.0	-1.9	-1.5	-0.9	-1.0	-1.0	1.0
BHVO-1	-0.9	-1.1	-0.4		-0.3	-0.5	0.4
BIR-1	-0.6	-0.5	-0.6		-0.7	-0.3	0.5
DNC-1	-0.8	-0.8	-1.0		-0.4	-0.8	0.8
MAG-1	-3.2	-3.6	-1.9		-3.6	-3.6	3.6
PCC-1		-0.6	-0.6		-0.7	-0.8	0.7
W-2	-0.5	-1.6	-0.6	-0.3	-0.4	-0.3	0.3

The loss of volatile elements during heating causes a large reduction in weight, from 0.3% to 3.6%. This has a large effect on the uncertainties of any calculations which include the weight of the samples.

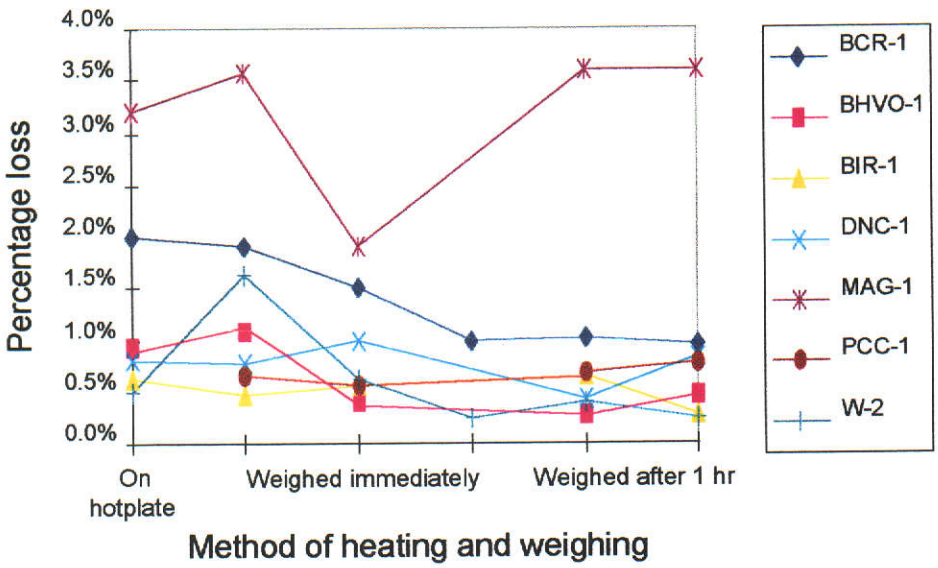

Figure 2-14 Percentage weight loss of GRMs after heating.

The concentrations of the GRMs (Sands and Rosman, 1997) were based on a dry weight, which was based on percentage changes in weight of: BCR-1, -1 %; BHVO-1, -0.4 %; BIR-1, -0.6 %; DNC-1, -0.8 %;

MAG-1, -3.6 %; PCC-1, -0.7 % and W-2, -0.3 %. These percentages were taken from the average of the two samples weighed after cooling for one hour (columns 6 and 7 in Table 2-17). There were two exceptions, BIR-1 and DNC-1, -0.6% for BIR-1 was the average of the first four columns and -0.8 % for DNC-1 of all the measurements.

2.7 Reduction of volatile elements in cadmium metal, Gd_2O_3 and Sm_2O_3

Before preparing the gravimetrically prepared cadmium, gadolinium and samarium standards careful measurements were made of weight loss during heating.

The change in weight of 99 mg of cadmium metal was measured by Differential Thermal Analysis. There was no indication of any mass change greater than 0.05% (Figure 2-15). The melting point for cadmium is around 350°C.

30 g samples of Specpure Gd_2O_3, and Sm_2O_3 were heated at 20°C/minute to 1400°C in air, in a Thermo Gravimetric Analyser, allowed to cool for 2 hours and then heated again to 1400°C.

A total mass loss of 1% was observed in the Gd_2O_3 (Figure 2-16). The initial loss of 0.6%, probably due to water, occurs in the first 450°C. From 450°C to 1400°C another change of state results in an 0.4% loss. On re-heating to 1400°C no further detectable mass loss was detected.

The Sm_2O_3 shows a total mass loss of about 11% (Figure 2-17). The initial loss was probably due to water (1.5%), then to the change in state of crystallisation of various hydrides (a further 7.5%). Over 500°C a further 2% mass loss indicates a further two stage change of state. Over 1200°C no further mass loss occurs. On re-heating to 1400°C no further detectable mass loss occurs.

Based on these observations, before preparing the gravimetric standards (Section 2.9), Gd_2O_3 and Sm_2O_3 were heated in an oven to 1100°C and 800°C respectively, these temperatures were maintained for 2 hours.

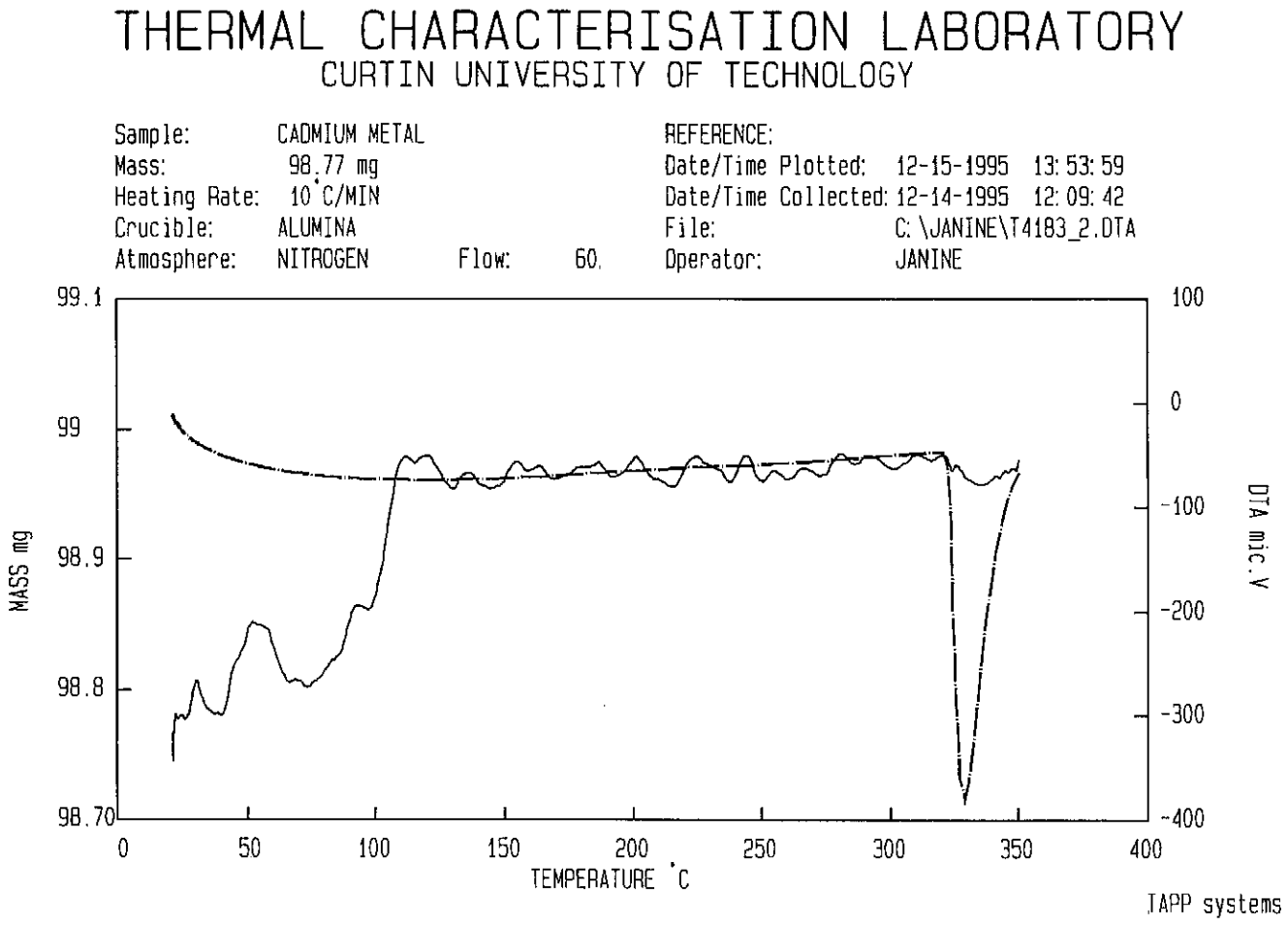

Figure 2-15 Mass loss with temperature of cadmium metal.

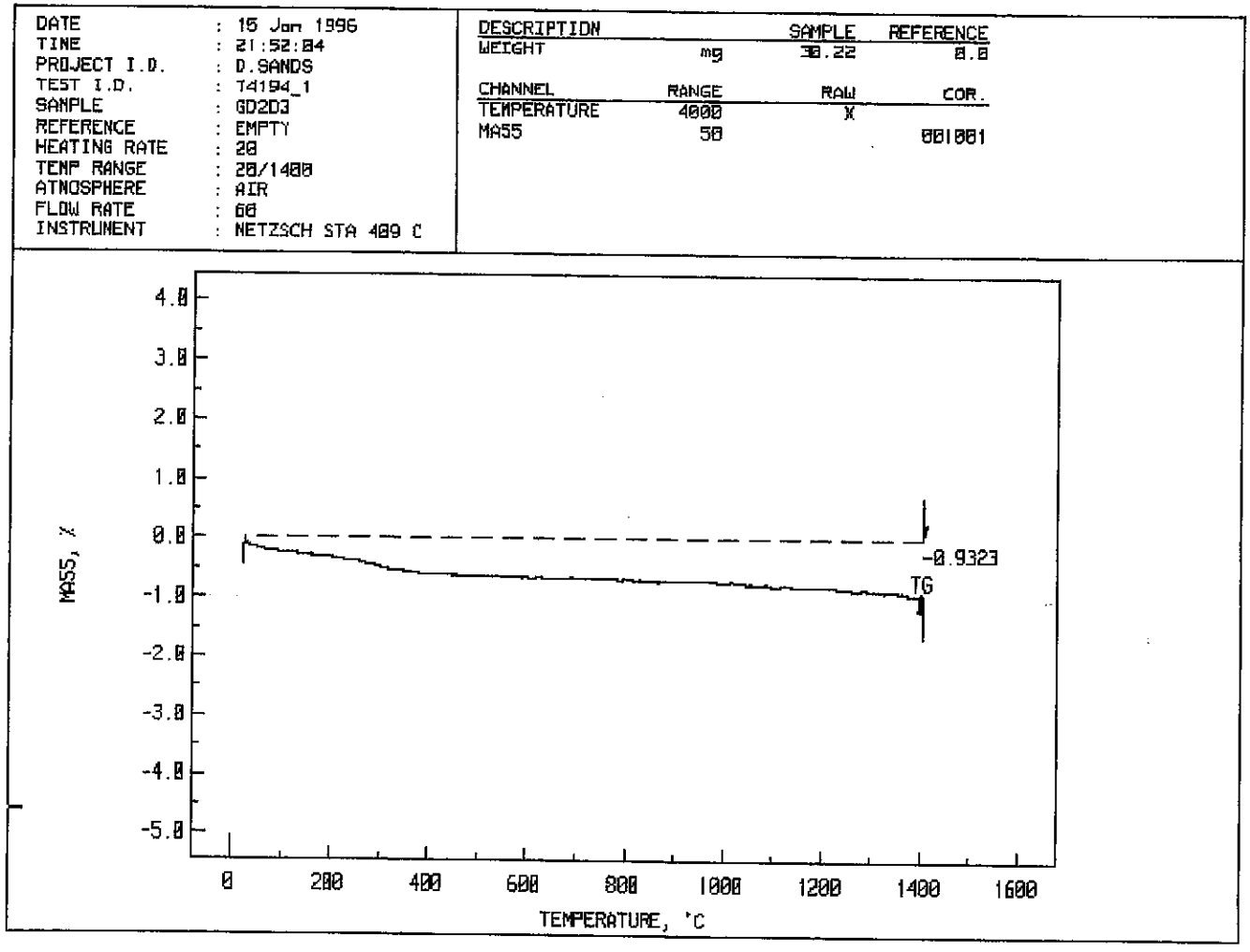

Figure 2-16 Mass loss with temperature of Gd_2O_3.

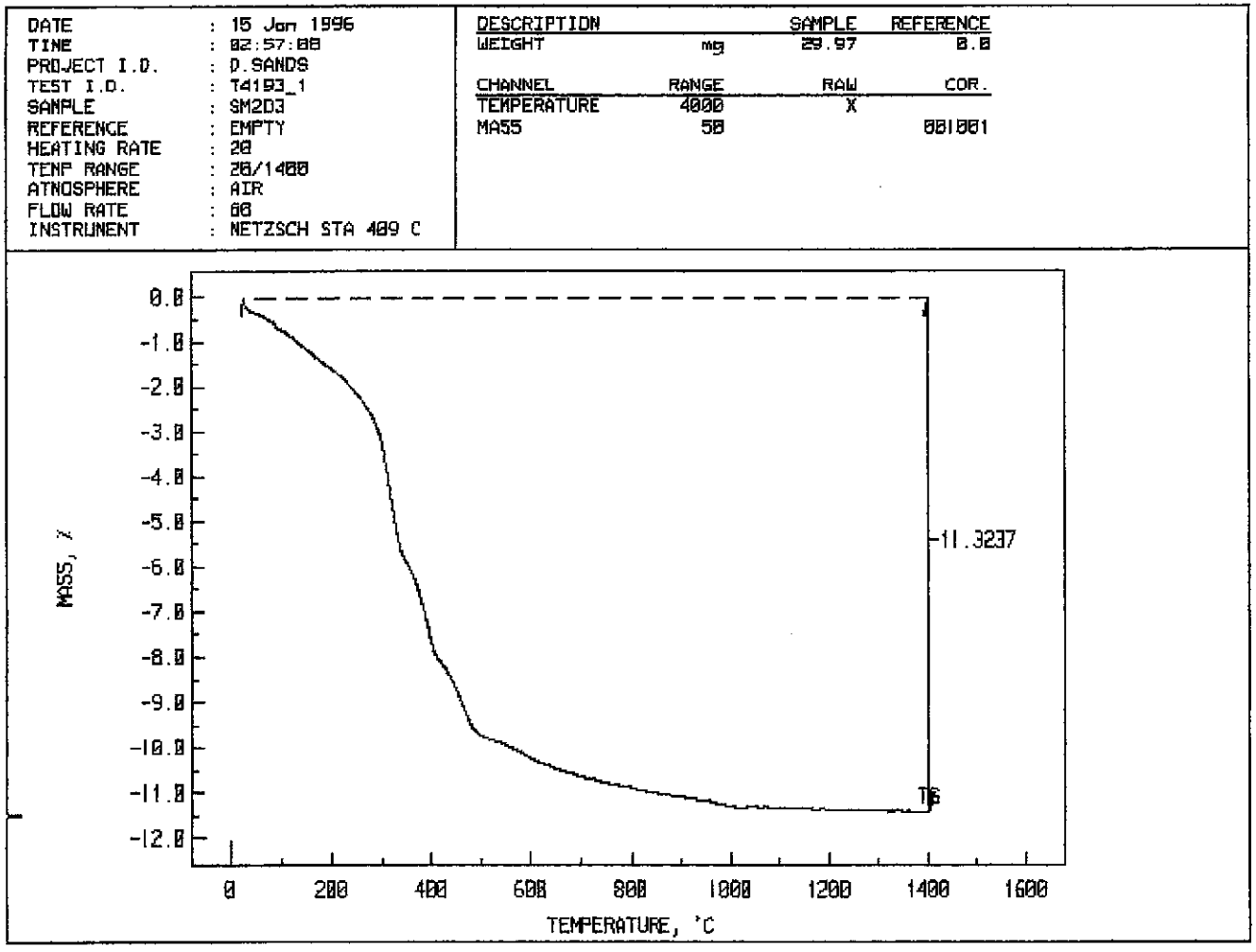

Figure 2-17 Mass loss with temperature of Sm_2O_3.

2.8 Preparation and calibration of tracers

Solutions of isotopic tracers are prepared from materials enriched in ^{106and111}Cd (enriched to 24.580% and 66.459% abundances respectively), ^{152}Gd (enriched to 41.20% abundance), and ^{147}Sm (enriched to 98.34% abundance) (Oak Ridge National Laboratory, USA) (Table 2-18, Figures 2-18 and 2-19). They are then calibrated against accurate gravimetrically prepared standard solutions (Section 2.9) using IDMS with a thermal ionisation mass spectrometer.

Each tracer was calibrated twice with each of the gravimetrically prepared standards.

Table 2-18 The isotopic abundances of the $^{106 and 111}$Cd, ^{152}Gd and ^{147}Sm tracers (%) (Oak Ridge National Laboratory, USA).

Cd isotopes	$^{106-111}$Cd tracer	Gd isotopes	^{152}Gd tracer	Sm isotopes	^{147}Sm tracer
106	24.580±0.014	**152**	41.20±0.1	**144**	0.05±0.02
108	0.1751±0.003	**154**	4.68±0.05	**147**	98.34±0.10
110	1.525±0.002	**155**	16.24±0.05	**148**	0.84±0.10
111	66.459±0.027	**156**	14.12±0.06	**149**	0.34±0.05
112	4.388±0.003	**157**	7.83±0.03	**150**	0.10±0.05
113	0.822±0.001	**158**	9.87±0.05	**152**	0.20±0.05
114	1.605±0.002	**160**	6.13±0.03	**154**	0.12±0.05
116	0.447±0.001				

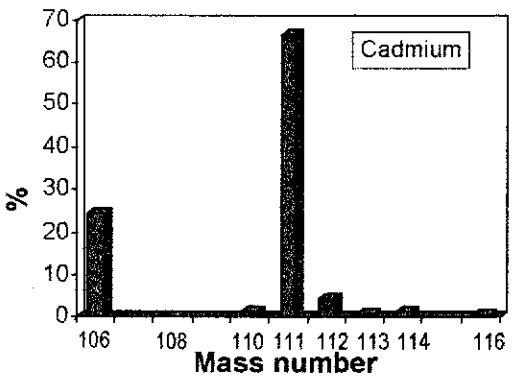

Figure 2-18 The isotopic abundances of the $^{106 and 111}$Cd tracer.

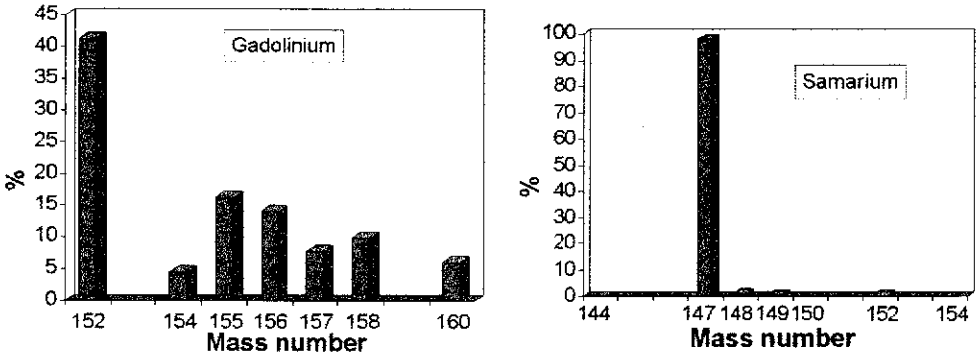

Figure 2-19 The isotopic abundances of the ^{152}Gd and ^{147}Sm tracers.

Table 2-19 The concentrations of the cadmium, gadolinium and samarium tracers used in this work, two of each.

Calibrated tracers	Concentration of tracers
$^{106 \text{ and } 111}$Cd	0.6349±0.0017 ppm
$^{106 \text{ and } 111}$Cd	33.83±0.13 ppb
^{152}Gd	10.446±0.017 ppm
^{152}Gd	2.082±0.005 ppm
^{147}Sm	11.643±0.014 ppm
^{147}Sm	1.8138 ±0.0032 ppm

2.9 Preparation and calibration of standards

Solutions with known concentrations were gravimetrically prepared from high purity cadmium metal and pure oxides of gadolinium and samarium (Johnson Matthey, Specpure).

The standards were prepared in a clean laboratory supplied with HEPA filtered air, wearing protective gloves, coats and shoes and with two people present to check each stage. Before any weighing of apparatus or standards, the electronic balance was calibrated.

For cadmium a standard with a concentration of around 1000 ppm was first prepared, then used to prepare two lower concentration standards of around 10 ppm. Four further standards of about 100 ppb are prepared from the 10 ppm standards (Figure 2-20).

The clean flasks had been stored filled with dilute HNO_3. The cadmium metal and its surroundings were cleaned with ethanol, and the

end of the cadmium metal rod discarded. The cadmium metal was dissolved in 0.5 M HNO_3.

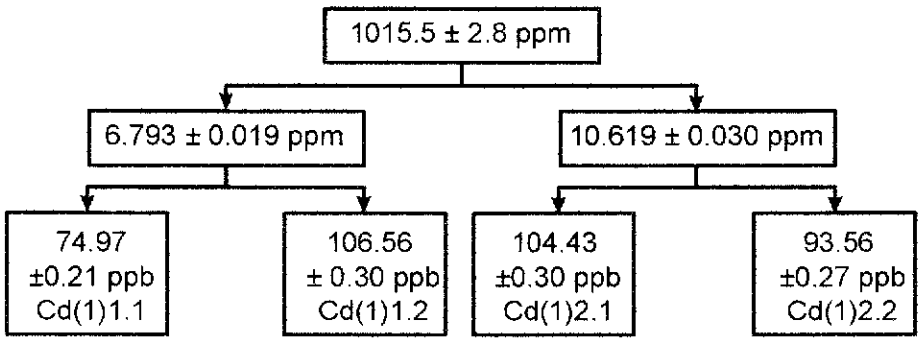

Figure 2-20 Preparation of the cadmium standards

For gadolinium and samarium two standards with concentrations around 1000 ppm were first prepared and then used to prepare two lower concentration standards of around 10 ppm (Figures 2-21 and 2-22). Every action and measurement were recorded at each stage.

Both the Gd_2O_3 and Sm_2O_3 powders were placed into a weighed Vycor vial which was then re-weighed. With a loose lid added, the vial was placed on a Vycor base and into a high temperature furnace. The Gd_2O_3 and Sm_2O_3 powders were heated in a Thermolyne (Sybran) Type 46200 High Temperature Furnace to remove any water or other volatile contaminants. Gd_2O_3 was heated to 1100°C and Sm_2O_3 to 800°C at 15°C/minute, these temperatures were maintained for 2 hours. The samples were removed in the vials while still hot and placed with a desiccant in a reduced vacuum environment. A weight loss of 0.7% for gadolinium and 14% for samarium was recorded.

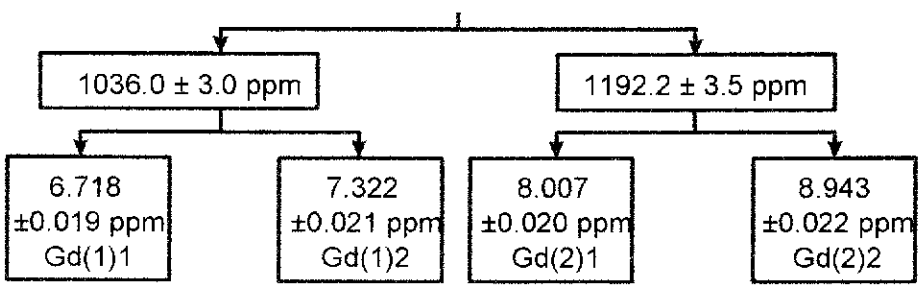

Figure 2-21 Preparation of gadolinium standards

Wide necked borosilicate Schott bottles, stored filled with dilute HNO_3, were used for dissolving the powder, so that the Vycor vials containing the gadolinium and samarium could be place directly into them. Both the gadolinium and samarium were dissolved in 1 M HCl.

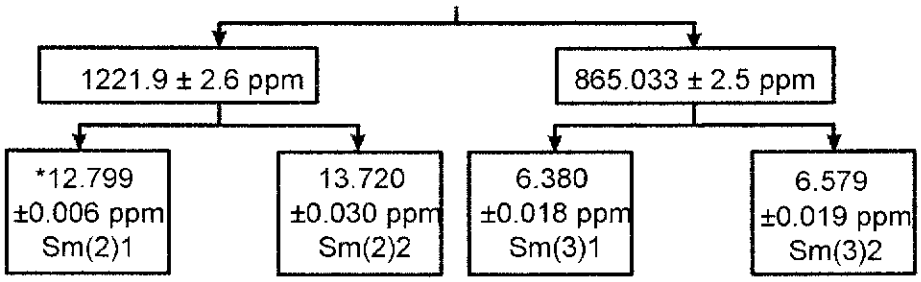

*Sm(2)1 was not used for calibration as there was a possibility that a micropipette malfunction resulted in contamination.

Figure 2-22 Preparation of samarium standards

2.10 The laboratory

The sample processing took place in a dedicated clean-air laboratory supplied with HEPA-filtered air.

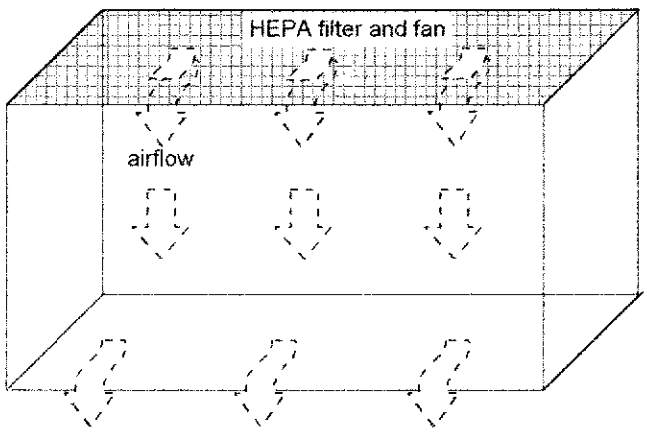

Figure 2-23 Laminar flow clean hood.

The use of metal was minimised in the construction of the laboratory, and where metal had been used it was covered in silastic, or plastic tape (for example unused power points). The walls were newly painted with

lead free paint (Croda 306A Regnapoxide + Croda 306B hardener). Two laminar flow hoods have HEPA filtered air flowing from above (Figure 2-23).

2.11 Preparation of chemical reagents

Concentrated reagents are purified in laboratories supplied with coarsely filtered air, while lower concentrations of acids are prepared in a laboratory with HEPA filtered air and with laminar-flow clean air hoods. Purified reagents were used for all cleaning and chemistry unless stated otherwise.

The measurement of any contamination in the reagents was by high precision isotope dilution mass spectrometry (IDMS). The analytical blanks are summarised in Table 2-20 at the end of this Section.

2.11.1 Milli-Q Water (MQW)

Tap water was filtered in an Aqua-Pure filter, then pre-treated by reverse osmosis, giving Milli-RO water, having removed at least 97% of dissolved organic material. This was followed by a five stage finishing unit using dry packed carbon, ion exchange resins, and a further membrane filter unit for Milli-Q water (Millipore Corp., Bedford, MA, USA). This procedure removes all particles and micro organisms larger than 0.22 μm.

Cadmium, gadolinium and samarium blanks in the MQW were 0.5 pg/g, 0.3 pg/g and 0.5 pg/g respectively.

2.11.2 Hydrofluoric acid.

Ajax Univar Analytical Grade (70%) hydrofluoric acid was distilled in a two-bottle teflon still (Figure 2-24), then stored in a 1 litre LDPE bottle.

The concentration of cadmium, gadolinium, and samarium in the distilled acid was 0.07 pg/g, <0.3 pg/g, and 0.3 pg/g respectively.

2.11.3 Hydrochloric acid.

Matheson Technical Grade (99%) pressurised gas hydrochloric acid was bubbled through MQW until the solution was saturated, then stored

in a 1 litre LDPE bottle. The concentration of cadmium, gadolinium, and samarium in the acid was 0.5 pg/g, 0.5 pg/g, and 0.4 pg/g respectively.

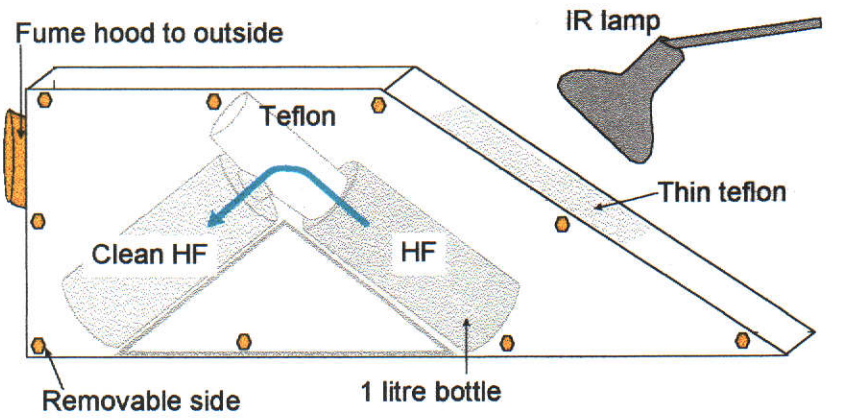

Figure 2-24 Apparatus for distilling concentrated HF.

2.11.4 Nitric acid.

Ajax Univar Analytical Grade (70%) nitric acid was distilled in a sub-boiling quartz still (Figure 2-25), then stored in a 2 litre LDPE bottle. Cadmium, gadolinium and samarium blanks were 0.4 pg/g, 0.2 pg/g and 0.3 pg/g respectively.

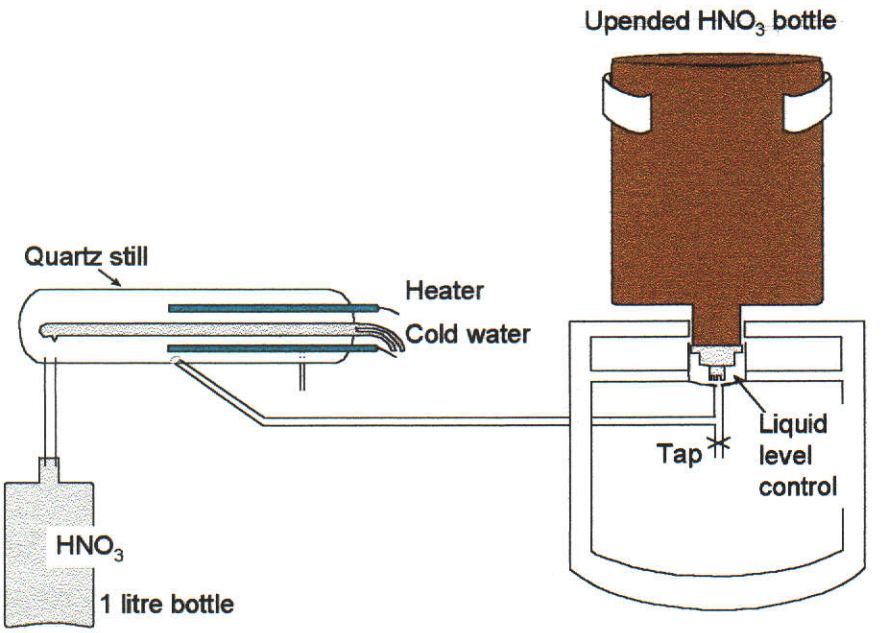

Figure 2-25 Apparatus for distilling concentrated HNO_3.

2.11.5 Methyl lactic acid.

Methyl lactic acid (2-mla) (Aldrich Chemical Co.) was used at concentrations of 0.4 M and 0.2 M, with pH=4.6±0.1 and 4.3±0.1. The 0.4 M acid was used for equilibrating the resin during pre-cleaning, two litres at a time of 0.2 M acid was prepared for the separation of the rare earth elements. Dedicated beakers and flasks were used to mix and weigh the crystals (molecular weight 104.1054 g/mole) and MQW.

Unbuffered 0.2 M methyl lactic acid was stored in a 4 litre high density polyethylene (HDPE) bottle. It was used unbuffered for loading gadolinium samples onto the filaments for the mass spectrometer. For separation of gadolinium and samarium the pH was adjusted to pH = 4.3 (pH = 4.6 for GRMs) using up to 11 ml of saturated ammonium solution (BDH Ammonium solution, 35% NH_3 Aristar), adding a little at a time and leaving it overnight each time to equilibrate. Gadolinium and samarium were present in this reagent at levels of 8 pg/g and <18 pg/g respectively, so no further cleaning was required.

The 0.4 M methyl lactic acid prepared for pre-cleaning the resin was adjusted to pH = 4.6 using up to 13 ml of saturated ammonia solution.

Table 2-20 Summary of the analytical blanks in the reagents used in this work (pg/g).

	Cd (pg/g)	Gd (pg/g)	Sm (pg/g)
Milli-Q water	0.5	0.3	0.5
Hydrofluoric acid	0.07	<0.3	0.3
Hydrochloric acid.	0.5	0.5	0.4
Nitric acid.	0.4	0.2	0.6
Methyl lactic acid		8	<18

2.11.6 pH meter

The acidity of the methyl lactic acid was measured with a Hanna Instruments Portable Microprocessor pH meter, with an uncertainty of ±0.1. Each time it was used the instrument was calibrated to pH = 7 and

pH = 4, using purchased buffer solutions. Between each use the bulb was rinsed in MQW and dried with a tissue, then placed with the temperature probe in the acid and left for 20 to 30 minutes, to minimise the effect of any drifting.

2.12 Cleaning the apparatus

2.12.1 New labware (Polyethylene, Teflon and Glassware)

All new labware was cleaned by wiping inside and out with dichloromethane to remove dust and grease, followed by immersion in a bath of aqua regia (AR grade) for 10-15 minutes, then in baths of 25% AR grade HCl and 20% AR grade HNO_3 for one week in each. Each item was rinsed in MQW between each stage.

In the clean-air laboratory the new disposable pipettes and pipette tips were cleaned over several weeks. They were first rinsed in MQW, placed in turn in tanks of dilute HCl and dilute HNO_3 at 40°C, then stored in dilute HNO_3, having been rinsed in MQW between each stage.

2.12.2 Used labware

Separate cleaning tanks were maintained for cleaning apparatus used for composition measurements and for those used for concentration measurements, where a tracer is used.

Both low density polyethylene (LDPE) and Vycor columns were rinsed in MQW, then stored in dilute HNO_3, in tanks specially reserved for the columns.

PFA beakers, with the lids screwed on, were refluxed on a hot plate at 80 °C for a minimum of 24 hours, with approximately 3 ml aqua regia, followed by heating for 20 seconds in a microwave oven on high. After rinsing in MQW they spent 24 hours in a tank of dilute HCl then dilute HNO_3, both at 80°C. The PFA beakers were then transferred to tanks of dilute HCl and dilute HNO_3, both at 40°C, for one week in each. They were stored with their lids on, filled with dilute HNO_3, in a tank of dilute HNO_3. Immediately before use about 3 ml dilute HNO_3, or concentrated HF and/or HCl was placed in the beakers, sealed in a plastic bag, and

heated for 20 seconds in a microwave oven. The reagent used depending on whether they are to be used for cadmium or gadolinium and samarium chemistry.

2.13 Sm contamination and BaF interference

An extended cleaning regime was incorporated after problems were experienced with samarium contamination in the PFA beakers while measuring the seven GRMs (Sands and Rosman, 1997). Two cleaning steps were added, the initial reflux with aqua regia, and the final clean with HF immediately before use. This reduced samarium contamination to the low picogram level.

Cleaning with concentrated HF before use was also an attempt to minimise barium fluoride interference on the mass spectrometer. This procedure not only reduced barium fluoride contamination, it also improved the ionisation of gadolinium and samarium in the mass spectrometer. It is thought that this process reduced a build up of silicates in the PFA beakers. This cleaning step also removed residual HCl in the beaker, reducing ammonium chloride contamination.

2.14 Preparation of resins

Three different resins were used for the separation of cadmium, gadolinium and samarium.

Anion exchange resin (Bio-Rad AG1x8, 100 - 200 mesh)

Cation exchange resin (Bio-Rad AG50x8, 200 - 400 mesh), and

Lanspec Resin (Eichrom Lanthanide Specific Resin, small bead size, 25 g).

The anion and cation exchange resins were examined for damage under a JEOL JSM-35C Scanning Electron Microscope, both before and after cleaning (Figures 2-26 and 2-27). It was observed that about 20% of the resin was damaged before cleaning, with no increase in damage following cleaning, but with a reduction in small broken pieces, which had been washed away.

2.14.1 Anion and cation exchange resin

The Bio-Rad Analytical Grade Anion Exchange Resin AG1x8 100-200 mesh is a strongly basic anion exchange resin used for the cadmium separation, and the separation of the rare earth element group from the matrix elements. The amount of cross linking determines the bead pore size, x8 indicates 8% cross linking and excludes molecules of molecular weight >1000. Mesh refers (in inches) to openings on the screen used to size the resins, so 100-200 mesh corresponds to a particle size of 74 to 149 μm. The ion on the resin is Cl^-, which has a high selectivity for the resin. When ions from a sample are exchanged onto the resin specific ions can be eluted by introducing an ion with higher affinity for the resin, or a high concentration of an anion with equivalent affinity.

The Bio-Rad Analytical Grade Cation Exchange Resin AG50x8, 200 - 400 mesh is a strongly acid cation exchange resin. 200 - 400 mesh corresponds to a particle size of 38 to 75 μm, the resolution increases and the flow rate decreases with a smaller particle size. The ions on the resin are replaced by ions of the same charge from the sample. If H^+ has a selectivity of 1 for the resin, Cd^{+2} has 2.95. 0.5 M HCl elutes cadmium and 0.2 M methyl lactic acid (pH = 4.3) the rare earth elements.

The anion and cation exchange resins were used for cadmium separation and the cation resin was also used to separate the rare earth element group. For cadmium the two resins were bulk pre-cleaned by rinsing alternately with 4 M HCl and MQW in one litre HDPE bottles. The old MQW was carefully poured out of the jar, so that no resin was lost, the acid added to the resin and the bottle shaken so that all the resin was suspended in the fluid, then it was left soaking for several weeks, when the process was repeated with the MQW. This was repeated six times, then the resins were stored in 4 M HCl.

For HPLC a different bulk cleaning process was followed.

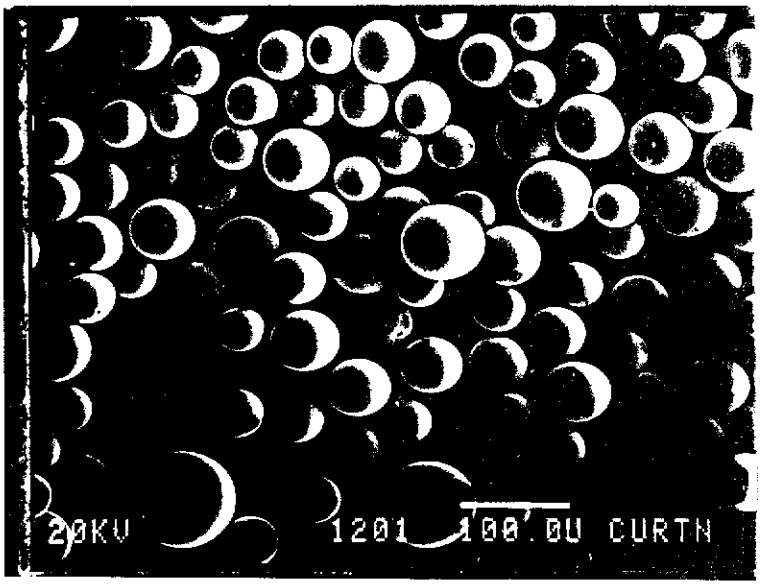

Figure 2-26 Cation exchange resin after cleaning (20% damaged) Magnification x 150.

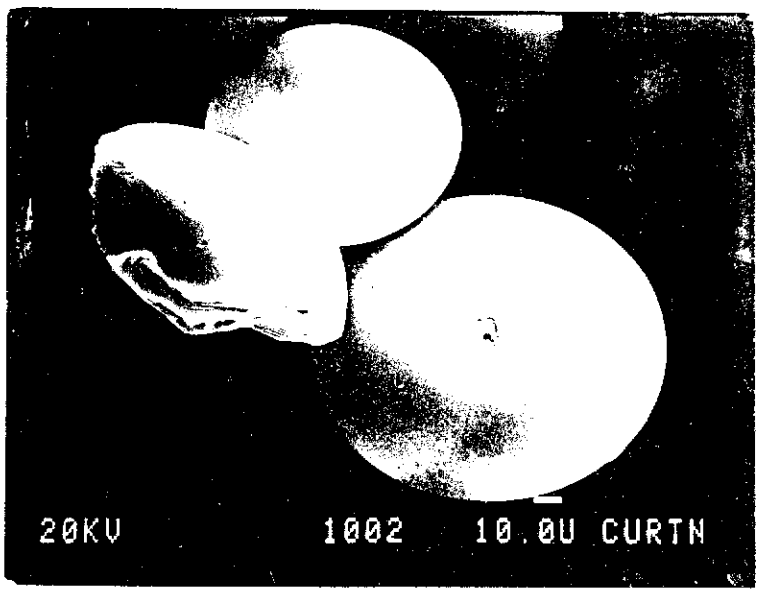

Figure 2-27 Damage observed in the anion exchange resin, before cleaning. Magnification x 500.

2.14.2 Cation exchange resin for HPLC

The Bio-Rad Analytical Grade Cation Exchange Resin, AG 50W-x8 200 - 400 mesh, was also used to separate gadolinium and samarium on the microcolumn, but it went through a different cleaning procedure (Fletcher, 1979 and Eugster et al., 1970b).

The dry resin was clean in bulk in a dedicated 20 x 1 cm glass column with a quartz frit (M Type Quartz Wool, Thermal Syndicate Ltd.). The resin is first washed into the column in MQW, then cleaned with two litres 4 M HCl to remove traces of rare earth elements and Ba. MQW was then passed through the column until the pH of the water going into the column was the same as the pH as it leaves the resin, approximately pH = 5.4 in this case.

250 ml 0.4 M methyl lactic acid of pH = 4.6 was then added to condition the resin, then it was washed again with about one litre of MQW until $pH_{in} = pH_{out}$ again. The top and bottom 2 cm of resin were discarded to remove any barium or REE left on the column, this cleaned resin was stored, covered with MQW, in a 50 ml LDPE bottle, away from light and in a plastic bag.

2.14.3 Lanspec Resin

The Lanspec Resin comes in the form of a fine powder. It was stored in dilute HCl in a new, cleaned PFA beaker. Pre-cleaning of the resin takes place on the column, using 6 to 7 column volumes of 6 M HCl.

Reports recommend the re-use of this resin, but it was found that it very easily becomes contaminated with samarium, so new resin was used for each separation.

2.14.4 Resin blanks

Measurement of any contamination in the resins was determined by IDMS, the analytical blanks are listed in Table 2-21.

Table 2-21 Analytical blanks measured in the resins.

	Cd (pg)	Gd (pg)	Sm (pg)
Anion resin for Cd separation	35		
Cation resin for Cd and REE group separation	48	20	40
Cation resin in microcolumn		20	25
Lanspec resin		15	24

2.15 Summary

In this Chapter an account has been given of the digestion, separation and purification procedures which have been followed to extract cadmium, gadolinium and samarium from terrestrial and lunar samples. Cadmium and the rare earth elements have been described, and a review of separation techniques compiled from the literature. The preparation and calibration of laboratory standards and tracers are detailed, as well as the measures taken to prepare and clean the laboratory, the apparatus, the reagents and the resins. Problems associated with contamination, and some of the solutions are outlined. Investigations have been made of the dry weight of samples, and the efficiency of the ion exchange columns.

The Chapter is supplemented by Appendices B, C and D.

3. Mass spectrometry

3.1 Instrumentation

3.1.1 Introduction

Two thermal ionisation mass spectrometers, an AEI (Associated Electronic Industries) model MS12 mass spectrometer and a VG (Vacuum Generators) model 354 mass spectrometer were used in this work.

3.1.2 AEI MS12 mass spectrometer

The AEI instrument was used for the early development work, but not for the critical measurements. It is a single focusing mass spectrometer with a 90 degree magnetic sector and 30.5 cm radius of curvature magnetic analyser. The vacuum system consists of two rotary pumps, a diffusion pump connected to the source and a Varian Vacion pump which maintains a constant vacuum in the analyser. The electronic system, vacuum system and data handling systems have already been well described (McCulloch, 1974, Smith, 1977, Mermelengas, 1980 and Loss, 1986).

3.1.3 VG 354 mass spectrometer

The VG instrument (Figures 3-1 and 3-2), which was used for the later development work and all the measurements, has been described in Loss (1986). The VG 354 has a 27 cm radius, 90° sector field, with extended geometry (Figure 3-3). An 8 kV HT accelerates the ions which are separated according to mass by a magnet with curved entrance and exit poles. The ions are counted by a Daly detector with photomultiplier or the new nine cup Faraday multi-collector, with independent movement of each cup, which was finally fitted in 1992. Electronic gains were always measured routinely and the accuracy was checked by comparison with published data.

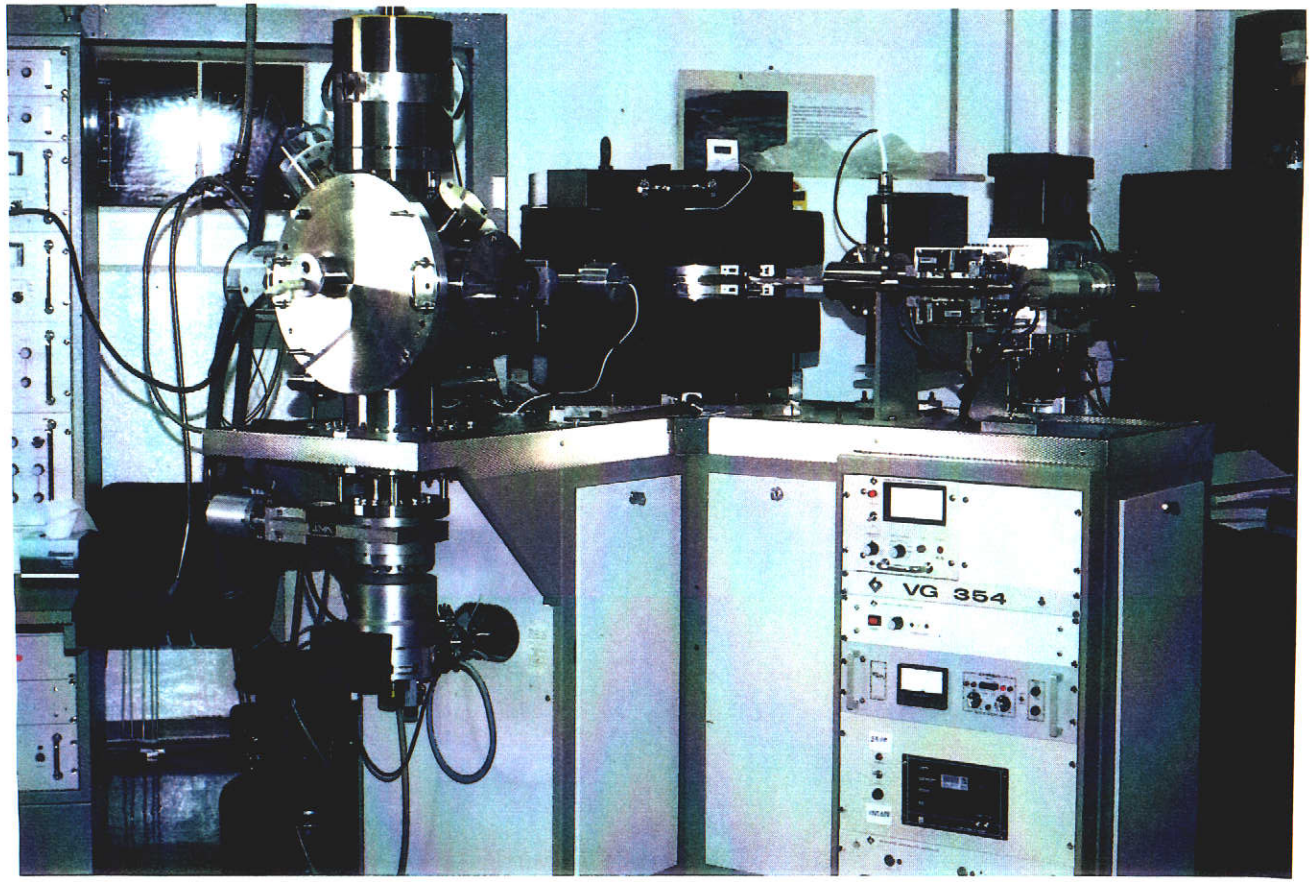

Figure 3-1 The VG353 thermal ionisation mass spectrometer.

Figure 3-2 Control instrumentation for the VG354 mass spectrometer, showing the HP computer, digital voltmeters for the nine multi collectors, temperature and magnetic field controls, pressure gauges, filament current, focussing and HT control.

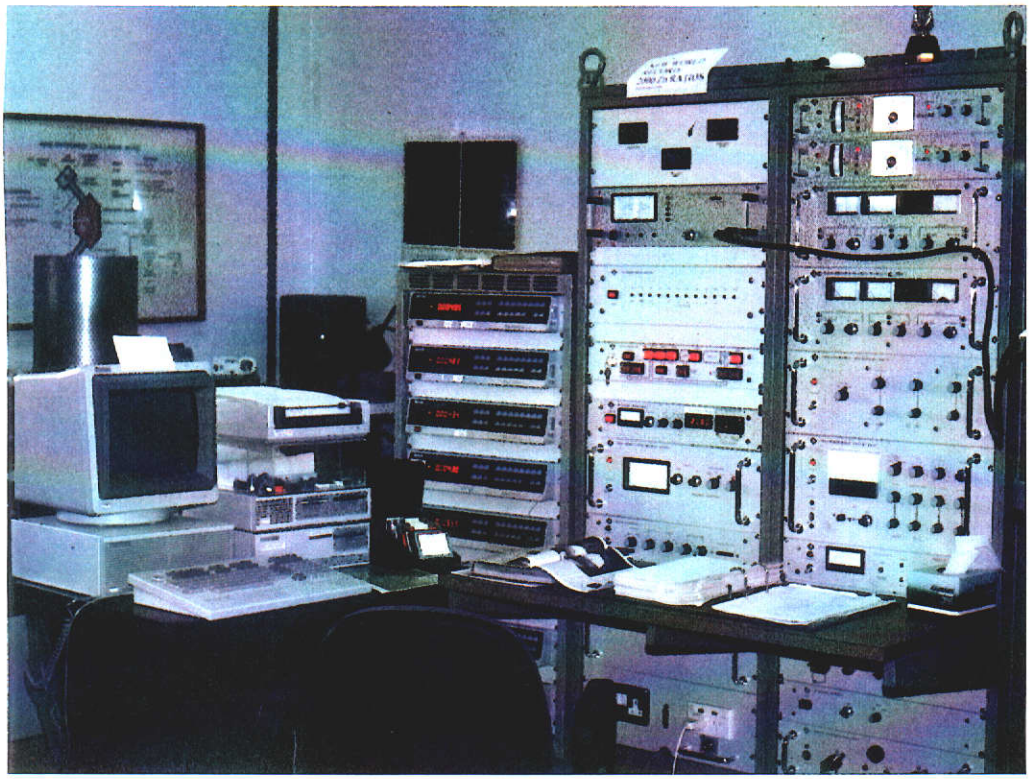

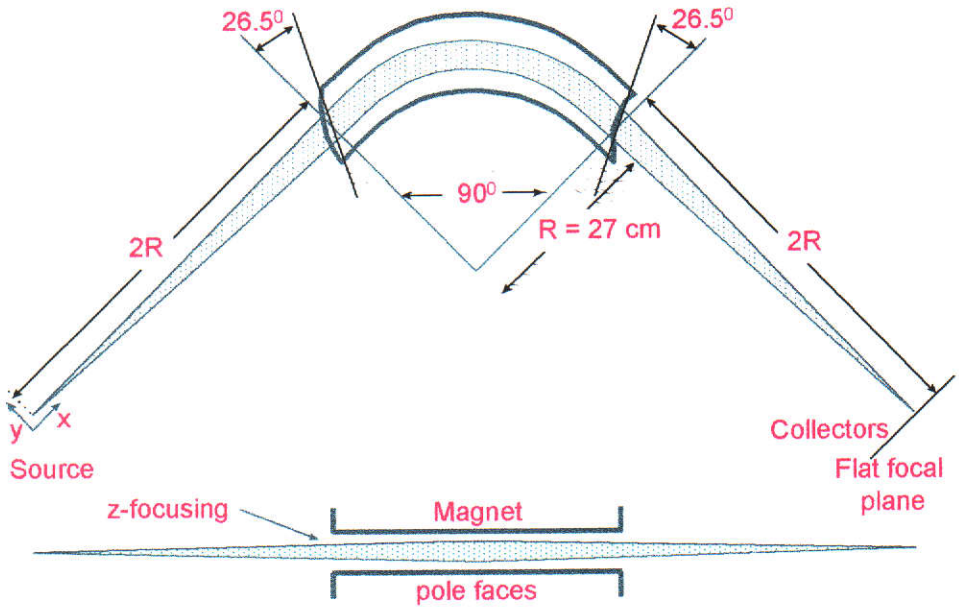

Figure 3-3 Ion optical system of the VG 354 mass spectrometer (taken from Loss, 1986).

A carousel (Figure 3-4) loaded with sixteen sample beads fitted into bead holders (Figure 3-5) is mounted into the source. The samples can be analysed manually, semi-automatically or automatically, controlled by a Hewlett Packard computer.

A pressure of $4x10^{-9}$ millibar (10^{-7} Pa) can be maintained in the analyser and $3\text{-}4x10^{-8}$ millibar (10^{-6} Pa) in the source by two Varian ion pumps, a Leybold Heraeus Turbovac 360CSV pump and rotary pumps.

3.1.4 Daly detector

The Daly knob electrode, which is maintained at a high negative potential, emits up to 8 electrons for each ion striking its surface. The electrons are accelerated to a scintillator connected to a photomultiplier.

One ion beam is measured at a time so the length of time taken to measure a set of isotopes can affect the precision and accuracy of the measurements in the presence of any electronic or ion beam instability.

Ion currents of 10^{-13} A to 10^{-15} A are displayed as 1 V to 10 mV (Table 3-1. A precision of 0.1% (at the 95% confidence level) can be achieved with an ion current of $3x10^{-13}$ A.

It takes over one hour to measure 100 ratios for five isotopes on this detector.

Table 3-1 The relationship between count rates, voltage and ion current on the Daly detector and the Faraday multi collectors.

Count rates (s^{-1})	DVM	Ion current
Daly		
1,000	10 mV	$1x10^{-15}$ A
100,000	1 V	$1x10^{-13}$ A
Faraday		
1,000	10 mV	$1x10^{-13}$ A
100,000	1 V	$1x10^{-11}$ A

Figure 3-4 The sixteen sample carousel for the VG 354 mass spectrometer, loaded with beads.

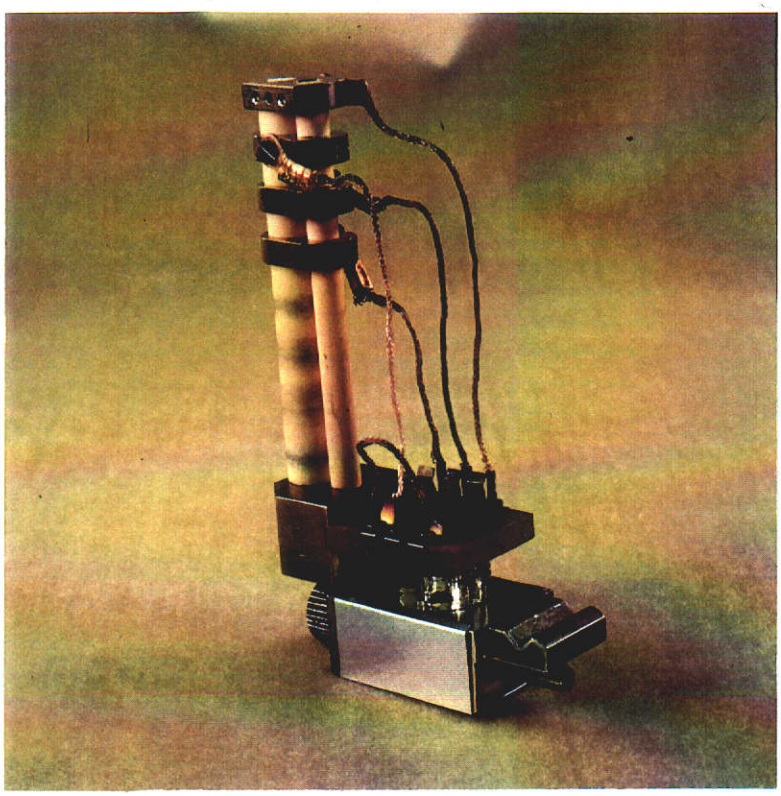

Figure 3-5 The bead is loaded in the base of the holder, with the filament facing down and covered with a cover slip with an exit slit.

3.1.5 Faraday multi-collector

The Faraday multi-collector has nine cups in the nearly flat focal plane. The axial collector is lowered to expose the Daly detector (Figure 3-6).

Cups are adjusted semi-automatically for a particular set of isotopes and the positions stored in Procedure files which can be recalled manually or included in an automated programme. In this work ion beams are measured in the static mode.

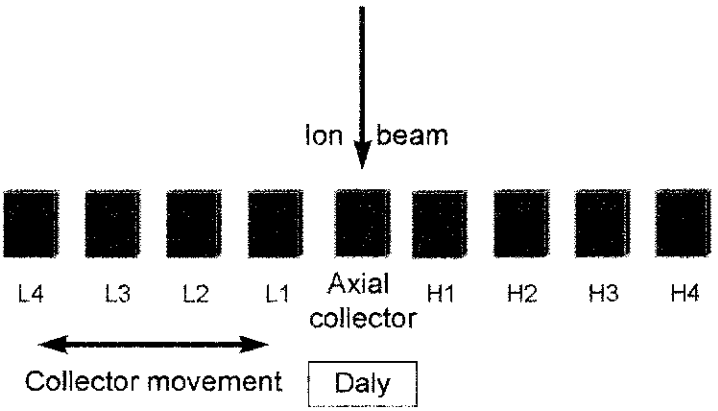

Figure 3-6 The nine cup Faraday multi-collector on the VG 354 mass spectrometer, L1 to L4 collect the low mass isotopes, H1 to H4, the high mass isotopes.

With a resistor of 10^{11} ohm ion currents of 10^{-13} A are displayed as 10 mV (Table 3-1), an ion current of 10^{-10} A is the maximum which can be measured reliably. A precision of 0.001% (at the 95% confidence level) can be achieved with an ion current of $3x10^{-11}$ A. The electronic gain from the nine channels can be monitored automatically or when requested. This is achieved by switching a constant current to each measurement channel. The gain is then normalised to a common value.

3.1.6 Ionisation

When a sample is heated on the filament in a mass spectrometer the efficiency of the ionisation process can be described by the Langmuir-Saha equation (Equation 3-1).

Equation 3-1 Langmuir-Saha equation

$$\frac{n^+}{n^0} = A \cdot \exp\left[\frac{(e(W-IP))}{kT}\right] = A \cdot \exp\left[\frac{(11600(W-IP))}{T}\right]$$

where

n^+ = the number of positive ions

n^0 = the number of neutral atoms

e = electronic charge (1.60×10^{-19} C)

IP = first ionisation potential of element (V)

W = work function of the filament surface (V)

k = Boltzmann's constant (1.38×10^{-23} J/K)

T = surface temperature (K)

For a high value of n^+/n^0 the work function of the filament material should be greater than the ionisation potential of the evaporating element, and the temperature as low as possible. If, however, the work function of the filament is lower than the ionisation potential of the element, then a higher temperature will increase ionisation. Rhenium filaments which have a high work function and melting point (Table 3-2) give efficient ionisation of samarium and gadolinium with high filament temperatures.

Cadmium is predicted to have very poor ionisation on any of these filaments so a silica gel/phosphoric acid activator is loaded with the sample onto a rhenium filament. It forms a glassy white matrix and allows nanogram samples of cadmium to produce ion beams of 10^{-13} A for several hours (Rosman and De Laeter, 1974a). Even further enhancement was achieved for the current measurements using the activator described by Gerstenberger and Haase (1997). With this activator a 10 ng cadmium sample yielded approximately 10^{-12} A ion beam for one hour.

Table 3-2 Work function of filaments, ionisation potential of elements and their melting points (MP).

	Work function (eV)	Ionisation potential (eV)	MP (^{O}C)
Re	5.10		3167
Ta	4.19		2996
W	4.52		3410
Cd		8.99	321
Sm		5.70	1072
Gd		6.16	1311

3.1.7 Data collection and analysis

In this work all samples are run semi-automatically as they are either very small or very valuable.

Two computer control programmes have been used for measuring the ion beams and calculating the ratios, General Peak Jumping (GPJIF) a modified version of VG supplied software, used with the Daly detector; and the General Multi-collector sequence (INTEG), used with the Faraday cups.

- Type files store the masses of the isotopes to be measured and by which Faraday cups, the ratios to be calculated and the multi collector cup positions (details of Type files are listed in Appendix E).
- Loaded samples in bead holders on the carousel are placed into the source, which is sealed and evacuated, the pyrometer placed to read the filament temperature and the samples degassed automatically.
- A sample can be run semi-automatically by moving the multi collector cups to the required positions and manually turning the carousel to align the ionising filament with the ion source collimator stack.
- Filaments are heated to just below the ionisation temperature, the LOS valve opened when the source pressure is close to 10^{-8} mbar, and the Scan programme set to scan across the mass range of interest. Peaks are manually focussed and centred and the temperature increased to produce the required stable ion beams.

- The Manual programme stores the parameters required for a particular sample; the programme GPJIF or INTEG; the Type file to be followed; the Daly or Faraday detector; the date and the number of blocks of ten sets of ratios required. Data collection is automatic but the temperature can be controlled manually.

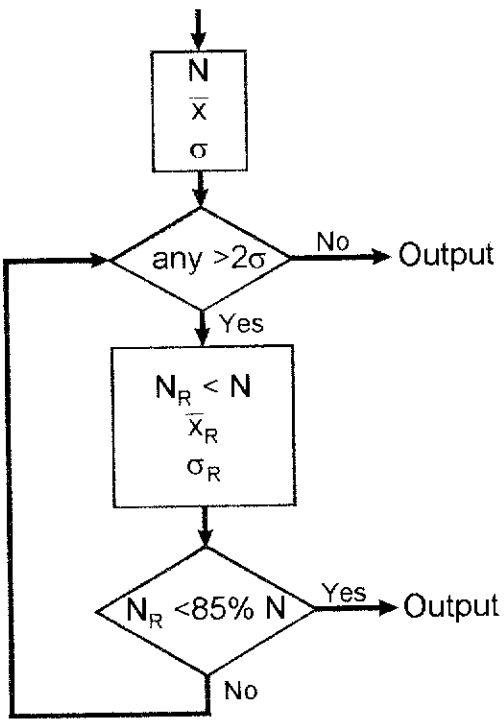

Figure 3-7 Initial rejection criteria on the VG 354 mass spectrometer. N, $\bar{x}$ and σ are the number of ratios, their mean and standard deviation "before rejection". N_R, $\bar{x}_R$ and σ_R are "after rejection" ratios when those with uncertainties >2σ have been rejected.

The isotopes in the spectrum are measured giving one set of ratios. The process is repeated ten times to give a block of data. These ratios are stored in a linear array R(*) and then go through the rejection procedure shown in Figure 3-7, where data deviating more than two standard deviations from the mean are rejected. These ratios, with no further processing, are defined as "raw" data in this work. Ratios can be transfered to a separate terminal for further processing as required.

3.2 General procedures

3.2.1 Introduction

The procedures for the measurement of cadmium, gadolinium and samarium in various circumstances and for different samples are detailed in the following Sections.

3.2.2 The Daly detector and the Faraday multi-collector cup configurations

One or two laboratory standards are run with every set of samples measured. One is used to check the position of the multi collector cups, the other to monitor instrument performance.

3.2.2.1 Cadmium

Cadmium standard samples larger than 10 ng and cadmium from rock and soil samples of more than 20 ng can be measured on the Faraday multi- collector. A further improvement in sensitivity of about five times was achieved with refinements of the activator (Section 3.2.3.1)

To monitor possible interferences from calcium phosphate ($CaPO_2$) and tin (discussed below) pre- and post-scans were included with the Daly detector in use and tin at mass 115 was measured in a dedicated cup with the Faraday multi collector.

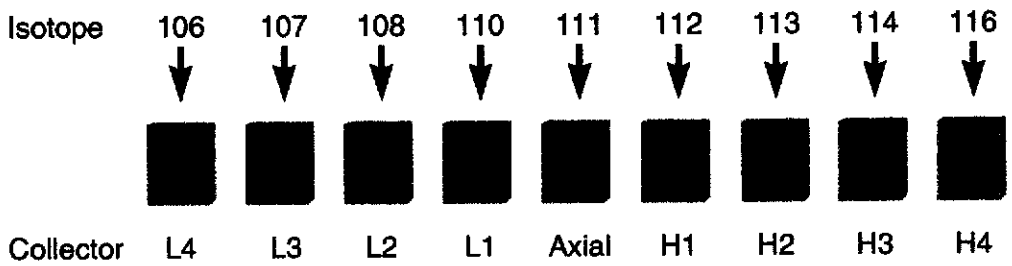

Figure 3-8 Multi-collector cup setting CD(111AX) used with Type 43 to measure cadmium isotopes.

The multi collector cups are set in two configurations, CD(111AX) and CD(112AX). CD(111AX) (Figure 3-8) with ^{111}Cd in the axial cup was used for concentration measurements of the GRMs, so that the double spiked tracer at ^{106}Cd and ^{111}Cd, and all eight cadmium isotopes are measured. This cup setting was in use up to August 1996.

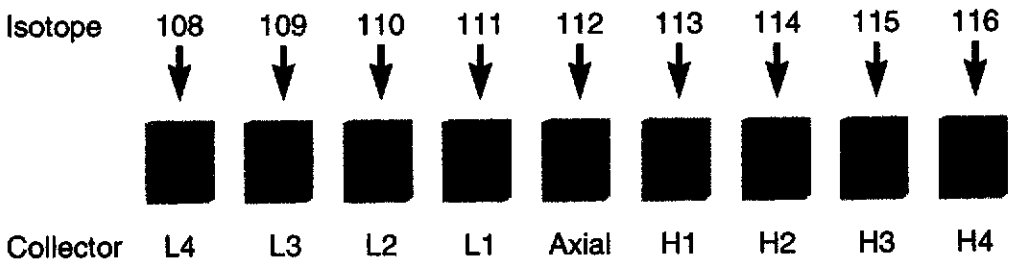

Figure 3-9 Multi-collector cup setting CD(112AX) to measure cadmium isotopes.

CD(112AX) (Figure 3-9), with ^{112}Cd in the axial cup, was used for isotopic composition measurements and, where the beam was large enough, concentration measurements of cadmium in the lunar samples. To monitor indium and tin ions at atomic mass 115 were included, ^{106}Cd was excluded as it is not possible to fit both 106 and 115 into a cup in this configuration. This setting was used from August 1996.

All cadmium ratios are calculated with reference to ^{112}Cd.

3.2.2.2 Gadolinium

Gadolinium was measured as the metal Gd^+.

All gadolinium samples smaller than about 300 ng were measured on the Daly detector. Additional isotopes, 149 and 163, were measured in pre- and post-scans on the Daly detector to monitor interferences from samarium at 149, and dysprosium at 163.

Only one configuration for the Faraday multi-collector cups was used for the measurement of gadolinium. GD(AX156) (Figure 3-10) with ^{156}Gd in the axial cup was used for all gadolinium concentration and composition measurements of the GRMs and of the lunar samples, when the ion beam was large enough. All seven gadolinium ions are included in this configuration, and samarium and dysprosium are monitored at atomic masses 150 and 163.

Gadolinium ratios are calculated with reference to ^{160}Gd.

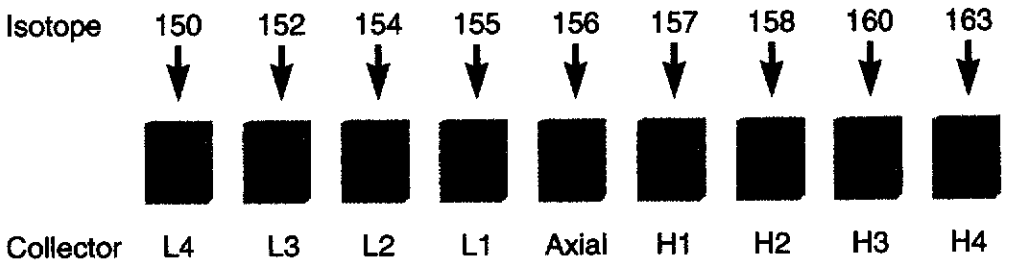

Figure 3-10 Multi-collector cup setting GD(AX156) to measure gadolinium metal ions.

3.2.2.3 Samarium

Samarium was measured as the metal Sm^+.

All samarium samples smaller than about 50 ng, loaded on a triple filament, and all samples smaller than 500 ng loaded on a single filament, were measured on the Daly detector.

To monitor interferences from barium fluoride mass position 157 was measured in the pre- and post-scans with the Daly.

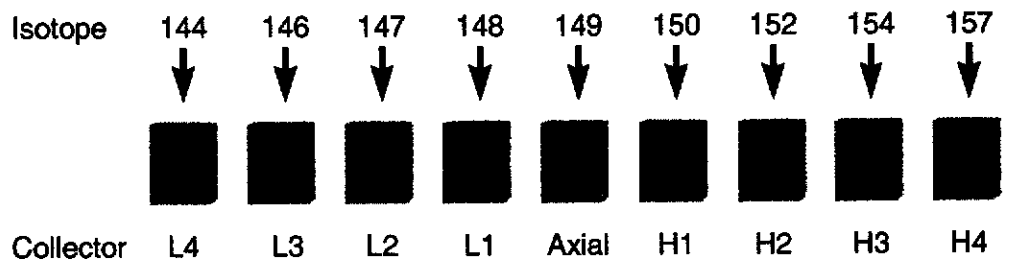

Figure 3-11 Multi-collector cup setting SM(149AX) to measure samarium metal ions.

Two positions for the multi-collector cups were used, SM(149AX) and SM(150AX). SM(149AX) (Figure 3-11) with ^{149}Sm in the axial cup was used for concentration measurement of the GRMs. All seven samarium isotopes are included and ions at atomic mass 146 and 157 are used to monitor neodymium oxide and barium fluoride. This setting was used up to July 1996.

From July 1996 SM(150AX) (Figure 3-12) with ^{150}Sm in the axial cup was used. All the lunar sample composition measurements, and where possible the concentration measurements, used this configuration. All

seven samarium isotopes were measured and ions at atomic mass 156 and 157 were used to better monitor barium fluoride.

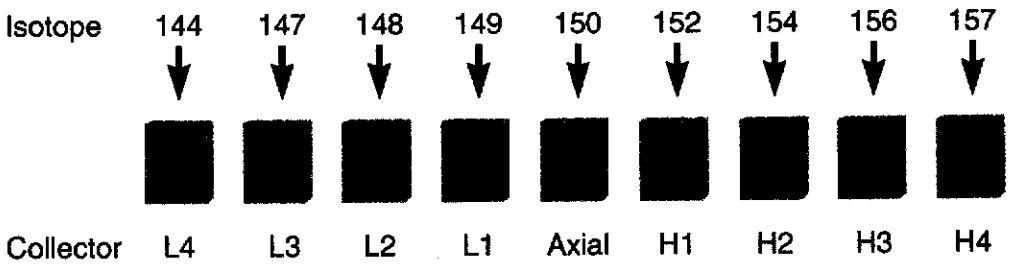

Figure 3-12 Multi-collector cup setting SM(150AX) to measure samarium metal ions.

All samarium ratios are calculated with reference to ^{152}Sm on the mass spectrometer, though it was found necessary to manually recalculate some to ^{154}Sm.

3.2.2.4 Temporal variability in the sensitivity of the multi collector cups

Faraday multi collector cup sensitivity can be monitored over time by observing changes in, for example, samarium standard ratios. All the normalised standards measured from 1995 to 1997 have been plotted in Figure 3-13 as $^{150}Sm/^{152}Sm$. Initial measurements used the cup configuration SM(149AX), after July 1996 SM(150AX). Thus, in earlier measurements $^{150}Sm/^{152}Sm$ was collected in cups High1/High 2, later in cups Axial/High 1. The Figure shows clearly a 0.09% change in the ratio when the cup setting was changed.

$^{148}Sm/^{152}Sm$ has been plotted in Figure 3-14 where initially cups Low 1/High 2 were used, and later cups Low 2/High 1. A different trend is observed where the sensitivity of Low 1 is seen to have changed by 0.06% over one year. The two Figures illustrate the different and varying sensitivity between the multi collector cups.

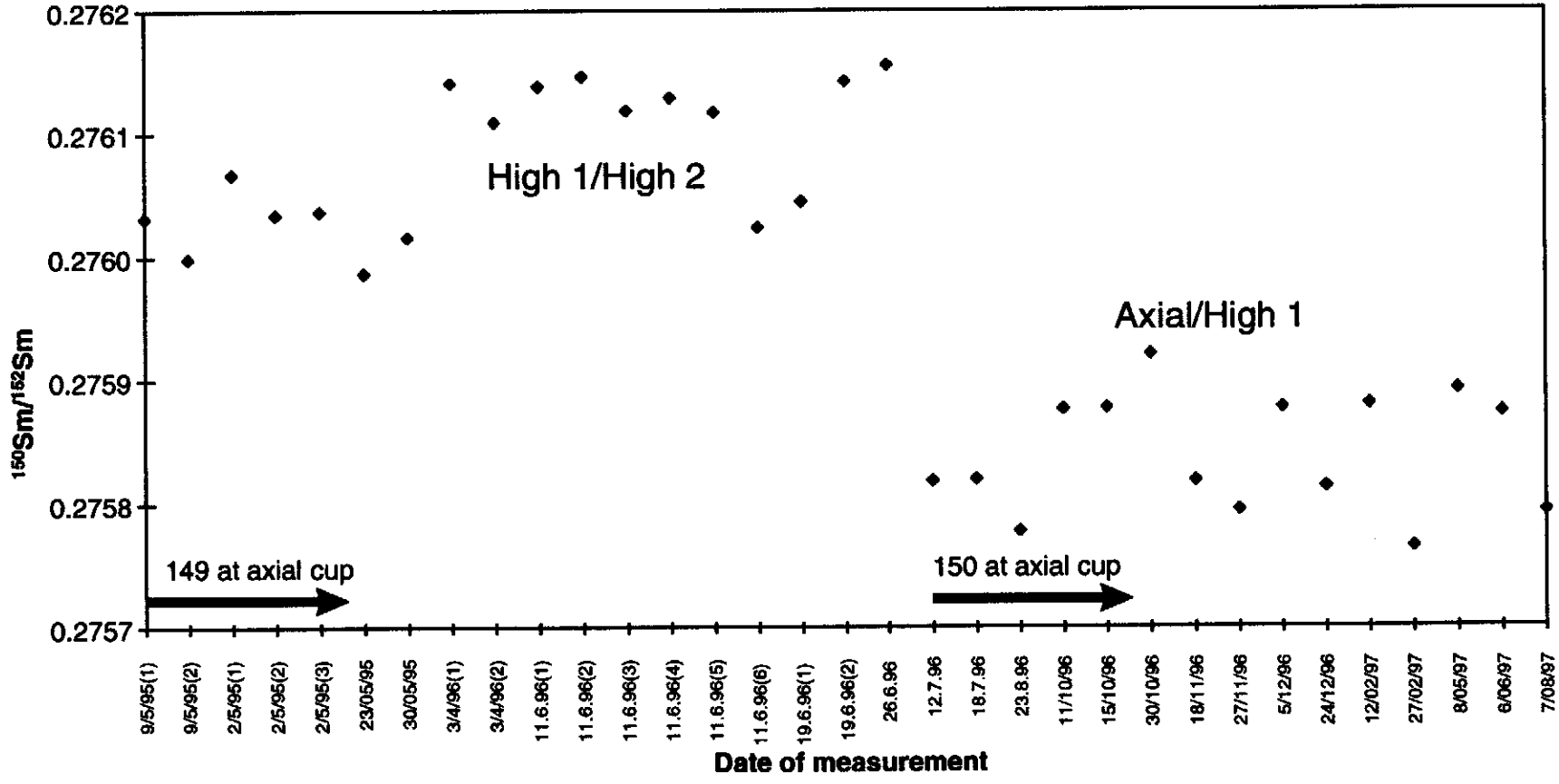

Figure 3-13 The graph shows $^{150}Sm/^{152}Sm$ measured over two years with two multi collector cup configurations, SM(149AX) and SM(150AX).

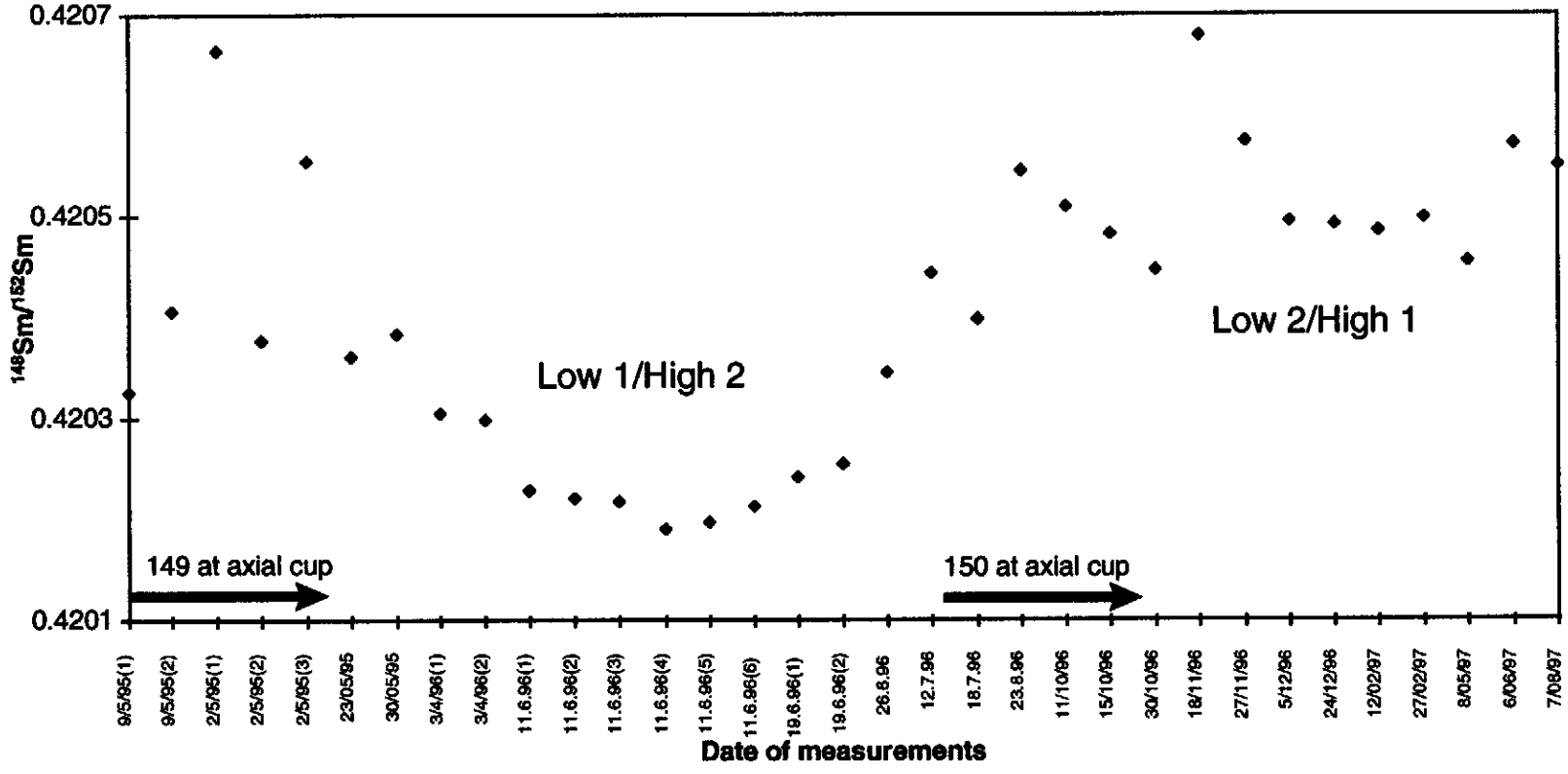

Figure 3-14 The graph shows $^{148}Sm/^{152}Sm$ measured over two years with the two multi collector cup configurations, SM(149AX) and SM(150AX).

To minimise the effect of any drift in cup sensitivity, neutron capture in cadmium, gadolinium and samarium were compared to standard measurements made in the same cup configurations and at the same time. Correction factors were never incorporated into the software.

3.2.3 Filaments and loading samples

Cathodeon glass beads, 5/8 inch in diameter by ¼ inch thick, with 0.040 inch diameter Nilo-K wire posts, shown in Figure 3-16 (a), (b) and (c), are used to load the samples into the mass spectrometer. Rhenium ribbon, 99.999% four pass zone refined (H Cross Co., New Jersey, 0.030 mm x 0.76mm), is spot welded onto either single or triple pairs of posts on the bead. The beads are then degassed at 4.5 A and 10^{-4} Pa for 30 minutes (Figure 3-15).

Figure 3-15 Before the sample is loaded eight beads are degassed at one time, in a vacuum system under the bell jar.

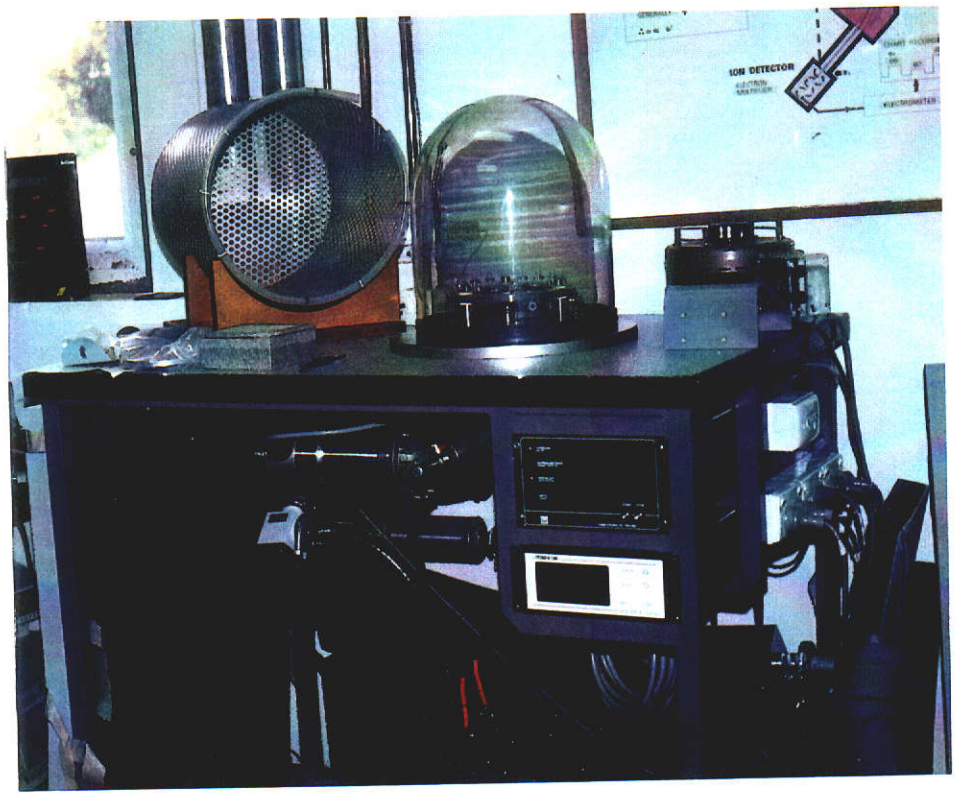

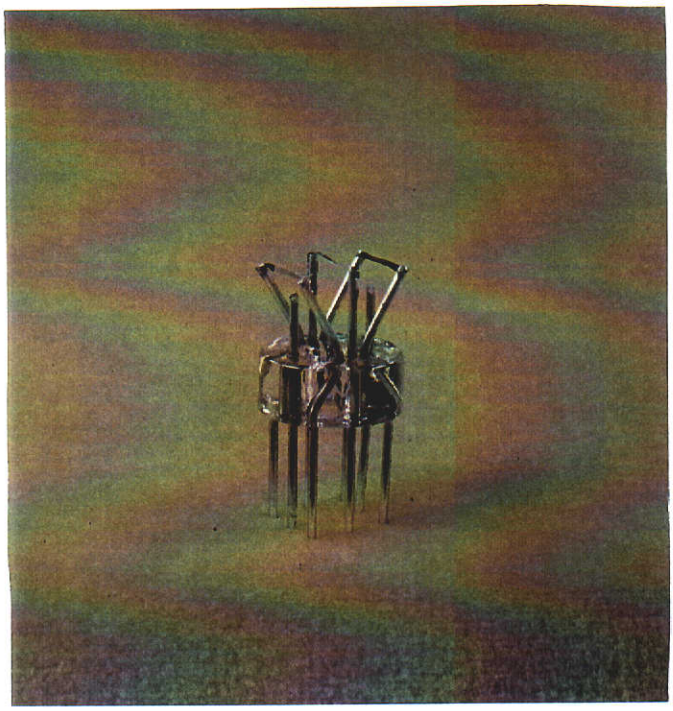

Figure 3-16 (a) A triple Re filament in the configuration for Cd.

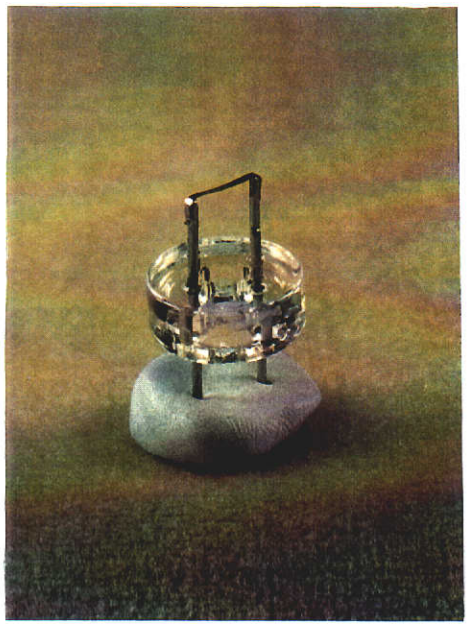

Figure 3-16 (b) A single Re filament, used for Sm.

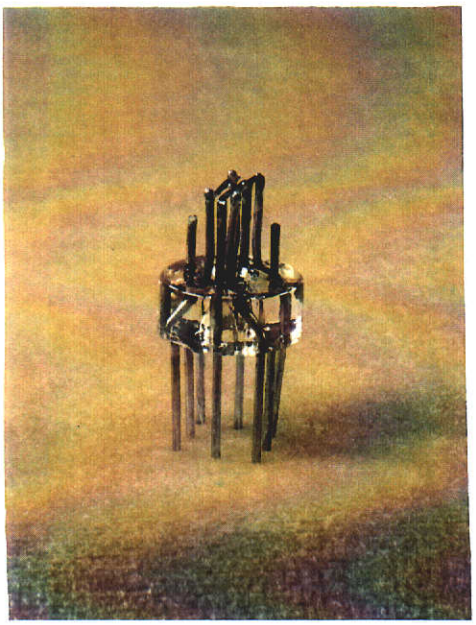

Figure 3-16 (c) A triple Re filament in the configuration for Gd or Sm.

Immediately before a sample was loaded on a filament the filament was cleaned with a 2 µl drop of 2 M HCl. With the beads in the source of the mass spectrometer, and the vacuum less than 10^{-6} mbar, the beads are degassed for a second time, with the line of sight (LOS) valve to the analyser still closed.

3.2.3.1 Cadmium

Cadmium was loaded onto the centre filament of the triple rhenium filament bead with the side filaments pulled wide apart as shown in Figure 3-16 (a) ("Oven" source, Rosman, 1992).

The cadmium sample was loaded in a silica gel activator (Aerosil, 2 g $SiCl_4$ in about 30 g MQW) mixed with phosphoric acid (Aristar (BDH) or Dom Merck, Germany Super Pure Phosphoric H_3PO_4, 50:50 mix, 2 g H_3PO_4 in about 30 g MQW). After June 1997 a new, finer, silica gel was used, (Merck Silicic acid colloidal solution, Darmstadt, ~15% methanol).

Table 3-3 The lunar samples showing which silica gel was used to load cadmium onto the filaments for both composition and concentration measurements.

Sample	**Aerosil or Merck silica gel**	
	Composition measurements	**Concentration measurements**
10017,341		Aerosil
14163,848	Aerosil Merck	Aerosil Merck
14310,615		Aerosil
15041,188		Aerosil
15059,240		Aerosil
60501,105	Aerosil Merck	Aerosil Merck
65701,23	Merck	Aerosil
72161,73	Merck	Aerosil
74220,125	Aerosil Merck	Aerosil Merck

All the GRM samples were loaded in the Aerosil silica gel. Some of the lunar samples were loaded in the same silica gel and some in the new Merck finer silica gel, Table 3-3 shows the details.

There was no discernible difference in ratios in either standard cadmium or lunar sample cadmium ratios when changing from one type of silica gel to another, although in some of the smaller lunar samples measured in the finer gel interference from tin was observed. The advantage of using the Merck Silicic acid colloidal solution is that a lunar sample that contains 10 ng to 12 ng of cadmium can now be measured on the Faraday multi collector cups where previously 20 ng to 30 ng of cadmium was the minimum size (Table 3-4).

To load the cadmium sample, contained in a 10 µl drop of phosphoric acid which had been added in the final evaporation stage of the chemistry, it was mixed with 4 µL silica gel and 2 µL phosphoric acid in a PFA beaker. The mix was loaded in 4 µL drops onto the centre filament of the triple rhenium filament and evaporated with the filament at 2 A, until the silica gel fumed and turned white. During the final degas in the mass spectrometer the centre filament was heated to 900 ^{0}C and the side filaments to 1100 ^{0}C.

Table 3-4 A comparison of cadmium ion beams on the Faraday multi collector, with the sample loaded in the Aerosil or Merck silica gel.

Cadmium std	**Aerosil silica gel**	**Merck silica gel**
2 ng	not possible	~$7x10^{-13}$ A
10 ng to 30 ng	0.3 to $6x10^{-12}$ A	$2x10^{-12}$ to $6x10^{-11}$ A
BCR-1		
30 ng	$8x10^{-13}$ A, $2x10^{-12}$ A	
10 ng	not possible	$3x10^{-13}$ to $2x10^{-12}$ A
5 ng	not possible	$2x10^{-12}$ A
2.5 ng	not possible	$2x10^{-13}$ A

Table 3-5 Some of the many methods trialled for loading gadolinium.

$^{158}Gd/^{160}Gd$ beam size (V)	Precision	Sample size	n*	Beaker	Beaker cleaning	Loaded in	Dried in	Filament	Filament cleaned in	GdO	BaF
1.9-4	good	1 µg	10	PFA	HNO_3	HNO_3	air	Ta-Re-Ta	HNO_3	no	no
0.7-1	very good	1 µg	23	PTFE	HNO_3	HNO_3	air	Ta-Re-Ta	HNO_3	yes	lots
0.2	good	3 µg	9	PFA	HCl	HNO_3	air	Ta-Re-Ta	HNO_3	no	lots
1.5-2.4	poor	3 µg	3	PFA	HCl	HNO_3	N_2/air	Ta-Re-Ta	HNO_3	yes	lots
1.5-2	very good	2.5 µg	16	PTFE	HCl	HNO_3	air	Ta-Re-Ta	HNO_3	yes	no
0.7	poor	1 µg	4	PTFE	HF	HCl	air	3xRe	HCl	no	no
0.6	very good	1 µg	21	PTFE	HF	HCl	N_2	3xRe	HCl	no	no
1.7	very good	1 µg	13	PFA	HF	2-mla	air	3xRe	HCl	yes	yes <0.1%
1.5-2	very good	1 µg	15	PFA	HF	2-mla	N_2	3xRe	HCl	no	no
2-6	good	5 µg	14	PFA	HF	2-mla	air	3xRe	HCl	yes	no
1.1-4	good	2.5 µg	14	PTFE	HCl	2-mla	N_2	3xRe	HCl	no	no
1.1	very good	2.5 µg	10	PTFE	HCl	2-mla	air	3xRe	HCl	no	no

*n is the number of sets of 10 ratios run before the ion beam decays.

3.2.3.2 Gadolinium

Gd^+ metal ions were measured in this work to avoid the oxygen corrections and interferences experienced when gadolinium is run as an oxide. Previous measurements of gadolinium by mass spectrometry have been of the oxides (Eugster et al., 1970a and 1970b, Lugmair and Marti, 1971), however Shima et al., 1994 and Hidaka et al., 1995 reported ion beams, with 1 μg of sample, of $2x10^{-11}$ A of ^{158}Gd for one hour with Ta-Re-Ta filaments and of $0.2x10^{-11}$ A ion beams with a triple rhenium filament.

Several loading variables were tested in the VG 354 mass spectrometer (summarised in Table 3-5), filaments (triple Re and triple Ta-Re-Ta), type of beaker (PFA or PTFE), methods of pre-cleaning the beakers (with HCl, HNO_3 or HF), acid for dissolving and loading the sample onto the filament (HNO_3, HCl, or methyl lactic acid), environment for evaporating the sample on the filament (air, or N_2), and pre-cleaning the filament before loading the sample (HNO_3 or HCl). Monitored during measurements was the ion beam size (in volts) , the precision of the measurements, the number of sets of 10 ratios before the ion beam decayed (n), the presence of gadolinium oxide isotopes and barium fluoride interference.

No Gd^+ metal ion beam currents were comparable in size to those achieved by Shima et al., 1994 and Hidaka et al., 1995 on Ta-Re-Ta filaments, so it was decided to use triple rhenium filaments, with the sample loaded in unbuffered methyl lactic acid and dried in air. The filament was pre-cleaned with a 2 μl drop of HCl.

For loading a sample 10 μl of unbuffered methyl lactic was added to the evaporated sample in a PFA beaker, then loaded in 4 μl drops onto the side filaments of a triple filament and slowly evaporated to dryness at 1.5 A, to minimise the formation of oxides. When samples are concentrated in 2 μl phosphoric acid the filament has to be heated to 2.5 A to fully evaporate the sample. Though this sometimes increased the production of gadolinium oxide it did not seem to affect the ionisation of the gadolinium metal beam to any great extent. After loading and drying

the sample the side filaments are moved as close as possible to the centre filament, as shown in Figure 3-16 (c).

For loading a sample 10 µl of unbuffered methyl lactic was added to the evaporated sample in a PFA beaker, then loaded in 4 µl drops onto the side filaments of a triple filament and slowly evaporated to dryness at 1.5 A, to minimise the formation of oxides. When samples are concentrated in 2 µl phosphoric acid the fflament has to be heated to 2.5 A to fully evaporate the sample. Though this sometimes increased the production of gadolinium oxide it did not seem to affect the ionisation of the gadolinium metal beam to any great extent. After loading and drying the sample the side filaments are moved as close as possible to the centre filament, as shown in Figure 3-16 (c).

In the mass spectrometer the gadolinium samples from the GRMs were degassed for five minutes with the centre filament at 1600 ^{0}C and the side filaments at 2.80 A. This was increased for the lunar samples to a 30 minute degas to reduce the loss of pressure experienced during sample measurements.

3.2.3.3 Samarium

Initially the GRM samarium samples were loaded on a single rhenium filament (Figure 3-16 (b)), in 2 M HCl. A change to triple rhenium filaments in May 1995 resulted in a ten times increase in ion beams. The triple filament (Figure 3-16 (c)) was used for all the lunar samples and the final GRMs (which filament was used is detailed in Appendix F, Section 1-3). As with gadolinium the lunar samples were evaporated in 2 µl phosphoric acid. All filaments were cleaned with a 2 µl drop of HCl before loading the sample.

For both single and triple rhenium filaments the loading procedure for samarium was the same. 10 µl of 2 M HCl was added to the evaporated sample in the PFA beaker, it was loaded in 4 µl drops onto a single filament or onto the sides of a triple filament and slowly evaporated to dryness at 1.5 A. With the lunar samples concentrated in 2 µl phosphoric acid the filament had to be heated to 2.5 A to fully evaporate the sample.

The side filaments are moved as close as possible to the centre filament, as shown in Figure 3-16 (c).

In the mass spectrometer the samarium samples from the GRMs were degassed for five minutes with the centre filament at 1500 ^{0}C and the side filaments at 1.4 A. For the lunar samples the degassing was extended to 30 minutes, though the loss of pressure was less with samarium than with the gadolinium samples.

3.2.4 Measurements on the mass spectrometer

When the samples are loaded in the mass spectrometer and the automatic degassing procedure is complete the LOS valve is opened so the measurements can begin.

3.2.4.1 Cadmium

The centre filament was heated to 1100 ^{0}C with the Daly detector in place. The largest isotope ^{114}Cd was focussed and centred (or ^{111}Cd if a tracer was included). If there was a steady ion beam close to $1x10^{-13}$ A from ^{114}Cd the axial collector was lifted and the Faraday multi collector cups put into use. Measurements of cadmium are made with the filament temperature at 1300 ^{0}C to 1350 ^{0}C, and sometimes as high as 1400 ^{0}C.

Cadmium standard samples less than 50 ng and measured on the Faraday had uncertainties for ^{114}Cd/^{112}Cd of 0.01% to 0.003% at the 95% confidence level.

For the GRM and lunar concentration measurements ion currents are 10^{-15} to 10^{-13} A so most measurements are on the Daly detector. For the composition measurements the Faraday was usually used, with ion currents over $2x10^{-13}$ A (details in Appendices F and G).

3.2.4.2 Gadolinium

Gadolinium metal ionises at high centre filament temperatures of 1700 ^{0}C to 1950 ^{0}C and side filament currents of 2.5 A to 4 A.

An initial centre filament temperature of 1650 ^{0}C and side filament current of 2 A was increased slowly to 1750 ^{0}C and 2.5 A to 3 A and sometimes higher, when ionisation occurs and ^{158}Gd can be focussed and centred.

Ion currents of 10^{-13} A to 10^{-15} A for $^{158}Gd/^{160}Gd$ were obtained for the GRM and lunar concentration measurements so most were measured on the Daly, currents of 10^{-12} A to 10^{-15} A allowed most of the composition measurements to be on the Faraday (details in Appendices E and G).

Gadolinium standard samples measured on the Faraday multi collector, with the beakers pre-cleaned in hydrofluoric acid, had uncertainties at the 95% confidence level of 0.001% to 0.0007% for $^{158}Gd/^{160}Gd$. Without beaker pre-cleaning uncertainties were 0.02% to 0.003%.

Rhenium starts evaporating at over 1900 ^{0}C so these high filament temperatures needed to be used with care.

3.2.4.3 Samarium

With the single rhenium filament the samarium oxides ionise at 1250 ^{0}C but decrease when the samarium metal starts ionising at 1350 ^{0}C. Ion beams of $4x10^{-12}$ A with 1 µg samarium laboratory standards, show uncertainties at the 95% confidence level for $^{154}Sm/^{152}Sm$ of from 0.01% to 0.008%.

Using a triple filament the initial temperature was set at 1500 ^{0}C, with the side filaments at 1 A. The samarium metal ionises with the centre filament at 1600 ^{0}C, and side filaments at 1.5 A, at these temperatures the samarium oxide beam decreases. Ionisation of the samarium metal sometimes increases steadily for some time if the side filament temperature is reduced, with good precision measurements resulting. Ion beams of $2x10^{-11}$ A are commonly obtained with 1 µg samarium standard samples. Before the procedures were changed to pre-cleaning the PFA beakers with hydrofluoric acid uncertainties of 0.03% to 0.003% at the 95% confidence level were found for $^{154}Sm/^{152}Sm$, afterwards uncertainties for $^{154}Sm/^{152}Sm$ were 0.001% to 0.003%.

About half of the lunar and GRM concentration measurements, which give ion currents of 10^{-12} A to 10^{-15} A, were on the Faraday multi collectors. When the change was made to triple filaments for the GRM samarium concentration measurements all the data were collected on the

Faraday multi collector, except for PCC-1 (details in Appendices F and G).

3.2.5 Instrument induced isotopic mass fractionation

Instrument induced mass dependent fractionation of isotopes on the mass spectrometer result in a near linear change in the isotope abundances with isotope mass. Normalisation and corrections for fractionation were made using the exponential law (Russell et al., 1978):

$(R^{i/j})_{measured} = (R^{i/j})_{true}(m_i/m_j)^{\phi}$, so $\phi = \ln((R^{i/j})_{measured}/(R^{i/j})_{true})/\ln(m_i/m_j)$,

where $(R^{i/j})$ is the ratio of isotopes i and j, and

for cadmium $(R^{i/j})_{true}$ is $^{110}Cd/^{112}Cd = 0.51928$,

for gadolinium $(R^{i/j})_{true}$ is $^{156}Gd/^{160}Gd = 0.9361$ (Eugster et al., 1970b),

for samarium $(R^{i/j})_{true}$ is $^{147}Sm/^{152}Sm = 0.56081$ (Lugmair, 1975).

So $(R^{i/j})_{true} = ((R^{i/j})_{measured})/(m_i/m_j)^{\phi}$ Equation 3-2.

3.2.5.1 Cadmium

Cadmium was normalised to $^{110}Cd/^{112}Cd = 0.51928$, which was the average value of $^{110}Cd/^{112}Cd$ measured in 1994 using the 111 axial configuration on the VG 354 mass spectrometer. This normalising value was retained in spite of an increase in the average value of $^{110}Cd/^{112}Cd$ of 0.14±0.03% caused by the change in the multi collector cup configuration and drifting in cup sensitivity since that time.

Figure 3-17 compares the raw and normalised data from this work to Rosman and De Laeter (1975). The precision of the Rosman and De Laeter (1975) data was significantly lower than in this work so it seemed appropriate to present the comparison normalised to $^{110}Cd/^{116}Cd$. The laboratory standard data were published uncorrected so has been normalised to $^{110}Cd/^{116}Cd = 1.67870$. The uncertainties in the Rosman and De Laeter (1975) data are to two standard errors of the mean.

The two data sets are in agreement for five ratios, but there is a small difference at 112 and a large one at 108 (-0.28%).

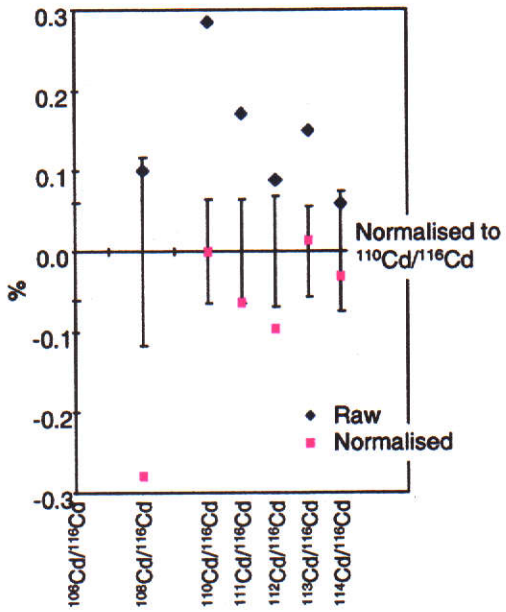

Figure 3-17 Cadmium standard showing the percentage deviation of raw and normalised data for 1997 from Rosman and De Laeter (1975) normalised to $^{110}Cd/^{116}Cd = 1.67870$. Uncertainties are shown at 2 standard deviations for the latter.

3.2.5.2 Gadolinium

Gadolinium was normalised to $^{156}Gd/^{160}Gd = 0.9361$ (from Eugster et al., 1970b). Figure 3-18 gives the percentage deviation from Eugster et al. (1970b) of the raw and normalised gadolinium standard measurements for 1997. Uncertainties which are smaller than the symbols are omitted, the percentage uncertainties on the raw gadolinium data are from measurements on 21/8/97.

There is a poor correspondence at $^{152}Gd/^{160}Gd$ and $^{154}Gd/^{160}Gd$, suggesting either the undetected presence of samarium in the measurements in this work (within experimental uncertainties no samarium was detected), or that Eugster et al. has overcorrected for samarium oxide at masses 168 and 170 (Equation 1, Eugster et al., 1970a). A possible cause of these differences is that the data in this paper are normalised and corrected by the exponential law, it is not clear what method was used by Eugster et al. (1970b).

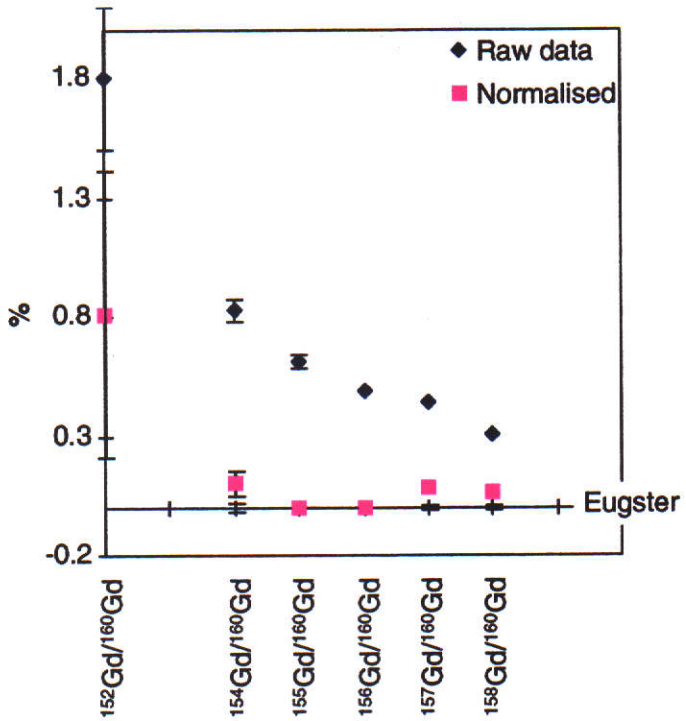

Figure 3-18 Gadolinium standard raw and normalised data for 1997 as a percentage deviation from Eugster et al. (1970b). Uncertainties are all at the 95% confidence level. Uncertainties on the raw data are from one measurements on 21/8/97.

$^{157}Gd/^{160}Gd$ and $^{158}Gd/^{160}Gd$ are 0.8‰ and 0.7‰ higher than Eugster et al. (1970b),possibly from interference by barium fluoride at mass 157 (uncertainties are 0.1‰ and 0.06‰ respectively). Barium fluoride at mass 157 would cause an interference of about 0.01% at ^{156}Gd and ^{155}Gd, too small to identify here, however there was no barium fluoride observed during these measurements. The discrepancy could also be caused by collector bias in the multi collector cups High 1 and High 2, used for $^{157}Gd/^{160}Gd$ and $^{158}Gd/^{160}Gd$. To minimise this possibility standards are always measured on the same day and with the same conditions as the samples.

The normalisation of gadolinium to $^{156}Gd/^{160}Gd$ in any sample which has experienced neutron capture poses a problem as $^{156}Gd/^{160}Gd$ will show an increase as a result of the neutron capture at $^{155}Gd/^{160}Gd$. The isotopes ^{155}Gd, ^{156}Gd, ^{157}Gd and ^{158}Gd are all affected by neutron capture so $^{152}Gd/^{160}Gd$ and $^{154}Gd/^{160}Gd$ are the only possible alternative normalising ratios. However ^{152}Gd and ^{154}Gd are low abundance

isotopes, so measured ratios are of low precision, an uncertainty of about 0.7% in $^{154}Gd/^{160}Gd$ in this work.

Hidaka et al. (1995) measured $^{154}Gd/^{160}Gd$ with an ion current of $>2x10^{-12}$ A, so was able to normalise his neutron irradiated samples to $^{154}Gd/^{160}Gd = 0.09972$. He uses three methods of correcting for the false discrimination effect: normalising to $^{154}Gd/^{160}Gd$, normalising to $^{156}Gd/^{160}Gd = 0.9361$, and normalising to a modified $^{156}Gd/^{160}Gd$, after balancing with a decrement of ^{155}Gd. The latter method is described here.

Table 3-6 Modified normalising values of $^{156}Gd/^{160}Gd$ (Hidaka et al., 1995).

Sample	Neutron fluence ($x10^{15}$ n/cm^2)	$^{156}Gd/^{160}Gd$ = (normalising value)
TMU-STD	0	0.9361
Irradiated STD1	5.94	0.93617
Irradiated STD2	11.2	0.93628
Irradiated STD3	14.0	0.93634

It is assumed that $^{155}Gd/^{160}Gd + ^{156}Gd/^{160}Gd$ is a constant, which is taken by Hidaka et al., 1995 to be 1.6129. For non-irradiated samples $^{156}Gd/^{160}Gd = 0.9361$ is taken as the normalising ratio. For an irradiated sample $^{155}Gd/^{160}Gd_{(1)}$ is first normalised to $^{156}Gd/^{160}Gd_{(1)} = 0.9361$, then a new normalising value $^{156}Gd/^{160}Gd_{(2)}$ is calculated from $1.6129 - ^{155}Gd/^{160}Gd_{(1)}$. A new $^{155}Gd/^{160}Gd_{(2)}$ is found by normalising to $^{156}Gd/^{160}Gd_{(2)}$. This is continued until $^{156}Gd/^{160}Gd_{(n)} = ^{156}Gd/^{160}Gd_{(n+1)}$ and it is repeated for each irradiated sample (Table 3-6).

In this work all samples were normalised to $^{156}Gd/^{160}Gd = 0.9361$. In addition the lunar samples were normalised to values of $^{156}Gd/^{160}Gd$ calculated by the Hidaka et al. (1995) iterative method.

3.2.5.3 Samarium

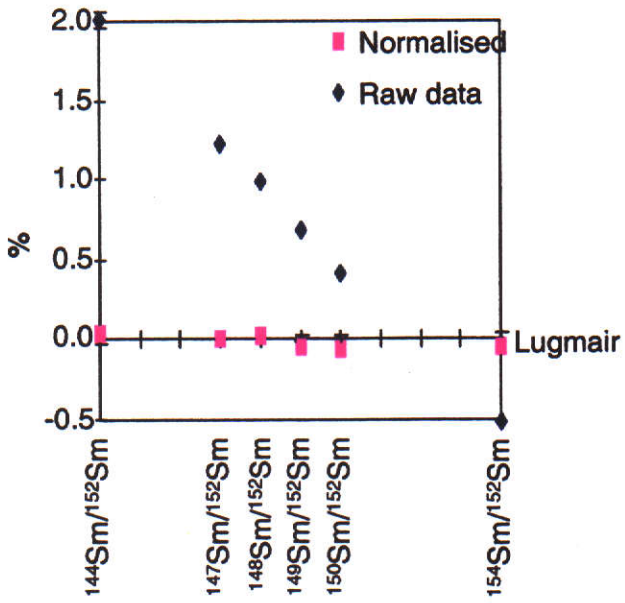

Figure 3-19 Samarium standard raw and normalised data for 1997 as a percentage deviation from Lugmair (1975). Uncertainties are all at the 95% confidence level. Uncertainties on the raw data are from one measurements on 6/6/97.

Figure 3-19 gives the percentage deviation from Lugmair (1975) of the raw and normalised samarium standard measurements for 1997 from this work. The percentage uncertainties on the raw samarium data are from measurements on 6/6/97, if uncertainties are smaller than the symbols they are not included. Samarium was normalised to $^{147}Sm/^{152}Sm = 0.56081$ (from Lugmair, 1975). There was a good correspondence with the normalised data which were at the most 0.06% from the Lugmair (1975) values.

As neutron capture on samarium occurs at ^{149}Sm only ^{149}Sm and ^{150}Sm are affected, so no modification needs to be made of the normalising ratio, which is $^{147}Sm/^{152}Sm = 0.56081$.

3.2.6 Interferences

3.2.6.1 Cadmium

Interferences from palladium (at isotopes 106, 108 and 110), tin (at isotopes 112, 114 and 116) and indium (at isotope 113) are possible (listed in Table 2-4) and a visual check was always made. No palladium interferences were observed, tin and indium were additionally monitored at mass 115. Any indium detected in concentration measurements was always less than 0.2% of the cadmium ratio at $^{113}Cd/^{112}Cd$, and if observed $^{111}Cd/^{113}Cd$ was not used for the calculations. Because of the low abundance of tin at mass 115 this is not the ideal isotope to monitor, but the wide mass range of cadmium and tin isotopes do not fit into the multi-collector cups. Section 6.3.1 describes the minimal amount of tin found in some of the smaller lunar samples.

Table 3-7 Calculated isotopic interferences from $CaPO_2$ and H_2CaPO_2.

Isotope	Cadmium (%)	Abundance ratios of $CaPO_2$ relative to 103	Abundance ratios of H_2CaPO_2 relative to 105
103		1	
104		0.00037089	
105		0.00864845	1
106	1.2	0.00134452	0.0005209
107		0.02199507	0.0086485
108	0.9	0.00001364	0.0013458
109		0.00007799	0.0219953
110	12.4	0.00000003	0.0000169
111	12.8	0.00184704	0.0000780
112	24.0	0.00000069	0.0000000
113	12.3	0.00000378	0.0018470
114	28.8	0	0.0000010
115			0.0000038
116	7.6		0

Frequently seen interferences at low temperatures were combinations of $CaPO_2^+$ and related molecular ions, listed in Table 3-7, observed from mass 103 to 109. The interferences were always negligible at the

operating temperatures used to measure cadmium (1300 ^{0}C to 1350 ^{0}C). They are shown in Figure 3-20 at 1149 ^{0}C, 1170 ^{0}C and 1227 ^{0}C.

In the Figure related interferences are observed at 105, 106, 107, 108 an 109, while at $^{110}Cd/^{112}Cd$ there is no such interference. It can be seen that the data points in Figure 3-20 at 1227 ^{0}C for $^{106}Cd/^{112}Cd$, $^{108}Cd/^{112}Cd$ and $^{110}Cd/^{112}Cd$ are in proportion to cadmium isotopes, whose ratios at these masses are $^{106}Cd/^{112}Cd$ = 0.05418, $^{108}Cd/^{112}Cd$ = 0.037067 and $^{110}Cd/^{112}Cd$ = 0.5128.

In Figure 3-21 similar data at temperatures of 1256 ^{0}C to 1329 ^{0}C confirm that the molecular ions at 103/112 and 105/112 are not present at 113/112, so do not interfere at $^{113}Cd/^{112}Cd$. The scatter at $^{113}Cd/^{112}Cd$ is around $^{113}Cd/^{112}Cd$ = 0.506171. Other measurements have confirmed that the same is true for $^{111}Cd/^{112}Cd$, $^{114}Cd/^{112}Cd$ and $^{116}Cd/^{112}Cd$.

It was unclear exactly what combination of molecular ions were interfering, but they were no longer present at cadmium operating temperatures.

The interference from $CaPO_2$ and related ions was reduced when calcium was more efficiently removed from the cadmium sample during the chemistry and also from more effective degassing in the mass spectrometer. Because phosphoric acid (H_3PO_4) is used to load cadmium onto the filament it is unlikely that this interference can be completely eliminated.

Though a double tracer $^{106 \text{ and } 111}Cd$ was used for the concentration measurements, IDMS calculations have only been done with the enhanced ^{111}Cd because of the uncertainty caused by the $CaPO_2$ interference at mass ^{106}Cd.

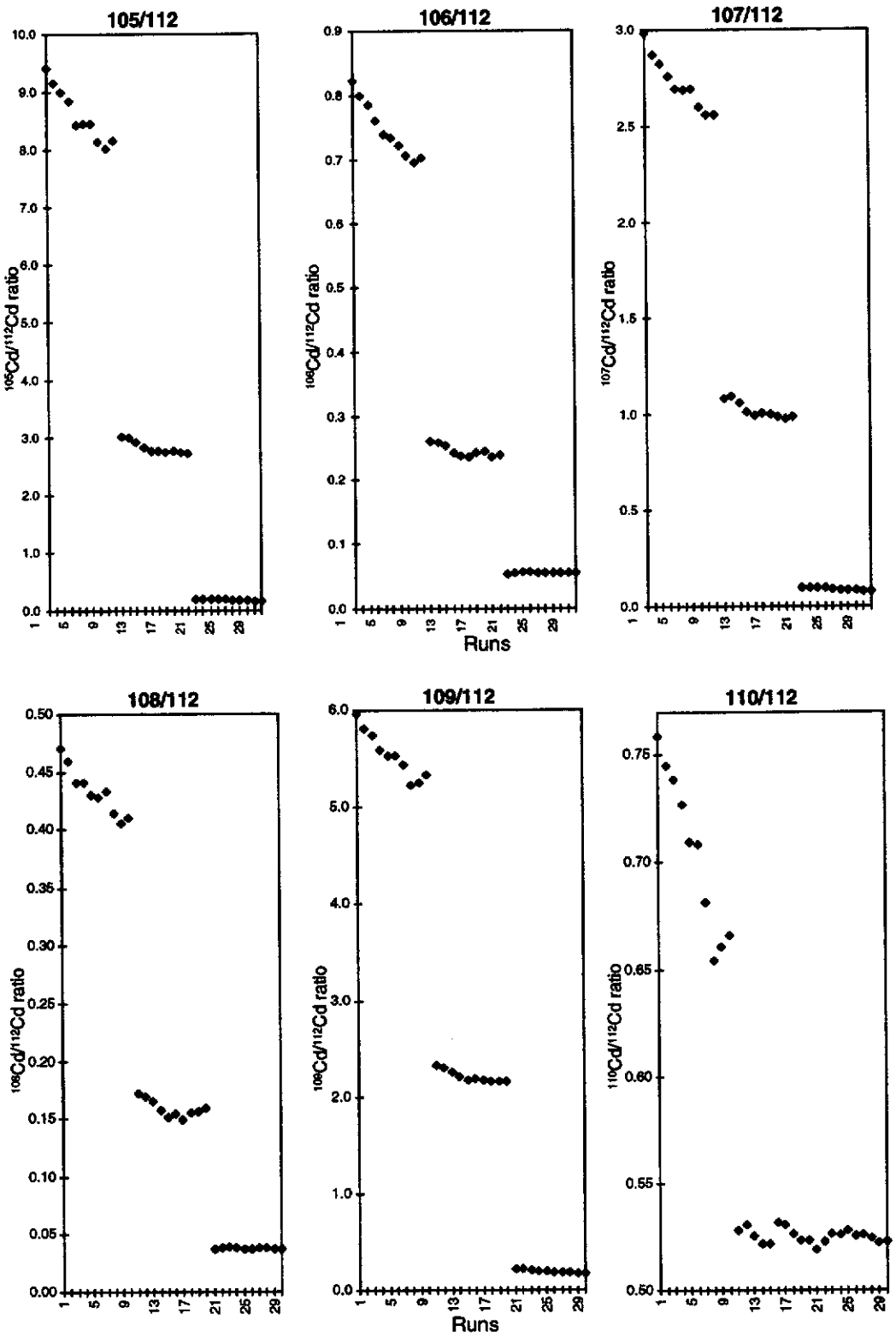

Figure 3-20 A comparison of six ratios referenced to ^{112}Cd at three filament temperatures, 1149 ^{0}C, 1170 ^{0}C and 1227 ^{0}C, to observe the relationship between molecular ions and cadmium.

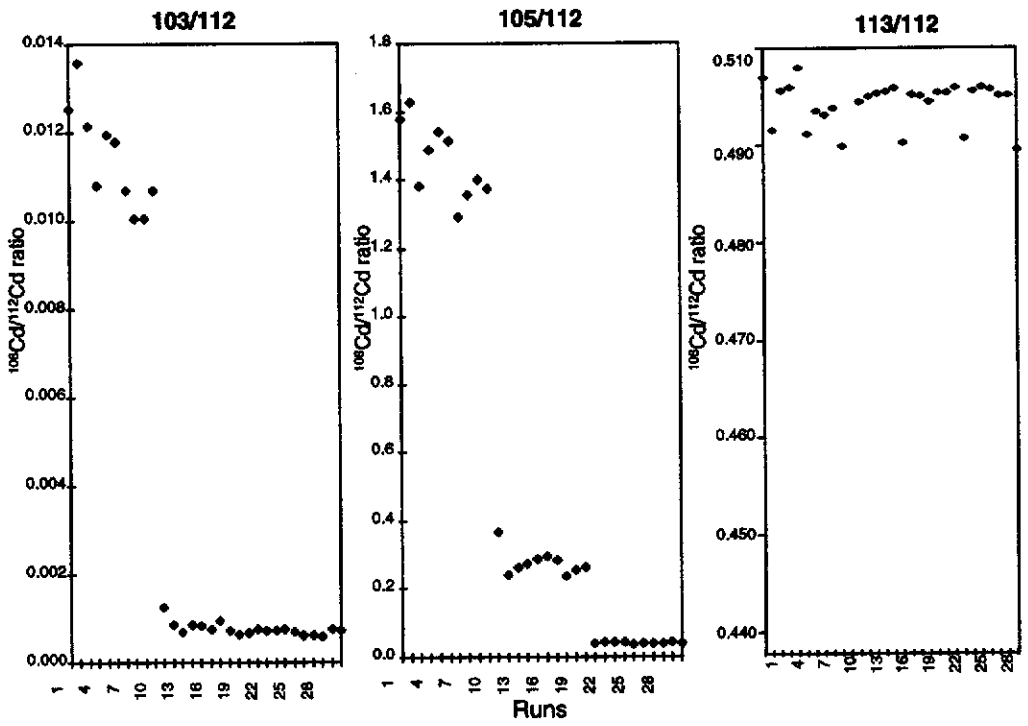

Figure 3-21 A comparison of three ratios referenced to ^{112}Cd at three filament temperatures, 1256 ^{0}C, 1282 ^{0}C and 1329 ^{0}C, to observe the relationship between molecular ions and cadmium.

3.2.6.2 Gadolinium

Samarium, samarium oxide, barium fluoride, barium oxide, dysprosium and several rare earth oxides are likely to interfere with gadolinium metal isotopes (listed in Chapter 2, Table 2-15). Efficient chemistry can remove most of the rare earths from the sample, but it was necessary to monitor lanthanum oxide (which interferes with gadolinium at mass 155), neodymium oxide (at masses 158 and 160), dysprosium (at 156, 158 and 160) and samarium (at 152 and 154). Lanthanum, neodymium and dysprosium ionise at lower temperatures than gadolinium, so do not usually cause a problem. Barium oxide was rarely seen, and was not present at the higher temperatures needed to ionise gadolinium.

Samarium can interfere at mass 152 which is the position of the ^{152}Gd tracer, so samarium must always be monitored at 149 or 150 during concentration measurements.

Improved chemistry and cleaning of beakers has minimised interference by barium fluoride which can interfere with gadolinium at ^{154}Gd to ^{157}Gd. If any barium fluoride is detected it will decay at the high

temperatures used to ionise gadolinium. Barium fluoride can be monitored at 149, 151 or 153, though at 149 it can be concealed by samarium and at 151 and 153 by europium. Barium fluoride isotopes do not occur at masses 152, 158 or 160, so can be disregarded during concentration measurements.

3.2.6.3 Samarium

Only gadolinium, neodymium or barium fluoride are likely to interfere with samarium metal ions (Chapter 2, Table 2-15). Neodymium was rarely present and decays at a low temperature, whereas gadolinium requires too high an ionisation temperature to interfere with samarium. Barium fluoride was monitored at mass 157.

3.3 Summary

The main features of the two thermal ionisation mass spectrometers used in this work, the VG 354 and AEI MS12, were described in this Chapter, including the procedures for measuring cadmium, gadolinium and samarium, sample loading techniques, and the filaments and beads on which samples are loaded. The manual positioning of the multi-collector cups and controlling the VG 354 mass spectrometer are covered; laboratory standard measurements compared to published data; and machine induced mass fractionation and normalisation described. Interfering isotopes, isobaric with cadmium, gadolinium and samarium, were considered.

The Chapter is supplemented by Appendix E.

4. The lunar samples

4.1 The Moon

4.1.1 Introduction

Since 1969 and the first manned lunar landings the understanding of the formation and history of the Moon has expanded rapidly. US and Soviet manned and unmanned missions have brought back new data, and approximately 382 kg of soil and rock. More recently ten lunar meteorites have been collected from Antarctica. The chemical and physical measurements of this material, together with new data from satellites such as Galileo, Clementine and the Lunar Prospector, are the main sources of recent information about the Moon.

4.1.2 Lunar evolution

Pyroxene, olivine, plagioclase and ilmenite are the major mineral types on the Moon, suggesting that after accretion and melting about 4.6 billion years ago the Moon cooled slowly and differentiated. It is thought that an outer low density plagioclase crust (dated 4.3 to 4.6 billion years) floated on a deep layer of essentially olivine and pyroxene with a magma ocean rich in incompatible trace elements sandwiched between the two.

The oldest of the highland rocks are ferroan anorthosites, 75% plagioclase, rich in Ca and Al. Also found in the highlands are magnesium-rich rocks and KREEP rocks enriched in potassium, rare earth elements and phosphorous with high levels of U and Th (dated 4.35 billion years). The highlands cover 70% of the nearside and almost all the far side of the Moon.

The average lunar crust has a positive europium anomaly compared to the other rare earth elements, while the average mare basalts have a negative europium anomaly, suggesting that the europium rich plagioclase was separated from the deep magmas, which were the source regions for the varied Fe and Ti-rich mare basalts.

Mare volcanism was active 3.9 billion years ago, while the Moon was still being heavily bombarded, but ceased about 3 billion years ago.

4.1.3 Lunar surface layer, surface mixing

The lunar surface has been cratered and the surface broken down to a fine grained powdery layer (the regolith) by the continuous bombardment of high velocity meteorites ranging in size from micro-meteoroids less than 1 mm in diameter to meteorites 100s of km in diameter. Between 3.92 and 3.85 billion years ago the cratering was very intense and resulted in the massive basins which were subsequently filled with lava. Impacts have continued at a reduced rate resulting in a regolith, layered by ejecta, and well mixed to several metres. In contrast to the surface of the earth the lunar surface is relatively undisturbed by erosion and weathering, meteorite impact is the major transport process, so most of the surface is more than 4 billion years old. Taylor (1975 and 1982) provide informative overviews of research following the Apollo Missions.

Small impacts by centimetre and smaller particles erode the lunar rocks with an erosion rate of $1mm/10^6$ years on a typical 1 kg rock, while larger impacts will fragment it.

4.2 The lunar samples

From 1964 to 1974 various US (Ranger and Surveyor) and Russian (Luna) unmanned flights landed on the Moon and returned photographs, data on the soil, chemical analyses and radiation environmental studies. Between 1970 and 1976 Luna 16, Luna 20 and Luna 24 returned 300 g of mare soil and highland material from on and near Mare Fecunditatis and Mare Crisium. Six manned Apollo missions landed on the Moon in 1969, 1971 and 1972 and returned with 382 kg of rock and soil samples.

Nine lunar soil samples are held by this laboratory. Only five of the samples have been previously measured for samarium and gadolinium isotopic abundances. None have previously been measured for cadmium isotope abundances.

4.2.1 Lunar samples

Samples are handled and processed to ensure that they are always physically protected and their integrity maintained.

The samples from the Apollo 11, 12 and 14 missions were taken to the Lunar Receiving Laboratory where they were placed in quarantine until

biological tests had been completed under vacuum. All the samples are stored and studied in cabinets filled with flowing high purity nitrogen gas (Morris et al., 1983a).

Table 4-1 The lunar samples held at this laboratory.

Mission	Sample	Description	Weight (g)
Apollo 11	**10017,341**	Internal, documented + locatable chips	1.003
Apollo 14	**14163,848**	Fines (<1 mm)	0.505
	14310,615	3 interior chips	1.014
Apollo 15	**15041,188**	<1 mm	0.501
	15059,240	4 fresh interior chips	0.511
Apollo 16	**60501,105**	Fines (<1 mm)	0.501
	65701,23	Spare (<1 mm)	0.510
Apollo 17	**72161,73**	Fines (<1 mm)	0.501
	74220,125	Reserve	1.000

Nearly all samples were sieved. Apollo 14, 15, 16 and 17 were screened at 10 mm, 4 mm, 2 mm and 1 mm grain sizes.

Lunar samples held by this laboratory are listed in Table 4-1

4.2.2 Numbering of samples

The Apollo missions are identified by the first one or two numbers, for example 10 is for Apollo 11, then 12, 14 and 15 for Apollo 12, 14 and 15 and 6 and 7 for Apollo 16 and 17.

For Apollo 11 to 15 samples the final 3 digits identify the sample, for example 10084 is sample number 84 collected on the Apollo 11 mission, 15455 is sample 455 from Apollo 15.

For Apollo 16 and 17 the second number becomes that of the station on the traverse, so that 66095 is sample 095 from station 6 of Apollo 16. The final digit specifies whether the sample is an unsieved soil (0), a sieved fraction of a soil (1 to 4) or a rock (5 to 9).

Splits from samples are listed by additional digits, separated by a comma, for example 15455,20 is split 20 from rock 15455 (Heiken et al., 1991 and Morris et al., 1983a).

4.2.3 Apollo 11

4.2.3.1 Apollo 11 landing site

This first manned landing on 20th July, 1969, lasted just under 2½ hours and collected a total of 21.6 kg of samples. The landing site ($0^0$67' N and $23^0$49' E) in the south west of Mare Tranquillitatis is about 40 km from the mare/highland boundary. The surface is flat, with many craters of 0.3 to 20 m in diameter and a few large boulders, and sits between the rays of the 180 m diameter West crater.

Two chemically distinct basalts of different ages have been identified, suggesting two lava flows. Some samples have their sources in the highlands (Heiken et al., 1991).

4.2.3.2 Apollo 11 sample collection at the lunar surface

The teflon sampler bag, aluminium scoops and return containers and other tools were designed for ease of use and minimum contamination. The 47.5 cm x 28.75 cm x 20 cm aluminium Apollo lunar sample return containers (ALSRC) maintained the bulk samples in a vacuum for the return journey. A 1 kg "contingency sample" of rock fragments and soil was returned to earth in a cloth bag. A 15 kg bulk sample was scooped and placed in the ALSRC 1003.

Two 2 cm drive tube core samples, sealed on the lunar surface, and a final 6 kg of selected samples (including 10017) were returned in ALSRC 1004 (Morris et al., 1983a).

4.2.3.3 Apollo 11 sample handling

Samples removed from the spacecraft were taken to the Mobile Quarantine Facility, enclosed in plastic bags, then transferred to the Lunar Receiving Laboratory.

During the description and splitting operation of sample 10017 (and some others) a leak developed in one of the gloves, but the pressure did not rise above 2 cm of mercury (about $3x10^3$ Pa). The whole system was then re-sterilised with dry heat before reducing the pressure again to $1.3x10^{-4}$ Pa, and continuing classification (Kramer et al., 1977).

4.2.3.4 Sample 10017,341

10017,341 is part of rock 10017 (16 cm x 11 cm x 6 cm and 973 g) and comes from a subdivision of the chip 10017,280 (13.07 g) which was split from 10017,15 (8 cm x 6 cm x 4.5 cm, 197.4 g), which was split from 10017. Sample 10017,341 is from the interior of rock 10017. Photographs of the preparation of sample 10017,341 are shown in Appendix H, Figures 1-1 (a), (b), (c) and (d).

Sample 10017 is described as a vesicular basalt, black and white on fresh surfaces to steel grey on sawed (Kramer et al., 1977). It is a high-Ti mare basalt; with the major minerals pyroxene, olivine, plagioclase and ilmenite (Heiken et al., 1991).

4.2.4 Apollo 14

4.2.4.1 Apollo 14 landing site

The third successful landing on 31st January, 1971 was at the Fra Mauro formation ($3^0$40' S and $17^0$28' E). It lasted 9 hours 23 minutes, covered 3½ km and 42.3 kg of material was collected.

A hilly region north of the ancient Fra Mauro Crater, the area has impact-ejecta ridges made of large blocks radiating from the Imbrium Basin containing highland debris and a variety of mare basalt fragments. The Cone Crater breaks one of the ridges, this was the first highland site visited, and had a large number of craters (Heiken et al., 1991). All samples were breccias and breccias within breccias except for the soils and four crystalline rocks (Taylor, 1975).

4.2.4.2 Apollo 14 sample collection at the lunar surface

A contingency sample was collected first. Most samples were documented by photographs from different angles both before and after the samples were collected.

A special trenching tool was used on this mission and three 2 cm drive tube cores collected. The "Modularised Equipment Transporter", somewhat like a wheelbarrow, was pulled by the astronaut and contained tools and samples (Morris et al., 1983a).

4.2.4.3 Apollo 14 handling

Samples were processed in stainless steel nitrogen filled glove cabinets, under negative pressure. They were sieved into >1 cm, 4-10 mm, 2-4 mm, 1-2 mm and <1 mm fractions which were stored in stainless steel cans (Morris et al., 1983a).

4.2.4.4 Sample 14163,848

The soil sample 14163 was collected 15 m NW of the Lunar Module at the end of the first sortie. It was a surface sample, with scoop depths of several centimetres from the bottom of a one metre secondary crater, with glass in the bottom (Morris et al., 1983a). The sample contains a high proportion of fused soil, and some highland material.

Sample 14163,848 is <1 mm fines.

4.2.4.5 Sample 14310,615

This crystalline rock sample was collected on the way back from the second outing to the rim of Cone Crater at Station G. The position was not well documented, with no surface photos. The rock had a mass of 3439.0 g and was 19 cm x 14 cm x 11 cm and is unusual in that the rounded and smooth upper surface has been exposed for some time, while the lower, angular, surface has been buried in the regolith with no tumbling.

Sample 14310,615 was chipped from the upper exterior surface of 14310,35 (626 g), which was sawn from 14310, photographs are shown in Appendix H, Figures 2-1 (a), (b), (c), (d), (e), (f) and (g).

Rock 14310 is a medium, grey, blocky melted rock, fine grained and homogeneous in mineralogy (Carlson and Walton, 1978). Though it was at first presumed igneous, it is a polymict rock, melted during an impact, and enriched in meteoroid siderophile elements. It shows enrichment in the light rare earth elements and a negative europium anomaly (Heiken et al., 1991).

4.2.5 Apollo 15

4.2.5.1 Apollo 15 landing site

The Apollo mission landed on 30th July, 1971 at the Hadley-Apennine region ($26^0$06' N and $3^0$39' E) at the eastern end of the Imbrium Basin. The mission lasted 18½ hours, covering 28 km and collecting over 77 kg of material assisted by the Lunar Roving Vehicle (LRV), which was first used on this mission.

The lava filled landing site on Palus Putredinis is situated at a complex highland-mare boundary, where the east of the Imbrium Basin meets with the massifs and highlands of the Apennine region. The site is crossed by rays and the long, deep, Hadley Rille.

The great variety of samples reflects the varied history of the site, two distinct basalts were found here, highland material of a variety of rock types, and two unusual volcanic materials, an aluminous non mare basalt, rich in KREEP and an emerald green glass of primitive composition (Ryder, 1985).

4.2.5.2 Apollo 15 sample collection at the lunar surface

A contingency sample was collected first. An adjustable scoop skimmed the upper 1 cm, or scooped 1 to 5 cm, or selected from layers exposed in trench walls. The rake used to collect small rock samples was also used to collect the accompanying soil. Documentation was assisted by photographs taken from different directions both before and after sample collection. Three 4 cm drive cores were collected, and one drill core, 237 cm deep (Morris et al., 1983a).

4.2.5.3 Apollo 15, 16 and 17 handling

The samples from these missions were handled in a similar way. No more quarantine was required so samples were processed in stainless steel nitrogen filled glove boxes. Documented bags were opened, photographed and described and rocks >1 cm were removed. The remains were sieved as with the Apollo 14 samples. Any large or spectacular fragments were picked from the drill cores (Morris et al., 1983a).

4.2.5.4 Sample 15041,188

This dark grey <1 mm soil was collected from near the surface of the deep trench located 12 m SW of a 5 m diameter crater at Station 8, near the Apollo Lunar Surface Experiments Package (ALSEP). There is a smooth hummocky surface of fine grained material with rare, cobbled sized fragments not visibly related to any particular crater. The trench wall was uniform, with perhaps slight colour darkening in the middle part above a hard layer at about 35 cm (Morris et al., 1983a). Sample 15041,188 was part of the 269.6 g 15041 sample.

4.2.5.5 Sample 15059,240

This angular, tough, dull grey rock was also collected at Station 8, 15 m S of the ALSEP central station. Sample 15059,240 consists of four fresh interior chips from 15059,235 which was chipped from 15059,0, which was sawn from 15059,0 (Appendix H, Figures 3-1 (a), (b), (c), (d), (e) and (f)). 15059 is a glass coated regolith breccia containing mare basalt and KREEP basalt fragments and glass (Ryder, 1985).

It shows enrichment in the light rare earth elements and a negative europium anomaly.

4.2.6 Apollo 16

4.2.6.1 Apollo 16 landing site

This mission to the lunar highlands landed on 21st April, 1972 on heavily cratered plains near the Descartes highlands ($8^0$60' S and $15^0$31' E). Twenty seven kilometres was covered in just over 20 hours and 96 kg of material was collected.

None of the expected volcanic rocks were found at this site in the central lunar highlands, a very heavily cratered area. Samples, all impact products, were taken from the Cayley plains, the hilly Descartes material, and the lunar highlands, distant from any mare.

4.2.6.2 Apollo 16 sample collection at the lunar surface

The same equipment and procedures were used as Apollo 15. On this mission five 4 cm drive cores, and one 2 cm drill core 221 cm deep were collected (Morris et al., 1983b).

4.2.6.3 Sample 60501,105

The sample was raked surface soil <1 mm collected at Station 10 near ALSEP, and approximately 100 m SW of the Lunar Module. The surrounding area is level with 2-3 cm pebbles exposed on the surface. 60601,105 is part of the 433.8 g 60501 sample.

4.2.6.4 Sample 65701,23

This olive grey <1 mm soil was from the interior wall of a 20 m diameter crater, very close to the rim, near Station 5 and is surface soil to accompany a rake sample. The sample area has a mostly sandy surface with no large blocks nearby.

65701,23 was part of the 171.3 g 65701 sample.

4.2.7 Apollo 17

4.2.7.1 Apollo 17 landing site

The Taurus-Littrow valley ($20^0$10' N and $30^0$46' E) was the landing site of the Apollo 17 mission, on 11th December, 1972. Thirty kilometres were covered in 22 hours, and 110½ kg collected.

The steep sided Taurus-Littrow Valley, flooded with mare basalt, is situated at the highland/mare boundary of the south east rim of the Serenitatis Basin. Large boulders have rolled down the slopes and some of the many craters are covered by an avalanche from the South Massif.

The valley floor was found to consist of several high-Ti basalts, 3.8 to 3.7 billion years. The North and South Massifs could be deposited ejecta from the Serenitatis basin, dated 3.87 billion years. Orange and black glass fragments with high-Ti basaltic composition, 3.64 billion years, were found on the valley floor (Heiken et al., 1991).

4.2.7.2 Apollo 17 sample collection at the lunar surface

Collection and documentation are the same as for Apollo 15 and 16. Samples were collected without leaving the LRV. Photographs were taken before reaching the sample area, then the astronauts drove up and collected samples. Three trenches were dug and five 4 cm drive cores and one 2 cm drill core 292 cm deep were extracted (Morris et al., 1983b).

4.2.7.3 Sample 72161,73

This olive grey <1 mm soil sample was a surface sample from a "typical dark matter" flat area with sparse fragments collected from the LRV Station 3, between ALSEP and Station 2. 72161,73 was from the 162.5 g 72161 sample.

4.2.7.4 Sample 74220,125

This soil is from a 0.8 m wide band of orange glass (high Ti with Cd higher than in the mare basalts), bordered by light grey soil and underlain by a black clastic deposit, collected from a 6-8 cm deep trench near the low place on the rim of 120 m diameter Shorty Crater at Station 4 (Morris et al., 1983b).

74220,125 comes from the 1171.0 g 74220 sample held in reserve.

5. Elemental abundance of cadmium, gadolinium and samarium

Elemental concentration measurements using the technique of isotope dilution mass spectrometry (IDMS) from Webster (1960), is described in Section 5.1.

The concentrations of cadmium, gadolinium and samarium in seven geochemical reference materials are presented in Section 5.2, the lunar samples in Section 5.3 and the analytical blanks in Section 5.4.

A detailed description of the procedures used during the mass spectrometry measurements are in Appendix F.

5.1 Isotope dilution mass spectrometry (IDMS)

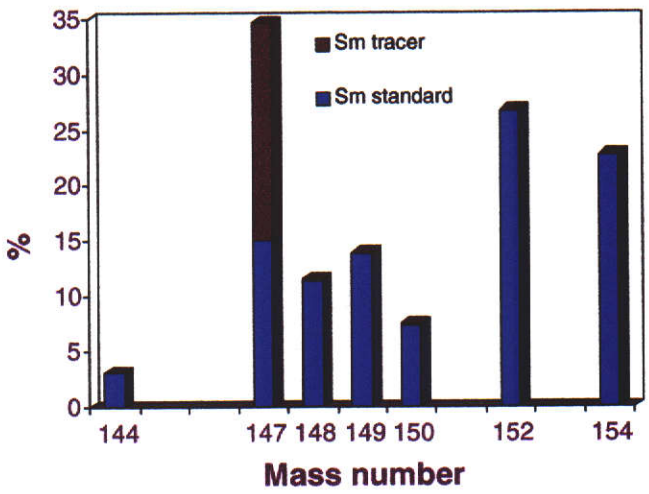

Figure 5-1 A samarium terrestrial standard sample with a measured mass of ^{147}Sm tracer added.

In IDMS a known quantity of tracer is added to a sample. The change in the abundances of the isotopes of the element being measured allows the mass of the element in the sample to be calculated, using Equation 5-1.

5.1.1 Calculation of the concentrations

The following equation is used to calculate the concentrations (Webster, 1960):

$$W_N = W_T \times \frac{\sum_{i=1}^{i=n} N_{ik} M'_i}{\sum_{i=1}^{i=n} T_{ik} M'_i} \times \left[\frac{T_{ik} - M_{ik}}{M_{ik} - N_{ik}} \right]$$

Equation 5-1

Where T_{ik}, M_{ik} and N_{ik} are the ratios of isotope i and reference isotope k of the Tracer, Mix (of Natural and Tracer) and Natural samples. W_T and W_N are the mass of the tracer added to the sample and the mass in the sample of the element being measured. M'_i is the atomic mass of the ith isotope of the element being measured. The atomic masses used in the calculation are listed in Table 5-1.

Having found W_N, the concentration of the element in the sample is found by:

$$\text{Concentration} = \frac{(W_N - \text{Blank})}{\text{Sample} \cdot \text{Mass}}$$

where Blank is the analytical blank for the complete digestion, extraction and mass spectrometry process.

In this work two different reference isotopes k have been used for each element, for cadmium, the ratios $^{111}Cd/^{112}Cd$ and $^{111}Cd/^{113}Cd$, for gadolinium $^{152}Gd/^{160}Gd$ and $^{152}Gd/^{158}Gd$, and for samarium $^{147}Sm/^{152}Sm$ and $^{147}Sm/^{149}Sm$. The mean of the two calculations of W_N is recorded.

Table 5-1 The atomic masses of cadmium, gadolinium and samarium used for IDMS.

Atomic masses of cadmium isotopes (Audi and Wapstra, 1993)							
106	**108**	**110**	**111**	**112**	**113**	**114**	**116**
105.906461	107.9041863	109.903006	110.904182	111.9027577	112.9044014	113.9033586	115.904756

Atomic masses of gadolinium (Audi and Wapstra, 1993)						
152	**154**	**155**	**156**	**157**	**158**	**160**
151.919789	153.920862	154.922619	155.922120	156.923957	157.924101	159.927051

Atomic masses of samarium (Audi and Wapstra, 1993)						
144	**147**	**148**	**149**	**150**	**152**	**154**
143.911996	146.914894	147.914832	148.917180	149.918656	151.919729	153.922206

5.1.2 Uncertainty in concentration calculations

Uncertainties in the concentration of the element are calculated using the equations below for each part of Equation 5-1. Equation 5-2 and Equation 5-3 give the uncertainty of the terms in brackets and those outside the brackets respectively.

The general principles used in this work to calculate the uncertainties are:

- For addition and subtraction the absolute uncertainty is found from the square root of the sum of the squares of the absolute uncertainties for each term.
- For division and multiplication the fractional uncertainty is found from the square root of the sum of the squares of the fractional uncertainties of each term.

The uncertainty of the terms inside the brackets in Equation 5-1 is:

$$\sqrt{\left[\frac{(\Delta M_{ik})^2+(\Delta N_{ik})^2}{(M_{ik}-N_{ik})^2}\right]+\left[\frac{(\Delta T_{ik})^2+(\Delta M_{ik})^2}{(T_{ik}-M_{ik})^2}\right]} \qquad \text{Equation 5-2}$$

where Δ is the absolute uncertainty and N, M and T are the same ratios as in Equation 5-1. The uncertainties of the measured ratios are in all cases at the 95% confidence level.

The uncertainty of the terms not in the brackets in Equation 5-1 is:

$$\left[\frac{\Sigma\left(\Delta N_{ik}^{\ 2}\right)}{(\Sigma N_{ik}M')^2}\right]+\left[\frac{\Sigma\left(\Delta T_{ik}^{\ 2}\right)}{(\Sigma T_{ik}M')^2}\right]+\left(\frac{\Delta W_T}{W_T}\right)^2 \qquad \text{Equation 5-3}$$

The absolute uncertainty in the mass of the element in the sample (ΔW_N) is found by taking the square root of the sum of Equation 5-2 and Equation 5-3, then multiplying by the calculated mass of the element (W_N).

$\Delta W_N = W_N * \sqrt{(}$Equation 5-2 +Equation 5-3)

The absolute uncertainties ΔN_{ik} and ΔT_{ik} in Equation 5-3 have been calculated with the assistance of a programme which uses the Monte Carlo method (Holmes and Rosman, 1995).

The uncertainty in the concentration requires another step:

$$\Delta Conc = Conc * \sqrt{\left(\frac{(\Delta W_N)^2 + (\Delta Blank)^2}{(W_N - Blank)^2}\right) + \left(\frac{\Delta W_{sample}}{W_{sample}}\right)^2} \qquad \text{Equation 5-4}$$

where the absolute uncertainty in the concentration of the element and in the analytical blank are $\Delta Conc$ and $\Delta Blank$, and Conc is the measured concentration.

The uncertainties in the concentration measurements therefore includes uncertainties in the measured ratios (at the 95% confidence level), in the tracer calibration (0.2% to 0.4%), in the weight of the tracer added (0.2%), the weight of the sample (0.2%), and in the analytical blank.

5.2 Cadmium, gadolinium and samarium concentrations in the geochemical reference materials (GRM)

The concentration of cadmium, gadolinium and samarium in seven GRMs, measured in this work by IDMS, are presented in Tables 5-3, 5-4, and 5-5. Details of the mass spectrometry procedures are given in Section 5.2.1 and Appendix F, Section 1.

5.2.1 General procedures for the GRM samples

Seven United States Geological Survey (USGS) GRMs, supplied as rock powders in glass bottles, were analysed in this study. In Table 5-2 details of the samples, the original weight and the dry weight (described in Chapter 2, Section 2.6).

Cadmium, gadolinium and samarium tracers were added to the samples at the start of the digestion (details of tracers added to each sample are listed in Appendix F, Section 1). Uncertainties in the weight of the tracer solutions are ±0.2 mg for measurements taken to one decimal

place and ±0.05 mg for measurements taken to two decimal places. The uncertainty in the concentration of the tracer (at the 95% confidence level) was included in the final uncertainty.

Table 5-2 The seven geochemical reference materials with the initial weight and the dry weight after heating.

Sample	Sample weight (mg)	Dry weight (mg)	Date
BCR-1 Columbia River basalt split 76 position 29	138.7 115.6	136.1 113.4	22/9/94 22/9/94
BHVO-1 Hawaiian basalt split 8 position 1	154.7 141.1 132.65	153.0 139.6 131.23	22/9/94 9/11/94 6/6/95
BIR-1 Icelandic basalt no. 1135	101.1 168.6 124.9 125.13	100.6 167.8 124.3 124.55	9/11/94 9/11/94 12/1/95 8/5/95
DNC-1 North Carolina dolerite no. 0478	108.7 105.0 157.09 137.5 120.43	107.9 104.2 155.88 136.4 119.50	6/2/95 6/2/95 8/5/95 8/5/95 6/6/95
MAG-1 Marine mud, Gulf of Maine, split 63 position 19	116.6 133.9	112.4 129.1	9/1/95 9/1/95
PCC-1 East Austin Creek peridotite split 51 position 10	102.8 203.4 209.81	102.1 202.1 208.47	6/2/95 27/2/95 6/6/95
W-2 Centreville diabase no. 1221	194.6 115.4 129.25	191.4 113.5 127.13	27/2/95 27/2/95 6/6/95

The samples of MAG-1 and PCC-1 had a very fine carbon residue left after digestion was complete, but of negligible mass compared to the sample.

5.2.2 Concentrations in the geochemical reference materials

The cadmium, gadolinium and samarium concentrations in BCR-1, BHVO-1, BIR-1, DNC-1, MAG-1, PCC-1 and W-2, listed below, have been published in Sands and Rosman (1997).

5.2.2.1 Cadmium

Cadmium concentrations in seven GRMs are presented in Table 5-3. Details of the mass spectrometry procedures are listed in Appendix F, Section 1.2. The uncertainties for this work are at the 95% level of confidence and for the literature, two standard deviations as quoted by the authors. The average analytical blank for cadmium was 140 ± 30 pg, which is less than 1.5% of the cadmium in the samples, except for PCC-1, where it is less than 5%. The measurement of the analytical blanks is described in Section 5.4 and includes the digestion, separation chemistry and mass spectrometry, blanks for all three elements are summarised in Table 5-13.

The concentrations of cadmium shown in Table 5-3 for BCR-1 and PCC-1 agree within uncertainties with the mean of previously published IDMS values. In the absence of published IDMS concentrations for BHVO-1, BIR-1, DNC-1, MAG-1 or W-2 published values measured by atomic absorption spectrometry (AAS) are quoted. Comparing the average concentrations from this work with AAS values only MAG-1 agrees within experimental uncertainties. The range of values seen in DNC-1 suggest that this sample is heterogeneous.

One BIR-1 and one PCC-1 sample are excluded due to chemistry and mass spectrometry problems.

These are the first cadmium concentration measurements of BHVO-1, BIR-1, DNC-1, MAG-1 and W-2 using the high precision technique of IDMS. New concentration measurements are presented for BCR-1 and PCC-1.

Table 5-3 The concentration of cadmium in seven GRMs, by IDMS.

Date	Sample	This work (ppb)	Mean (ppb)	Literature values by IDMS (ppb) ± 95% CI	Mean of literature values by AAS (ppb) ± 2 sd
22/9/94 22/9/94	**BCR-1**	134±1 134±1	134	122±7,125±4,139±5 (Rosman and De Laeter, 1974 & 1980) 136±1 (Loss et al., 1984)	135±36 (Gladney et al., 1990)
22/9/94 9/11/94 6/6/95	**BHVO-1**	88±1 99.3±0.7 93.3±0.6	94		76±12 (Gladney and Roelandts, 1988a)
9/11/94 9/11/94 12/1/95 8/5/95	**BIR-1**	97.1±0.6 92.2±0.6 none 102±1	97		354±300 (Gladney and Roelandts, 1988b)
6/2/95 6/2/95 8/5/95 8/5/95 6/6/95	**DNC-1**	83.4±0.9 82.0±0.6 97.9±0.8 131±1 74.0±0.5	94		178 (Gladney and Roelandts, 1988b)
9/1/95 9/1/95	**MAG-1**	184±9 205±1	195		193±32 (Gladney and Roelandts, 1988a)
6/2/95 27/2/95 6/6/95	**PCC-1**	none 16.2±0.1 16.0±0.1	16	15±2 (Rosman and De Laeter, 1974b)	
27/2/95 27/2/95 6/6/95	**W-2**	74.3±0.5 78.9±0.5 77.1±0.6	77		332 (Gladney and Roelandts, 1988b)

5.2.2.2 Gadolinium

Gadolinium concentration measurements are presented in Table 5-4. Details of mass spectrometry procedures are in Appendix F, Section 1.3. The average analytical blank was 74±3 pg, less than 0.01% of the gadolinium in the samples. The uncertainties shown for this work are at the 95% level of confidence and, quoted by the authors in the literature, two standard deviations.

The concentration of gadolinium in BCR-1 agrees with the mean of 32 previously published IDMS values, within experimental uncertainties. The 32 published values range from 6.34 ppm to 7.2 ppm, most with uncertainties of 4% (two standard deviations). BHVO-1 was 6% higher than the previously published IDMS values and the BIR-1 average was the same as the one published IDMS value, within uncertainties, which was measured by spark source mass spectrometry (SSMS).

The two samples of PCC-1 reported in this work and the one published IDMS value differ markedly, suggesting that gadolinium is not homogeneous in PCC-1 for 100 mg size samples. This is also true for samarium and will be discussed in the next Section.

In the absence of published IDMS gadolinium concentrations for DNC-1, MAG-1 or W-2 published values by neutron activation analysis (NAA) are shown in the Table. Of the measurements presented here DNC-1 and W-2 agree within experimental uncertainties with the NAA values, but the MAG-1 concentration was 30% lower than the reported NAA mean.

Five measurements have been rejected, due to chemistry or mass spectrometry problems, or a large divergence from other results perhaps due to isotopic interference in the mass spectrometry.

These are the first gadolinium concentration measurements by IDMS of DNC-1, MAG-1 and W-2, and new concentration measurements are presented for BCR-1, BHVO-1, BIR-1 and PCC-1.

Table 5-4 The concentration of gadolinium in seven GRM, by IDMS.

Date	Sample	This work (ppm)	Mean (ppm)	Literature values by IDMS (ppm) ± 2 sd	Mean of literature values by NAA (ppm) ± 2 sd
22/9/94 22/9/94	**BCR-1**	6.74±0.05 6.85±0.04	6.8	6.7 ± 0.4; n=32*	
22/9/94 9/11/94 6/6/95	**BHVO-1**	6.37±0.02 ~~7.29±0.14~~ 6.48±0.04	6.42	6.01±0.24 (Sun et al., 1979) 6.24 (Rautenschlein et al., 1985)	
9/11/94 9/11/94 12/1/95 8/5/95	**BIR-1**	none 1.942±0.007 1.86±0.03 1.90±0.01	1.90	1.6 (Jochum et al., 1994) by ID-SSMS ± 6-20%	
6/2/956/ 2/95 8/5/95 8/5/95	**DNC-1**	none 2.01±0.08 ~~0.0022±.0037~~ 2.30±0.37	2.2		2.2±0.6 (Gladney and Roelandts, 1988b)
9/1/95 9/1/95	**MAG-1**	5.95±0.01 6.18±0.03	6.07		8.5±1.6 (Gladney and Roelandts, 1988a)
6/2/95 27/2/95 6/6/95	**PCC-1**	0.006±0.002 ~~0.92±0.01~~ 0.054±0.003	_	0.028 (Hooker et al., 1975)	
27/2/95 27/2/95 6/6/95	**W-2**	4.0±0.4 4.06±0.07 3.81±0.01	3.9		3.9±1.0 (Gladney and Roelandts, 1988b)

*n=32; the mean of selected references from Gladney et al., 1990; all were sighted.

5.2.2.3 Samarium

Samarium concentration measurements in seven GRMs are presented in Table 5-5. Details of the mass spectrometry procedures are listed in Appendix F, Section 1.4. The average analytical blank for samarium was 100±40 pg, which is less than 0.01% of the samarium in the samples. The uncertainties shown for this work are at the 95% level of confidence and for the literature two standard deviations as quoted by the authors.

Samarium concentrations in all seven GRMs agree within experimental uncertainties with the four previously published IDMS values and the three NAA values in the Table, except for BHVO-1 and PCC-1.

The 43 published values for BCR-1 range from 6.22 ppm to 7.44 ppm, most with stated uncertainties of 4% (two standard deviations). The mean samarium concentration in BHVO-1 was about 8% higher than the two previously published IDMS values.

There are no published IDMS samarium concentration values for DNC-1, MAG-1 or W-2, so the mean of concentrations measured by NAA are shown in Table 5-5. The values reported here for DNC-1, MAG-1 and W-2 agree with these values within experimental uncertainties.

The concentration of samarium in the first two PCC-1 samples reported here are the same within experimental uncertainties as the 'compiled' values from Gladney and Roelandts (1991), of 0.0066±0.0036 ppm, though the third sample differs markedly. The ratio of samarium to gadolinium concentrations in each sample is usually similar for each type of rock (Table 5-6). For PCC-1 the ratios from this work are 1.60 (sample dated 6/2/95) and 1.96 (sample dated 6/6/95). The values published by Hooker et al. (1975) give a ratio of 0.25.

Table 5-5 The concentration of samarium in seven GRM, by IDMS.

Date	Sample	Individual analyses, this work (ppm)	Mean (ppm)	Literature values by IDMS(ppm) ± 2sd	Mean of literature values by NAA (ppm) ± 2sd
22/9/94 22/9/94	**BCR-1**	6.65±0.04 6.74±0.05	6.70	6.6 ± 0.4; n=43*	
22/9/94 9/11/94 6/6/95	**BHVO-1**	6.41±0.04 6.46±0.06 6.47±0.04	6.45	5.79 (Sun et al., 1979) 6.16 (Rautenschlein et al., 1985)	
9/11/94 9/11/94 12/1/95 8/5/95	**BIR-1**	none 1.136±0.008 none 1.140±0.007	1.138	1.11 (Jochum et al., 1994) by ID-SSMS ± 6-20%	
6/2/95 6/2/95 8/5/95 8/5/95	**DNC-1**	none ~~9.6±6.7~~ 1.48±0.01 1.458±0.009	1.47		1.41±0.30 (Gladney and Roelandts, 1988b)
9/1/95 9/1/95	**MAG-1**	7.69±0.06 7.87±0.05	7.78		7.7±1.2 (Gladney and Roelandts, 1988a)
6/2/95 27/2/95 6/6/95	**PCC-1**	0.0096±0.0004 0.0073±0.0002 0.1056±0.0008	_	0.007 (Hooker et al., 1975)	
27/2/95 27/2/95 6/6/95	**W-2**	~~18±38~~ 3.47±0.04 3.43±0.02	3.45		3.28±0.46 (Gladney and Roelandts, 1988b)

*n=43; the mean of selected references from Gladney et al., 1990; all were sighted.

Table 5-6 The ratio of samarium and gadolinium concentrations for each pair of independent measurements of the GRM samples.

Sample	Samarium/gadolinium
BCR-1	0.99, 0.98
BHVO-1	1.0, 1.0
BIR-1	0.6, 0.6
DNC-1	0.7, 0.6
MAG-1	1.3, 1.3
PCC-1	1.60, 1.96
W-2	0.9, 0.9

This suggests either that the Hooker et al. (1975) gadolinium concentration in PCC-1 is not correct, that the concentrations of gadolinium and samarium in some grains are not related or that neither of the gadolinium concentrations in this work are correct. It is more likely, however, that all the rare earth concentrations may be correct and PCC-1 is heterogeneous.

Five of the samples are not included because of problems with the chemistry, the mass spectrometry or a large divergence from the other results.

These are the first samarium concentration measurements by IDMS of DNC-1, MAG-1 and W-2, and new concentration measurements are presented for BCR-1, BHVO-1, BIR-1 and PCC-1.

5.3 Concentrations in the lunar samples

The concentration of cadmium, gadolinium and samarium in the lunar samples measured in this work using IDMS are given in Tables 5-10, 5-11 and 5-12 respectively. Details of the mass spectrometry procedures are given in Appendix F, Section 2.

5.3.1 General procedures for the lunar samples

After the digestion of a lunar sample and before the final evaporation stage about 5% by volume of the solution was removed using a clean pipette, for the concentration measurements (Table 5-7). Cadmium, gadolinium and samarium tracers are added to the extracted 5% at this stage, the mass of tracer added in each case is listed in Tables 5-8 and

5-9. After evaporation the cadmium, gadolinium and samarium mix was separated on anion and cation exchange columns dedicated to IDMS work, described in Chapter 2.

The digestion procedure left one or two very fine chips of negligible weight in some of the samples, marked with a tick in Table 5-7.

Table 5-7 Sample sizes used for the lunar sample concentration measurements by IDMS.

Lunar sample	Size of sample digested (mg) (±0.2 mg)	Sample removed for IDMS (vol. % of solution)	Sample size used for IDMS (mg) ±4%	Date	Digestion residue
10017,341	264.4	4%	9.3	9/4/97	✓
14163,848	200.8	5%	9.6	21/3/97	x
	235.8	4%	9.6	15/7/97	x
14310,615	215.8	6%	13.3	9/4/97	x
15041,188	203.0	4%	7.9	9/4/97	✓
15059,240	246.3	5%	11.7	9/4/97	x
60501,105	208.7	5%	11.2	16/1/97	✓
	258.3	4%	10.1	15/7/97	x
65701,23	195.8	4%	7.8	9/4/97	✓
72161,73	198.7	5%	9.6	9/4/97	x
74220,125	210.1	4%	9.1	21/3/97	✓
	207.6	5%	9.6	15/7/97	x

5.3.1.1 Cadmium

Most cadmium concentration measurements were made using the Daly detector, ion currents were between 10^{-15} A and 10^{-13} A. Details of mass spectrometry procedures are in Appendix F, Section 2.1.

Table 5-8 Details of the tracers for cadmium concentration measurements of the lunar samples. The tracer added was 33.83 ppb $^{106\text{-}111}$Cd.

Sample	$^{106\text{-}111}$Cd tracer (pg) (±8 pg)	Date
10017,341	849	9/4/97
14163,848	941	21/3/97
	842	15/7/97
14310,615	896	9/4/97
15041,188	907	9/4/97
15059,240	785	9/4/97
60501,105	934	16/1/97
	809	15/7/97
65701,23	880	9/4/97
72161,73	856	9/4/97
74220,125	795	21/3/97
	839	15/7/97

5.3.1.2 Gadolinium and samarium

Table 5-9 Details of the tracers added for the gadolinium and samarium concentration measurements of the lunar samples. The gadolinium tracer is 2.082 ppm ^{152}Gd, the samarium tracer 1.8138 ppm ^{147}Sm.

Sample	^{152}Gd tracer added (ng) (±0.4 ng)	^{147}Sm tracer added (ng) (±0.4 ng)	Date
14163,848	56.0	44.8	21/3/97
	53.7	46.1	15/7/97
60501,105	54.8	76.0	16/1/97
	54.1	47.3	15/7/97
74220,125	54.6	42.8	21/3/97
	51.4	46.4	15/7/97

Gadolinium and samarium were measured using the Daly and Faraday detectors with ion currents between 10^{-16} A and 10^{-14} A and 10^{-15} A and 10^{-12} A respectively. Details of mass spectrometry procedures are in Appendix F, Section 2.2 and 2.3.

5.3.2 Cadmium, gadolinium and samarium concentrations in the lunar samples

Cadmium, gadolinium and samarium concentration in the lunar samples are in Tables 5-10, 5-11 and 5-12.

Table 5-10 Cadmium concentrations in the lunar samples measured by IDMS, with the analytical blanks which were measured at the same time as each set of samples.

Date	Sample	Concentrations, this work (ppb) ± 95% CI	Blanks (pg)	Literature values of similar samples (ppb)
9/4/97	**10017,341**	10.0±0.2	87±7	68 (Anders et al., 1971) #10017,87
21/3/97 15/7/97	**14163,848**	~~1.04±0.02 ppm~~ ~~800±15 ppb~~	173±5 340±20	139, 140 (Morgan et al., 1972) #14163,57, 196 (Baedecker et al., 1972) #14163,115
9/4/97	**14310,615**	1.51±0.02	87±7	2.6 (Morgan et al., 1972) #14310,119, 8.4 (Baedecker et al., 1972) #141310,120
9/4/97	**15041,188**	32.8±0.6	115±7	
9/4/97	**15059,240**	34.9±0.3	87±7	35.5 (Ganapathy, 1973 from Ryder, 1985)
16/1/97 15/7/97	**60501,105**	~~3.59±0.11 ppm~~ 112±2 ppb	173±5 340±20	96 (Wasson et al., 1975) #60501,32
9/4/97	**65701,23**	68.3±0.8	115±7	77 (Boynton et al., 1976) #65700,4
9/4/97	**72161,73**	57.0±0.6	115±7	58 (Baedecker et al., 1974) #72161,19
21/3/97 15/7/97	**74220,125**	300±7 ppb ~~2.85±0.17 ppm~~	173±5 340±20	320, 92, 260 (Morgan et al., 1974) #74220,54, #74220,54,1, #74220,54,2
				314, bulk 157, 500-62 μm 232, 62-20 μm 505, 20-0.1 μm (Wasson et al., 1975) #74220,233,19

The uncertainties shown for this work are at the 95% level of confidence.

5.3.2.1 Cadmium

The analytical blanks, measured at the same time as the lunar samples, are listed in Table 5-10. The measurement of the analytical blank is described in Section 5.4 and includes the digestion, separation chemistry and mass spectrometry.

As traces of indium were observed (less than 0.2% of the sample in all cases at mass 113), the ratio $^{111}Cd/^{113}Cd$ was not used to calculate the concentrations, only $^{111}Cd/^{112}Cd$ was used for all the lunar cadmium concentration calculations.

Samples 10017,341, 14310,615, 15041,188, 15059,240, 65701,23, and 72161,73 have precise concentration measurements in the low ppb range, the range expected for cadmium in lunar samples. These first high precision cadmium measurements by IDMS are not always in agreement with earlier data, which used various types of neutron activation analysis.

The two 14163,848 samples give concentrations of cadmium of 1.04 ppm and 800 ppb, about five times higher than the literature values. This sample was contaminated by small pieces of plastic, and showed no neutron capture in cadmium (Section 6.3), in spite of evidence of neutron capture on gadolinium and samarium, so these cadmium data have had to be rejected.

The first 60501,105 sample shows an anomalously high concentration (3.59 ppm) of cadmium. If the concentration of 112 ppb for the sample dated 15/7/97 is correct (it is of the same order as the value from Wasson et al. (1975)) then this suggests contamination of the first sample by about 35 ng of cadmium. However, the $^{114}Cd/^{112}Cd$ versus $^{113}Cd/^{112}Cd$ correlation diagram (Figure 6-29) indicates high neutron capture (an increase in $^{114}Cd/^{113}Cd$ of 0.5%) in this possibly contaminated sample, suggesting there is no terrestrial cadmium contamination. Under the circumstances it would seem that this sample must have become contaminated during processing, even though this was not evident in the blanks taken at the same time.

The blank for the concentration measurement of the first 60501,105 sample (16/1/97) was 173 pg (Table 5-10), and for the composition measurement 89 pg (Table 6-9), both insignificant in terms of the contamination experienced here.

Another possibility is that all the 60501,105 is contaminated, but this would contradict the second concentration value of 112 ppb and the clear

evidence of neutron capture. Perhaps some of the small pieces of plastic seen in 14163,848 were also in 60501,105. It is a possibility.

For 74220,125 dated 21/3/97 a concentration of 300 ppb is well within the range of the concentrations found by Morgan et al. (1974), whereas 74220,125 dated 15/7/97, with a concentration of 2.85 ppm, is ten times greater than expected, so has been rejected. Any neutron capture effects on this sample would be the minimum detectable, so it is unclear whether the very small neutron capture effect seen (less than the uncertainties) is real or not (Section 6.3.1).

Analytical blanks are measured with every set of samples analysed (Table 5-10). For the small (8 to 11 mg) samples used for concentration measurements the blank was mostly less than 15% of the cadmium content of each of the samples. This indicates that the high concentration measurements in three samples was not caused by contamination from the digestion, separation chemistry or mass spectrometry.

The first cadmium concentration measurements of lunar soils and rocks by IDMS are presented here and include two cadmium concentration measurements of samples not measured before, 15041,188 and 15059,240.

5.3.2.2 Gadolinium and samarium

Analytical blanks of 74±3 pg, taken from the GRM blanks, have been assumed for these gadolinium samples, due to poor or non-existent ionisation of the low picogram blanks. The gadolinium concentration of the 14163,848 sample dated 21/3/97 was rejected because of samarium contamination seen visually and during mass spectrometry measurements.

Table 5-11 Gadolinium concentrations in the lunar samples measured by IDMS.

Date	Sample	Concentrations this work (ppm)	Literature values of similar samples (ppm)
21/3/97 15/7/97	**14163,848**	none 21±7	42.7, 35.9 (Hubbard et al., 1972) #14163,65
16/1/97 15/7/97	**60501,105**	3.26±0.05 5.8±0.3	
21/3/97 15/7/97	**74220,125**	8.1±0.2 8.6±0.1	8.52 (BVSP, 1981)

For the samarium lunar measurements an average analytical blank of 116±9 pg was obtained.

The gadolinium and samarium concentrations for 14163,848 are 50% and 20% lower than the literature values. However, the Sm/Gd concentration ratios of 1.2 and 1.4 are close to the values expected for an Apollo 14 basalt.

Table 5-12 Samarium concentrations in the lunar samples measured by IDMS.

Date	Sample	Concentrations this work (ppm)	Literature values of similar samples (ppm)
21/3/97 15/7/97	**14163,848**	24.3±0.4 29.8±0.5	29.0, 36.5, 30.0 (Hubbard et al., 1972) #14163,65
16/1/97 15/7/97	**60501,105**	2.68±0.04 14±2	
21/3/97 15/7/97	**74220,125**	6.3±0.1 6.8±0.1	6.53 (BVSP, 1981)

In sample 60501,105 (dated 15/7/97) the samarium concentration was higher than expected. In the Apollo 16 highland material the concentration of samarium is generally lower than that of gadolinium so, though there were no interferences detected in the mass spectrometry, some doubt must be cast on this value, especially in view of the problems experienced with samarium contamination.

As expected the rare earth concentrations found here indicate a higher rare earth concentration in the Apollo 14 basalts compared to the Apollo 16 highland material.

The 74220,125 orange glass concentrations of gadolinium and samarium are the same as those of Rhodes (1974) from BVSP (1981).

These are the first gadolinium and samarium concentration measurements of samples 60501,105, and new concentration measurements are presented for 14163,848 and 74220,125.

5.4 Analytical blanks

5.4.1 Analytical blanks for concentration measurements

Every time a set of samples was processed a measurement was made of any contamination, the analytical blank. Exactly the same digestion, separation chemistry and mass spectrometry procedures are used for the blank and it was processed at the same time as the samples. Cadmium, gadolinium and samarium tracers are added to the blank at the same time as they are added to the sample.

For the GRMs the tracer was added close to the start of the digestion procedure. For the lunar samples, where 5% of the sample was extracted at the end of the digestion process, the tracers are added to the extract before the final evaporation.

Analytical blanks are calculated by IDMS. As the total magnitude of the blank was required, not the concentration, the uncertainties are found using a modified version of the calculations in Section 5.1.2.

5.4.2 Analytical blanks for composition measurements

As in the previous Section, an analytical blank was run with every set of samples. For composition measurements tracers are added to the blank when the digestion an separation chemistry was complete, before measurement by IDMS.

5.4.3 Other analytical blanks

The analytical blanks for the rhenium filaments and digestion are listed in Table 5-13, also total chemistry and mass spectrometry blanks for the elemental concentration and composition measurements.

Table 5-13 Various analytical blanks (pg) measured in this work.

	Cd (pg)	Gd (pg)	Sm (pg)
Filament blanks	5	1	2
Digestion	75	1.4	22
Total chemistry and mass spectrometry for IDMS	140	75	116
Total chemistry and mass spectrometry for composition	46	12	50

5.5 Summary

Presented in this chapter are cadmium, gadolinium and samarium concentration measurements in the seven geochemical reference materials, BCR-1, BHVO-1, BIR-1, DNC-1, MAG-1, PCC-1 and W-2 using the high precision technique of IDMS.

Included are the first IDMS measurements of cadmium in BHVO-1, BIR-1, DNC-1, MAG-1 and W-2, of gadolinium in DNC-1, MAG-1 and W-2 and of samarium in DNC-1, MAG-1 and W-2.

Also presented are the first cadmium, gadolinium and samarium concentrations measurements using IDMS in lunar rocks and soils, cadmium concentrations in samples 10017,341, 14163,848, 14310,615, 15041,188, 15059,240, 60501,105, 65701,23, 72161,73 and 74220,125, and gadolinium and samarium concentrations in 14163,848, 60501,105 and 74220,125. These are also the first cadmium concentrations measured in 15041,188 and 15059,240 and the first gadolinium and samarium concentrations measured in 60501,105.

The Chapter is supplemented by Appendix F.

6. The isotopic composition of cadmium, gadolinium and samarium

The isotopic composition of laboratory standards and BCR-1 are listed in Sections 6.1 and 6.2, followed by the isotopic composition of the lunar samples in Section 6.3. The ratios of $^{113}Cd/^{112}Cd$, $^{114}Cd/^{112}Cd$, $^{155}Gd/^{160}Gd$, $^{156}Gd/^{160}Gd$, $^{157}Gd/^{160}Gd$, $^{158}Gd/^{160}Gd$, $^{149}Sm/^{152}Sm$ and $^{150}Sm/^{152}Sm$ in the lunar samples are compared to these ratios in the laboratory standards and in BCR-1 to identify possible neutron capture.

6.1 Laboratory standards

Cadmium, gadolinium and samarium isotopic abundance measurements on the mass spectrometer are given in Tables 6-1, 6-2, 6-3 and 6-4. Details of the conditions and procedures during mass spectrometry measurements are described in detail in Appendix G, Section 1.

6.1.1 Cadmium

All the cadmium standards were measured by the Faraday detectors, with ^{112}Cd centred on the axial collector. They were loaded on the filaments in an older silica gel mix before June 1997 and in the finer silica gel since that time. One hundred or more measurements were made of each sample with ion currents of 10^{-12} A to 10^{-11} A at mass 114, samples were usually between 10 and 50 ng. Details of the collector array, sample size, ion current and the number of ratios measured for each sample are listed in Appendix G, Table 1-1. $^{106}Cd/^{112}Cd$ has not been measured because of the constraints of the Faraday multi-collector cups, described in Chapter 3.

Table 6-1 The isotopic composition of cadmium laboratory standards.

Sample	$^{106}Cd/^{112}Cd$	$^{108}Cd/^{112}Cd$	$^{110}Cd/^{112}Cd$	$^{111}Cd/^{112}Cd$	$^{113}Cd/^{112}Cd$	$^{114}Cd/^{112}Cd$	$^{116}Cd/^{112}Cd$	$^{114}Cd/^{113}Cd$
(Rosman and De Laeter, 1975)	0.05415 ±0.00003	0.03810 ±0.00002	0.52542 ±0.00010	0.53430 ±0.00010	0.50240 ±0.00011	1.17383 ±0.00011	0.30147 ±0.00008	
8/8/96(1)		0.037118 ±0.000019	0.51928	0.531526 ±0.000025	0.506126 ±0.000017	1.188719 ±0.000072	0.309071 ±0.000039	2.34866 ±0.00016
4/8/96(2)		0.037132 ±0.000094	0.51928	0.53137 ±0.00012	0.50602 ±0.00010	1.18875 ±0.00042	0.30947 ±0.00011	2.34921 ±0.00097
23/8/96		0.037118 ±0.000049	0.51928	0.53166 ±0.00019	0.50637 ±0.00012	1.18892 ±0.00023	0.30932 ±0.00014	2.34795 ±0.00074
5/12/96		0.03720 ±0.00011	0.51928	0.53156 ±0.00014	0.50660 ±0.00012	1.18930 ±0.00025	0.30931 ±0.00017	2.34760 ±0.00074
12/2/97(1)		0.037038 ±0.000021	0.51928	0.53113 ±0.00010	0.50626 ±0.00011	1.18973 ±0.00012	0.309376 ±0.000067	2.35004 ±0.00054
12/2/97(2)		0.037063 ±0.000065	0.51928	0.531445 ±0.000064	0.506606 ±0.000099	1.18994 ±0.00015	0.30955 ±0.00014	2.34886 ±0.00054
26/5/97(1)		0.037049 ±0.000079	0.51928	0.530930 ±0.000080	0.506065 ±0.000090	1.18959 ±0.00024	0.30953 ±0.00012	2.35067 ±0.00064
26/5/97(2)		0.037063 ±0.000053	0.51928	0.531289 ±0.000071	0.505613 ±0.000087	1.18800 ±0.00034	0.30894 ±0.00014	2.34977 ±0.00078

Continued

Table 6-1 continued.

Sample	$^{106}Cd/^{112}Cd$	$^{108}Cd/^{112}Cd$	$^{110}Cd/^{112}Cd$	$^{111}Cd/^{112}Cd$	$^{113}Cd/^{112}Cd$	$^{114}Cd/^{112}Cd$	$^{116}Cd/^{112}Cd$	$^{114}Cd/^{113}Cd$
14/6/97(2)		0.037082 ±0.000005	0.51928	0.53092 ±0.00022	0.50581 ±0.00021	1.188986 ±0.000063	0.309194 ±0.000024	2.35064 ±0.00099
24/6/97(1)		0.037115 ±0.000080	0.51928	0.531095 ±0.000051	0.505983 ±0.000089	1.18900 ±0.00019	0.30926 ±0.00013	2.34988 ±0.00056
24/6/97(2)		0.037073 ±0.000022	0.51928	0.531161 ±0.000091	0.506295 ±0.000075	1.18954 ±0.00013	0.309362 ±0.000050	2.34949 ±0.00043
8/7/97		0.037029 ±0.000041	0.51928	0.53085 ±0.00018	0.50623 ±0.00018	1.19004 ±0.00010	0.309550 ±0.000049	2.35079 ±0.00087
14/8/97		0.037086 ±0.000018	0.51928	0.531133 ±0.000070	0.506244 ±0.000064	1.189532 ±0.000055	0.309245 ±0.000039	2.34972 ±0.00032
Average of 1996 & 97		0.037090 ±0.000025	0.51928	0.53124 ±0.00014	0.50617 ±0.00015	1.18923 ±0.00031	0.30932 ±0.00010	2.34947 ±0.00054
Average of 1997		0.037067 ±0.000017	0.51928	0.53111 ±0.00012	0.50612 ±0.00019	1.18937 ±0.00041	0.30933 ±0.00013	2.34997 ±0.00042

Cadmium from this work is normalised to $^{110}Cd/^{112}Cd = 0.51928$. The standards published by Rosman and De Laeter (1975) have not been normalised or corrected for fractionation. Uncertainties in this work are at the 95% confidence level and in Rosman and De Laeter (1975), one standard error of the mean. All measured standards with uncertainties greater than 0.04% for $^{114}Cd/^{113}Cd$ ratio have been excluded.

The cadmium standards for 1996 and 1997 are listed in Table 6-1 and plotted as $^{114}Cd/^{112}Cd$ versus $^{113}Cd/^{112}Cd$ in Figure 6-1. The data in both Table and Figure are normalised to $^{110}Cd/^{112}Cd = 0.51928$ (Section 3.2.5) and the uncertainties are at the 95% confidence level. In view of the spread of data for 1996 and 1997 shown in Figure 6-1 the average of the 1997 data has been used as the cadmium standard in this work.

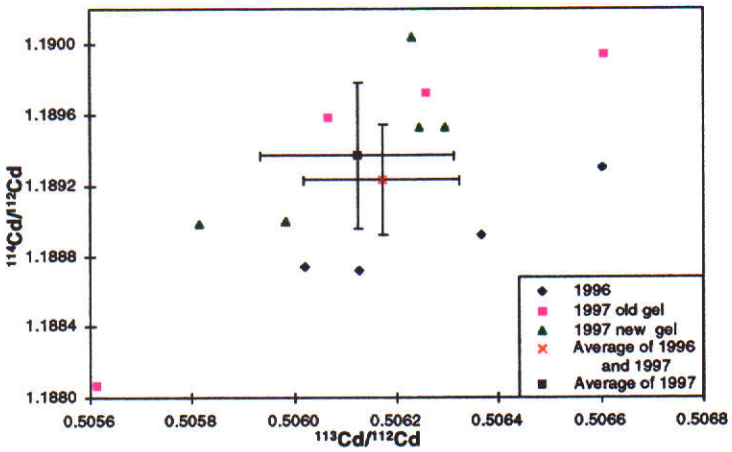

Figure 6-1 Cadmium standard measurements for 1996 and 1997.

6.1.2 Gadolinium

All gadolinium standards were measured on the Faraday multi-collectors with ^{156}Gd centred on the axial collector. One hundred or more measurements were made of each sample with ion currents of 10^{-11} A at mass 158, samples were usually between 1 and 5 µg. Details of the collector array, sample size, ion current and the number of ratios measured for each sample are listed in Appendix G, Table 1-2.

The gadolinium standards for 1996 and 1997 are listed in Table 6-2 and plotted as $^{158}Gd/^{160}Gd$ versus $^{157}Gd/^{160}Gd$ in Figure 6-2. The data in both Table and Figure are normalised to $^{156}Gd/^{160}Gd = 0.9361$ (Section 3.2.5) and uncertainties are at the 95% confidence level. In view of the spread of data for 1996 and 1997 shown in Figure 6-2 the average of the 1997 data has been used as the gadolinium standard in this work.

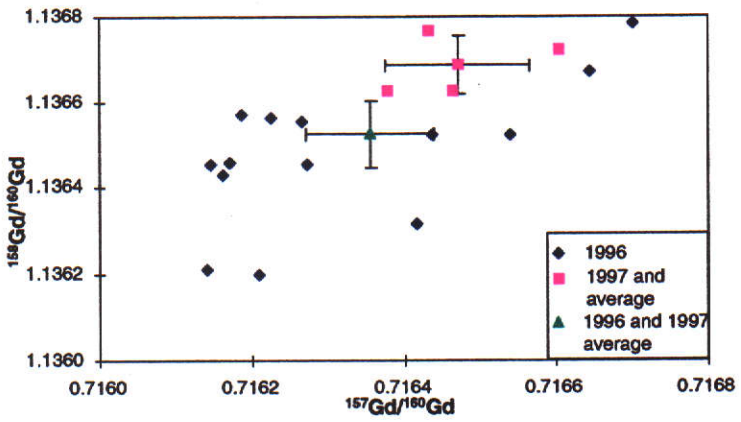

Figure 6-2 Gadolinium standards for 1996 and 1997.

6.1.3 Samarium

All samarium standards were measured on the Faraday multi-collectors with ^{150}Sm centred on the axial collector. One hundred or more measurements were made of each sample with ion currents of 10^{-11} A at mass 154, samples were usually between 1 and 4 μg. Details of the collector array, sample size, ion current and the number of ratios measured for each sample are listed in Appendix G, Table 1-3.

The samarium standards for 1996 and 1997 are listed in Table 6-3 (with ^{152}Sm as the reference isotope) and Table 6-4 (referenced to ^{154}Sm). They are plotted as $^{150}Sm/^{152}Sm$ versus $^{149}Sm/^{152}Sm$ in Figure 6-3. The data in the first Table and the Figure are normalised to $^{147}Sm/^{152}Sm = 0.56081$ (Section 3.2.5) and in Table 6-4 to $^{147}Sm/^{154}Sm = 0.65914$. In both Tables the uncertainties are at the 95% confidence level.

Table 6-2 The isotopic composition of gadolinium laboratory standards.

Sample	$^{152}Gd/^{160}Gd$	$^{154}Gd/^{160}Gd$	$^{155}Gd/^{160}Gd$	$^{157}Gd/^{160}Gd$	$^{158}Gd/^{160}Gd$	$^{158}Gd/^{157}Gd$
Eugster et al., 1970b	0.00928 ±0.00002	0.09975 ±0.00002	0.67692 ±0.00009	0.71589 ±0.00004	1.13590 ±0.00009	
Hidaka et al., 1995	0.009263 ±0.000008	0.099722 ±0.000002	0.676840 ±.000008	0.715826 ±.000006	1.135861 ±.000008	
20/3/96(1)	0.009520 ±0.000032	0.099957 ±0.000028	0.676958 ±0.000025	0.716267 ±0.000017	1.136554 ±0.000016	1.586775 ±0.000044
20/3/96(2)	0.009348 ±0.000009	0.099806 ±0.000011	0.676961 ±0.000016	0.716161 ±0.000021	1.136431 ±0.000033	1.586839 ±0.000065
20/3/96(3)	0.009361 ±0.000012	0.099828 ±0.000010	0.676975 ±0.000021	0.716438 ±0.000027	1.136523 ±0.000030	1.586353 ±0.000073
8/6/96	0.009454 ±0.000018	0.099898 ±0.000017	0.677179 ±0.000076	0.716170 ±0.000030	1.136458 ±0.000029	1.586856 ±0.000078
12/6/96(1)	0.009375 ±0.000006	0.099820 ±0.000009	0.676969 ±0.000024	0.716187 ±0.000047	1.136569 ±0.000024	1.58697 ±0.00011
12/6/96(2)	0.009368 ±0.000005	0.099847 ±0.000005	0.676949 ±0.000013	0.716644 ±0.000013	1.136673 ±0.000015	1.586104 ±0.000035
19/6/96	0.009536 ±0.000010	0.099961 ±0.000013	0.677179 ±0.000054	0.716211 ±0.000026	1.136199 ±0.000032	1.586404 ±0.000074
26/6/96	0.009221 ±0.000010	0.099706 ±0.000020	0.676971 ±0.000027	0.716226 ±0.000007	1.136565 ±0.000008	1.586880 ±0.000019
18/7/96	0.009290 ±0.000012	0.099765 ±0.000010	0.676925 ±0.000011	0.716147 ±0.000008	1.136455 ±0.000016	1.586903 ±0.000029

Continued

Table 6-2 continued.

Sample	$^{152}Gd/^{160}Gd$	$^{154}Gd/^{160}Gd$	$^{155}Gd/^{160}Gd$	$^{157}Gd/^{160}Gd$	$^{158}Gd/^{160}Gd$	$^{158}Gd/^{157}Gd$
1/8/96	0.009426	0.099925	0.676940	0.716416	1.136316	1.586112
	±0.000026	±0.000027	±0.000008	±0.000022	±0.000009	±0.000051
12/9/96	0.009351	0.099813	0.676999	0.716141	1.136213	1.586578
	±0.000018	±0.000022	±0.000048	±0.000023	±0.000057	±0.000094
20/9/96	0.009338	0.099824	0.676921	0.716274	1.136456	1.586623
	±0.000008	±0.000008	±0.000014	±0.000018	±0.000020	±0.000049
2/10/96	0.009327	0.099831	0.677017	0.716540	1.136523	1.58613
	±0.000011	±0.000010	±0.000033	±0.000054	±0.000044	±0.00013
15/10/96	0.009395	0.099877	0.67717	0.716702	1.136786	1.58613
	±0.000029	±0.000028	±0.00011	±0.000080	±0.000045	±0.00019
11/2/97	0.009321	0.099837	0.677003	0.716434	1.136766	1.586701
	±0.000011	±0.000015	±0.000022	±0.000010	±0.000018	±0.000034
8/5/97	0.00933	0.09981	0.67681	0.716604	1.13672	1.58626
	±0.00013	±0.00014	±0.00027	±0.000051	±0.00013	±0.00021
6/6/97	0.009321	0.099819	0.676963	0.716379	1.136628	1.58663
	±0.000036	±0.000032	±0.000042	±0.000072	±0.000082	±0.00020
21/8/97	0.009449	0.099935	0.676993	0.716465	1.136629	1.586440
	±0.000029	±0.000029	±0.000015	±0.000019	±0.000025	±0.000055
Av 1996 & 1997	0.009374	0.099848	0.676993	0.716356	1.136526	1.58654
	±0.000036	±0.000031	±0.000044	±0.000085	±0.000078	±0.00014
Average 1997	0.009355	0.099851	0.676942	0.716471	1.136687	1.58651
	±0.000062	±0.000056	±0.000090	±0.000094	±0.000068	±0.00019

Gadolinium is normalised to $^{156}Gd/^{160}Gd = 0.9361$ (from Eugster et al., 1970b). Uncertainties in this work are at the 95% confidence level, and in Eugster et al. (1970b) and Hidaka et al. (1995), 2 standard error of the mean. All measured standards with uncertainties greater than 0.01% for the $^{158}Gd/^{157}Gd$ ratio have been excluded.

Table 6-3 The isotopic composition of samarium laboratory standards, referenced to ^{152}Sm.

Date	$^{144}Sm/^{152}Sm$	$^{148}Sm/^{152}Sm$	$^{149}Sm/^{152}Sm$	$^{150}Sm/^{152}Sm$	$^{154}Sm/^{152}Sm$	$^{150}Sm/^{149}Sm$
Lugmair et al., 1975	0.11502 ±0.00004	0.42045 ±0.00003	0.51683 ±0.00004	0.27602 ±0.00002	0.85082 ±0.00005	
Hidaka et al., 1995	0.114962 ±0.000002	0.420456 ±0.000004	0.516862 ±0.000003	0.276002 ±0.000002	0.850824 ±0.000006	
11/10/96,	0.115045 ±0.000004	0.420509 ±0.000005	0.516662 ±0.000006	0.275877 ±0.000005	0.850497 ±0.000017	0.533959 ±0.000022
15/10/96,	0.115043 ±0.000005	0.420483 ±0.000011	0.516685 ±0.000009	0.275878 ±0.000006	0.850467 ±0.000016	0.533938 ±0.000028
30/10/96,	0.115021 ±0.000003	0.420447 ±0.000006	0.516734 ±0.000007	0.275920 ±0.000003	0.850668 ±0.000012	0.533970 ±0.000018
18/11/96,	0.115089 ±0.000004	0.420679 ±0.000006	0.516601 ±0.000010	0.275818 ±0.000005	0.850005 ±0.000018	0.533910 ±0.000026
5/12/96	0.115051 ±0.000005	0.420496 ±0.000008	0.516683 ±0.000007	0.275878 ±0.000007	0.850436 ±0.000016	0.533940 ±0.000030
17/12/96,	0.115067 ±0.000002	0.420528 ±0.000004	0.516638 ±0.000003	0.275842 ±0.000004	0.850279 ±0.000012	0.533917 ±0.000017
17/12/96,	0.115046 ±0.000003	0.420479 ±0.000006	0.516664 ±0.000009	0.275879 ±0.000005	0.850471 ±0.000016	0.533963 ±0.000025
24/12/96,	0.115055 ±0.000008	0.420492 ±0.000013	0.516591 ±0.000015	0.275813 ±0.000012	0.850274 ±0.000027	0.533909 ±0.000053

Continued

Table 6-3 continued.

Date	$^{144}Sm/^{152}Sm$	$^{148}Sm/^{152}Sm$	$^{149}Sm/^{152}Sm$	$^{150}Sm/^{152}Sm$	$^{154}Sm/^{152}Sm$	$^{150}Sm/^{149}Sm$
12/2/97	0.115031 ±0.000008	0.420486 ±0.000008	0.516693 ±0.000011	0.275881 ±0.000011	0.850718 ±0.000026	0.533935 ±0.000044
27/2/97	0.115068 ±0.000010	0.420498 ±0.000011	0.516561 ±0.000011	0.275765 ±0.000021	0.850335 ±0.000021	0.533848 ±0.000081
6/6/97	0.115058 ±0.000005	0.420571 ±0.000012	0.516646 ±0.000015	0.275874 ±0.000014	0.850523 ±0.000033	0.533971 ±0.000057
7/8/97	0.115070 ±0.000021	0.420550 ±0.000087	0.516542 ±0.000016	0.275794 ±0.000012	0.850195 ±0.000078	0.533924 ±0.000053
Average of 1996 & 1997	0.115054 ±0.000011	0.420518 ±0.000036	0.516641 ±0.000034	0.275851 ±0.000027	0.85041 ±0.00012	0.533932 ±0.000020
Average of 1997	0.115057 ±0.000018	0.420526 ±0.000040	0.516610 ±0.000070	0.275828 ±0.000057	0.85044 ±0.00022	0.533919 ±0.000051

Ratios are normalised to $^{147}Sm/^{152}Sm = 0.56081$ (from Lugmair et al., 1975). Uncertainties in this work and for Hidaka et al. (1995) are at the 95% confidence level, for Lugmair et al. (1975), 2 standard errors of the mean. Data have been rejected where the uncertainties for $^{150}Sm/^{149}Sm$ are greater than 0.02%.

Table 6-4 The isotopic composition of samarium laboratory standards for 1997, recalculated using ^{154}Sm as the reference isotope.

Date	$^{144}Sm/^{154}Sm$	$^{148}Sm/^{154}Sm$	$^{149}Sm/^{154}Sm$	$^{150}Sm/^{154}Sm$	$^{152}Sm/^{154}Sm$	$^{150}Sm/^{149}Sm$
Lugmair et al., 1975	0.13519 ±0.00004	0.49417 ±0.00003	0.60745 ±0.00004	0.32442 ±0.00002	1.17534 ±0.00005	
12/02/97	0.135193 ±0.000011	0.494221 ±0.000008	0.607310 ±0.000009	0.324270 ±0.000011	1.175438 ±0.000026	0.533944 ±0.000020
27/2/97	0.135210 ±0.000012	0.494268 ±0.000014	0.607233 ±0.000013	0.324197 ±0.000024	1.175819 ±0.000021	0.533892 ±0.000042
6/6/97	0.135211 ±0.000005	0.494337 ±0.000012	0.607294 ±0.000013	0.324293 ±0.000012	1.175632 ±0.000033	0.533997 ±0.000023
7/8/97	0.135202 ±0.000021	0.49434 ±0.00011	0.607240 ±0.000012	0.324254 ±0.000011	1.175958 ±0.000078	0.533980 ±0.000021
Average for 1997	0.135204 ±0.000008	0.494292 ±0.000057	0.607269 ±0.000038	0.324253 ±0.000040	1.17571 ±0.00022	0.533953 ±0.000074

Ratios are normalised to $^{147}Sm/^{154}Sm = 0.65914$ (from Lugmair et al., 1975). Uncertainties are at the 95% confidence level. Data have been rejected where the uncertainties for $^{150}Sm/^{149}Sm$ are greater than 0.008%.

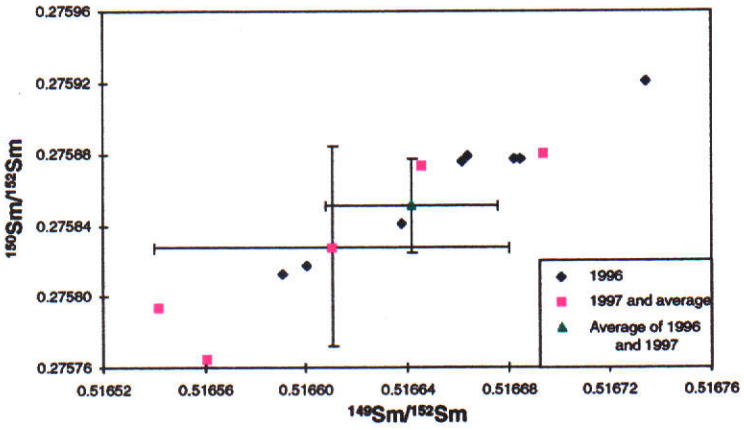

Figure 6-3 Samarium standards for 1996 and 1997.

In view of the spread of data for 1996 and 1997 shown in Figure 6-3 the average of the 1997 data has been used as the samarium standard in this work.

A review of the data suggests an instability in the multi-collector cup which counts the ^{152}Sm ions (High 1). For this reason the samarium standard and lunar sample ratios were recalculated using ^{154}Sm as the reference isotope.

6.2 BCR-1

The isotopic composition of cadmium, gadolinium and samarium in the GRM BCR-1 is included for comparison with the lunar samples, in addition to the laboratory standards. Samples were loaded and run in the same way as the standard samples. The ratios are listed in Tables 6-5, 6-6 and 6-7. Details of the mass spectrometry procedures are in Appendix G, Section 2.

6.2.1 Cadmium

All BCR-1 samples were measured with the Faraday detectors, with ^{112}Cd centred on the axial collector. Only the sample measured on 24/6/97 was loaded on the filament in the new silica gel. One hundred or more measurements of each ratio were made of each sample with ion currents of 10^{-12} A to 10^{-13} A. The high $^{116}Cd/^{112}Cd$ ratios suggests the presence of tin, but none was observed in any measurement.

Table 6-5 The isotopic composition of cadmium in BCR-1.

	$^{108}Cd/^{112}Cd$	$^{111}Cd/^{112}Cd$	$^{113}Cd/^{112}Cd$	$^{114}Cd/^{112}Cd$	$^{116}Cd/^{112}Cd$	$^{114}Cd/^{113}Cd$
20/09/96	0.037183	0.531542	0.50605	1.18892	0.31066	2.3494
	±0.000078	±0.000098	±0.00017	±0.00042	±0.00019	±0.0011
11/10/96(1)	0.03712	0.53127	0.50640	1.18909	0.31008	2.3481
	±0.00016	±0.00019	±0.00027	±0.00059	±0.00019	±0.0017
11/10/96(2)	0.03705	0.53133	0.50637	1.18930	0.31014	2.3487
	±0.00015	±0.00019	±0.00026	±0.00049	±0.00020	±0.0016
3/4/97	0.03709	0.531183	0.50624	1.18934	0.31046	2.34936
	±0.00011	±0.000090	±0.00012	±0.00029	±0.00015	±0.00080
24/6/97(1)	0.03707	0.53118	0.50589	1.18833	0.31025	2.3490
	±0.00019	±0.00026	±0.00030	±0.00049	±0.00078	±0.0017
24/6/97(3)	0.03712	0.53101	0.50543	1.18789	0.31056	2.3502
	±0.00016	±0.00025	±0.00025	±0.00034	±0.00070	±0.0014

Cadmium is normalised to $^{110}Cd/^{112}Cd = 0.51928$. Uncertainties are at the 95% confidence level. Sets of 10 measurements on the mass spectrometer are rejected when a ratio varies more than 0.1% from the mean. The number in parenthesis refer to different measurements made on the same day.

Table 6-6 The isotopic composition of gadolinium in BCR-1.

	$^{152}Gd/^{160}Gd$	$^{154}Gd/^{160}Gd$	$^{155}Gd/^{160}Gd$	$^{157}Gd/^{160}Gd$	$^{158}Gd/^{160}Gd$	$^{158}Gd/^{157}Gd$
24/12/96	0.00987	0.10031	0.677030	0.71657	1.136402	1.585887
	± 0.00017	±0.00013	±0.000038	±0.00012	±0.000080	±0.000033
27/2/97	0.00931	0.09965	0.67698	0.7171	1.13552	1.5836
	±0.00089	±0.00080	±0.00051	±0.0014	±0.00066	±0.0032

Gadolinium is normalised to $^{156}Gd/^{160}Gd = 0.9361$. Uncertainties are at the 95% confidence level. Sets of 10 measurements on the mass spectrometer are rejected when a ratio varies more than 0.4% from the mean.

Table 6-7 The isotopic composition of samarium in BCR-1

	$^{144}Sm/^{152}Sm$	$^{148}Sm/^{152}Sm$	$^{149}Sm/^{152}Sm$	$^{150}Sm/^{152}Sm$	$^{154}Sm/^{152}Sm$	$^{150}Sm/^{149}Sm$
11/10/96	0.115471	0.420481	0.51630	0.27568	0.85358	0.53395
	± 0.000050	±0.000057	±0.00014	±0.00012	±0.00065	± 0.00027
24/12/96	0.115067	0.420552	0.516610	0.275830	0.850277	0.533924
	±0.000004	±0.000008	±0.000010	±0.000004	±0.000021	± 0.000013
24/12/96	0.115052	0.420492	0.516707	0.276009	0.85056	0.53417
	±0.000067	±0.000051	±0.000097	±0.000081	±0.00012	± 0.00019
27/2/97	0.115040	0.420556	0.516605	0.275894	0.850202	0.53405
	±0.000045	±0.000032	±0.000035	±0.000064	±0.000069	± 0.00013

Samarium ratios are normalised to $^{147}Sm/^{152}Sm = 0.56081$. Uncertainties are at the 95% confidence level. Sets of 10 measurements on the mass spectrometer are rejected when a ratio varies more than 0.4% from the mean.

The measurements on 3/4/97 in Table 6-5 were compared to the lunar samples as they have the highest precision of the 1997 samples and were measured at the same time, they are plotted on the correlation diagrams in Figures 6-4 and 6-29.

6.2.2 Gadolinium

All BCR-1 samples were measured by the Faraday detectors, with ^{156}Gd centred on the axial collector. About two hundred measurements of each ratio were made of each sample with ion currents of 10^{-11}. Details of each sample are listed in Appendix G, Table 2-2.

The measurements of 24/12/96 in Table 6-6 were compared to the lunar samples because of the poor precision of the 1997 measurements, they were plotted on the correlation diagrams in Figures 6-30 and 6-33.

6.2.3 Samarium

All BCR-1 samples were measured by the Faraday detectors, with ^{150}Sm centred on the axial collector. Two hundred or more measurements of each ratio were made of each sample with ion currents of 10^{-11} A. Details of each sample are listed in Appendix G, Table 2-3.

The measurements of 27/2/97 in Table 6-7 were used with the lunar samples as they are of good precision and were measured at the same time as the lunar samples, they were plotted on the correlation diagram in Figure 6-36.

6.3 Lunar samples

Lunar samples were stored in sealed bags in a clean laboratory until needed. After weighing the surplus sample was immediately re-sealed.

Small curved pieces of plastic were found in both samples of 14163,848. Possibly as a result of this the cadmium in the sample was found to be contaminated with natural cadmium, so that no changes caused by neutron capture could be detected and the concentration measurements were far higher than expected from the literature. For gadolinium and samarium the concentrations were in the accepted range and clear evidence of neutron capture was seen in this sample.

Table 6-8 The weight of lunar samples analysed.

Date of digestion	Sample	Size of sample digested (±0.2 mg)	Size of sample removed for IDMS
14/3/97	**14163,848**	200.8	5%
2/7/97		235.8	4%
16/1/97	**60501,105**	208.7	5%
2/7/97		258.3	4%
9/4/97	**65701,23**	195.8	4%
9/4/97	**72161,73**	198.7	5%
14/3/97	**74220,125**	210.1	4%
2/7/97		207.6	5%

The concentration of cadmium in samples 10017,341, 14310,615, 15041,188 and 15059,240 is too low for composition measurements of sufficient precision at this time. Composition measurements of cadmium, gadolinium and samarium in 14163,848, 60501,105 and 74220,125 and cadmium only in 65701,23 and 72161,125 have been completed.

Cadmium, gadolinium and samarium isotopic abundance measurements of the lunar samples are given in Tables 6-10, 6-19 and 6-27 (raw data), Tables 6-11, 6-20, 6-28, 6-29 and 6-30 (normalised data) and Tables 6-18 and 6-24 (cadmium and gadolinium modified data). "Raw" data has been defined in Section 3.1.7, and refers to the ratios calculated from the ion currents measured on the mass spectrometer, data is rejected which varies by more than two standard deviations from the mean. No other normalisation procedure has been applied.

Details of the mass spectrometry procedures are listed in Appendix G, Section 3.

6.3.1 Cadmium

Each lunar sample had one hundred or more sets of cadmium isotope ratios measured, with ion currents of 10^{-14} A to 10^{-11} A, both the Daly and Faraday detectors were used, all samples were loaded in the older silica gel, except where indicated in Appendix F. Details of the mass spectrometry procedures for each sample are listed in Appendix F, Table 3-1.

Neutron capture on cadmium is observed in three of the lunar samples, 60501,105, 65701,23 and 72161,73, and evidence of mass fractionation is also demonstrated.

The Apollo 14 sample 14163,848 was too contaminated by terrestrial cadmium for any anomalies to be observed. Any neutron capture in the orange glass, 74220, 125, was less than the precision of the measurements. No fractionation was observed in either of these two samples.

Some interference from tin, such a small amount that it was undetectable during measurements, was subtracted from the isotopic measurements of the lunar samples. Modifications to the mass fractionation corrections are described and applied below.

The measurements of 74220,125 dated 14/3/97 were rejected as the sample ionised poorly, with very poor precision on both the Faraday and the Daly detectors.

Table 6-9 Cadmium analytical blanks for the lunar composition measurements.

Date	Sample	Cd (pg)
14/3/97 2/7/97	**14163,848**	38 ± 3 89 ± 4
16/1/97 2/7/97	**60501,105**	not measured 89 ± 4
2/7/97	**65701,23**	10.2 ± 0.5
2/7/97	**72161,73**	10.2 ± 0.5
14/3/97 2/7/97	**74220,125**	38 ± 3 89 ± 4

Analytical blanks were measured with every set of samples analysed (Table 6-9), the procedure is described in Section 5.4. The analytical blanks for the composition measurements were less than 0.01% of the cadmium in the samples, suggesting that any contamination observed in these samples was not from the chemistry or mass spectrometry.

Table 6-10 Isotopic abundances of cadmium in the lunar samples, raw data.

Date	Sample	$^{108}Cd/^{112}Cd$	$^{110}Cd/^{112}Cd$	$^{111}Cd/^{112}Cd$	$^{113}Cd/^{112}Cd$	$^{114}Cd/^{112}Cd$	$^{116}Cd/^{112}Cd$
1997	**Laboratory standard**	0.037138 ±0.000046	0.51979 ±0.00033	0.53136 ±0.00025	0.50587 ±0.00011	1.18823 ±0.00056	0.30875 ±0.00031
14/3/97	**14163,848**	0.03722 ±0.00013	0.51994 ±0.00011	0.53170 ±0.00010	0.50598 ±0.00010	1.18805 ±0.00027	0.30861 ±0.00016
2/7/97	**14163,848**	0.037108 ±0.000025	0.51938 ±0.00013	0.53138 ±0.00014	0.505870 ±0.000040	1.18894 ±0.00025	0.30909 ±0.00015
16/1/97	**60501,105 (Daly)**		0.52023 ±0.00048		0.50391 ±0.00053	1.1880 ±0.0014	
2/7/97	**60501,105**	0.0368 ±0.0010	0.51594 ±0.00060	0.53017 ±0.00081	0.50601 ±0.00043	1.19680 ±0.00064	0.3140 ±0.0015
9/4/97	**65701,23**	0.03651 ±0.00021	0.51369 ±0.00036	0.52804 ±0.00039	0.50661 ±0.00025	1.20229 ±0.00052	0.3189 ±0.0017
9/4/97	**72161,73**	0.03606 ±0.00037	0.51307 ±0.00048	0.52812 ±0.00045	0.50709 ±0.00046	1.2020 ±0.0014	0.3171 ±0.0014
14/3/97	**74220,125 (Faraday)**	0.0353 ±0.0027	0.5187 ±0.0022	0.5384 ±0.0059	0.5011 ±0.0032	1.1827 ±0.0020	0.340 ±0.030
	(Daly)		0.5258 ±0.0022	0.5342 ±0.0018	0.5052 ±0.0014	1.1758 ±0.0043	
2/7/97	**74220,125**	0.037355 ±0.000053	0.52113 ±0.00017	0.53186 ±0.00025	0.505146 ±0.000037	1.18538 ±0.00049	0.30745 ±0.00032

Uncertainties are at 95% confidence levels.

Table 6-11 Isotopic abundances of cadmium in the lunar samples, normalised to $^{110}Cd/^{112}Cd = 0.51928$, but with no additional modifications for tin or anomalies in the exponential law caused by large mass fractionation effects.

Date	Sample	$^{108}Cd/^{112}Cd$	$^{111}Cd/^{112}Cd$	$^{113}Cd/^{112}Cd$	$^{114}Cd/^{112}Cd$	$^{116}Cd/^{112}Cd$	$^{114}Cd/^{113}Cd$
1997	**Laboratory standard**	0.037067 ±0.000017	0.53111 ±0.00012	0.50612 ±0.00019	1.18937 ±0.00041	0.30933 ±0.00013	2.34997 ±0.00042
14/3/97	**14163,848**	0.03713 ±0.00013	0.531359 ±0.000065	0.50630 ±0.00014	1.18954 ±0.00032	0.30938 ±0.00018	2.34979 ±0.00090
2/7/97	**14163,848**	0.037093 ±0.000020	0.531332 ±0.000081	0.505918 ±0.000093	1.189162 ±0.000071	0.309201 ±0.000035	2.35051 ±0.00045
16/1/97	**60501,105 (Daly)**			0.50455 ±0.00058	1.1912 ±0.0016		2.3602 ±0.0042
2/7/97	**60501,105**	0.03707 ±0.00020	0.531545 ±0.000096	0.50500 ±0.00018	1.19017 ±0.00030	0.30953 ±0.00035	2.35675 ±0.0010
9/4/97	**65701,23**	0.03732 ±0.00021	0.53090 ±0.00025	0.50391 ±0.00036	1.18957 ±0.00053	0.3122 ±0.0014	2.3602 ±0.0019
9/4/97	**72161,73**	0.03687 ±0.00037	0.53138 ±0.00030	0.50374 ±0.00050	1.1884 ±0.0014	0.3094 ±0.0011	2.3566 ±0.0039
~~14/3/97~~	~~**74220,125 (Faraday)**~~	~~0.0354 ±0.0025~~	~~0.5387 ±0.0064~~	~~0.5008 ±0.0038~~	~~1.1815 ±0.0048~~	~~0.339 ±0.028~~	~~2.352 ±0.021~~
	~~**(Daly)**~~		~~0.53084 ±0.00082~~	~~0.5084 ±0.0013~~	~~1.1905 ±0.0088~~		~~2.342 ±0.018~~
2/7/97	**74220,125**	0.037088 ±0.000044	0.53092 ±0.00017	0.506032 ±0.000088	1.18952 ±0.00016	0.30958 ±0.00015	2.35068 ±0.00051

Uncertainties are at 95% confidence levels.

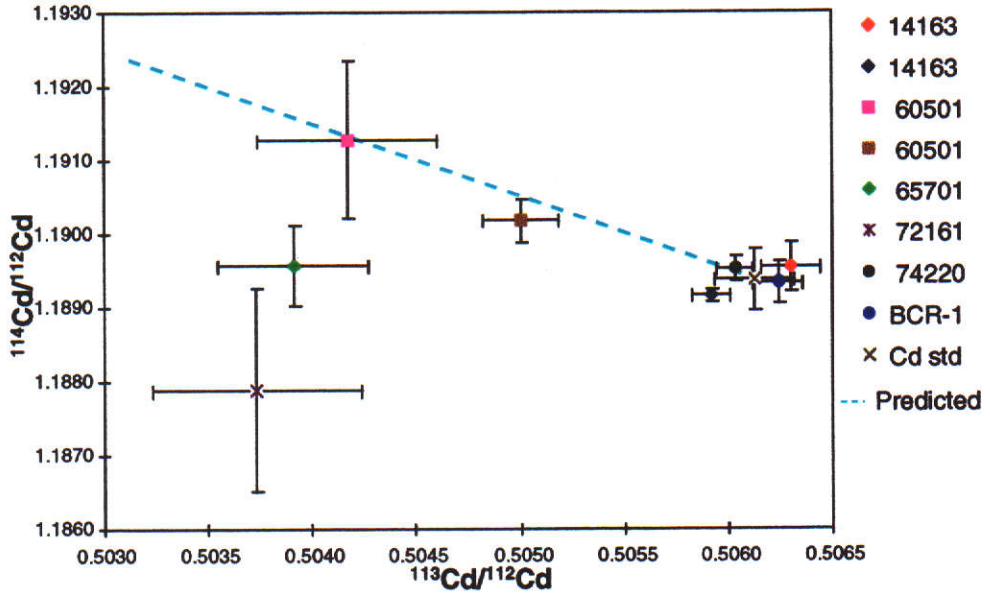

Figure 6-4 Correlation diagram of $^{114}Cd/^{112}Cd$ versus $^{113}Cd/^{112}Cd$ in the lunar samples showing the predicted line for neutron capture. No corrections have been made for interferences, ratios are normalised to $^{110}Cd/^{112}Cd = 0.51928$.

The cadmium lunar data, normalised to $^{110}Cd/^{112}Cd = 0.51928$ and corrected for instrumental mass fractionation, are shown on a $^{114}Cd/^{112}Cd$ versus $^{113}Cd/^{112}Cd$ correlation diagram in Figure 6-4, and are compared with the predicted path for neutron capture. The cluster of data to the right of the Figure contain the cadmium standard, BCR-1, 14163,848 and 74220,125. No neutron capture is evident in 14163,848 or 74220,125. The two 14163,848 samples would be expected to show the significant neutron capture observed with gadolinium (Figure 6-30) and samarium (Figure 6-36). However contamination from a source of terrestrial cadmium, probably the plastic pieces described above, suggests that these data should be rejected.

74220,125 is the same as terrestrial cadmium within experimental uncertainties. This either indicates contamination with terrestrial cadmium, that the neutron capture is too low to be identified or there is no neutron capture. For gadolinium and samarium the reduction in $^{157}Gd/^{160}Gd$ and $^{149}Sm/^{154}Sm$ with this sample is 0.02% and 0.04% respectively (Tables 6-22 and 6-32). A decrease of 0.06% in $^{113}Cd/^{112}Cd$,

or 0.04% in $^{114}Cd/^{113}Cd$, is the minimum which can be detected with the present precision.

Possible neutron capture effects are seen in 60501,105, 65701,23 and 72161,73, though two of the data points are well below the predicted line. This will be examined in the next Section and modified data displayed at the end of Section 6.3.1.

The two data points for 60501,105 fall on the predicted line for neutron capture, though the first point (a pink square, measured on the Daly) shows greater changes in $^{114}Cd/^{113}Cd$ from neutron capture than the second (0.5% compared to 0.3%, Table 6-12). The concentration of cadmium in the first 60501,105 sample (3.59 ppm) suggests it is highly contaminated though there is no sign of such contamination by terrestrial cadmium in Figure 6-4, the second 60501,105 sample (yellow square), dated 2/7/97, shows the possibility of slight contamination. This contradiction suggests that the source of the contamination is not spread evenly throughout the sample.

Table 6-12 Percentage change in the abundances of $^{113}Cd/^{112}Cd$, $^{114}Cd/^{112}Cd$ and $^{114}Cd/^{113}Cd$ in lunar samples compared to the laboratory standard abundances of these isotopes. All are normalised data.

	$^{113}Cd/^{112}Cd$	$^{114}Cd/^{112}Cd$	$^{114}Cd/^{113}Cd$
14163,848	0.04%	0.01%	0.02%
14163,848	-0.04%	-0.02%	0.02%
60501,105	-0.39%	0.16%	0.55%
60501,105	-0.22%	0.07%	0.29%
65701,23	-0.44%	0.02%	0.45%
72161,73	-0.47%	-0.13%	0.35%
74220,125	-0.02%	0.01%	0.03%

Samples 65701,23 and 72161,73 show changes in the $^{114}Cd/^{113}Cd$ ratio of 0.5% and 0.4%, but with a possible interference from tin this is not necessarily from neutron capture. This problem will be examined in the next Sections.

6.3.1.1 Effect of isobaric tin and mass fractionation

In the next Sections it will be shown that in samples 60501,105, 65701,23 and 72161,73 the cadmium isotopes were contaminated by small amounts of tin and that the samples showed evidence of 0.3% to 0.6% per mass unit of lunar mass fractionation. Cadmium standards measured since 1994 were checked for similar mass fractionation effects. Modified ratios and correlation diagrams for the lunar samples will be presented later.

Contamination by tin is considered first, the abundance of the tin isotopes are listed in Table 6-13. The $^{114}Cd/^{112}Cd$ versus $^{113}Cd/^{112}Cd$ correlation diagram in Figure 6-5 shows the predicted effect of subtracting tin from the two lunar samples 65701,23 and 72161,73. The arrowed lines have been calculated by subtracting increasing amounts of tin from the raw data for isotopes 112, 114 and 116, then normalising the data to $^{110}Cd/^{112}Cd = 0.51982$.

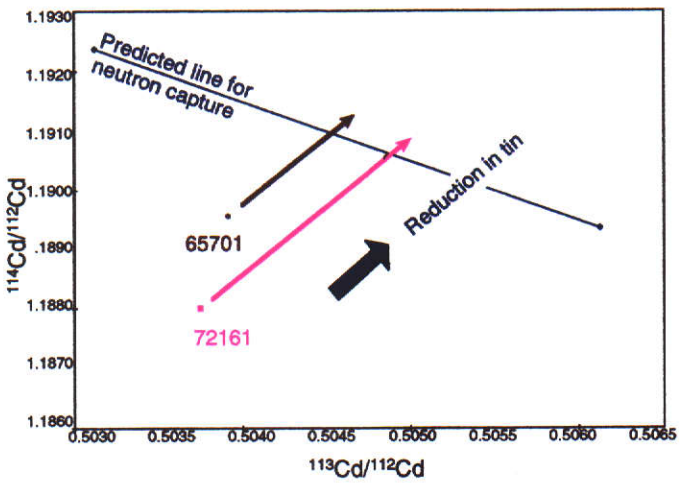

Figure 6-5 Two displaced lunar samples, showing the locus of the data points with the subtraction of tin isotopes.

For samples 65701,23 and 72161,73 the arrowed lines cross the predicted line for neutron capture when the tin content of isotope 112 is 0.0008 (0.08%) and 0.0014 (0.14%) respectively, though this will be true only if interference by tin is the single cause of the observed anomalies.

Table 6-13 The abundances of the tin isotopes.

Isotope	112	114	115	116	117
Sn (%)	1.0	0.65	0.35	14.4	7.6
Isotope	118	119	120	122	124
Sn (%)	24.1	8.6	32.8	4.7	5.8

However, it will be shown that the anomalies here were not necessarily all caused by tin.

A modification to the fractionation correction is described in Section 6.3.1.5 below. Figure 6-6 shows the effect of this correction on the position of the lunar sample data points.

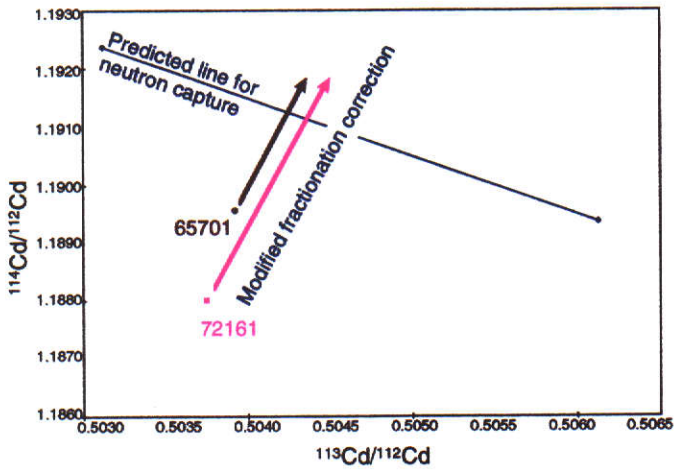

Figure 6-6 Two displaced lunar samples, showing the locus of the data points with a modification to the fractionation correction.

6.3.1.2 Is the interference tin?

To assess the influence of tin the cadmium standards measured on the Faraday multi-collector during 1996 and 1997 were re-examined. The scatter of the raw cadmium standard data (not listed in this thesis) were compared to the raw lunar data (listed in Table 6-10). The raw data are shown as a percentage deviation from the average of all the normalised cadmium standards measured in 1996 and 1997.

In Figures 6-7, 6-8 and 6-9 the raw ratios $^{110}Cd/^{112}Cd$, $^{116}Cd/^{112}Cd$ and $^{111}Cd/^{112}Cd$ are plotted as a percentage deviation from the relevant normalised ratios. The mean of the raw data, shown as a pink dotted line on each graph, was calculated from all the cadmium standard

measurements made with the 112 axial cup setting on the mass spectrometer in 1996 and 1997. Excluded were two anomalous measurements made on 15/2/97 and one on 9/7/97, marked in green on the graphs.

The $^{110}Cd/^{112}Cd$ ratios in Figure 6-7 are presented as a percentage deviation from $^{110}Cd/^{112}Cd = 0.51928$. The mean over two years of the $^{110}Cd/^{112}Cd$ raw data is 0.14±0.03% above this value.

Figure 6-7 suggests that the interference in the three standards measured on 15/2/97 and on 9/7/97, and in lunar samples 60501,105, 65701,23 and 72161,73 could be caused by tin at mass 112. Tin has isotopes isobaric with cadmium at mass numbers 112, 114 and 116 (Table 6-13).

To confirm the presence of tin the $^{116}Cd/^{112}Cd$ raw data ratios were plotted as a percentage deviation from $^{116}Cd/^{112}Cd = 0.30931$, and also $^{111}Cd/^{112}Cd$ as a percentage from $^{111}Cd/^{112}Cd = 0.53120$, shown in Figures 6-8 and 6-9. The average of the $^{116}Cd/^{112}Cd$ cadmium standard ratios is -0.27±0.06% from the normalised value and for $^{111}Cd/^{112}Cd$ 0.06±0.03%.

Mass 116 has the largest abundance tin isotope of those that overlap with cadmium (14.4%), and the three $^{116}Cd/^{112}Cd$ measurements on 15/2/97, 9/7/97, and in the lunar samples 60501,105, 65701,23 and 72161,73 (seen in Figure 6-8 and listed in Table 6-14) strongly suggest that the interference is tin. One anomaly here is that sample 65701,23 is showing a greater deviation from the mean than sample 72161,73, for the $^{110}Cd/^{112}Cd$ ratio this was reversed.

The $^{114}Cd/^{112}Cd$ ratios, not plotted here, show similar results to $^{116}Cd/^{112}Cd$. If the interference was caused by tin the $^{114}Cd/^{112}Cd$ ratio would be 0.65/14.4 times the magnitude of $^{116}Cd/^{112}Cd$, that this is not so can be seen in Table 6-14. In each case, except for sample 65701,23, the deviation from the mean of $^{114}Cd/^{112}Cd$ is half that experienced by $^{116}Cd/^{112}Cd$, a suggestion that lunar mass fractionation may be present.

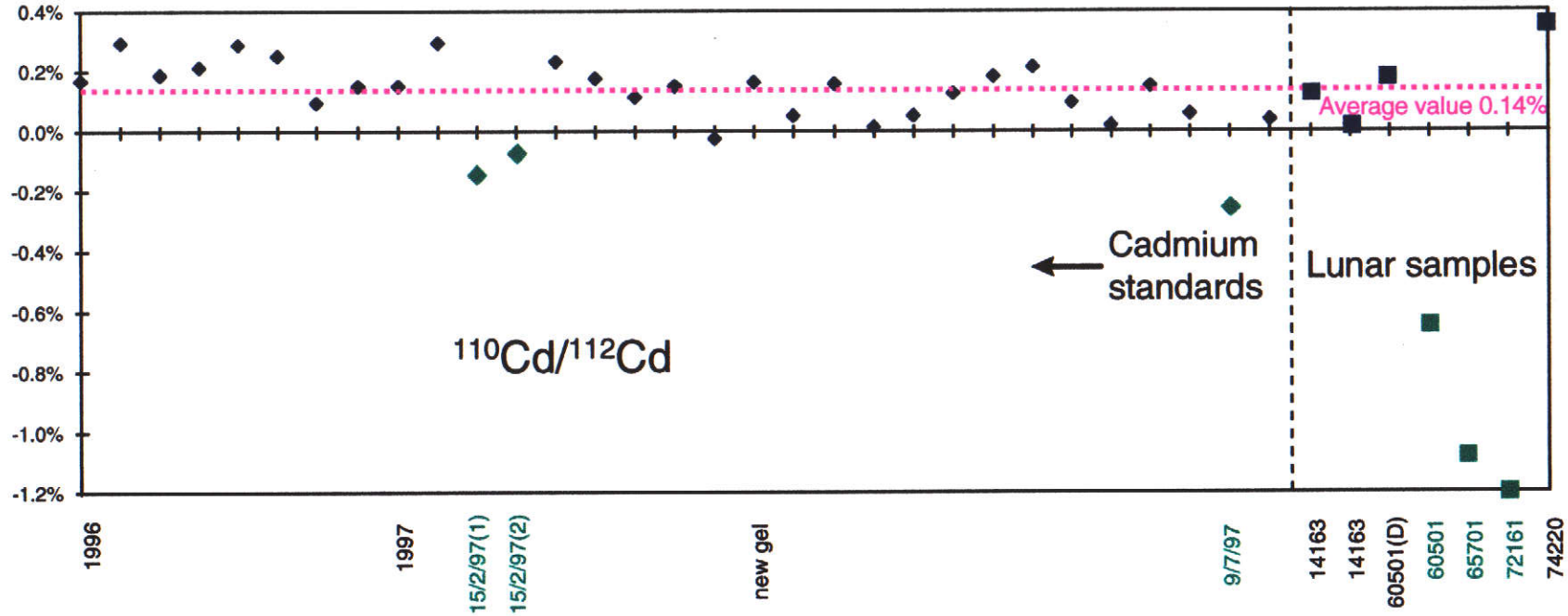

Figure 6-7 Percentage deviation of the raw $^{110}Cd/^{112}Cd$ cadmium standard measurements (1996 to 1997) and the lunar samples from $^{110}Cd/^{112}Cd = 0.51928$.

The pink dotted line, 0.14±0.03%, is the average of the $^{110}Cd/^{112}Cd$ raw cadmium standard data measurements for 1996 and 1997 excluding the three extreme data points coloured in turquoise blue.

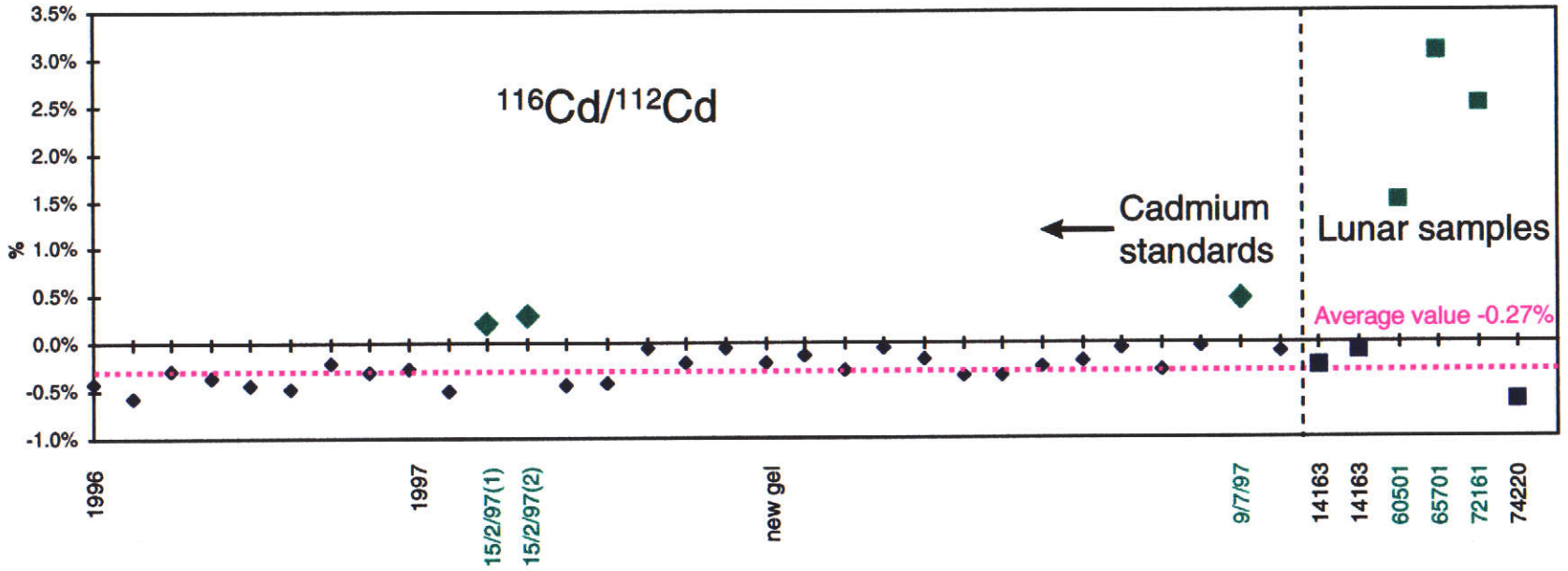

Figure 6-8 Percentage deviation of the raw cadmium standard measurements (1996 to 1997) and the lunar samples from $^{116}Cd/^{112}Cd = 0.30931$, to determine if tin is present.

The pink dotted line, -0.27±0.06%, is the average of the $^{116}Cd/^{112}Cd$ raw cadmium standard data measurements for 1996 and 1997, excluding the three extreme data points coloured in turquoise blue.

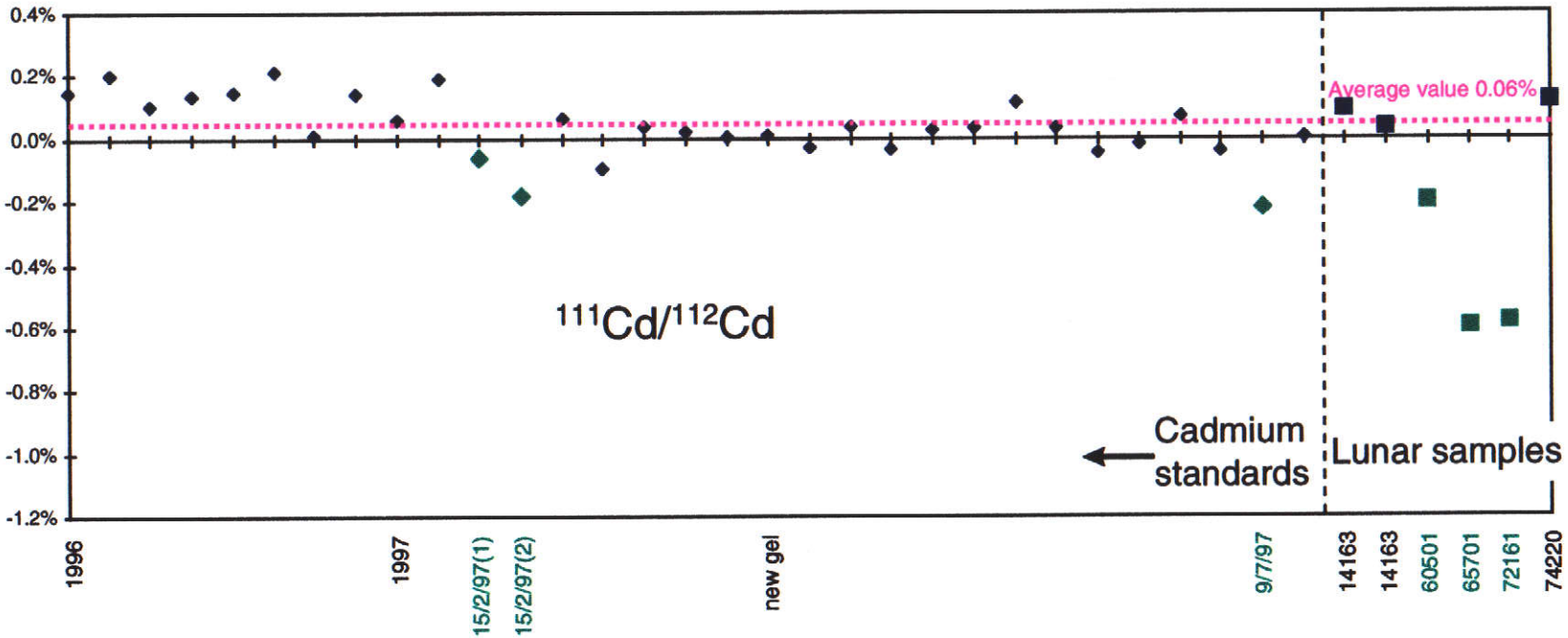

Figure 6-9 Percentage deviation of the raw cadmium standard measurements (1996 to 1997) and the lunar samples from $^{111}Cd/^{112}Cd = 0.53120$, to determine if tin is present.

The pink dotted line, 0.06±0.03%, is the average of the $^{111}Cd/^{112}Cd$ raw cadmium standard data measurements for 1996 and 1997, excluding the three extreme data points coloured in turquoise blue.

Figure 6-9 shows the $^{111}Cd/^{112}Cd$ ratio for the raw data for 1996, 1997 and the lunar samples. If the interference was tin the $^{111}Cd/^{112}Cd$ data would be similar to $^{110}Cd/^{112}Cd$ as the abundance of ^{111}Cd is of similar magnitude to ^{110}Cd and there is no tin at masses 110 or 111, only at mass 112. However, comparing the $^{110}Cd/^{112}Cd$ and $^{111}Cd/^{112}Cd$ ratios in Figures 6-7 and 6-9 and in Table 6-14 it can be seen that there is a similar type of interference in the standards measured on 15/2/97 and on 9/7/97, and in lunar samples 60501,105, 65701,23 and 72161,73, but their relative magnitude suggests mass fractionation, with the low mass isotopes showing reduced abundance.

Table 6-14 Percentage deviation of measured raw data from the mean of the 1996 and 1997 cadmium standard raw data, seen in Figures 6-7, 6-8 and 6-9. Included are the three anomalous standards and three lunar samples under discussion.

	$^{110}Cd/^{112}Cd$	$^{111}Cd/^{112}Cd$	$^{113}Cd/^{112}Cd$	$^{114}Cd/^{112}Cd$	$^{116}Cd/^{112}Cd$
15/2/97 (1)	-0.3	-0.1	+0.06	+0.2	+0.5
15/2/97 (2)	-0.2	-0.2	+0.04	+0.3	+0.6
9/7/97	-0.4	-0.3	+0.09	+0.4	+0.7
60501,105	-0.8	-0.3	+0.1	+0.8	+1.8
65701,23	-1.2	-0.7	+0.1	+1.2	+3.4
72161,73	-1.3	-0.5	+0.2	+1.25	+2.8

Table 6-14 summarises the divergence from the mean of the three standard samples and the three lunar samples. They are listed as a percentage deviation from the mean of the 1996 and 1997 cadmium standard raw data for each ratio and all show evidence of mass fractionation.

The results for the three cadmium standards and the three lunar samples are considered below. The standard samples were examined first and the lunar samples after Section 6.3.1.6.

6.3.1.3 Three anomalous cadmium standards

Mass fractionation of 0.1%, 0.1% and <0.2% per mass unit is seen in the three cadmium laboratory standards which were identified in Figures 6-7, 6-8 and 6-9; no tin is observed. The raw data for one of the samples

are plotted in Figure 6-10 as a percentage deviation from the mean of the 1997 laboratory standards, also raw data.

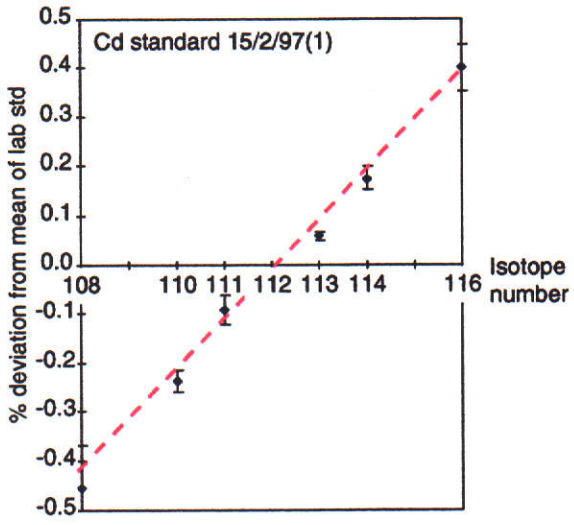

Figure 6-10 The raw data for the cadmium standard measured on 15/2/97(1) plotted as a percentage deviation from the mean of the standards, showing fractionation of 0.1% per mass unit. Uncertainties are at the 95% confidence level.

In all the cadmium standards measurements since early 1994 fewer than 9% have shown this effect, and none show fractionation greater than 0.2% per mass unit. Of this 9%, 75% had been used to check the positions of the multi-collector cups before collecting standard data. It is therefore possible that the lighter isotopes had been preferentially evaporated before the measurements were started.

The mass fractionation observed in the lunar samples, discussed below, is much greater than that observed in these cadmium standard samples and in addition the data from the lunar samples were recorded as soon as the cadmium ionised in the mass spectrometer, so mass fractionation of this type seen in the lunar samples is unlikely to be from systematic effects.

The three lunar samples showing mass fractionation have been through the same chemistry and mass spectrometry procedures as samples 14163,848 and 74220,125 and BCR-1, which show no signs of

mass fractionation. This suggests that the mass fractionation in 60501,105, 65701,23 and 72161,73 is unlikely to be caused by these procedures. The mass of cadmium measured in BCR-1 is similar to that in sample 60501,105, so fractionation cannot be attributed to mass differences.

6.3.1.4 Correcting for fractionation and interference

Anomalies found in samples 60501,105, 65701,23 and 72161,73 are modified by the subtraction of picogram amounts of tin at masses 112, 114 and 116. A small correction has also been made to the fractionation correction procedure (described in the next Section 6.3.1.5).

An iterative procedure is used to subtract tin from isotopes 112, 114 and 116 and to correct for fractionation. There are four conditions which need to be satisfied before the iteration is complete.

First the raw data are plotted as a percentage deviation from the average of the 1997 raw standard data (Figures 6-14, 6-19 and 6-24). A line of best fit is drawn through $^{108}Cd/^{112}Cd$, $^{110}Cd/^{112}Cd$, $^{111}Cd/^{112}Cd$ and mass 112 (which is fixed at zero), the slope identifying the magnitude of the mass fractionation. With no interference from tin the line should also pass through $^{116}Cd/^{112}Cd$, and in the presence of neutron capture the line should pass between $^{113}Cd/^{112}Cd$ and $^{114}Cd/^{112}Cd$.

It has been assumed that the mass fractionation is linear, but it is possible that the increased abundance of $^{116}Cd/^{112}Cd$ seen in all three samples is not from tin, but from a non-linearity in the lunar mass fractionation, though with neutron capture causing anomalies at $^{113}Cd/^{112}Cd$ and $^{114}Cd/^{112}Cd$ it is not possible to be certain. To take this into account calculations are made both with tin subtracted and without.

So the first condition is that after tin has been subtracted from masses 112, 114 and 116 the fractionation line must pass through the data point $^{116}Cd/^{112}Cd$.

For the second condition, the normalised data are plotted as a percentage deviation from the average of the 1997 normalised standard data. If there is no interference from tin or any other effect all the points

should plot on the line, except in the presence of neutron capture when $^{113}Cd/^{112}Cd$ should be below and $^{114}Cd/^{112}Cd$ above the line.

However, it has been found that when highly fractionated samples are normalised to $^{110}Cd/^{112}Cd = 0.51928$ using the exponential law, the results vary directly with the magnitude of the fractionation. This effect is discussed in the next Section, and a small modification to the normalisation procedure is described.

So the second condition is that after tin has been subtracted and the fractionation correction modified $^{114}Cd/^{112}Cd$ must plot above the line and $^{113}Cd/^{112}Cd$ below the line, and at the correct separation for neutron capture. Though all other points should plot on the line, this is not always true with $^{116}Cd/^{112}Cd$. The presence of tin has the greatest effect at $^{116}Cd/^{112}Cd$ and there are uncertainties in the magnitude of the tin correction, especially when the linearity of the lunar mass fractionation is not established. It will also be shown in the next Section that the exponential law is inadequate to precisely reduce data in the presence of large mass fractionation effects. At $^{116}Cd/^{112}Cd$ this effect is magnified.

The third condition refers to the correct separation of $^{114}Cd/^{112}Cd$ and $^{113}Cd/^{112}Cd$ above and below the line when there is neutron capture. For the cadmium standard $^{114}Cd/^{112}Cd = 1.189372$ and $^{113}Cd/^{112}Cd = 0.506123$, so when ^{113}Cd captures a neutron $^{113}Cd/^{112}Cd$ decreases and $^{114}Cd/^{112}Cd$ increases. They do so in the ratio $0.506123/1.189372 \approx 0.43$. When $^{114}Cd/^{112}Cd$ increases by 0.43%, $^{113}Cd/^{112}Cd$ decreases by 1%, so this requirement is the third condition.

For the fourth condition the normalised data are plotted on $^{114}Cd/^{112}Cd$ versus $^{113}Cd/^{112}Cd$ correlation diagrams where data showing neutron capture should lie on the predicted line.

During the iterative procedure increasing amounts of tin are subtracted and the fractionation correction is modified by increasing percentages until the four conditions are satisfied. It is applied to the three lunar samples, 60501,105, 65701,23 and 72161,73 in Sections 6.3.1.6, 7 and 8.

6.3.1.5 The modified mass fractionation correction

Figure 6-11 shows the effect of mass fractionation when raw data showing different initial fractionation are normalised to $^{110}Cd/^{112}Cd$ = 0.51928 using the exponential law. To examine this effect the average 1997 cadmium standard raw data was first linearly fractionated over a range of +1% to -1% per mass unit (assuming that lunar mass fractionation is linear). It was then normalised to $^{110}Cd/^{112}Cd$ = 0.51928 and plotted as a percentage deviation from the starting composition (also normalised). It can be seen in Figure 6-11 that positive fractionation of between 0% and 1% per mass unit results in an increase in normalised $^{116}Cd/^{112}Cd$ of up to 0.03% at the maximum where the fractionation is 0.45% per mass unit, with a lesser effect on $^{114}Cd/^{112}Cd$ and $^{113}Cd/^{112}Cd$ of 0.008% and 0.001% (Figure 6-11).

Russell et al. (1978) described the same effect when highly fractionated measured ratios are unable to be reduced with sufficient precision by exponential, linear or Rayleigh fractionation laws.

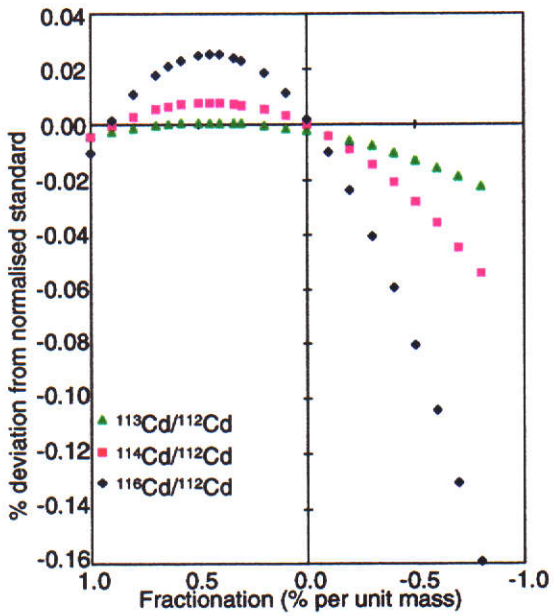

Figure 6-11 The cadmium standard fractionated by +1% to -1% per mass unit by calculation are plotted as a percentage deviation from the normalised cadmium standard. The x-axis displays the calculated fractionation.

Figure 6-12 shows the effect at each isotope when cadmium which has been linearly fractionated by 0.45% per mass unit, is then normalised to

$^{110}Cd/^{112}Cd$ = 0.51928 using the exponential law. The average uncertainty on each point is ±0.05%.

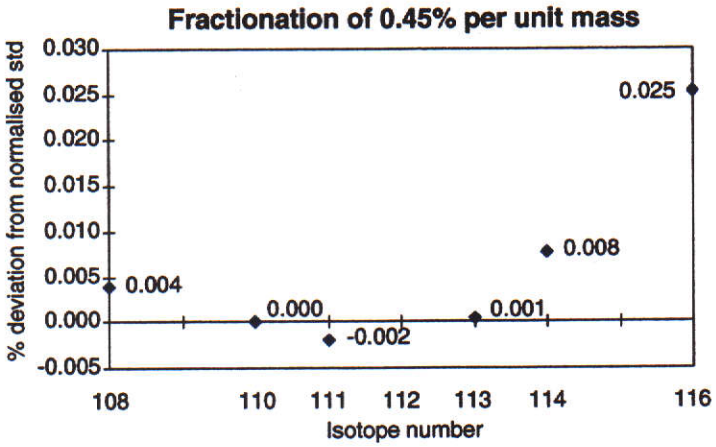

Figure 6-12 Cadmium standard fractionated to 0.45% per mass unit and normalised to $^{110}Cd/^{112}Cd$ = 0.51928 shown as a percentage deviation from the normalised, unfractionated standard.

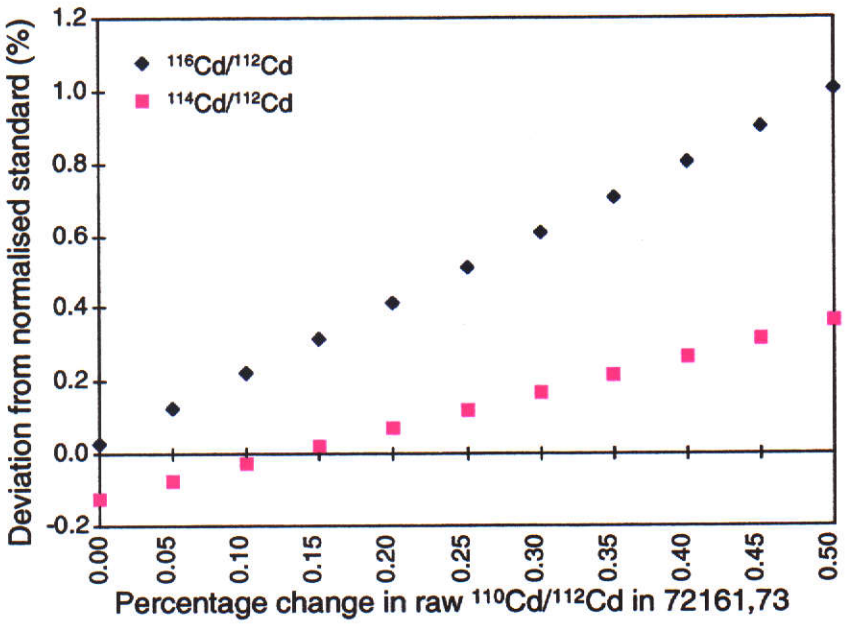

Figure 6-13 The variation of the normalised $^{114}Cd/^{112}Cd$ and $^{116}Cd/^{112}Cd$ in 72161,73 with percentage increases in the raw $^{110}Cd/^{112}Cd$. The sample is fractionated by 0.54% per mass unit.

From Figure 6-11 it can be seen that a small decrease in the raw value of $^{110}Cd/^{112}Cd$ (the normalising ratio) caused by fractionation will alter the normalised values of $^{114}Cd/^{112}Cd$ and $^{116}Cd/^{112}Cd$. If the raw $^{110}Cd/^{112}Cd$ is deliberately increased by a small amount the normalised $^{116}Cd/^{112}Cd$

will increase by twice this amount, while $^{114}Cd/^{112}Cd$ will increase by slightly less, this is illustrated for sample 72161,73 in Figure 6-13.

The normalised lunar samples will be affected by these biases and a modification to $^{110}Cd/^{112}Cd$ before normalisation will be made when correcting for interferences in the following Sections.

6.3.1.6 Modifications to sample 60501,105 to reduce the effects of tin and mass fractionation

The unmodified raw cadmium data for 60501,105 are plotted as a percentage deviation from the 1997 raw laboratory standard measurements in Figure 6-14.

The line of best fit passes through $^{108}Cd/^{112}Cd$, $^{110}Cd/^{112}Cd$, $^{111}Cd/^{112}Cd$ and mass 112, and just below $^{116}Cd/^{112}Cd$. $^{114}Cd/^{112}Cd$ and $^{113}Cd/^{112}Cd$ lie above and below the line, showing mass fractionation of 0.30% per mass unit. $^{116}Cd/^{112}Cd$ lies just above the fractionation line, suggesting either interference from tin or non-linearity in the fractionation.

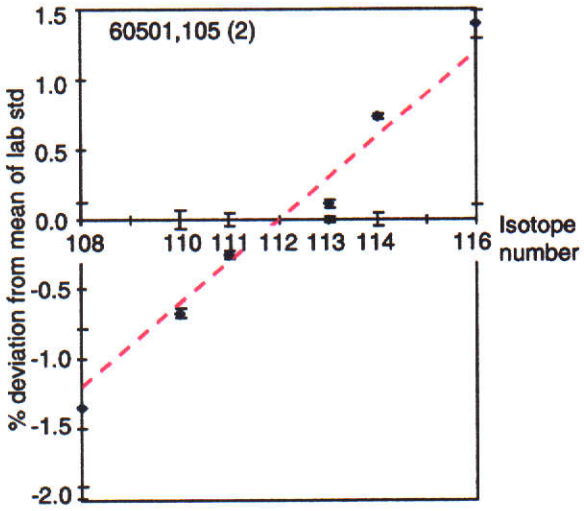

Figure 6-14 The raw cadmium data for the lunar sample 60501,105 plotted as a percentage deviation from the 1997 raw laboratory standard, showing 0.30% fractionation per mass unit. Uncertainties are at the 95% confidence level.

These same data, normalised to $^{110}Cd/^{112}Cd = 0.51928$, and with no corrections for tin or lunar mass fractionation, are shown as a yellow

diamond in the $^{114}Cd/^{112}Cd$ versus $^{113}Cd/^{112}Cd$ correlation diagram in Figure 6-18 and as a light blue diamond in Figure 6-17.

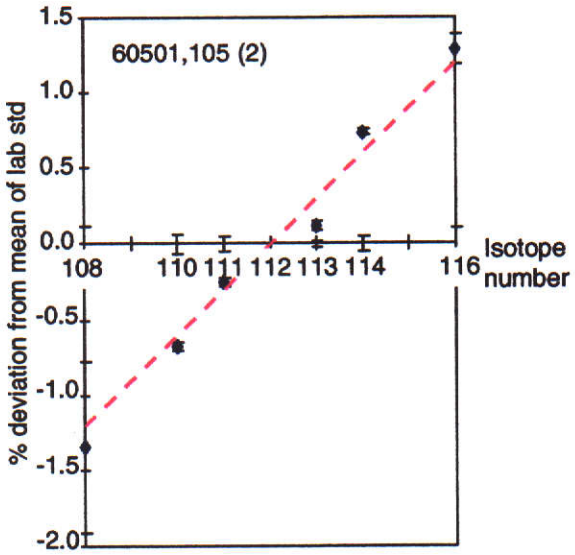

Figure 6-15 The raw cadmium data for the lunar sample 60501,105, with approximately 10 pg of tin subtracted and the line of best fit passing though $^{116}Cd/^{112}Cd$.

The iteration procedure described in Section 6.3.1.4 was applied to the raw data. Figure 6-15 shows the raw data corrected for tin interferences tin at masses 112, 114 and 116. Assuming the fractionation to be linear it was found that 0.11% of the 116 isotope was ^{116}Sn, (i.e. about 10 pg total of tin in the measured sample on the unlikely assumption of equal ionisation efficiency of tin and cadmium).

The effect of subtracting the tin can be seen in Figures 6-17 and 6-18 (dark blue diamonds).

When the normalised data (with no tin subtracted) are plotted on Figure 6-11, (results seen in Figure 6-16), $^{114}Cd/^{112}Cd$ and $^{116}Cd/^{112}Cd$ initially lie 0.06% above the standard normalised data, within the uncertainties of the fractionated data. With tin subtracted $^{114}Cd/^{112}Cd$ is still at +0.06% though $^{116}Cd/^{112}Cd$ lies 0.04% below the standard value. This casts doubt on the validity of the tin subtraction, and for this reason a second set of calculations, with no subtraction for tin, is included.

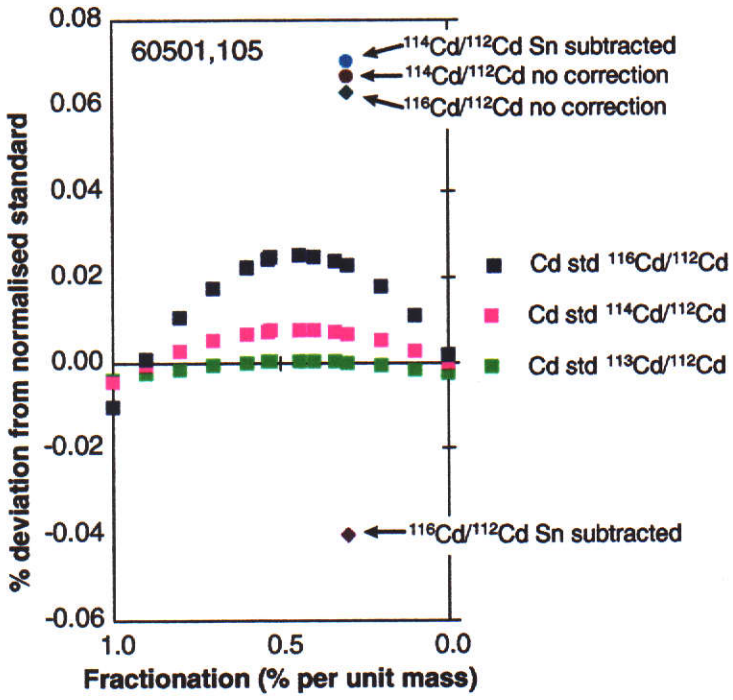

Figure 6-16 Normalised data plotted against fractionation showing the positions of $^{114}Cd/^{112}Cd$ and $^{116}Cd/^{112}Cd$ for 60501,105 both before and after tin has been subtracted.

After the subtraction of tin the raw value of $^{110}Cd/^{112}Cd$ was increased by 0.02% following the method described in 6.3.1.5 (0.02% is less than the uncertainty in the $^{110}Cd/^{112}Cd$ ratio which is 0.1% at the 95% confidence level). This results in $^{116}Cd/^{112}Cd$ lying on the line in Figure 6-17 (pink diamonds), with $^{114}Cd/^{112}Cd$ and $^{113}Cd/^{112}Cd$ above and below the line in the expected configuration. In the correlation diagram, Figure 6-18, the data point for 60501,105 now lies on the predicted line for neutron capture (a pink diamond again).

An alternative approach is examined where the assumption is made that the lunar mass fractionation is non-linear and no tin is present. The raw data are modified at $^{110}Cd/^{112}Cd$ by an increase of 0.024%, then normalised to $^{110}Cd/^{112}Cd = 0.51928$. No tin is subtracted. All isotope ratios except for $^{116}Cd/^{112}Cd$ are unchanged compared to the results achieved above. $^{116}Cd/^{112}Cd$ is 0.1% higher than the standard (seen in Figure 6-17, the green diamond).

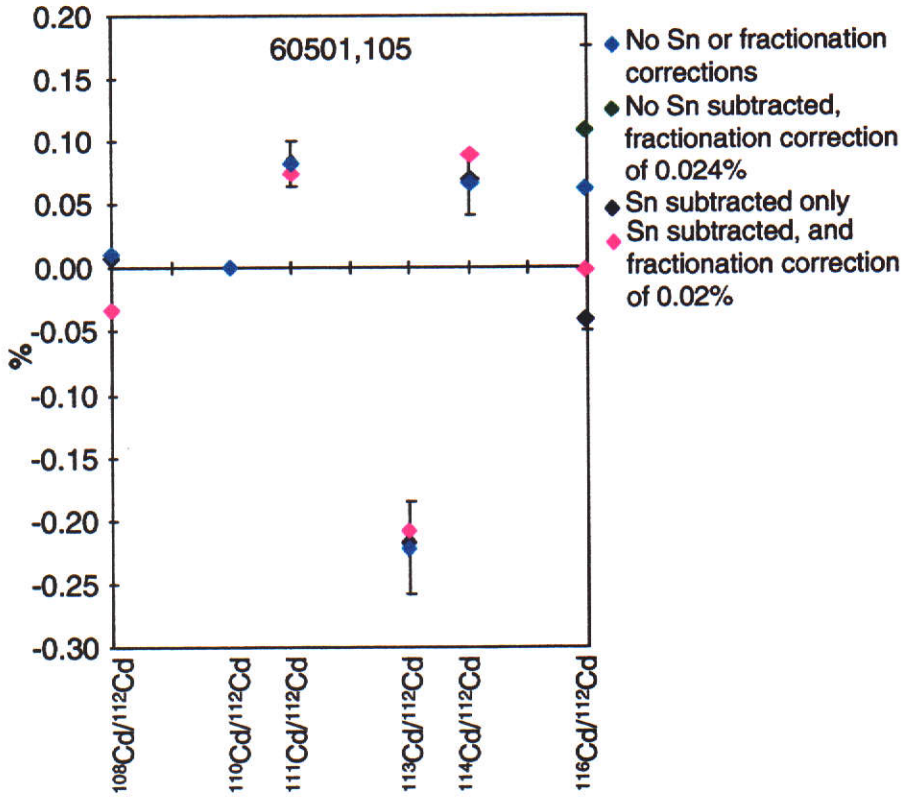

Figure 6-17 Sample 60501,105, data normalised to $^{110}Cd/^{112}Cd$ = 0.51928, is plotted as a percentage deviation from the normalised standard. Data have been modified by the subtraction of tin and by a modification to the mass fractionation correction.

Summarising, the data in Figure 6-17 show 60501,105, normalised to $^{110}Cd/^{112}Cd$ = 0.51928. Data where no tin has been subtracted and no modifications made in the normalisation calculation, are shown as light blue diamonds. The dark blue diamonds are data with only tin subtracted. These data are then modified by increasing the raw $^{110}Cd/^{112}Cd$ by 0.02% (pink diamonds). The green point is the result of a modification of 0.024% in $^{110}Cd/^{112}Cd$, with no tin subtraction. An interference is evident at $^{111}Cd/^{112}Cd$, which could also be seen in the raw data in Figure 6-9.

The normalised data for 60501,105 are shown on the correlation diagram in Figure 6-18. The data point with no modifications is the yellow diamond, the effect of the subtraction of tin is shown with the dark blue diamond and the pink data point is the position after the subtraction of tin as well as the 0.02% increase in the raw $^{110}Cd/^{112}Cd$ before normalisation.

The same final point results from a 0.024% increase in the raw $^{110}Cd/^{112}Cd$ with no tin subtracted.

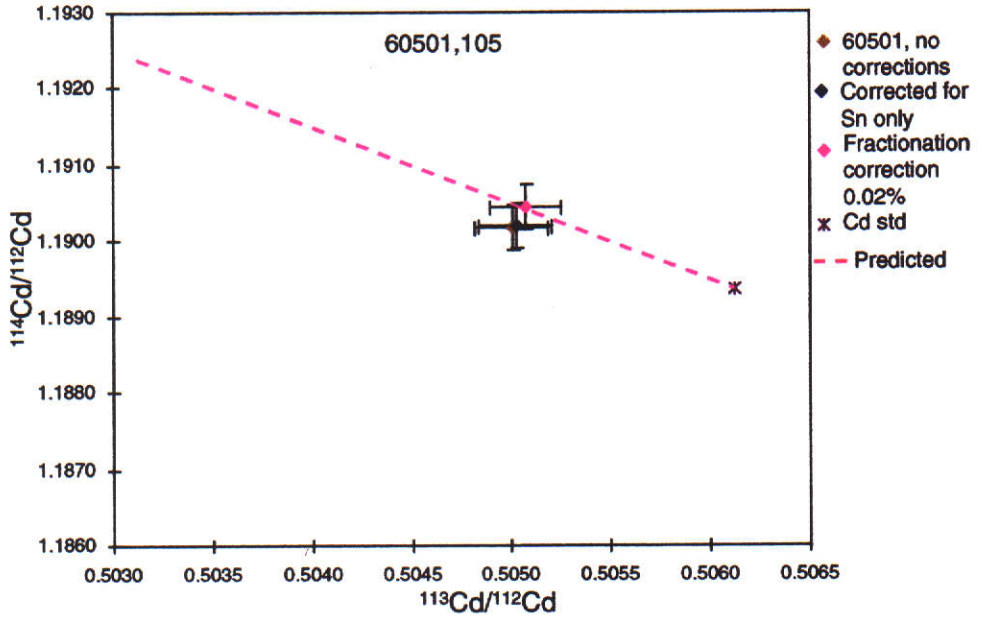

Figure 6-18 $^{114}Cd/^{112}Cd$ and $^{113}Cd/^{112}Cd$ correlation diagram showing 10 pg tin subtracted from 60501,105, and the modification of $^{110}Cd/^{112}Cd$ by 0.02%, with the predicted line for neutron capture.

As a result of the iteration procedure the four conditions were satisfied when 10 pg of tin was subtracted and $^{110}Cd/^{112}Cd$ was increased by 0.02%, or when no tin was subtracted and the raw $^{110}Cd/^{112}Cd$ was increased by 0.024% (except that here $^{116}Cd/^{112}Cd$ is 0.1% higher than expected).

Neutron capture on ^{113}Cd results in a decrease of 0.21% in $^{113}Cd/^{112}Cd$ and for $^{114}Cd/^{112}Cd$, an increase of 0.09%. The change in $^{114}Cd/^{113}Cd$ is 0.30%.

A summary of subtractions and corrections are listed in Table 6-15.

6.3.1.7 Modifications to sample 65701,23 to reduce the effects of tin and mass fractionation

Using the same arguments as in the previous section, the unmodified raw cadmium data for 65701,23 are plotted as a percentage deviation from the 1997 raw laboratory standard measurements in Figure 6-19.

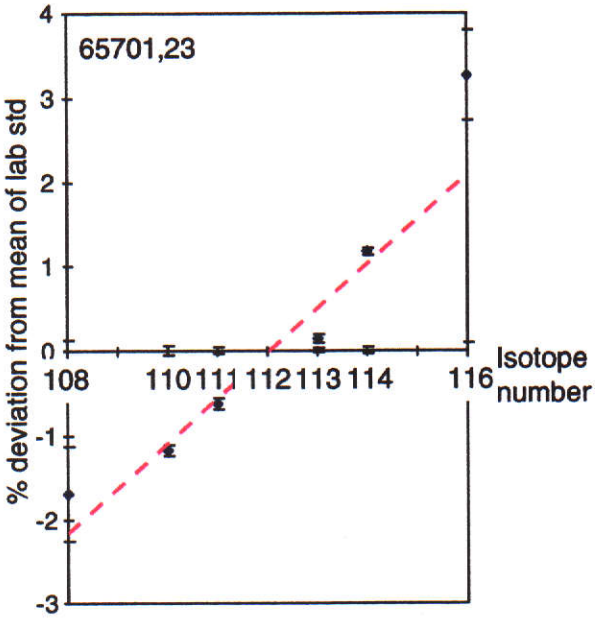

Figure 6-19 The raw cadmium data for the lunar sample 65701,23 plotted as a percentage deviation from the 1997 raw standard showing fractionation of 0.53% per mass unit. Uncertainties are at the 95% confidence level.

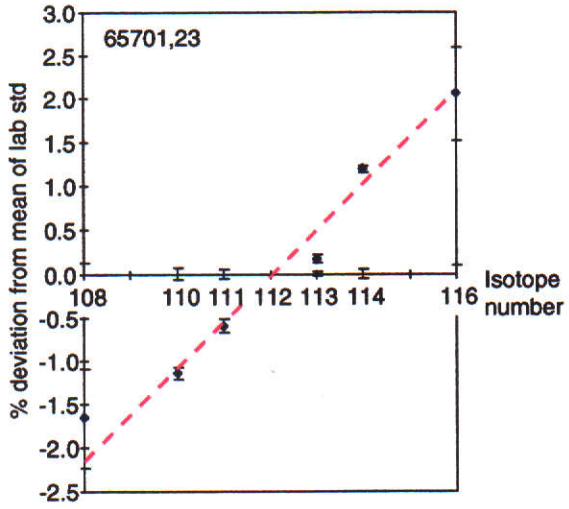

Figure 6-20 The raw cadmium data for the lunar sample 65701,23, with approximately 77 pg of tin subtracted.

The fractionation line goes through $^{108}Cd/^{112}Cd$, $^{110}Cd/^{112}Cd$, $^{111}Cd/^{112}Cd$ and mass 112, and between $^{113}Cd/^{112}Cd$ and $^{114}Cd/^{112}Cd$, showing mass fractionation of 0.53% per mass unit. $^{116}Cd/^{112}Cd$ is 1.1% above the fractionation line indicating the presence of tin, which also obscures any non-linearity in the fractionation.

The data shown in Figure 6-19, normalised to $^{110}Cd/^{112}Cd = 0.51928$, with no corrections for tin or lunar mass fractionation, are shown as a yellow diamond in the $^{114}Cd/^{112}Cd$ versus $^{113}Cd/^{112}Cd$ correlation diagram in Figure 6-23 and in Figure 6-22 as light blue diamonds.

Figure 6-20 shows the same raw data corrected for tin interference at masses 112, 114 and 116. Assuming the fractionation to be linear it was found that 1.183% of the 116 isotope was ^{116}Sn, (i.e. about 77 pg total of tin in the measured sample on the unlikely assumption of equal ionisation efficiency of tin and cadmium). The effect of subtracting the tin can also be seen in Figures 6-22 and 6-23 (dark blue diamonds).

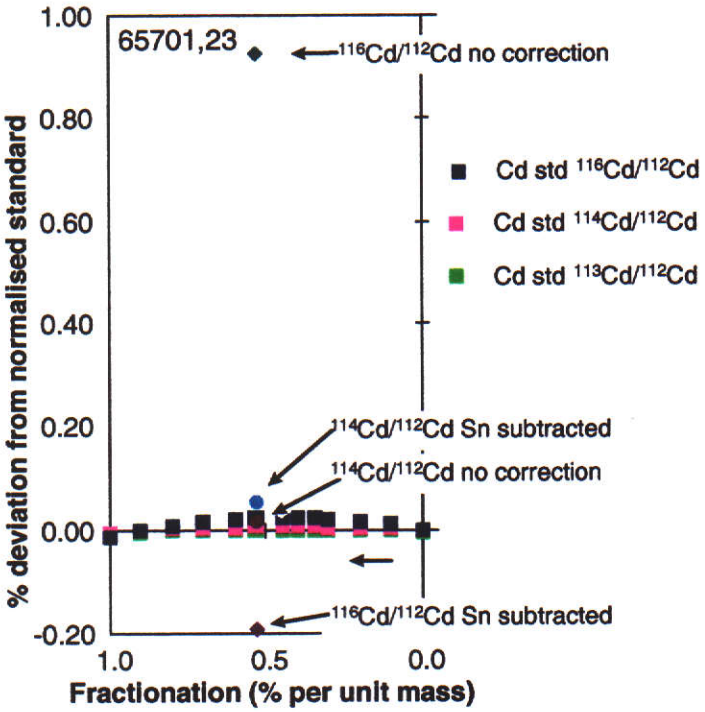

Figure 6-21 Normalised data plotted against fractionation showing the positions of $^{114}Cd/^{112}Cd$ and $^{116}Cd/^{112}Cd$ for 65701,23 both before and after tin has been subtracted.

When the normalised data (with no tin subtracted) are plotted on Figure 6-11, (results seen in Figure 6-21), $^{116}Cd/^{112}Cd$ initially lies 0.9% above the standard data. With tin subtracted $^{116}Cd/^{112}Cd$ lies 0.2% below the standard value. This casts doubt on the magnitude of the tin subtraction, and for this reason a second set of calculations, with no subtraction for tin, is included, though in this case at least part of the

$^{116}Cd/^{112}Cd$ +0.9% anomaly is likely to be tin. $^{114}Cd/^{112}Cd$ lies in approximately the same position as the standard, fractionated, data both before and after the subtraction of tin.

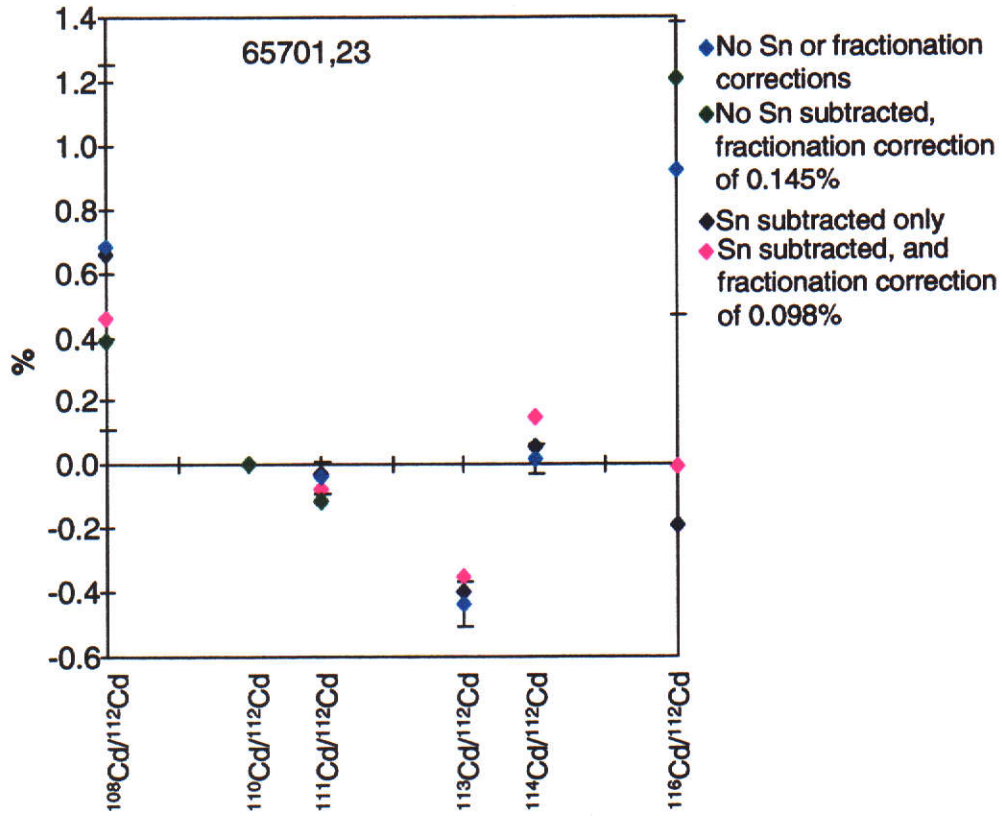

Figure 6-22 Sample 65701,23, normalised to $^{110}Cd/^{112}Cd = 0.51928$, is plotted as a percentage deviation from the normalised standard. Data have been modified by the subtraction of tin and by a modification to the mass fractionation correction.

With tin subtracted the raw value of $^{110}Cd/^{112}Cd$ was increased by 0.098% (greater than the uncertainty in this ratio which is 0.07% at the 95% confidence level), following the method described in 6.3.1.5. This leaves the normalised values of $^{114}Cd/^{112}Cd$ and $^{113}Cd/^{112}Cd$ above and below the line (Figure 6-22, pink diamonds), in the required proportions and $^{116}Cd/^{112}Cd$ lying on the line. In the correlation diagram (Figure 6-23) the data point for 65701,23 now lies on the predicted line for neutron capture (pink diamond).

If the assumption is made that all the $^{116}Cd/^{112}Cd$ anomaly is from non-linear mass fractionation the raw $^{110}Cd/^{112}Cd$ is increased by 0.145% for the modification to the mass fractionation correction and then the ratios

are normalised to $^{110}Cd/^{112}Cd$ = 0.51928. These normalised data are shown in Figure 6-22 as green diamonds. Though $^{113}Cd/^{112}Cd$ and $^{114}Cd/^{112}Cd$ are unchanged by this calculation the position of all the other isotopes now differ, the green diamonds compared to the pink diamonds in Figure 6-22.

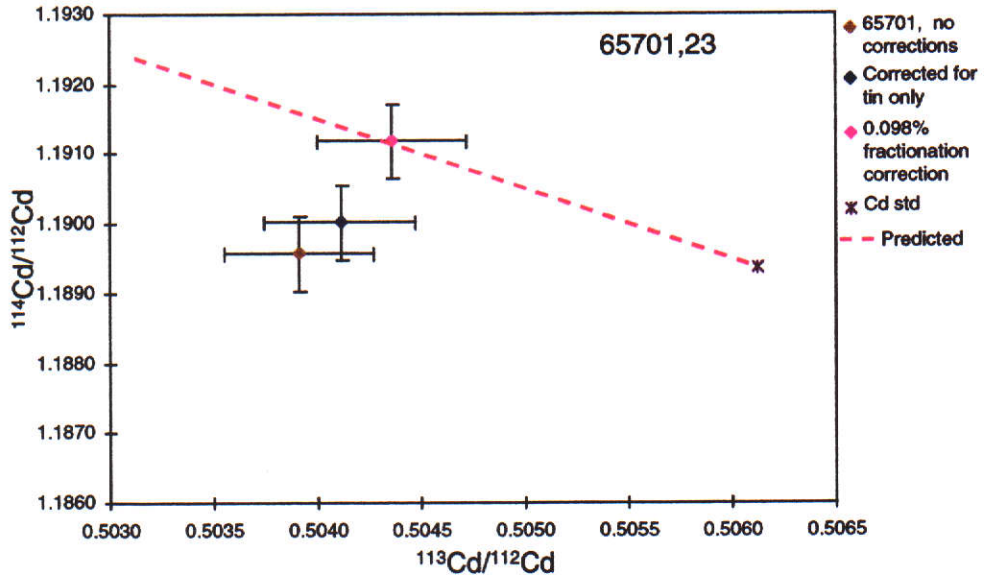

Figure 6-23 $^{114}Cd/^{112}Cd$ and $^{113}Cd/^{112}Cd$ correlation diagram showing the effect of subtracting 77 pg tin from samples 65701,23, and the modification of $^{110}Cd/^{112}Cd$ by 0.098%.

Summarising, the data in Figure 6-22 show sample 65701,23 normalised to $^{110}Cd/^{112}Cd$ = 0.51928 with tin subtracted (dark blue diamonds), but with no further modification for lunar fractionation, while the pink diamonds show these data with an increase in the raw $^{110}Cd/^{112}Cd$ of 0.098%. The light blue diamonds show data where no tin has been subtracted and no modifications have been made to the normalisation procedures. The data represented by the green diamonds have no tin subtracted and the raw $^{110}Cd/^{112}Cd$ has been increased by 0.145% before normalisation.

As a result of the iteration procedure the four conditions were satisfied when 77 pg of tin was subtracted and the raw $^{110}Cd/^{112}Cd$ was increased by 0.098%, also when tin was not subtracted and $^{110}Cd/^{112}Cd$ was

increased by 0.145%. In the latter case $^{116}Cd/^{112}Cd$ does not satisfy the conditions.

Neutron capture on ^{113}Cd shows $^{113}Cd/^{112}Cd$ with a decrease of 0.35% and $^{114}Cd/^{112}Cd$ an increase of 0.15%. The change in $^{114}Cd/^{113}Cd$ is 0.50%.

A summary of subtractions and corrections are listed in Table 6-15.

6.3.1.8 Modifications to sample 72161,73 to reduce the effects of tin and mass fractionation

The unmodified raw cadmium data for 72161,73 are plotted as a percentage deviation from the 1997 raw laboratory standard measurements in Figure 6-24.

The fractionation line goes through $^{108}Cd/^{112}Cd$, $^{110}Cd/^{112}Cd$, $^{111}Cd/^{112}Cd$, mass 112, and through $^{116}Cd/^{112}Cd$ within uncertainties, and between $^{113}Cd/^{112}Cd$ and $^{114}Cd/^{112}Cd$ and shows mass fractionation of 0.54% per mass unit.

The isotopic ratio $^{116}Cd/^{112}Cd$ is just above the fractionation line, suggesting either interference from tin or non-linearity in the fractionation. These unmodified data, when normalised to $^{110}Cd/^{112}Cd = 0.51928$, are seen in Figure 6-27 as light blue diamonds. The data points for $^{114}Cd/^{112}Cd$ and $^{113}Cd/^{112}Cd$ are lower than the cadmium standard, with $^{116}Cd/^{112}Cd$ equal to the standard. The same data are shown as a yellow diamond in the $^{114}Cd/^{112}Cd$ versus $^{113}Cd/^{112}Cd$ correlation diagram in Figure 6-28.

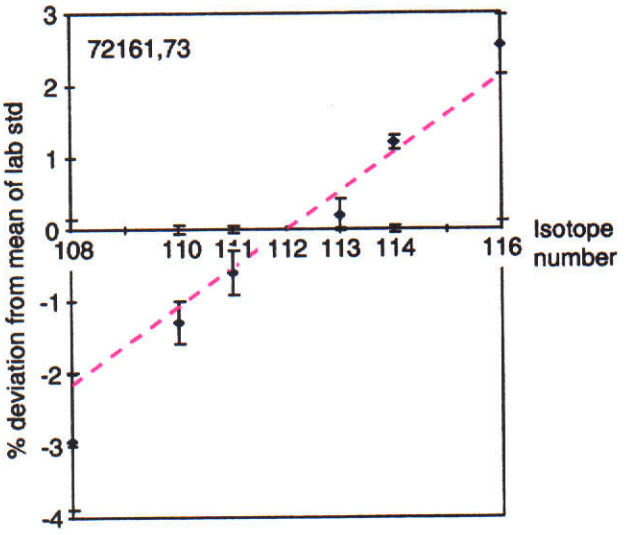

Figure 6-24 The raw cadmium data for the lunar sample 72161,73 plotted as a percentage deviation from the 1997 raw standard showing 0.54% per mass unit fractionation. Uncertainties are at the 95% confidence level.

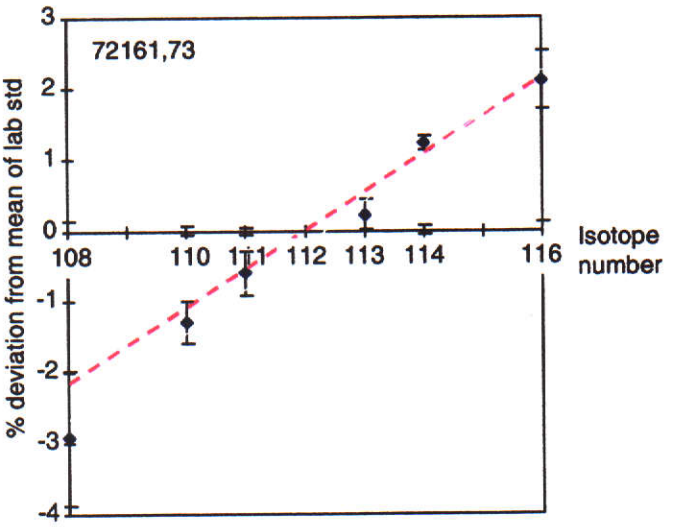

Figure 6-25 The raw cadmium data for the lunar sample 72161,73, with approximately 24 pg of tin subtracted, and the line of best fit now passing through the $^{116}Cd/^{112}Cd$ point.

Figure 6-25 shows the same raw data corrected for tin at masses 112, 114 and 116. Assuming the fractionation to be linear it was found that 0.45% of the 116 isotope could be ^{116}Sn, (i.e. about 24 pg total of tin in the measured sample on the unlikely assumption of equal ionisation efficiency of tin and cadmium). The effect of subtracting the tin can also be seen in Figures 6-27 and 6-28 (dark blue diamonds).

When the normalised data are plotted on Figure 6-11 it is found that the subtraction of tin moved $^{116}Cd/^{112}Cd$ from 0.03% above to 0.4% below the standard value (Figure 6-26). For this reason a second set of calculations is included later, with no subtraction for tin.

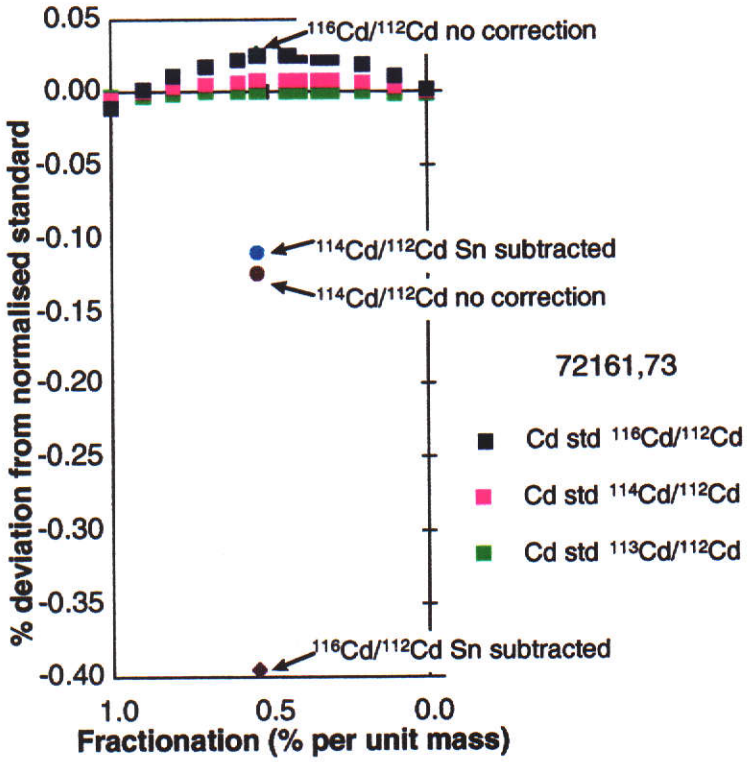

Figure 6-26 Normalised data plotted against fractionation showing the positions of $^{114}Cd/^{112}Cd$ and $^{116}Cd/^{112}Cd$ for 72161,73 both before and after tin has been subtracted.

With tin subtracted the raw value of $^{110}Cd/^{112}Cd$ was increased by 0.258% (greater than the uncertainty in this ratio which is 0.09% at the 95% confidence level). With the data normalised the result is seen in Figure 6-27 (the pink diamonds), with $^{114}Cd/^{112}Cd$ and $^{113}Cd/^{112}Cd$ above and below the line in the required proportions and in Figure 6-28.

Assuming that all the $^{116}Cd/^{112}Cd$ anomaly is from non-linear mass fractionation the raw $^{110}Cd/^{112}Cd$ is increased by 0.28%, then normalised to $^{110}Cd/^{112}Cd = 0.51928$ (Figure 6-27, the green diamonds). All isotopes show very small changes, except for $^{113}Cd/^{112}Cd$ and $^{114}Cd/^{112}Cd$ which remain the same and $^{116}Cd/^{112}Cd$ which is nearly 0.6% above the cadmium standard.

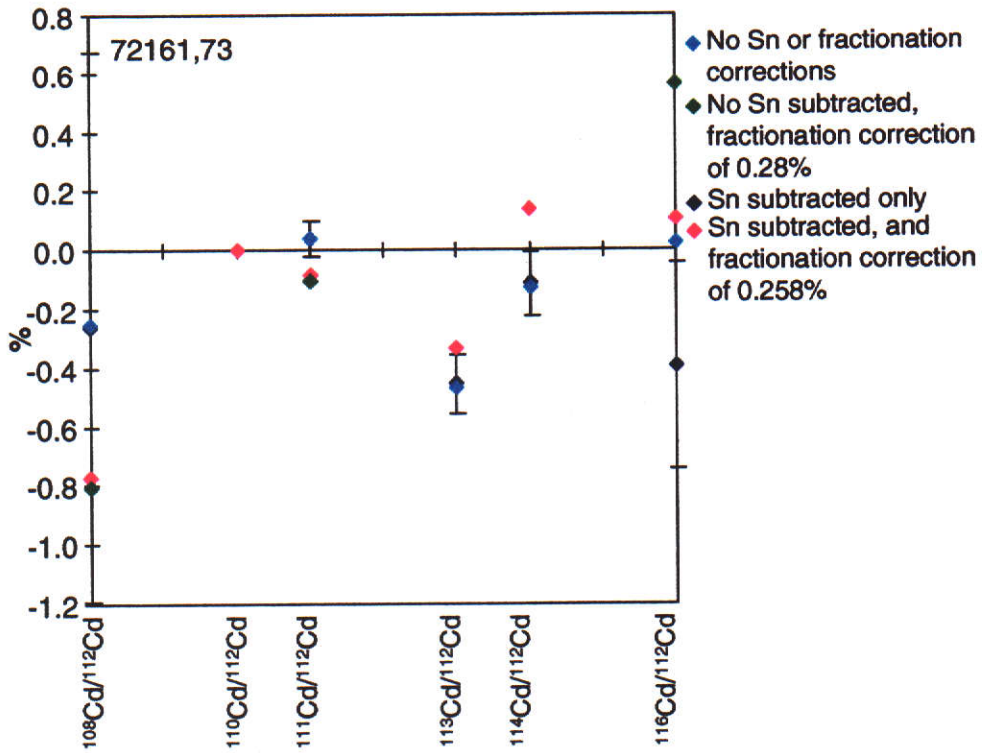

Figure 6-27 Sample 72161, normalised to $^{110}Cd/^{112}Cd = 0.51928$, is plotted as a percentage deviation from the normalised standard. Data have been modified by the subtraction of tin and by a modification to the mass fractionation correction

To summarise Figure 6-27, where all data are normalised to $^{110}Cd/^{112}Cd = 0.51928$, light blue diamonds are data where no tin has been subtracted and no modifications made for mass fractionation. The dark blue diamonds are data with tin subtracted. These data are then modified by increasing the raw $^{110}Cd/^{112}Cd$ by 0.258% (pink diamonds). The green diamonds show the result of increasing $^{110}Cd/^{112}Cd$ by 0.28%, with no tin subtracted.

The modified data are seen in Figure 6-28, on the predicted line for neutron capture (the pink diamond).

As a result of the iteration procedure the four conditions were satisfied when 24 pg of tin was subtracted and the raw $^{110}Cd/^{112}Cd$ was increased by 0.258%, also when tin was not subtracted and $^{110}Cd/^{112}Cd$ was increased by 0.28%. Neutron capture on ^{113}Cd results in a decrease of

0.33% in $^{113}Cd/^{112}Cd$ and for $^{114}Cd/^{112}Cd$ an increase of 0.14%. The change in $^{114}Cd/^{113}Cd$ from neutron capture is 0.47%.

A summary of subtractions and corrections are listed in Table 6-15.

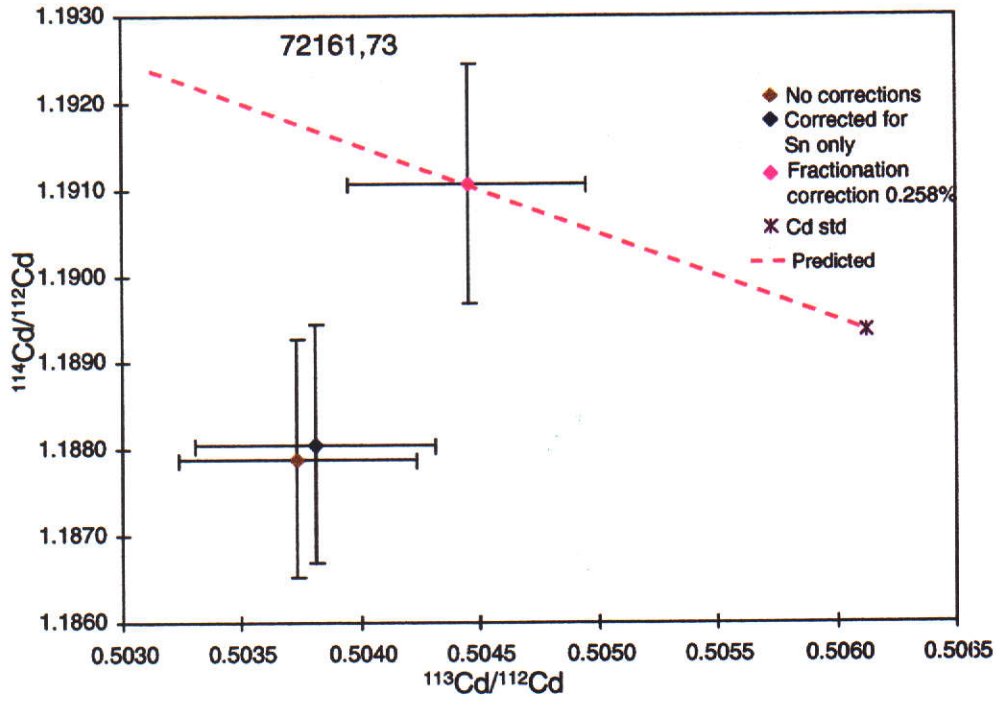

Figure 6-28 $^{114}Cd/^{112}Cd$ and $^{113}Cd/^{112}Cd$ correlation diagram showing the effect of subtracting 24 pg tin from sample 72161,73, then the modification of $^{110}Cd/^{112}Cd$ by 0.258%, with the predicted line for neutron capture.

6.3.1.9 Summary

Table 6-15 below summarises the analysis of the three fractionated lunar samples. Table 6-16 gives the percentage deviation of the raw ratios of the lunar samples from the 1997 raw cadmium standard, the subtraction of tin is the only modification. This Table differs from Table 6-14 as the percentage deviations in that Table were compared to the average of all the 1996 and 1997 standards and tin had not been subtracted.

Table 6-15 The mass fractionation found in lunar samples, corrections made for tin interferences and computational biases.

	Fractionation (% per mass unit)	Tin subtracted at atomic number 116 (%)	Increase in raw $^{110}Cd/^{112}Cd$ (%) after tin subtraction	Increase in raw $^{110}Cd/^{112}Cd$ (%), no tin subtraction
60501,105	0.30	0.11	0.02	0.024
65701,23	0.53	1.18	0.098	0.145
72161,73	0.54	0.65	0.258	0.28

Table 6-16 The percentage deviation of the lunar sample raw data from the mean of the 1997 cadmium standard raw data. These data are corrected for interference by tin at 112, 114 and 116.

	$\frac{^{108}Cd}{^{112}Cd}$	$\frac{^{110}Cd}{^{112}Cd}$	$\frac{^{111}Cd}{^{112}Cd}$	$\frac{^{113}Cd}{^{112}Cd}$	$\frac{^{114}Cd}{^{112}Cd}$	$\frac{^{116}Cd}{^{112}Cd}$
60501,105	-1.3±0.6	-0.68±0.03	-0.25±0.03	+0.12±0.03	+0.74±0.02	+1.3±0.1
65701,23	-1.7±0.6	-1.15±0.07	-0.60±0.07	+0.17±0.05	+1.19±0.04	+2.1±0.5
72161,73	-2.9±1.0	-1.3±0.1	-0.6±0.1	+0.2±0.1	+1.2±0.2	+2.1±0.4

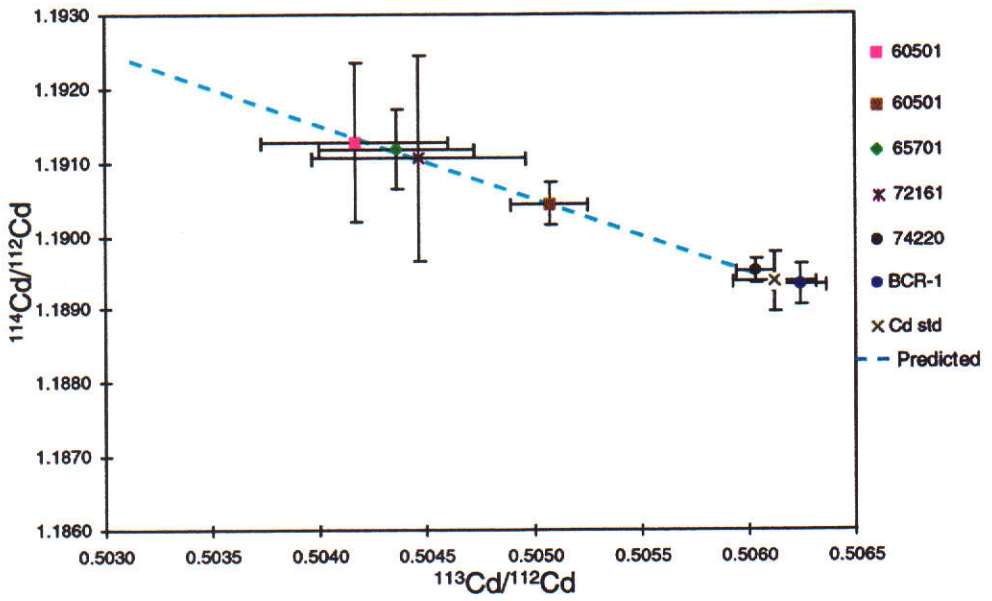

Figure 6-29 Correlation diagram of $^{114}Cd/^{112}Cd$ versus $^{113}Cd/^{112}Cd$ in lunar samples, showing neutron capture. Tin has been subtracted and modifications made to the normalisation correction.

The assumption has been made that the mass fractionation in the lunar samples is linear and therefore the interferences at isotope 116 are caused by tin. There is also the possibility that lunar mass fractionation is

non-linear and samples 60501,105 and 72161,73 have no tin interference and sample 65701,23 has less tin than has been assumed.

The modified $^{113}Cd/^{112}Cd$ and $^{114}Cd/^{112}Cd$ ratios are plotted on a correlation diagram in Figure 6-29. This Figure shows clear evidence of neutron capture on ^{113}Cd. Samples 60501,105, 65701,23 and 72161,73 show a change in $^{114}Cd/^{113}Cd$ of 0.5%. The second 60501,105 sample, which is suspected of being contaminated, shows an increase of only 0.3% in $^{114}Cd/^{113}Cd$. The percentage decrease in the $^{113}Cd/^{112}Cd$, and increase in the $^{114}Cd/^{112}Cd$ and $^{114}Cd/^{113}Cd$ ratios are summarised in Table 6-17.

The cadmium isotopic ratios for the lunar samples, modified by the subtraction of tin and by a correction to the normalising ratio, are listed in Table 6-18. The data are normalised to $^{110}Cd/^{112}Cd = 0.51928$.

Table 6-17 Percentage change in the abundances of $^{113}Cd/^{112}Cd$, $^{114}Cd/^{112}Cd$ and $^{114}Cd/^{113}Cd$ in lunar samples compared to laboratory standard abundances, attributed to neutron capture. Tin interferences have been subtracted and modifications made for the normalisation correction.

	$^{113}Cd/^{112}Cd$	$^{114}Cd/^{112}Cd$	$^{114}Cd/^{113}Cd$
60501,105	-0.310%	0.154%	0.466%
60501,105	-0.208%	0.090%	0.298%
65701,23	-0.348%	0.152%	0.502%
72161,73	-0.328%	0.141%	0.471%
74220,125	-0.018%	0.012%	0.030%

Table 6-18 Isotopic abundances of cadmium in the lunar samples, with tin interferences subtracted and modifications made to the normalisation correction to compensate for mass fractionation effects.

Date	Sample	$^{108}Cd/^{112}Cd$	$^{111}Cd/^{112}Cd$	$^{113}Cd/^{112}Cd$	$^{114}Cd/^{112}Cd$	$^{116}Cd/^{112}Cd$	$^{114}Cd/^{113}Cd$
1997	**Laboratory standard**	0.037067 ±0.000017	0.53111 ±0.00012	0.50612 ±0.00019	1.18937 ±0.00041	0.30933 ±0.00013	2.34997 ±0.00042
16/1/97	**60501,105**			0.504553 ±0.000577	1.191204 ±0.001639		2.360912 ±0.004222
2/7/97	**60501,105**	0.03706 ±0.00020	0.531499 ±0.000096	0.50507 ±0.00018	1.19044 ±0.00030	0.30633 ±0.00035	2.3570 ±0.0010
9/4/97	**65701,23**	0.03723 ±0.00021	0.53070 ±0.00025	0.50436 ±0.00036	1.19118 ±0.00053	0.3093 ±0.0014	2.3618 ±0.0020
9/4/97	**72161,73**	0.03678 ±0.00034	0.53067 ±0.00032	0.50446 ±0.00050	1.1911 ±0.0014	0.3093 ±0.0012	2.3610 ±0.0036
2/7/97	**74220,125**	0.037088 ±0.000044	0.53092 ±0.00017	0.506032 ±0.000088	1.18952 ±0.00016	0.30958 ±0.00015	2.35068 ±0.00051

The ratios are normalised to $^{110}Cd/^{112}Cd = 0.51928$. Uncertainties are at 95% confidence levels.

Table 6-19 Isotopic abundances of gadolinium in the lunar samples, raw data.

Date	Sample	$^{152}Gd/^{160}Gd$	$^{154}Gd/^{160}Gd$	$^{155}Gd/^{160}Gd$	$^{156}Gd/^{160}Gd$	$^{157}Gd/^{160}Gd$	$^{158}Gd/^{160}Gd$
1997	**Laboratory standard**	0.00945 ±0.00013	0.10058 ±0.00087	0.6860 ±0.0019	0.9406 ±0.0021	0.7190 ±0.0013	1.1394 ±0.0013
14/3/97	**14163,848**	0.00975 ±0.00082	0.10058 ±0.00043	0.67872 ±0.00074	0.9389 ±0.0010	0.71642 ±0.00080	1.14031 ±0.00073
2/7/97	**14163,848**	0.00984 ±0.00073	0.10043 ±0.00067	0.67841 ±0.00072	0.93873 ±0.00062	0.71538 ±0.00061	1.13913 ±0.00068
16/1/97	**60501,105 (Daly)**			0.6851 ±0.0023	0.9482 ±0.0039	0.7311 ±0.0042	1.1444 ±0.0015
2/7/97	**60501,105**	0.0139 ±0.0047	0.1047 ±0.0041	0.67993 ±0.00078	0.9415 ±0.0015	0.7164 ±0.0015	1.14358 ±0.00063
14/3/97	**74220,125 (Daly)**			0.691 ±0.0023	0.9510 ±0.0034	0.7251 ±0.0018	1.1461 ±0.0015
	(Faraday)	0.009381 ±0.000090	0.10023 ±0.00027	0.6787 ±0.0022	0.9383 ±0.0024	0.7180 ±0.0010	1.1383 ±0.0013
2/7/97	**74220,125 (Daly)**			0.734 ±0.032	0.975 ±0.011	0.773 ±0.022	1.1473 ±0.0037

Uncertainties are at 95% confidence levels.

Table 6-20 Isotopic abundances of gadolinium in the lunar samples. The ratios are normalised to $^{156}Gd/^{160}Gd = 0.9361$.

Date	Sample	$^{152}Gd/^{160}Gd$	$^{154}Gd/^{160}Gd$	$^{155}Gd/^{160}Gd$	$^{157}Gd/^{160}Gd$	$^{158}Gd/^{160}Gd$	$^{158}Gd/^{157}Gd$
1997	**Laboratory standard**	0.009355 ±0.000062	0.099851 ±0.000056	0.676942 ±0.000090	0.716471 ±0.000094	1.136687 ±0.000068	1.58651 ±0.00019
14/3/97	**14163,848**	0.00969 ±0.00081	0.10012 ±0.00035	0.67616 ±0.00026	0.71448 ±0.00087	1.13860 ±0.00024	1.5936 ±0.0020
2/7/97	**14163,848**	0.01002 ±0.00072	0.10013 ±0.00068	0.67602 ±0.00044	0.71415 ±0.00025	1.13791 ±0.00015	1.59337 ±0.00061
~~16/1/97~~	~~**60501,105**~~ **(Daly)**			~~0.6742~~ ~~±0.0019~~	~~0.7241~~ ~~±0.0035~~	~~1.1372~~ ~~±0.0019~~	~~1.5704~~ ~~±0.0081~~
2/7/97	**60501,105**	0.0137 ±0.0046	0.1038 ±0.0039	0.67509 ±0.00089	0.71287 ±0.00066	1.1399 ±0.0012	1.5989 ±0.0022
14/3/97	**74220,125 (Daly)**			0.6768 ±0.0011	0.71614 ±0.00047	1.1366 ±0.0012	1.5871 ±0.0020
	(Faraday)	0.00934 ±0.00013	0.09987 ±0.00013	0.67673 ±0.00013	0.71670 ±0.00037	1.13693 ±0.00019	1.58634 ±0.00087
~~2/7/97~~	~~**74220,125**~~ **(Daly)**			~~0.697~~ ~~±0.020~~	~~0.750~~ ~~±0.026~~	~~1.1242~~ ~~±0.0039~~	~~1.500~~ ~~±0.053~~

Uncertainties are at 95% confidence levels.

6.3.2 Gadolinium

Ninety or more sets of gadolinium isotope ratios were measured for each lunar sample. Ion currents were between 10^{-15} A and 10^{-12} A with both the Daly and Faraday detectors being used. Details of the procedures used for each sample are listed in Appendix G, Table 3-2.

Neutron capture on gadolinium ^{155}Gd and ^{157}Gd in two lunar samples 14163,848 and 60501,105 is presented here. Ratios are normalised both to ^{156}Gd/^{160}Gd = 0.9361 and to calculated values of ^{156}Gd/^{160}Gd. Calculated values of ^{156}Gd/^{160}Gd are required when neutron capture on ^{155}Gd increases the ^{156}Gd/^{160}Gd ratio.

The raw and normalised gadolinium isotopic ratios for each of the lunar samples are listed in Tables 6-19 and 6-20.

Ratios for 60501,105 (16/1/97) and 74220,125 (2/7/97) were rejected because of ionisation and chemistry problems (described in Appendix G). The two measurements of 74220,125 on 14/3/97 were of one sample, using both the Daly and Faraday detectors, both were of reasonable precision so both were retained.

In the presence of neutron capture ^{156}Gd/^{160}Gd, the normalising ratio, will be increased by the capture of neutrons at ^{155}Gd, so when samples showing neutron capture are normalised to ^{156}Gd/^{160}Gd = 0.9361 all the isotopes will be anomalously low (discussed in Section 3.2.5.2). Calculations to compensate for this effect are discussed below.

The ^{152}Gd/^{160}Gd and ^{154}Gd/^{160}Gd ratios in 14163,848 and 60501,105 show interferences caused by samarium contamination at ^{152}Gd and ^{154}Gd. As samarium isotopes are not isobaric with $^{155\text{-}160}$Gd, where neutron capture occurs, this interference does not affect the evidence of neutron capture.

The analytical blanks shown in Table 6-21 are negligible, representing <0.08% of the gadolinium in the samples.

Table 6-21 Gadolinium analytical blanks for the composition measurements.

Date	Sample	(pg)
14/3/97 2/7/97	**14163,848**	1.37±.03 ng 11.6±4.5 pg
16/1/97 2/7/97	**60501,105**	<0.9 pg 11.6±4.5 pg
14/3/97 2/7/97	**74220,125**	1.37±.03 ng 11.6±4.5 pg

The significant gadolinium isotopic ratios measured in the lunar samples, BCR-1 and the laboratory standard are plotted in Figure 6-30. Included is the theoretical line showing changes in ratios in the presence of neutron capture. The slope is -0.763 to compensate for the false discrimination effect on $^{156}Gd/^{160}Gd$ caused by neutron capture (Russ, 1974).

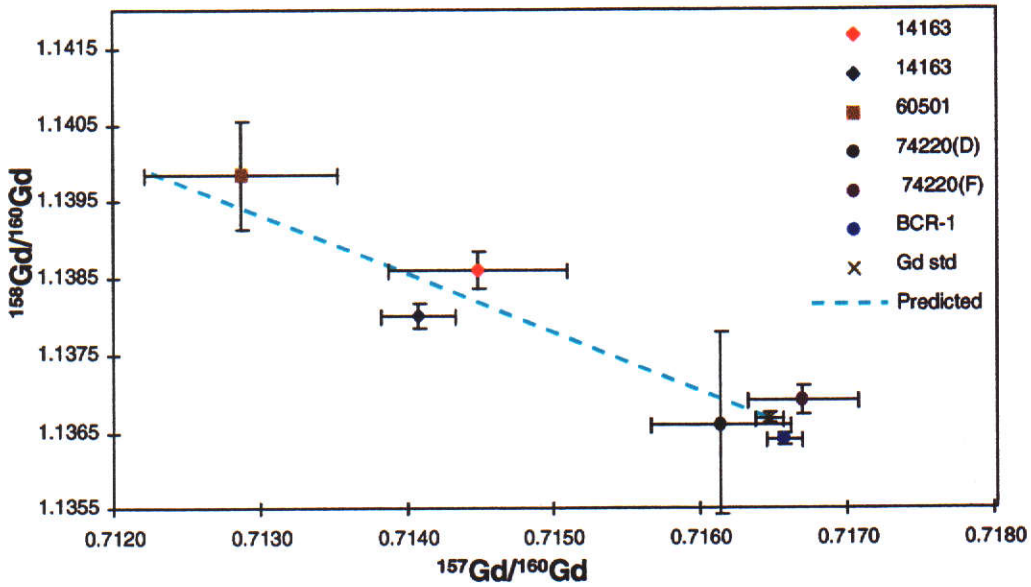

Figure 6-30 Correlation diagram of $^{158}Gd/^{160}Gd$ versus $^{157}Gd/^{160}Gd$ showing neutron capture on ^{157}Gd in lunar samples. Ratios are normalised to $^{156}Gd/^{160}Gd = 0.9361$. Theoretical slope is -0.763.

Two samples, 14163,848 and 60501,105, show evidence of neutron capture. One measurement of 14163,848 does not plot within uncertainties of the predicted line. No neutron capture was observed for

74220,125. The percentage changes in the ratios are listed in Table 6-22.

Table 6-22 Percentage change in $^{157}Gd/^{160}Gd$, $^{158}Gd/^{160}Gd$ and $^{158}Gd/^{157}Gd$ in lunar samples compared to laboratory standards. Data are normalised to $^{156}Gd/^{160}Gd = 0.9361$.

	$^{157}Gd/^{160}Gd$	$^{158}Gd/^{160}Gd$	$^{158}Gd/^{157}Gd$
14163,848	-0.28%	0.17%	0.45%
14163,848	-0.32%	0.11%	0.43%
60501,105	-0.50%	0.28%	0.78%
74220,125(D)	-0.05%	-0.007%	0.04%
74220,125(F)	0.03%	0.02%	-0.01%

To remove the bias caused by normalising to $^{156}Gd/^{160}Gd = 0.9361$ in the presence of neutron capture alternative methods are considered (Section 3.2.5.2). It is not possible to normalise the lunar data in this work to $^{154}Gd/^{160}Gd$ because the uncertainties in the ratio are too large (0.2% to 1%), and there is also an occasional interference detected at ^{154}Gd, from samarium.

The iteration method described by Hidaka et al. (1995), and discussed in Section 3.2.5.2, was adopted for the corrections. Normalising ratios were determined so that $^{156}Gd/^{160}Gd = 0.93651$, 0.93654 and 0.93707 for 14163,848 (two) and 60501,105 (Table 6-23). The constant used for the iterations, the sum of the average laboratory standard ratios measured during 1997, $^{155}Gd/^{160}Gd$ and $^{156}Gd/^{160}Gd$, is 1.61304.

The new normalising values for the three lunar samples are 0.04%, 0.05% and 0.1% higher than $^{156}Gd/^{160}Gd = 0.9361$. Use of these normalising constants increases the isotopic ratios (Figure 6-32), an increase of less than 0.0002 in 14163 (this work and Russ et al., 1971) and 0.0004 in 60501 (this work).

The advantages of modifying the normalising ratio by the iteration method, instead of normalising to $^{156}Gd/^{160}Gd = 0.9361$ and then correcting for the bias caused, is that there is no requirement to use neutron capture cross sections in the calculations. The new data can be used without further modification for the calculation of $\varepsilon_{Sm}/\varepsilon_{Gd}$.

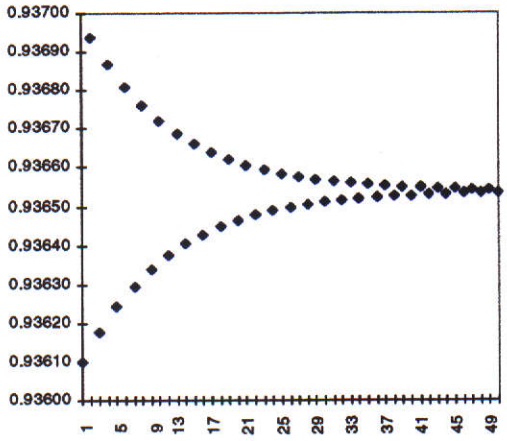

Figure 6-31 The convergence of the normalising constant to $^{156}Gd/^{160}Gd = 0.93654$, for 14163,848.

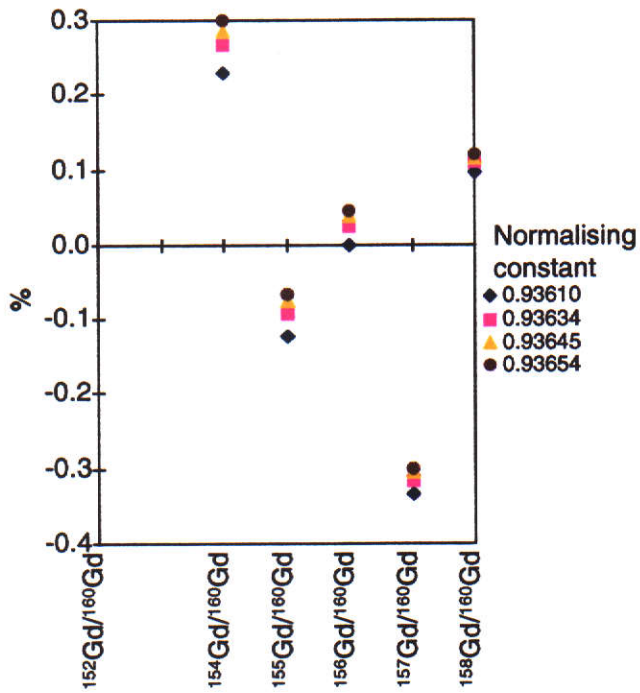

Figure 6-32 The percentage deviation from the 1997 gadolinium standard of 14163,848 as the normalising constant converges to $^{156}Gd/^{160}Gd = 0.93654$.

Table 6-23 Normalising values $^{156}Gd/^{160}Gd$ for the lunar samples calculated by iteration.

Sample	Normalising value	Number of iterations
14163,848 (14/3/97)	0.93651	56
14163,848 (2/7/97)	0.93654	49
60501,105	0.93707	64

Table 6-24 Isotopic abundances of gadolinium in the lunar samples normalised to the $^{156}Gd/^{160}Gd$ ratio in Table 6-23.

Date	Sample	$^{152}Gd/^{160}Gd$	$^{154}Gd/^{160}Gd$	$^{155}Gd/^{160}Gd$	$^{156}Gd/^{160}Gd$	$^{157}Gd/^{160}Gd$	$^{158}Gd/^{160}Gd$	$^{158}Gd/^{157}Gd$
1997	**Laboratory standard**	0.009355 ±0.000062	0.099851 ±0.000056	0.676942 ±0.000090	0.9361 ±0.0009	0.716471 ±0.000094	1.136687 ±0.000068	1.58651 ±0.00019
14/3/97	**14163,848**	0.00970 ±0.00081	0.10019 ±0.00035	0.67653 ±0.00026	0.93651	0.71472 ±0.00061	1.13885 ±0.00024	1.5934 ±0.0014
2/7/97	**14163,848**	0.00996 ±0.00069	0.10020 ±0.00065	0.67641 ±0.00045	0.93654	0.71429 ±0.00025	1.13818 ±0.00015	1.59344 ±0.00061
2/7/97	**60501,105**	0.0104 ±0.0014	0.1012 ±0.0039	0.67597 ±0.00089	0.93707	0.71343 ±0.00066	1.14044 ±0.00071	1.5985 ±0.0018

Uncertainties are at 95% confidence levels.

Table 6-24 shows the modified gadolinium data. They are plotted on a $^{158}Gd/^{160}Gd$ versus $^{157}Gd/^{160}Gd$ correlation diagram (Figure 6-33), with the theoretical line for neutron capture having a gradient of -1. The changes caused by neutron capture of the $^{157}Gd/^{160}Gd$, $^{158}Gd/^{160}Gd$ and $^{158}Gd/^{157}Gd$ ratios, expressed as percentage deviations from the laboratory standard, are listed in Table 6-25.

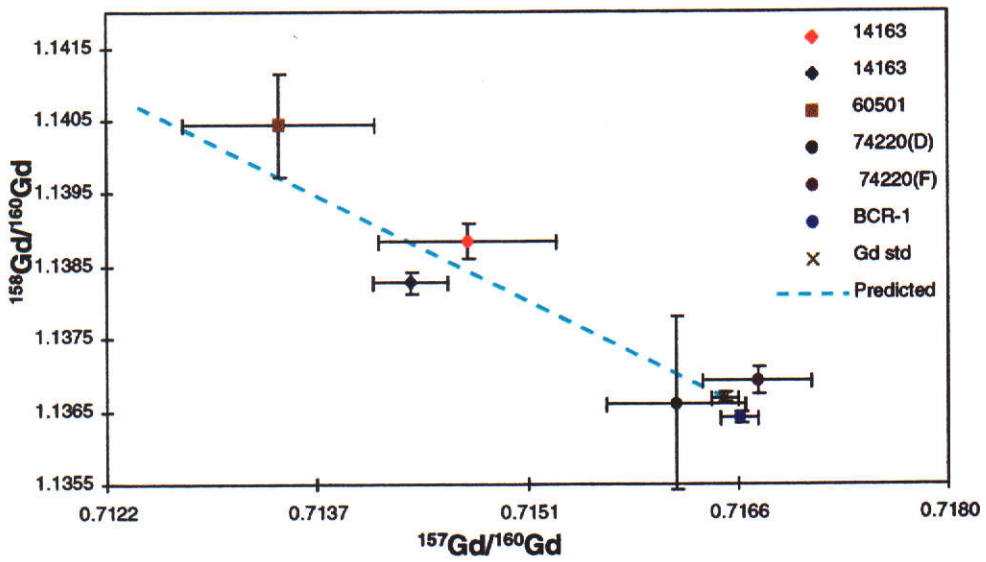

Figure 6-33 Correlation diagram of $^{158}Gd/^{160}Gd$ versus $^{157}Gd/^{160}Gd$ showing neutron capture on ^{157}Gd in lunar samples.

Table 6-25 Percentage deviation of the $^{157}Gd/^{160}Gd$, $^{158}Gd/^{160}Gd$ and $^{158}Gd/^{157}Gd$ ratios in lunar samples from the laboratory standards, with modified values of $^{156}Gd/^{160}Gd$.

	$^{157}Gd/^{160}Gd$	$^{158}Gd/^{160}Gd$	$^{158}Gd/^{157}Gd$
14163,848	-0.25%	0.19%	0.44%
14163,848	-0.30%	0.14%	0.44%
60501,105	-0.43%	0.33%	0.76%

Neutron capture by ^{155}Gd can now be plotted on a $^{156}Gd/^{160}Gd$ versus $^{155}Gd/^{160}Gd$ correlation diagram (Figure 6-34). Changes in the isotopic ratios $^{155}Gd/^{160}Gd$, $^{156}Gd/^{160}Gd$ and $^{156}Gd/^{155}Gd$ caused by neutron capture and compared to laboratory standard values are listed in Table 6-26.

Percentage uncertainties at the 95% confidence level, for the two 14163,848 and one 60501,105 sample shown in Figures 6-34 and 6-35 are, for $^{155}Gd/^{160}Gd$, ±0.04%, ±0.07% and ±0.12%, for $^{156}Gd/^{160}Gd$, ±0.11%, ±0.07% and ±0.02% and for $^{157}Gd/^{160}Gd$, ±0.09%, ±0.04% and ±0.09%, they are not shown on the graphs for clarity. Absolute uncertainties are listed in Table 6-24.

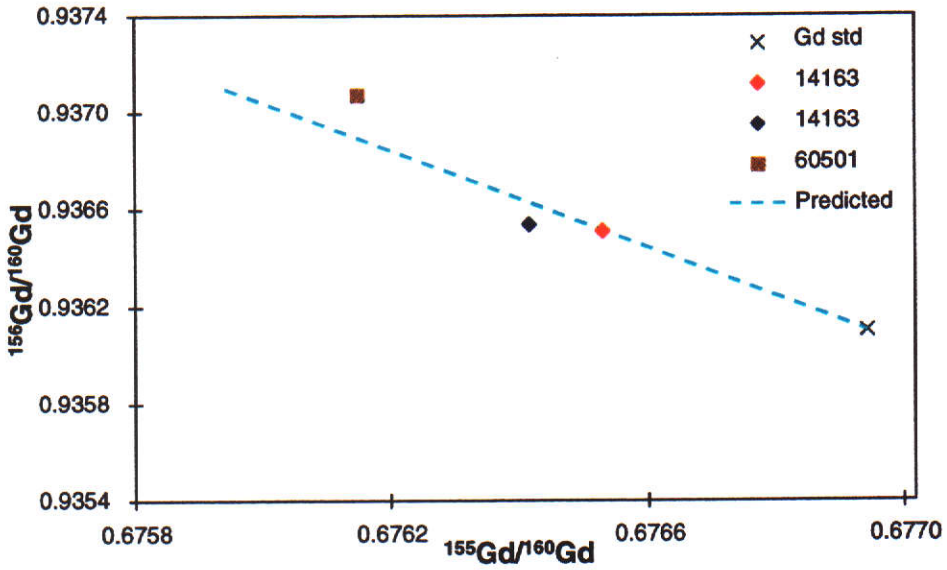

Figure 6-34 Correlation diagram of $^{156}Gd/^{160}Gd$ versus $^{155}Gd/^{160}Gd$ showing neutron capture on ^{155}Gd in lunar samples. Samples are normalised to various values of $^{156}Gd/^{160}Gd$.

Table 6-26 Percentage deviation of the $^{155}Gd/^{160}Gd$, $^{156}Gd/^{160}Gd$ and $^{156}Gd/^{155}Gd$ ratios in lunar samples from the laboratory standards, with modified values of $^{156}Gd/^{160}Gd$.

	$^{155}Gd/^{160}Gd$	$^{156}Gd/^{160}Gd$	$^{156}Gd/^{155}Gd$
14163,848	-0.06%	0.04%	0.11%
14163,848	-0.08%	0.05%	0.12%
60501,105	-0.14%	0.10%	0.25%

The two gadolinium isotopes with high thermal neutron capture cross sections, ^{157}Gd and ^{155}Gd, are plotted in Figure 6-35. The slope of the predicted line is equal to the ratio of the ^{157}Gd and ^{155}Gd neutron capture cross sections, i.e. $\sigma^{157}/\sigma^{155} = 4.19$ ($\sigma^{155}/\sigma^{157} = 0.2386$ Eugster et al., 1970b from Moeller, 1960). All three points lie on the predicted line,

within experimental uncertainties, confirming the relative values of the two cross sections.

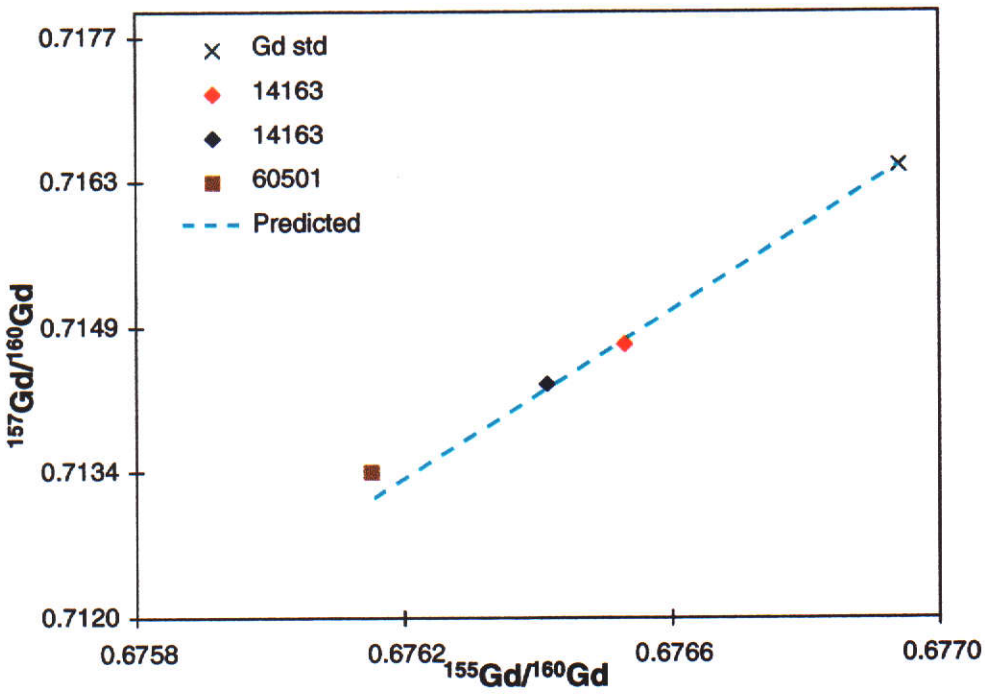

Figure 6-35 Correlation diagram of $^{157}Gd/^{160}Gd$ versus $^{155}Gd/^{160}Gd$. Samples with neutron capture are normalised to the calculated values of $^{156}Gd/^{160}Gd$.

The measurement precision and sensitivity is not sufficient to resolve neutron capture effects in gadolinium in the other samples which were available.

6.3.3 Samarium

Two hundred or more sets of samarium isotope ratios were measured on each lunar sample. Ion currents were between 10^{-13} A and 10^{-11} A, only the Faraday detector was used. Details of the procedures used for each sample are listed in Appendix G, Table 3-3.

Table 6-27 Isotopic abundances of samarium in the lunar samples with ^{152}Sm as the reference isotope, raw data.

	Sample	$^{144}Sm/^{152}Sm$	$^{147}Sm/^{152}Sm$	$^{148}Sm/^{152}Sm$	$^{149}Sm/^{152}Sm$	$^{150}Sm/^{152}Sm$	$^{154}Sm/^{152}Sm$
1997	**Laboratory standard**	0.11734 ±0.00021	0.56766 ±0.00065	0.42461 ±0.00036	0.52036 ±0.00037	0.27716 ±0.00014	0.84642 ±0.00040
14/3/97	**14163,848**	0.11633 ±0.00014	0.56454 ±0.00040	0.42291 ±0.00024	0.51716 ±0.00022	0.277918 ±0.000083	0.84809 ±0.00024
2/7/97	**14163,848**	0.11645 ±0.00013	0.56504 ±0.00035	0.42315 ±0.00022	0.51756 ±0.00020	0.278030 ±0.000075	0.84793 ±0.00022
16/1/97	**60501,105**	0.11586 ±0.00012	0.56321 ±0.00030	0.42204 ±0.00019	0.51563 ±0.00019	0.27827 ±0.00038	0.84872 ±0.00017
2/7/97	**60501,105**	0.11561 ±0.00044	0.5624 ±0.0022	0.4217 ±0.0013	0.5154 ±0.0012	0.27824 ±0.00027	0.8493 ±0.0013
14/3/97	**74220,125**	0.11641 ±0.00028	0.56489 ±0.00085	0.42303 ±0.00052	0.51871 ±0.00046	0.27669 ±0.00016	0.84797 ±0.00050
2/7/97	**74220,125**	0.11651 ±0.00066	0.5622 ±0.0016	0.42179 ±0.00098	0.5180 ±0.0010	0.2776 ±0.0010	0.8494 ±0.0011

Uncertainties are at 95% confidence levels.

Table 6-28 Isotopic abundances of samarium in the lunar samples with ^{152}Sm as the reference isotope, normalised to $^{147}Sm/^{152}Sm = 0.56081$.

	Sample	$^{144}Sm/^{152}Sm$	$^{148}Sm/^{152}Sm$	$^{149}Sm/^{152}Sm$	$^{150}Sm/^{152}Sm$	$^{154}Sm/^{152}Sm$	$^{150}Sm/^{149}Sm$
1997	**Laboratory standard**	0.115057 ±0.000018	0.420526 ±0.000040	0.516610 ±0.000070	0.275828 ±0.000057	0.85044 ±0.00022	0.533919 ±0.000051
14/3/97	**14163,848**	0.115091 ±0.000028	0.420682 ±0.000017	0.515127 ±0.000021	0.277191 ±0.000027	0.850284 ±0.000025	0.538102 ±0.000057
2/7/97	**14163,848**	0.115040 ±0.000042	0.420624 ±0.000032	0.515249 ±0.000019	0.277205 ±0.000030	0.850422 ±0.000048	0.53808 ±0.00021
16/1/97	**60501,105**	0.115060 ±0.000047	0.420610 ±0.000058	0.514332 ±0.000041	0.277979 ±0.000083	0.850138 ±0.000085	0.54047 ±0.00017
2/7/97	**60501,105**	0.11507 ±0.00033	0.420687 ±0.000061	0.514466 ±0.000078	0.27792 ±0.00018	0.850218 ±0.000059	0.54022 ±0.00036
14/3/97	**74220,125**	0.115065 ±0.000016	0.420584 ±0.000019	0.516483 ±0.000018	0.275914 ±0.000017	0.850378 ±0.000037	0.534217 ±0.000037
~~2/7/97~~	~~**74220,125**~~	~~0.11606 ±0.00051~~	~~0.42008 ±0.00053~~	~~0.51727 ±0.00066~~	~~0.27731 ±0.00090~~	~~0.85023 ±0.00094~~	~~0.5361 ±0.0019~~

Uncertainties are at 95% confidence levels.

Table 6-29 Isotopic abundances of samarium in the lunar samples with ^{154}Sm as the reference isotope. The ratios are normalised to $^{147}Sm/^{154}Sm = 0.65914$.

	Sample	$^{144}Sm/^{154}Sm$	$^{148}Sm/^{154}Sm$	$^{149}Sm/^{154}Sm$	$^{150}Sm/^{154}Sm$	$^{152}Sm/^{154}Sm$	$^{150}Sm/^{149}Sm$
1997	**Laboratory standard**	0.135204 ±0.000008	0.494292 ±0.000057	0.607269 ±0.000038	0.324253 ±0.000040	1.17571 ±0.00022	0.533953 ±0.000074
14/3/97	**14163,848**	0.135233 ±0.000033	0.494489 ±0.000020	0.605559 ±0.000023	0.325882 ±0.000030	1.175869 ±0.000025	0.538151 ±0.000054
2/7/97	**14163,848**	0.13513 ±0.00011	0.494375 ±0.000064	0.6057003 ±0.000038	0.325865 ±0.000081	1.175712 ±0.000047	0.53799 ±0.00014
16/1/97	**60501,105**	0.135186 ±0.000058	0.494416 ±0.000065	0.604645 ±0.000054	0.32662 ±0.00043	1.176015 ±0.000084	0.54018 ±0.00071
2/7/97	**60501,105**	0.135209 ±0.000385	0.494499 ±0.000068	0.604795 ±0.000080	0.32675 ±0.00021	1.175935 ±0.000059	0.54027 ±0.00036
14/3/97	**74220,125**	0.135209 ±0.000029	0.494370 ±0.000027	0.607134 ±0.000021	0.324369 ±0.000032	1.175768 ±0.000036	0.534264 ±0.000055

Uncertainties are at 95% confidence levels.

Table 6-30 Isotopic abundances of samarium in the lunar samples with ^{148}Sm as the reference isotope. The ratios are normalised to $^{147}Sm/^{148}Sm = 1.33359$.

	Sample	$^{144}Sm/^{148}Sm$	$^{149}Sm/^{148}Sm$	$^{150}Sm/^{148}Sm$	$^{152}Sm/^{148}Sm$	$^{154}Sm/^{148}Sm$	$^{150}Sm/^{149}Sm$
1997	**Laboratory standard**	0.273603 ±0.000050	1.22849 ±0.00020	0.65591 ±0.00015	2.37797 ±0.00065	2.02233 ±0.00056	
14/3/97	**14163,848**	0.273994 ±0.000093	1.224051 ±0.000097	0.658423 ±0.000054	2.37362 ±0.00046	2.01680 ±0.00055	0.537905 ±0.000060
2/7/97	**14163,848**	0.27366 ±0.00033	1.22491 ±0.00034	0.65888 ±0.00018	2.3758 ±0.0015	2.0199 ±0.0017	0.53790 ±0.00021
16/1/97	**60501,105**	0.27378 ±0.00021	1.22256 ±0.00026	0.66020 ±0.00082	2.3756 ±0.0016	2.0189 ±0.0018	0.54001 ±0.00046
2/7/97	**60501,105**	0.27396 ±0.00089	1.22246 ±0.00031	0.66014 ±0.00024	2.3735 ±0.0017	2.0165 ±0.0019	0.54001 ±0.00021
14/3/97	**74220,125**	0.273739 ±0.000097	1.22777 ±0.00015	0.65576 ±0.00017	2.37608 ±0.00068	2.01993 ±0.00082	0.53410 ±0.00012

Uncertainties are at 95% confidence levels.

Neutron capture by samarium in the three lunar samples 14163,848, 60501,105 and 74220, 125 is presented here. Samarium has not been measured in 65701,23 or 72161,73 in this work. To investigate possible anomalies at ^{152}Sm or ^{154}Sm ratios have been referenced to ^{148}Sm, ^{152}Sm and ^{154}Sm. The plotted lunar data are referenced to ^{154}Sm due to a suspected instability in the multi-collector cup which measures ^{152}Sm.

The samarium isotopic abundances in the lunar samples is given in Table 6-27 (raw data) and in Table 6-28 (referenced to ^{152}Sm), Table 6-29 (referenced to ^{154}Sm) and Table 6-30 (referenced to ^{148}Sm) (all normalised data).

Measurements of sample 74220,125 dated 2/7/97 were rejected due to poor ionisation.

No anomalies have been detected at ^{152}Sm or ^{154}Sm. An unknown interference at $^{148}Sm/^{154}Sm$ of less than 0.04% showed no relationship to neutron capture anomalies. There is some evidence of 0.1% to 0.2% fractionation in the lunar samples which needs further observations.

Table 6-31 Samarium analytical blanks for the composition measurements.

Date	Sample	(pg)
14/3/97	**14163,848**	34±28 ng
16/1/97	**60501,105**	57±3 pg
14/3/97	**74220,125**	34±28 ng

Analytical blanks, shown in Table 6-31, are <4% of the samarium in the samples, reflecting the problems with contamination.

The significant samarium isotopic ratios measured in the lunar samples, BCR-1 and the laboratory standard are plotted in Figure 6-36. Included is the theoretical line for neutron capture. Ratios are normalised to $^{147}Sm/^{154}Sm = 0.65914$.

Neutron capture is shown for the first time on 74220,125 and new measurements on 14163,848 and 60501,105, with increases in $^{150}Sm/^{149}Sm$ of 0.06%, 0.8% and 1.2% respectively (Table 6-32).

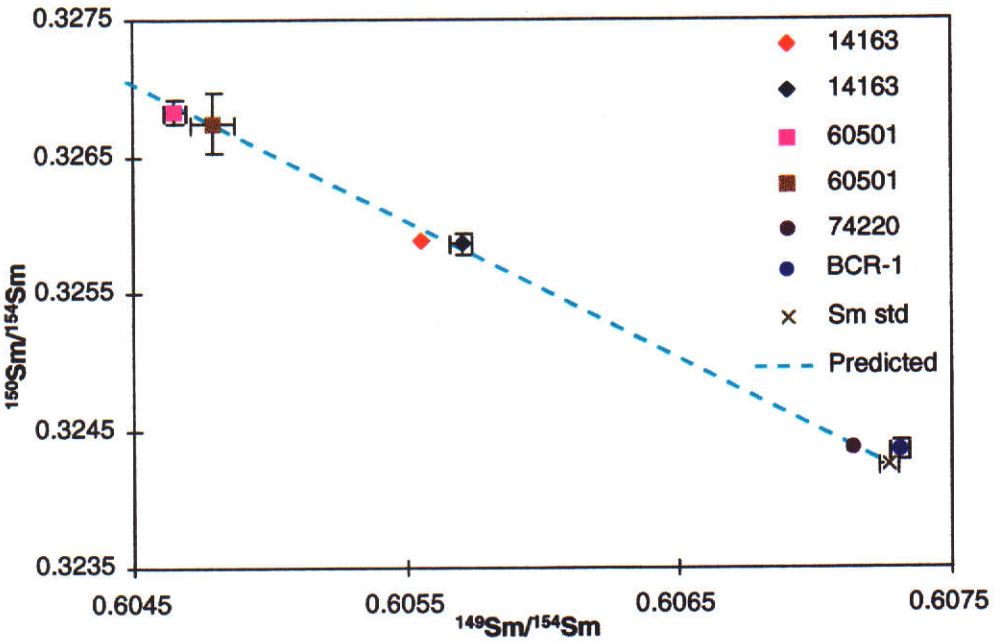

Figure 6-36 Correlation diagram of $^{150}Sm/^{154}Sm$ versus $^{149}Sm/^{154}Sm$ showing neutron capture on ^{149}Sm in lunar samples. Uncertainties smaller than the size of the symbol have been omitted.

Table 6-32 Percentage deviation of the $^{149}Sm/^{154}Sm$ and $^{150}Sm/^{154}Sm$ ratios in lunar samples from the laboratory standards.

	$^{149}Sm/^{154}Sm$	$^{150}Sm/^{154}Sm$	$^{150}Sm/^{149}Sm$
14163,848	-0.28%	0.50%	0.79%
14163,848	-0.26%	0.50%	0.76%
60501,105	-0.43%	0.80%	1.23%
60501,105	-0.41%	0.77%	1.18%
74220,125	-0.02%	0.04%	0.06%

6.4 Summary

Cadmium, gadolinium and samarium laboratory standard measurements have been presented here, together with isotope abundance measurements for BCR-1.

Neutron capture on cadmium has been shown for the first time, with changes of up to 0.5% in $^{114}Cd/^{113}Cd$ in three lunar samples 60501,105, 65701,23 and 72161,73.

Mass fractionation in cadmium in lunar samples has also been observed for the first time, with values of 0.5% and 0.3% per mass unit.

A modification to the procedure used to normalise fractionated data has been developed, as the exponential law is no longer valid with such high mass fractionation. Isobaric interferences caused by tin have been identified in the spectrum and corrected.

Neutron capture measurements have been presented for gadolinium in two lunar samples 14163,848 and 60501,105 amounting to changes in the $^{158}Gd/^{157}Gd$ ratio of 0.4% and 0.8 % respectively.

The first measurements of neutron capture on samarium in 74220,125 have been measured showing an increase in $^{150}Sm/^{149}Sm$ of 0.06%. Further measurements in two lunar samples 14163,848 and 60501,105 analysed previously gave increases in the $^{150}Sm/^{149}Sm$ ratio of 0.8% and 1.2% respectively.

The Chapter is supplemented by Appendix G.

7. Discussion

In this Chapter neutron capture on lunar samples is examined and compared with published data, the neutron energy spectrum is discussed and the presence of lunar mass fractionation in cadmium is considered.

7.1 Neutron capture

In Tables 7-1 and 7-2 neutron capture in ^{113}Cd, ^{155}Gd, ^{157}Gd and ^{149}Sm from this work and from published data are compared. Neutron capture data for ^{149}Sm in lunar surface soils are plotted in Figure 7-1.

The $^{150}Sm/^{149}Sm$ ratios for samples from all six Apollo Missions (Russ et al., 1971 and 1972 and Curtis and Wasserburg, 1975 and 1977b), for 14163,848, 60501,105 and 74220,125 from this work, and for samples irradiated by thermal neutrons from Hidaka et al. (1995) are included in Figure 7-1.

The data reflect irradiation by neutrons of from $6x10^{15}$ neutrons/cm^2 (Hidaka et al., 1995) to $(5.60\pm0.06)x10^{16}$ neutrons/cm^2 (Curtis and Wasserburg, 1975).

$^{150}Sm/^{149}Sm$ from Apollo 11, 12 and 14 surface soils all indicate a neutron fluence of approximately $2x10^{16}$ neutrons/cm^2 (Russ et al., 1971), so the two 14163,848 samples measured in this work, which plot in the same area, will have experienced a similar fluence. The 14163 sample from this work and from Russ et al. (1971) both show an increase in $^{150}Sm/^{149}Sm$ of 0.8% compared to the terrestrial values (listed in Tables 7-1 and 7-2).

Gadolinium in the same samples shows an increase in $^{158}Gd/^{157}Gd$ of 0.4% in this work and of 0.5% in Russ et al. (1971), the same within uncertainties.

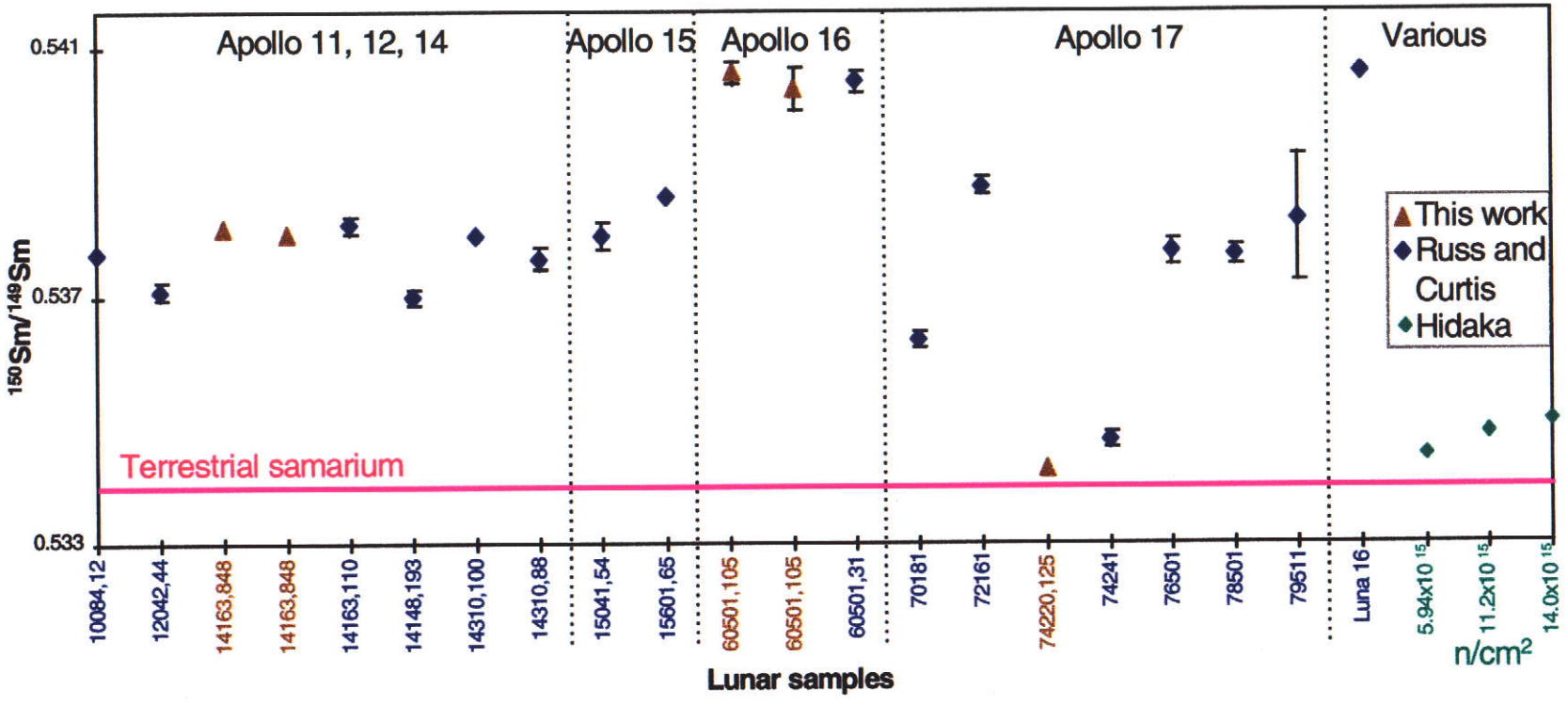

Figure 7-1 Neutron capture effects on $^{150}Sm/^{149}Sm$ in lunar surface soil samples from the Apollo 11, 12, 14, 15, 16 and 17 missions. Samples labelled "Russ and Curtis" are from Russ et al., 1971 and 1972 and Curtis and Wasserburg, 1975 and 1977b. Three irradiated samples from Hidaka et al., 1995 are shown.

Uncertainties from this work and the literature are at the 95% confidence level and two standard deviations respectively. Samples with no error bars have uncertainties less than the size of the symbol.

Table 7-1 Isotopic ratios of cadmium, gadolinium and samarium sensitive to neutron capture. Percent differences are given relative to the corresponding terrestrial ratios. All uncertainties are at the 95% confidence level.

Date	Sample	$^{114}Cd/^{113}Cd$	% change	$^{156}Gd/^{155}Gd$*	% change	$^{158}Gd/^{157}Gd$*	% change	$^{150}Sm/^{149}Sm$	% change
1997	**Laboratory standard**	2.34997 ±0.00042	0%	1.382837	0%	1.58651 ±0.00019	0%	0.533953 ±0.000051	0%
14/3/97	**14163,848**			1.384291	0.1%	1.5944 ±0.0014	0.4%	0.538151 ±0.000054	0.8%
2/7/97	**14163,848**			1.384558	0.1%	1.59350 ±0.00061	0.4%	0.53800 ±0.00014	0.8%
16/1/97	**60501,105**	2.3628 ±0.0029	0.6%					0.54054 ±0.00016	1.2%
2/7/97	**60501,105**	2.3570 ±0.0010	0.3%	1.385899	0.2%	1.5985 ±0.0018	0.8%	0.54027 ±0.00036	1.2%
9/4/97	**65701,23**	2.3618 ±0.0020	0.5%						
9/4/97	**72161,73**	2.3610 ±0.0036	0.5%						
14/3/97	**74220,125**							0.534264 ±0.000055	0.06%

*Normalised to calculated values of $^{156}Gd/^{160}Gd$.

Table 7-2 Published isotopic ratios of gadolinium and samarium. Percent differences are given relative to the corresponding terrestrial values in each study. All uncertainties are two standard deviations of the mean.

	$^{158}Gd/^{157}Gd$	% change	References	$^{150}Sm/^{149}Sm$	% change	References
14163,110	1.59452 ±0.00013	0.5%	Russ et al., 1971	0.53815 ±0.00013	0.8%	Russ et al., 1971
60501,31	1.60460 ±0.00018	1.1%	Russ, 1973	0.54046 ±0.00016	1.2%	Curtis and Wasserburg, 1975
60501,31	1.60428 ±0.00019	1.1%	Curtis and Wasserburg, 1975			
72161	1.59732 ±0.00037	0.7%	Curtis and Wasserburg, 1977b	0.53877 ±0.00014	0.9%	Curtis and Wasserburg, 1977b

The Apollo 16 sample 60501 shows the same high neutron capture in this work and in Curtis and Wasserburg (1975) (Figure 7-1), reflecting a fluence of (5.60±0.06)x10^{16} neutrons/cm^2 (Curtis and Wasserburg, 1975). The increase in $^{150}Sm/^{149}Sm$ of 1.2% is the same in both studies.

Also in sample 60501 the $^{158}Gd/^{157}Gd$ ratio has increased by 0.8% in this work, compared to 1.1% in Russ (1973) and Curtis and Wasserburg (1975). However, $^{114}Cd/^{113}Cd$ increased by 0.6% and 0.3% in this sample compared to terrestrial values (0.3% is from the sample suspected of contamination, discussed earlier).

The Apollo 16 sample 65701,23, where only cadmium was measured, shows the expected high neutron capture already found in other Apollo 16 samples, with a 0.5% increase in $^{114}Cd/^{113}Cd$ compared to terrestrial values (Table 7-1).

The Apollo 17 surface soil samples seen in Figure 7-1 show a varied history, with some heavily exposed materials (72161, 76501, 78501 and 79511 (Curtis and Wasserburg, 1977b)), similar to Apollo 14 samples, some exposed for only a short time (74220 (this work) and 74241 (Curtis and Wasserburg, 1975)), and one sample, 70181 (Curtis and Wasserburg, 1975) with an intermediate exposure.

The Apollo 17 sample 74220,125, measured for the first time in this study, is the orange glass from the rim of Shorty Crater. A small increase due to neutron capture of 0.06% in $^{150}Sm/^{149}Sm$ was observed and is compatible with the low exposure age of 30 million years (Arvidson et al., 1975 from Huneke, 1973). A similar change is seen in sample 74241, also from the rim of Shorty Crater, where it was probably deposited after being excavated from depth (Curtis and Wasserburg, 1975). Comparing 74220,125 in Figure 7-1 with the irradiated material measured by Hidaka et al. (1995) indicates that 74220 has experienced a neutron fluence of less than 6x10^{15} neutrons/cm^2.

In the other Apollo 17 soil measured for cadmium, 72161,73, the 0.5% increase in $^{114}Cd/^{113}Cd$ is slightly lower than the 0.6% increase in $^{114}Cd/^{113}Cd$ found in 60501,105. From gadolinium isotopic measurements Curtis and Wasserburg (1977b) calculated a neutron fluence of (3.72± 0.10)x10^{16} neutrons/cm^2 for sample 72161.

These results are compatible with the shorter exposure time of the Apollo 14 basalts compared to the Apollo 16 highland material, and the low rare earth content of the Apollo 16 highland material, which enhances the capture of thermal neutrons. The varied irradiation history of the Apollo 17 samples reflects the relatively recent activity in the Taurus-Littrow Valley.

7.2 The neutron energy spectrum <0.2 eV

The relative changes in the isotopic composition of cadmium, gadolinium and samarium in the lunar samples can be used to decipher the energy spectrum of the low energy neutrons at the sites where the samples were collected. Each of the isotopes ^{113}Cd, ^{155}Gd, ^{157}Gd and ^{149}Sm preferentially capture neutrons at their resonance energies of 0.178 eV, 0.03 eV, 0.03 eV and 0.09 eV (Table 7-4), so the magnitude of the changes ε_{Cd}, ε_{Gd} and ε_{Sm} (using Equation 1.10, defined in Chapter 1, Section 1.9), modified by the relevant neutron capture cross section, will reflect the intensity of the thermal neutrons at each energy. Russ (1972 and 1973), Russ et al. (1972) and Curtis and Wasserburg (1975, 1977a and b) compared measurements of the ratio $\varepsilon_{Sm}/\varepsilon_{Gd}$ to the theoretical calculations of Lingenfelter et al. (1972). The additional measurements of cadmium presented in this paper allow an extension of these comparisons to the higher energy of 0.178 eV by plotting $\varepsilon_{Cd}/\varepsilon_{Gd}$ and $\varepsilon_{Cd}/\varepsilon_{Sm}$.

The calculated values from this work of ε_{Cd}, ε_{Gd} and ε_{Sm}, the number of neutrons captured per atom of a particular isotope, are listed in Table 7-3 and plotted in Figure 7-2 and the ratios $\varepsilon_{Cd}/\varepsilon_{Sm}$, $\varepsilon_{Cd}/\varepsilon_{Gd}$ and $\varepsilon_{Sm}/\varepsilon_{Gd}$ are listed in Table 7-6 and plotted in Figure 7-3. Values of ε_{Cd}, ε_{Gd} and ε_{Sm} from the literature have been calculated using the corresponding terrestrial ratios in each study.

Table 7-3 ε_{Cd}, $\varepsilon_{^{155}Gd}$, $\varepsilon_{^{157}Gd}$ and ε_{Sm}, the number of neutrons captured per atom of a particular isotope (defined in Chapter 1, Section 1.9), for the lunar samples measured in this work. The $\varepsilon_{^{157}Gd}$ and ε_{Sm} values in brackets for 72161 are calculated from Curtis and Wasserburg (1977b).

		ε_{Cd} ($\times10^{-3}$)	$\varepsilon_{^{155}Gd}$ ($\times10^{-3}$)	$\varepsilon_{^{157}Gd}$ ($\times10^{-3}$)	ε_{Sm} ($\times10^{-3}$)
14/3/97	**14163,848**		0.6 ±1.2	2.7 ±0.6	2.73 ±0.08
2/7/97	**14163,848**		0.7 ±1.1	2.7 ±0.3	2.6 ±0.1
16/1/97	**60501,105**	3.8 ±1.0			4.3 ±0.2
2/7/97	**60501,105**	2.1 ±0.4	1.3 ±1.2	4.6 ±0.8	4.1 ±0.3
9/4/97	**65701,23**	3.5 ±0.7			
9/4/97	**72161,73**	3.3 ±1.2		(4.2) (±0.2)	(3.1) (±0.1)
14/3/97	**74220,125**				0.20 ±0.08

Uncertainties are at the 95% confidence level (this work) and two standard deviations of the mean (Curtis and Wasserburg, 1975 and 1977b).

The measured changes in gadolinium and samarium in Table 7-3, $\varepsilon_{^{157}Gd}$ and ε_{Sm}, for 14163,848 are the same within uncertainties in this work as in Russ et al. (1971) where $\varepsilon_{^{157}Gd} = 3.0\pm0.2$ and $\varepsilon_{Sm} = 2.7\pm0.1$. In 60501,105 $\varepsilon_{^{157}Gd}$ in this work is 30% lower and ε_{Sm} the same as in Curtis and Wasserburg (1975), where $\varepsilon_{^{157}Gd} = 6.9\pm0.3$ and $\varepsilon_{Sm} = 4.2\pm0.1$.

In sample 72161,73 only cadmium has been measured in this work, so $\varepsilon_{^{157}Gd}$ and ε_{Sm} from Curtis and Wasserburg (1977b) are included in Table 7-3, and shown in brackets.

To gain a general picture of the relative intensity of the thermal neutrons at 0.03 eV, 0.09 eV and 0.178 eV the changes due to neutron capture, ε_{Cd}, $\varepsilon_{^{155}Gd}$, $\varepsilon_{^{157}Gd}$ and ε_{Sm}, listed in Table 7-3, have been plotted in Figure 7-2 against neutron energy. Four lunar samples are included, 14163,848, 60501,105, 65701,23 and 72161, and ε_{Cd}, $\varepsilon_{^{155}Gd}$, $\varepsilon_{^{157}Gd}$ and ε_{Sm} have been divided by the relevant thermal cross section

listed in Table 7-4, so that they are directly comparable. As no direct comparison is being made between samples the effective neutron capture cross section based on the composition of the soil at each site is not being used, as it is not relevant here.

A comparison of the data points for one sample compared to those for another sample reflects the total amount of neutron fluence each sample was exposed to, which is not being considered here. What is being considered is a comparison of the data points within one particular sample, which will show the relative intensity of the neutrons at different energies. For example, the relative positions of the ε_{Gd}, ε_{Sm} and ε_{Cd} data points within one sample reflects the relative intensity of neutrons with energies of 0.03 eV, 0.09 eV and 0.178 eV.

Table 7-4 Resonance energy and cross sections at thermal energies Holden, (1987).

Reaction	Resonance energy (eV) Holden (1987)	Thermal cross-section (barns) Holden (1987)
$^{155}Gd(n,\gamma)^{156}Gd$	0.0268±0.0002	60,900±500
$^{157}Gd(n,\gamma)^{158}Gd$	0.0314±0.0002	254,000±815
$^{149}Sm(n,\gamma)^{150}Sm$	0.0973±0.0002	40,140±600
$^{113}Cd(n,\gamma)^{114}Cd$	0.178±0.002	20,600±400

Points plotted in Figure 7-2 which are from one sample are joined. The single value of ε_{Cd} for sample 65701,23 and the additional ε_{Sm} point for 60501 are included. ε_{157Gd} and ε_{Sm} for sample 72161,73 are from Curtis and Wasserburg (1977b). To simplify the graph the extreme points of the uncertainties have been joined to form an envelope.

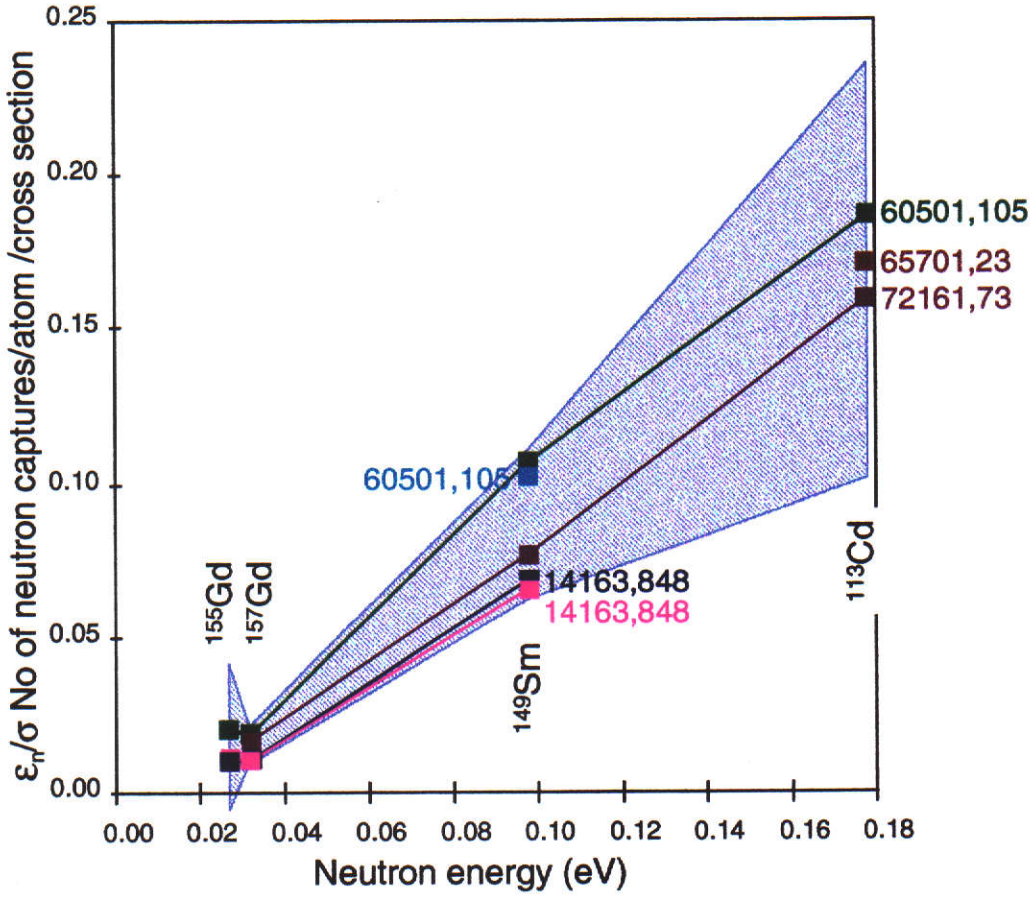

Figure 7-2 ε_{Cd}, $\varepsilon_{^{155}Gd}$,$\varepsilon_{^{157}Gd}$ and ε_{Sm}, divided by the appropriate thermal neutron capture cross sections, is plotted against neutron energy (eV) for four lunar samples. Extreme points of the uncertainties have been joined to form an envelope.

In Figure 7-2 the relative intensity of the neutrons at 0.03 eV and 0.09 eV for samples 14163,848 and 72161 appear to follow the same trend, so it is unfortunate that cadmium (0.178 eV) could not be measured in sample 14163,848 (due to heavy contamination) to confirm this.

Between 0.03 eV and 0.09 eV where the increase in the intensity of the neutron fluence is almost the same for the two 14163,848 samples and for 72161, the slope of the graph is measured as 0.9, 0.8, and 0.9 neutron captures/neutron energy respectively (Table 7-5). For sample 60501,105 the slope is 1.3 neutron captures/neutron energy, an increase in neutron intensity 1.5 times that of samples 14163,848 and 72161, showing that the energy spectrum of the neutrons varies between sites in the lower energies.

Between 0.09 eV and 0.178 eV the increase in the intensity of the neutron fluence is the same for 60501,105 and 72161, showing a slope of 1.0 neutron captures/neutron energy.

Not only does the neutron energy spectrum peak at higher energies than previously assumed (Lingenfelter, 1972), but the Apollo 16 soil has relatively fewer neutrons captured by ^{157}Gd at 0.03 eV compared to the other samples, showing a variation in the spectrum between sites.

Table 7-5 The slope of the graph in Figure 7-2, illustrating the relative changes in neutron intensity from 0.03 eV to 0.178 eV.

Sample	Change from 0.03 eV to 0.09 eV	Change from 0.09 eV to 0.178 eV
14163,848	0.87±0.05	
14163,848	0.83±0.06	
60501,105	1.34±0.07	0.98±0.61
72161,73	0.91±0.04	1.03±0.72

The peak of the thermal neutron fluence <0.2 eV was assumed by Lingenfelter et al. (1972), to be <0.1 eV. The shape of the gadolinium capture rate calculated by Lingenfelter et al. (1972) was found to be accurate, though too high, when compared to the Lunar Neutron Probe Experiment measurements (Woolum and Burnett, 1975). As the energy of the thermal neutrons is seen here to peak at higher energies than expected the fluence of neutrons at 0.03 eV will be relatively lower than assumed by Lingenfelter (1972). Re-calculating the ^{157}Gd capture rate with fewer 0.03 eV neutrons in the spectrum will reduce its magnitude, bringing it closer to the measured values.

Table 7-6 The thermal neutron energy spectrum, from this work. The numbers in brackets include data from Curtis and Wasserburg (1975) (ε_{Gd} for 60501) and Curtis and Wasserburg (1977b) (ε_{Gd} and ε_{Sm} for 72161).

Date	Sample	Σ_{eff} x10^{-2} cm^2/g	$\varepsilon_{Cd}/\varepsilon_{Gd}$	$\varepsilon_{Cd}/\varepsilon_{Sm}$	$\varepsilon_{Sm}/\varepsilon_{Gd}$
14/3/97	**14163,848**	0.91			1.0 ±0.2
2/7/97	**14163,848**	0.91			1.0 ±0.1
16/1/97	**60501,105**	0.48	0.83 (0.56) ±0.26 (±0.15)	0.90 ±0.24	0.9 (0.61) ±0.2 (±0.02)
2/7/97	**60501,105**	0.48		0.93 ±0.20	0.9 ±0.2
	72161,73	0.85	(0.79) (±0.29)	(1.07) (±0.39)	(0.74) (±0.04)

$\varepsilon_{Cd}/\varepsilon_{Gd}$, $\varepsilon_{Cd}/\varepsilon_{Sm}$ and $\varepsilon_{Sm}/\varepsilon_{Gd}$ are listed in Table 7-6 and plotted in Figure 7-3, $\varepsilon_{^{155}Gd}$ has not been included. The ratios $\varepsilon_{Cd}/\varepsilon_{Gd}$, $\varepsilon_{Cd}/\varepsilon_{Sm}$ and $\varepsilon_{Sm}/\varepsilon_{Gd}$ are a measure of the neutron energy spectrum below 0.2 eV and are compared here to the theoretical calculations of Lingenfelter et al. (1972). The uncertainties in these ratios are relatively large, so for clarity are not included in the Figure. $\varepsilon_{Cd}/\varepsilon_{Gd}$, $\varepsilon_{Cd}/\varepsilon_{Sm}$ and $\varepsilon_{Sm}/\varepsilon_{Gd}$ for sample 72161 are calculated with ε_{Gd} and ε_{Sm} from Curtis and Wasserburg (1977b). Additional values of $\varepsilon_{Cd}/\varepsilon_{Gd}$ and $\varepsilon_{Sm}/\varepsilon_{Gd}$ have been calculated for 60501 using ε_{Gd} = 6.9 from Curtis and Wasserburg (1975) (numbers and points in brackets in Table 7-6 and Figure 7-3) in view of the large difference in ε_{Gd} in both studies.

$\varepsilon_{Cd}/\varepsilon_{Gd}$, $\varepsilon_{Cd}/\varepsilon_{Sm}$ and $\varepsilon_{Sm}/\varepsilon_{Gd}$ are plotted against the macroscopic cross section in Figure 7-3. The macroscopic cross section (Σ_{eff}) for a particular sample is dependent on the neutron capture cross section of the individual elements which make up the soil where the sample was found (Lingenfelter et al. (1972)).

For this work Σ_{eff} = 0.91x10^{-2} cm^2/g is used for the Apollo 14 basalt, 14163. This value was calculated by Curtis and Wasserburg (1975) at a

sample temperature of 200 K for sample 14148, which is also a surface sample and of similar composition to 14163.

For the Apollo 16 sample 60501 a value of $\Sigma_{eff} = 0.48 \times 10^{-2}$ cm^2/g was calculated by Curtis and Wasserburg (1975), and for 72161 Curtis and Wasserburg (1977b) calculated $\Sigma_{eff} = 0.85 \times 10^{-2}$ cm^2/g.

Included in Σ_{eff} are Si, Ti, Al, Fe, Mg, Ca, Gd, Sm, Eu, O, Mn, Cr, Na and K, all elements with large neutron capture cross sections at thermal energies. Most of the cross sections are listed in Table 1-4 in Chapter 1, except for Mn, Cr, Na and K, which have cross sections of 13.3, 3.1, 0.53 and 2.1×10^{-24} cm^2 respectively (Curtis and Wasserburg, 1975).

Table 7-7 $\varepsilon_{Sm}/\varepsilon_{Gd}$ from the literature.

	$\varepsilon_{Sm}/\varepsilon_{Gd}$	References
Apollo 11, 12 and 14	0.83 to 0.89	Russ et al., 1971 and Curtis and Wasserburg, 1975
Apollo 15	0.75 to 0.77	Russ et al., 1972
Apollo 16	0.61	Curtis and Wasserburg, 1975
Apollo 17	0.71 to 0.91	Curtis and Wasserburg, 1975
Luna 16 G-2	0.76	Russ, 1972

Table 7-8 Literature values of $\varepsilon_{Sm}/\varepsilon_{Gd}$ for samples held at this laboratory.

Sample	$^{150}Sm/^{149}Sm$	$^{158}Gd/^{157}Gd$	$\varepsilon_{Sm}/\varepsilon_{Gd}$	References
14163,110	0.53815 ±0.0013	1.59452 ±0.00013	0.89 ±0.03	Russ et al., 1971
60501	0.54046 ±0.0016	1.60428 ±0.00019	0.61 ±0.02	Curtis and Wasserburg, 1975
72161	0.53876 ±0.0014	1.59732 ±0.00037	0.75 ±0.03	Curtis and Wasserburg, 1977b

The range of the published values of $\varepsilon_{Sm}/\varepsilon_{Gd}$ for surface soil samples from all the Apollo missions and a Luna mission are listed in Table 7-7 and vary from 0.61 in 60501 to 0.91 in sample 74241 (Curtis and Wasserburg, 1975). Published values of $\varepsilon_{Sm}/\varepsilon_{Gd}$ for samples measured in this work are in Table 7-8.

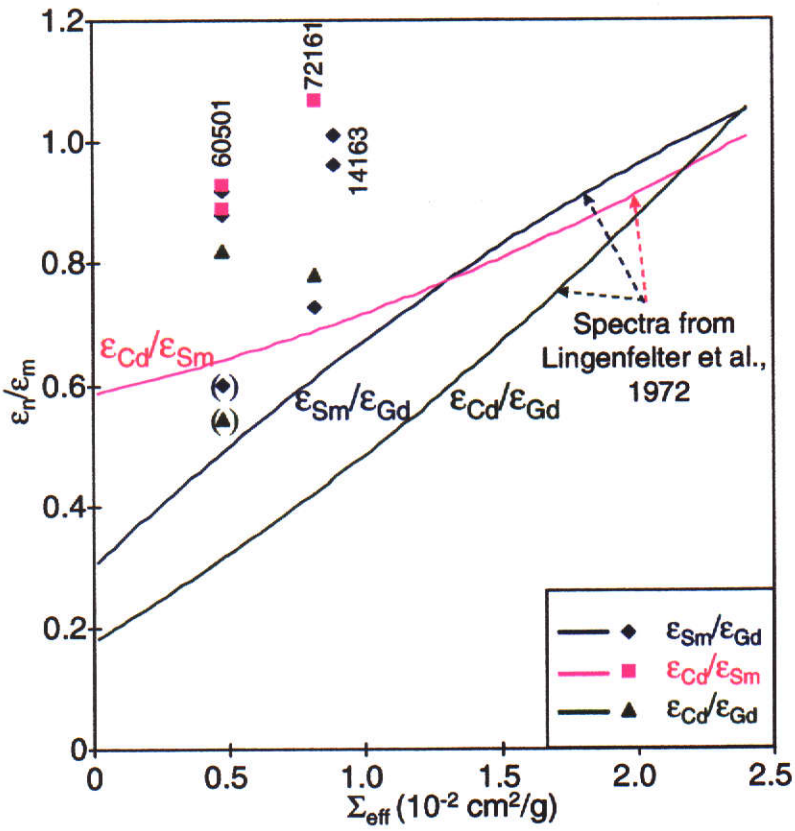

Figure 7-3 The neutron energy spectrum in lunar samples $\varepsilon_{Cd}/\varepsilon_{Gd}$, $\varepsilon_{Cd}/\varepsilon_{Sm}$ and $\varepsilon_{Sm}/\varepsilon_{Gd}$ plotted against the effective macroscopic cross section Σ_{eff}, and compared to the Lingenfelter et al. (1972) theoretical value. All data are from this work, except ε_{Gd} and ε_{Sm} for 72161 which is from Curtis and Wasserburg (1977b). The two points in brackets for 60501 are duplicate points calculated using ε_{Gd} from Curtis and Wasserburg (1975). Uncertainties are omitted to improve the clarity of the graph.

All of the $\varepsilon_{Cd}/\varepsilon_{Sm}$, $\varepsilon_{Cd}/\varepsilon_{Gd}$ and $\varepsilon_{Sm}/\varepsilon_{Gd}$ values plotted against Σ_{eff} in Figure 7-3 are higher than the Lingenfelter et al. (1972) theoretical predictions, but agree with the previously published data. All published $\varepsilon_{Sm}/\varepsilon_{Gd}$ data (Russ et al., 1971 and Burnett and Woolum, 1974) are 15% to 20% above the theoretical curve, which itself has uncertainties of ±30%.

The basalt, sample 14163,848, with two $\varepsilon_{Sm}/\varepsilon_{Gd}$ points plotted, is the same as Russ et al. (1972), within experimental uncertainties (1.0±0.3 and 1.0±0.1 in this work, 0.89±0.03 in Russ et al.). The points indicate a

more energetic neutron energy spectrum than was predicted by Lingenfelter et al. (1972), with either lower than expected neutron capture by gadolinium or higher by samarium.

In sample 60501,105 $\varepsilon_{Cd}/\varepsilon_{Gd}$, $\varepsilon_{Cd}/\varepsilon_{Sm}$ and $\varepsilon_{Sm}/\varepsilon_{Gd}$ are all well above the predicted lines (40% to 160%, Table 7-9) and $\varepsilon_{Sm}/\varepsilon_{Gd}$ is greater than the Curtis and Wasserburg (1975) value (0.9±0.2 compared to 0.61±0.02). As seen earlier in Figure 7-2 there are far fewer neutrons in this sample captured by ^{157}Gd at 0.03 eV than predicted by Lingenfelter (1972) and far more captured by ^{149}Sm and ^{113}Cd at 0.09 eV and 0.178 eV.

When $\varepsilon_{Cd}/\varepsilon_{Gd}$ and $\varepsilon_{Sm}/\varepsilon_{Gd}$ are re-calculated using the Curtis and Wasserburg (1975) value of ε_{Gd} the same result is obtained. These data points are enclosed in brackets in Figure 7-3.

Table 7-9 Measured $\varepsilon_n/\varepsilon_m$ relative to Lingenfelter et al. (1972) expressed as a percentage difference.

Sample	$\varepsilon_{Cd}/\varepsilon_{Gd}$	$\varepsilon_{Cd}/\varepsilon_{Sm}$	$\varepsilon_{Sm}/\varepsilon_{Gd}$
14163,848			60%
14163,848			50%
60501,105	160%	40%	85%
60501,105		45%	80%
60501 (Curtis and Wasserburg, 1975)	(75%)		(25%)
72161,73	80%	55%	20%

Sample 72161,73, with ε_{Gd} and ε_{Sm} taken from Curtis and Wasserburg (1977b) and ε_{Cd} from this work, shows a different trend to 60501, with more neutrons captured by ^{157}Gd at 0.03 eV relative to ^{113}Cd at 0.178 eV.

Comparing 60501,105 with 14163,848 and 72161, there are fewer 0.03 eV neutrons in sample 60501,105 relative to the other samples, suggesting a more energetic neutron energy spectrum in the highland material.

Gadolinium is very sensitive to changes in the abundance of low energy neutrons so would be expected to experience a high rate of neutron capture in Apollo 16 highland material, which contains few rare earths giving a high effective neutron capture cross section for gadolinium. However this is not observed here. One possible explanation for this puzzling anomaly is that length of exposure has a greater influence on gadolinium capture rates than does soil composition.

7.3 Lunar mass fractionation

There is strong evidence from this study that some lunar samples contain isotopically fractionated cadmium. Cadmium isotopes range from ^{106}Cd to ^{116}Cd which makes it an excellent element for the study of fractionation.

Samples 60501,105, 65701,23 and 72161,125 indicate fractionation of 0.30%, 0.53% and 0.54% per mass unit. It has been argued in Chapter 6 that the fractionation is not an artifact of the chemistry or mass spectrometry as no fractionation is seen in samples 14163,848, 74220,125 or BCR-1 which went through the same procedures as the fractionated samples, nor is it a function of the mass of cadmium in the sample.

The three fractionated samples 60501,105, 65701,23 and 72161,73 have concentrations of 112 ppb, 68.3 ppb and 57.0 ppb respectively; the lower concentration samples showing the greater fractionation. However, no fractionation is observed in BCR-1, which has a similar concentration of 134 ppb.

Cadmium mass fractionation plotted against concentration shows an inverse relationship (Figure 7-4). Sample 60501,105 showed evidence of a small amount of contamination by terrestrial cadmium, (Chapter 6 Section 6.3) so it is possible that this masks a higher mass fractionation effect than 0.30% per unit mass.

Table 7-10 Cadmium fractionation and elemental abundances found in three lunar samples.

	Fractionation (% per mass unit)	Concentration of cadmium (ppb)
60501,105	0.30	112
65701,23	0.53	68.3
72161,73	0.54	57.0

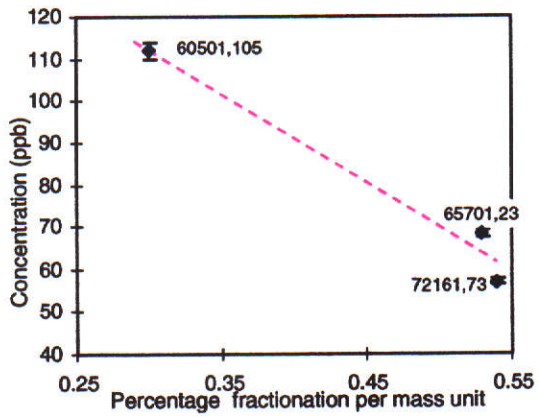

Figure 7-4 Concentration of cadmium plotted against fractionation in three lunar samples.

Cadmium from lunar samples collected from sheltered positions has been reported to have a higher concentration than similar samples from open areas (Morgan et al., 1974 and Baedecker et al., 1974). This reinforces the suggestions in the literature that fractionation could be caused by ion sputtering of grain surfaces and/or micro-meteorite impact melting and evaporation. Cadmium is a volatile element, so exposed samples bombarded for a long time could become depleted in cadmium, and fractionated.

Alternately, as cadmium fractionation has been observed in meteorites, it is possible that already fractionated cadmium from meteorites has been deposited on the lunar surface during accretion. However, so far only a few meteorites have shown cadmium fractionation so this is unlikely. The range of volatile fractionated elements found in lunar soil, breccia and impact melt coatings from a range of sites on the lunar surface does not suggest that accretion is the only source. The cadmium measured in this work was from well mixed surface soils, so no clear cause can be identified at this time.

8. Conclusions

The main aim of this work was to measure thermal neutron capture in ^{113}Cd in lunar samples for the first time, then combine these with new gadolinium and samarium neutron capture measurements to determine more fully the thermal neutron energy spectrum at the lunar surface. An additional aim was to search for mass fractionation in cadmium.

To achieve these goals the procedures for digestion and separation by ion exchange chemistry of cadmium, gadolinium and samarium in the samples were developed. Isotopic abundance measurements on the thermal ionisation mass spectrometer require very pure samples, with no isobaric interferences. Two independent procedures were developed to isolate cadmium and the rare earth elements.

A series of acid digestions using HF, HNO_3 and HCl dissolved the samples. The cadmium was separated and purified in anion and cation exchange columns while the rare earth elements were initially also separated with anion and cation columns, then an HPLC microcolumn and a Lanspec resin cation column. The extraction efficiencies of the ion exchange procedures for cadmium, gadolinium and samarium were 96%, 70% and 78% respectively.

Contamination was minimised through meticulous cleaning, storage and monitoring procedures.

A silica gel activator and single rhenium filament were used to optimise the ionisation of cadmium so that approximately 10 ng of cadmium from a lunar sample could be measured with a total ion current of over 10^{-12} A. Several hundred nanograms of gadolinium and samarium were analysed on triple rhenium filaments in methyl lactic acid and HCl, giving total ion currents of 10^{-12} A and $3x10^{-11}$ A respectively.

The digestion, separation and mass spectrometry procedures were trialled during measurements of the concentration of cadmium, gadolinium and samarium in seven geochemical reference materials, then modified where necessary for the lunar samples.

Concentration measurements in the seven geochemical reference materials BCR-1, BHVO-1, BIR-1, DNC-1, MAG-1, PCC-1 and W-2

were presented, some measured for the first time by IDMS. First cadmium concentration measurements by IDMS were determined for BHVO-1, BIR-1, DNC-1, MAG-1 and W-2, (averages of 94, 97, 94, 195 and 77 ppb respectively) with two new cadmium concentrations presented for BCR-1 and PCC-1 (134 ppb and 16 ppb) confirming previous results.

Three first measurements by IDMS of gadolinium and samarium concentrations in DNC-1, MAG-1 and W-2 were presented (averages of 2.0, 6.07 and 3.9 ppm respectively for gadolinium and 1.47, 7.78 and 3.45 ppm respectively for samarium). Three new IDMS concentrations confirming previous measurements for BCR-1, BHVO-1 and BIR-1 of 6.8ppm, 6.42ppm and 1.90 ppm respectively for gadolinium and 6.70 ppm, 6.45 ppm and 1.138 ppm respectively for samarium were presented. Anomalous gadolinium and samarium results for PCC-1 suggest that 100 mg samples are not homogeneous. During these measurements analytical blanks were 140 pg for cadmium, 74 pg for gadolinium and 100 pg for samarium.

The concentrations of cadmium, gadolinium and samarium in nine lunar samples have been measured for the first time by isotope dilution mass spectrometry using modified digestion, separation and mass spectrometry procedures. The cadmium concentrations in 10017,341, 14310,615, 15041,188, 15059,240, 60501,105, 65701,23, 72161,73 and 74220,125 are 10.0±0.2, 1.51±0.02, 32.8±0.6, 34.9±0.3, 112±2, 68.3±0.8, 57.0±0.6 and 300±7 ppb respectively. No satisfactory cadmium concentration measurements were made of 14163,848 because of contamination by pieces of plastic. This is the first time that cadmium concentrations have been measured in samples 15041,188 and 15059,240.

A gadolinium concentration of 21±7 ppm in 14163,848, 3.26±0.05 ppm and 5.8±0.3 ppm in 60501,105, and 8.1±0.2 ppm and 8.6±0.1 ppm in 74220,125 were presented as well as samarium concentrations of 24.3±0.4 ppm and 29.8±0.5 ppm in 14163,848, 2.68±0.04 ppm and

14±2 ppm in 60501,105, and 6.3±0.1 ppm and 6.8±0.1 ppm in 74220,125.

This is the first time that gadolinium and samarium concentrations in 60501,105 have been measured.

During these measurements the average analytical blanks were 160 pg for cadmium, 74 pg for gadolinium and 116 pg for samarium.

Isotopic composition measurements of laboratory standards and BCR-1 were compared to the lunar samples.

The isotopic composition of cadmium, gadolinium and samarium in laboratory standards, measured over several years, have been compared to published values and shown to be consistent with them.

The measurements of the isotopic composition of cadmium, gadolinium and samarium in lunar samples indicated changes due to neutron capture in five samples. The neutron capture measurements presented in this work are comparable with similar previously published measurements.

Increases in $^{114}Cd/^{113}Cd$ of 0.3% to 0.5% in lunar soil samples 60501,105, 65701,23 and 72161,73 indicated thermal neutron capture. No neutron capture was seen in 14163,848, due to terrestrial contamination, or in 74220,125 because the precision of the measurements were not sufficient. Changes in $^{114}Cd/^{113}Cd$ of more than 0.04% could be resolved. Analytical blanks for the cadmium composition measurements were less than 100 pg.

In gadolinium, increases of 0.4% and 0.8% in $^{158}Gd/^{157}Gd$ were observed in samples 14163,848 and 60501,105, confirming previous measurements of 14163,848, but lower than earlier values found on 60501,105. The precision of the measurements on 74220,125 were not sufficient to detect changes.

The method described by Hidaka et al. (1995) proved satisfactory in the modification of the normalising ratio $^{156}Gd/^{160}Gd$ to compensate for the increase in this ratio due to neutron capture. Analytical blanks for the gadolinium composition measurements were less than 1.5 ng.

Samarium isotopic abundance measurements indicate increases from neutron capture of 0.8%, 1.2% and 0.06% in $^{150}Sm/^{149}Sm$ in 14163,848,

60501,105 and 74220,125, which confirms and extends earlier measurements. Analytical blanks for the samarium composition measurements were less than 30 ng.

A comparison of the changes caused by thermal neutron capture on $^{158}Gd/^{157}Gd$, $^{150}Sm/^{149}Sm$ and $^{114}Cd/^{113}Cd$ has allowed a comparison of the relative intensity of neutrons with energies of 0.03 eV, 0.09 eV and 0.178 eV respectively. It has been shown that the energy spectrum of thermal neutrons peaks at higher energies than previously thought (Lingenfelter, 1972) and that the shape of the spectrum can vary between samples. The neutrons captured by sample 60501 were biased towards higher energies, whereas in 72161 more neutrons had lower energies.

The capture rate for gadolinium calculated by Lingenfelter, has been shown to be too high, this thesis indicates that re-calculations with a modified neutron energy spectrum, biased towards higher energies, could result in neutron capture rate by gadolinium closer to the measured rates.

Isotope fractionation of cadmium was detected in three samples, 60501,105, 65701,23 and 72161,73, at levels of 0.30%, 0.53% and 0.54% per mass unit respectively. Fractionation could be caused by ion sputtering, micro-meteorite impact melting or accretion of already fractionated materials, but more evidence is required to come to any firm conclusion.

Analyses of the samarium isotopic abundance data suggests that isotope fractionation may be present, but it is small in magnitude and will need to be confirmed.

Neutron capture effects have now been measured in cadmium samples as small as 12 ng leading the way to the application of these techniques to other lunar samples from other areas of the Moon, from the Apollo 17 drill core, and from meteorites with low cadmium concentrations. For a closer look at the neutron energy spectrum more cadmium neutron capture measurements are needed from samples already measured for gadolinium and samarium. Additional measurements of the three elements from several different sites on the

lunar surface could determine why the thermal neutron energy spectrum differs at different sites, whether the soil composition is the main cause of variations, or whether length of exposure has a greater effect.

Cadmium mass fractionation in lunar soils needs to be confirmed by the measurement of double spiked lunar samples. The measurement of cadmium fractionation in a wider range of lunar samples will identify variations between sites and throw some light on the causes of the fractionation.

References

Anders, E., Ganapathy, R., Keays, R.R., Laul, J.C. and Morgan, J.W. (1971) Volatile and siderophile elements in lunar rocks: Comparison with terrestrial and meteoritic basalts. *Proceedings of the Lunar Science Conference 2nd, Geochimica et Cosmochimica Acta Supplement.* 2:1021-1036.

Armstrong, T.W. and Alsmiller Jr, R.G. (1971) Calculation of cosmogenic radionuclides in the Moon and comparison with Apollo measurements. *Proceedings of the Lunar Science Conference 2nd, Geochimica et Cosmochimica Acta Supplement.* 2:1729-1745.

Arvidson, R., Crozaz, G., Drozd, R.J., Hohenberg, C.M. and Morgan, C.J. (1975) Cosmic ray exposure ages of features and events at the Apollo landing sites. *The Moon.* 13:259-276.

Audi and Wapstra (1993) The 1993 Atomic Mass Evaluation. (1) Atomic mass table. *Nuclear Physics.* A565:1-65.

Baedecker, P.A., Chou, C.-L. and Wasson, J.T. (1972) The extra lunar component in lunar soils and breccias. *Proceedings of the Lunar Science Conference 3rd, Geochimica et Cosmochimica Acta Supplement.* 2:1343-1359.

Baedecker, P.A., Chou, C.-L., Sundberg, L.L. and Wasson, J.T. (1974) Volatile and siderophilic trace elements in the soils and rocks of Taurus-Littrow. *Proceedings of the Lunar Science Conference 5th, Geochimica et Cosmochimica Acta Supplement.* 2:1625-1643.

Bogard, D.D., Nyquist, L.E., Bansal, B.M., Garrison, D.H., Wiesmann, H., Herzog, G.F., Albrecht, A.A., Vogt, S. and Klein, J. (1995) Neutron-capture ^{36}Cl, ^{41}Ca, ^{36}Ar, and ^{150}Sm in large chondrites: Evidence for high fluences of thermalized neutrons. *Journal of Geophysical Research.* 100(E5):9401-9416.

Boynton, W.V., Chou, C.-L., Robinson, K.L., Warren, P.H. and Wasson, J.T. (1976) Lithophiles, siderophiles and volatiles in Apollo 16 soils and rocks. *Proceedings of the Lunar Science Conference 7th, Geochimica et Cosmochimica Acta Supplement.* 1:727-742.

Buchanan, R.F. and Faris, J.P. (1964) Anion exchange characteristics of elements in HNO_3 medium. *Analytical Chemistry.* 36(6):1157-1158.

Burnett, D.S. and Woolum, D.S. (1974) Lunar neutron capture as a tracer for regolith dynamics. *Proceedings of the Lunar Science Conference 5th, Geochimica et Cosmochimica Acta Supplement.* 2:2061-2074.

Burnett, D.S., Huneke, J.C., Podosek, F.A., Russ, G.P., III and Wasserburg, G.J. (1971) The irradiation history of lunar samples. *Proceedings of the Lunar Science Conference 2nd, Geochimica et Cosmochimica Acta Supplement.* 2:1671-1679.

B.V.S.P. (1981) *Basaltic Volcanism in the Terrestrial Planets,* Pergamon, New York.

Carlson, I.C. and Walton, W.J.A., Jr (Eds.) (1978) *Apollo 14 Rock Samples,* NASA, Lyndon B. Johnson Space Center, Houston, Texas.

Cerrai, E. and Testa, C. (1963) Separation of rare earths by means of small columns of Kel-F supporting di(2-ethylhexyl) orthophosphoric acid. *Journal of Inorganic Nuclear Chemistry.* 25:1045-1050.

Commission of Atomic Weights and Isotopic Abundances (1986) Atomic Weights of the Elements 1985. *Pure and Applied Chemistry.* 58(12):1677-1692.

Crock, J.G., Lichte, F.E. and Wildeman, T.R. (1984) The Group Separation of the Rare-Earth Elements and Yttrium from Geologic Materials by Cation-Exchange Chromatography. *Chemical Geology.* 45:149-163.

Crock, J.G., Lichte, F.E., Riddle, G.O. and Beech, C.L. (1986) Separation and preconcentration of the rare earth elements and yttrium from geological materials by ion exchange and sequential acid elution. *Talanta.* 33(7):601-606.

Croudace, I.W. and Marshall, S. (1991) Determination of Rare Earth Elements and Yttrium in Nine Geochemical Reference Samples Using a Novel Group Separation Procedure Involving Mixed-Acid Elution Ion-Exchange Chromatography. *Geostandards Newsletter.* 15(1):139-144.

Curtis, D.B. and Wasserburg, G.J. (1975) Apollo 17 Neutron Stratigraphy - Sedimentation and Mixing in the Lunar Regolith. *The Moon.* 13:185-227.

Curtis, D.B. and Wasserburg, G.J. (1977a) Stratigraphic processes in the lunar regolith - additional insight from neutron fluence measurements on bulk soils and lithic fragments from the deep drill cores. *Proceedings of the Lunar Science Conference 8th, Geochimica et Cosmochimica Acta Supplement.* 3575-3593.

Curtis, D.B. and Wasserburg, G.J. (1977b) Transport and erosional processes in the Taurus-Littrow Valley - Inferences from neutron fluences in surface soils. *Proceedings of the Lunar Science Conference 8th, Geochimica et Cosmochimica Acta Supplement.* 3045-3057.

Elchuk, S. and Cassidy, R.M. (1979) Separation of the lanthanides on high efficiency bonded phases and conventional ion-exchange resins. *Analytical Chemistry.* 51(9):1434-1438.

Esat, T.M. and Williams, I.S. (1998) Rayleigh distillation and condensation of potassium isotopes. *Meteoritics and Planetary Science.* 33(4):A46.

Eugster, O., Tera, F., Burnett, D.S. and Wasserburg, G.J. (1970a) The Isotopic Composition of Gd and the Neutron Capture Effects in Samples from Apollo 11. *Earth and Planetary Science Letters.* 8:20-30.

Eugster, O., Tera, F., Burnett, D.S. and Wasserburg, G.J. (1970b) Isotopic Composition of Gadolinium and Neutron-Capture Effects in Some Meteorites. *Journal of Geophysical Research.* 75(14):2753-2768.

Eugster, O., Tera, F., Burnett, D.S. and Wasserburg, G.J. (1970c) Neutron capture effects in Gd from the Norton County meteorite. *Earth and Planetary Science Letters.* 7:436-440.

Evans, J.C., Reeves, J.H., Rancitelli, L.A. and Bogard, D.D. (1982) Cosmogenic nuclides in recently fallen meteorites: Evidence for galactic cosmic ray variations during the period 1967-1978. *Journal of Geophysical Research.* 87(B7):5577-5591.

Faris, J.P. (1960) Adsorption of the elements from hydrofluoric acid by anion exchange. *Analytical Chemistry.* 32:520-522.

Fidelis, I. and Siekierski, S. (1965) Use of 2-ethylhexyl phenylphosphonic acid in reversed phase partition chromatography. *Journal of Chromatography.* 17:542-548.

Fletcher, I.R. (1979) *Observations and comments on the design and operation of the Nd-Sm facility at University of California, San Diego,* Report Department of Applied Physics, Western Australian Institute of Technology, Perth, Western Australia.

Fletcher, I.R. (1982) *Procedures for the high purity separation of samarium and neodymium,* Report Western Australian Institute of Technology, Perth, Western Australia.

Fletcher, I.R. (1996) Personal communication.

Gerstenberger, H. and Haase, G. (1997) A highly effective emitter substance for mass spectrometric Pb isotope ratio determinations. *Chemical Geology.* 136:309-312.

Gladney, E.S. and Roelandts, I. (1988a) 1987 compilation of elemental concentration data for USGS BHVO-1, MAG-1, QLO-1, RGM-1, Sco-1, SDC-1, SGR-1 and STM-1. *Geostandards Newsletter.* 12(2):253-362.

Gladney, E.S. and Roelandts, I. (1988b) 1987 compilation of elemental concentration data for USGS BIR-1, DNC-1 and W-2. *Geostandards Newsletter.* 12(1):63-118.

Gladney, E.S., Jones, E.A., Nickell, E.J. and Roelandts, I. (1990) 1988 compilation of elemental concentration data for USGS basalt BCR-1. *Geostandards Newsletter.* 14(2):209-359.

Gladney, E.S., Jones, E.A., Nickell, E.J. and Roelandts, I. (1991) 1988 compilation of elemental concentration data for USGS DTS-1, G-1, PCC-1 and W-1. *Geostandards Newsletter.* 15(2):199-396.

Greenwood, N.N. and Earnshaw, A. (1984) *Chemistry of the Elements,* Pergamon Press, Oxford.

Heiken, G., Vaniman, D. and French, B.M. (1991) *Lunar Sourcebook A User's Guide to the Moon,* Cambridge University Press, Cambridge, U.K.

Hess, W.N., Canfield, E.H. and Lingenfelter, R.E. (1961) Cosmic ray neutron demography. *Journal of Geophysical Research.* 66:665-677.

Hidaka, H., Ebihara, M. and Shima, M. (1995) Determination of the isotopic compositions of samarium and gadolinium by thermal ionization mass spectrometry. *Analytical Chemistry.* 34:1437-1441.

Hidaka, H., Ebihara, M. and Yoneda, S. (1997) Samarium and gadolinium isotopic compositions of meteorites. *Meteoritics and Planetary Science.* 32:59.

Holden, N.E. (1987) personal communication .

Holmes, J.R. and Rosman, K.J.R. (1995) *Processing mass spectrometric data including uncertainties, employing Monte Carlo methods*, Report, Western Australian Isotope Science Research Centre, Curtin University of Technology, Perth.

Hooker, P.J., O'Nions, R.K. and Pankhurst, R.J. (1975) Determination of rare-earth elements in USGS standard rocks by mixed solvent ion exchange and mass spectrometric isotope dilution. *Chemical Geology.* 16:189-196.

Horwitz, E.P. and Bloomquist, C.A.A. (1975) Chemical separations for super-heavy element searches in irradiated uranium targets. *Journal of Inorganic Nuclear Chemistry.* 17:425-434.

Hubbard, N.J., Gast, P.W., Rhodes, J.M., Bansal, B.M., Wiesmann, H. and Church, S.E. (1972) Nonmare basalts: Part II. *Proceedings of the Lunar Science Conference 3rd, Geochimica et Cosmochimica Acta Supplement.* 2:1161-1179.

Humayun, M. and Clayton, R.N. (1995) Precise determination of the isotopic composition of potassium: Application to terrestrial rocks and lunar soils. *Geochimica et Cosmochimica Acta.* 59(10):2115-2130.

IUPAC (1986) Atomic weights of the elements 1985. *Pure and Applied Chemistry.* 58(12):1677-1692.

IUPAC (1998) Isotopic compositions of the elements 1997. *Pure and Applied Chemistry.* 70(1):217-235.

Jochum, K.P., Rehkamper, M. and Seufert, H.M. (1994) Trace element analysis of basalt BIR-1 by ID-SSMS, HPLC and LIMS. *Geostandards Newsletter.* 18(1):43-51.

Kiss, E. (1987) *Separation of rare-earth elements by reverse-phase partition chromatography. Preparation of Kel-F columns supporting Di(2-ethylhexyl)-orthophosphoric acid,* Report Research School of Earth Sciences, The Australian National University, Canberra, ACT 2601, Australia.

Korff, S.A. and Mendell, R.B. (1967) Neutron production by cosmic rays in the atmosphere. In *High-Energy Nuclear Reactions in Astrophysics,* ed B.S.P. Shen, Benjamin, Inc., New York.

Kornblum, J.J., Fireman, E.L., Levine, M. and Aronson, A. (1973) Neutrons in the Moon. *Proceedings of the Lunar Science Conference 4th, Geochimica et Cosmochimica Acta Supplement.* 2:2171-2182.

Kramer, F.E., Twedell, D.B. and Walton, W.J.A., Jr. (Eds.) (1977) *Apollo 11 Lunar Sample Information Catalogue (Revised),* NASA, Lyndon B. Johnson Space Center, Houston, Texas.

Kraus, K.A. and Nelson, F. (1955) Anion Exchange Studies of the Fission Products In *International Conference for Peaceful Uses of Atomic Energy*, Vol. VII (P/837) USA, pp. 113-124.

Laul, J.C. and Schmitt, R.A. (1973) Chemical composition of Apollo 15, 16, and 17 samples. *Proceedings of the Lunar Science Conference 4th, Geochimica et Cosmochimica Acta Supplement.* 2:1349-1367.

Lingenfelter, R.E., Canfield, E.H. and Hess, W.N. (1961) The Lunar Neutron Flux. *Journal of Geophysical Research.* 66(9):2665-2671.

Lingenfelter, R.E. (1963) The cosmic-ray neutron leakage flux. *Journal of Geophysical Research.* 68(20):5633-5639.

Lingenfelter, R.E. and Flamm, E.J. (1964) Neutron leakage flux from interactions of solar protons in the atmosphere. *Journal of Geophysical Research.* 69(11):2199-2207.

Lingenfelter, R.E., Flamm, E.J., Canfield, E.H. and Kellman, S. (1965a) High-Energy Solar Neutrons 1. Production in Flares. *Journal of Geophysical Research.* 70(17):4077-4086.

Lingenfelter, R.E., Flamm, E.J., Canfield, E.H. and Kellman, S. (1965b) High Energy Solar Neutrons 2. Flux at the Earth. *Journal of Geophysical Research.* 70(17):4087-4095.

Lingenfelter, R.E. and Ramaty, R. (1967) High energy nuclear reactions in solar flares. In *High-Energy Nuclear Reactions in Astrophysics* ed B.S.P. Shen, Benjamin, Inc, New York, 99-158.

Lingenfelter, R.E., Canfield, E.H. and Hampel, V.E. (1972) The Lunar Neutron Flux Revisited. *Earth and Planetary Science Letters.* 16:355-369.

Lockwood, J.A. (1973) Neutron Measurements in Space. *Space Science Review.* 14:663-719.

Loss, R.D. (1986) *Mobility of the fission valley elements from the Oklo fossil reactors*, PhD thesis, Department of Physics, University of Western Australia, Perth, Western Australia, pp. 324.

Lugmair, G.W. and Marti, K. (1971) Neutron Capture Effects in Lunar Gadolinium and the Irradiation Histories of Some Lunar Rocks. *Earth and Planetary Science Letters.* 13:32-42.

Lugmair, G.W., Scheinin, N.B. and Marti, K. (1975) Sm-Nd Age and History of Apollo 17 Basalt 75075: Evidence for Early Differentiation of the Lunar Exterior. *Proceedings of the Lunar Science Conference 6th, Geochimica et Cosmochimica Acta Supplement.* 1419-1429.

Maas, R. (personal communication) Sm-Nd separation using methyl-lactic acid and HDEHP methods .

Maas, R. and McCulloch, M.T. (1990) A Search for fossil nuclear reactors in the Alligator River uranium field, Australia: Constraints from Sm, Gd and Nd isotopic studies. *Chemical Geology.* 88:301-315.

Mason, B. and Moore, C.B. (1982) *Principles of Geochemistry.,* John Wiley and Sons.

McCulloch, M.T. (1974) *The isotopic and elemental abundance of lutetium*, Masters thesis, Department of Physics, Western Australian Institute of Technology, Perth, Western Australia, pp. 176.

Mermelengas, N. (1980) *Isotope studies on palladium*, Masters thesis, Department of Physics, Western Australian Institute of Technology, Perth, Western Australia, pp. 138.

Moeller, T. (1963) *The Chemistry of the Lanthanides.,* Reinhold Publishing Corp., New York.

Morgan, J.W., Ganapathy, R., Higuchi, H., Krahenbuhl, U. and Anders, E. (1974) Lunar basins: Tentative characterization of projectiles, from meteoritic elements in Apollo 17 boulders. *Proceedings of the Lunar Science Conference 5th, Geochimica et Cosmochimica Acta Supplement.* 2:1703-1736.

Morgan, J.W., Laul, J.C., Krahenbuhl, U., Ganapathy, R. and Anders, E. (1972) Major impacts on the moon: Characterization from trace elements in Apollo 12 and 14 samples. *Proceedings of the Lunar Science Conference 3rd, Geochimica et Cosmochimica Acta Supplement.* 2:1377-1395.

Morris, R.V., Score, R., Dardano, C. and Heiken, G. (Eds.) (1983a) *Handbook of Lunar Soils, Part I: Apollo 11-15.,* NASA, Planetary Materials Branch, Houston, Texas.

Morris, R.V., Score, R., Dardano, C. and Heiken, G. (1983b) *Handbook of Lunar Soils, Part II: Apollo 16-17.,* NASA, Planetary Materials Branch, Houston, Texas.

Nelson, F., Murase, T. and Kraus, K.A. (1964) Ion exchange procedures. I Cation exchange in concentrated HCl and $HClO_4$ solutions. *Journal of Chromatography.* 13:503-535.

Nelson, F., Rush, R.M. and Kraus, K.A. (1960) Anion adsorbability in HCl-HF solutions. 82:339-348.

Nemodruk, A.A., Novikov, Y.P., Lukin, A.M. and Kalinina, I.D. (1961) 2.7-bis-(4-chloro-2-phosphonobenzeneazo)-1.8-dihydroxynaphthalene-3.6-disulfonic acid (Chlorophosphonazo III), a new reagent for the photometric determination of uranium. *Zhurnal Analiticheskoi Khimii (in translation).* 16(2):180-184.

Nishiizumi, K., Regnier, S. and Marti, K. (1980) Cosmic ray exposure ages of chondrites, pre-irradiation and constancy of cosmic ray flux in the past. *Earth and Planetary Science Letters.* 50:156-170.

Peppard, D.F., Mason, G.W., Maier, J.L. and Driscoll, W.J. (1957) Fractional extraction of the lanthanides as their di-alkyl orthophosphates. *Journal of Inorganic Nuclear Chemistry.* 1:334-343.

Pierce, T.B. and Peck, P.F. (1962a) Use of di(2-ethylhexyl) orthophosphoric acid for the separation of the elements lanthanum-gadolinium by reverse phase partition chromatography. *Nature.* 194:84.

Pierce, T.B. and Peck, P.F. (1962b) Use of di(2-ethylhexyl) orthophosphoric acid for the separation of the rare earths by reverse phase partition chromatography. *Nature.* 195:594.

Pierce, T.B. and Hobbs, R.S. (1963) The separation of the rare earths by partition chromatography with reversed phase. Part I. Behaviour of column material. *Journal of Chromatography.* 12:74-80.

Rautenschlein, M., Jenner, G., Hertogen, J., Hofmann, A., Kerrich, R., Schmincke, H.-U. and White, W. (1985) Isotopic and trace element composition of volcanic glasses from the Akaki Canyon, Cyprus: implications for the origin of the Troodos ophiolite. *Earth and Planetary Science Letters.* 75:369-383.

Reedy, R.C. and Arnold, J.R. (1972) Interaction of Solar and Galactic Cosmic-Ray Particles with the Moon. *Journal of Geophysical Research.* 77(4):537-555.

Reedy, R.C., Arnold, J.R. and Lal, D. (1983) Cosmic-ray record in solar system matter. *Annual Review of Nuclear and Particle Science.* 33:505-537.

Rosman, K.J.R. (1992) Personal communication .

Rosman, K.J.R. (1997) Personal communication .

Rosman, K.J.R. and De Laeter, J.R. (1974a) The abundance of cadmium and zinc in meteorites. *Geochimica et Cosmochimica Acta.* 38:1665-1677.

Rosman, K.J.R. and De Laeter, J.R. (1974b) Mass spectrometric isotope dilution analyses of cadmium in standard rocks. *Chemical Geology.* 13:69-74.

Rosman, K.J.R. and De Laeter, J.R. (1975) The isotopic composition of cadmium in terrestrial minerals. *International Journal of Mass Spectrometry Ion Physics.* 16:385-394.

Rosman, K.J.R. and De Laeter, J.R. (1976) Isotopic fractionation in meteoritic cadmium. *Nature.* 261(5557):216-218.

Rosman, K.J.R. and De Laeter, J.R. (1978) A survey of cadmium isotopic abundances. *Journal of Geophysical Research.* 83(B3):1279-1287.

Rosman, K.J.R. and De Laeter, J.R. (1980) Mass spectrometric isotope dilution determination of cadmium in geochemical reference samples. *Geostandards Newsletter*, 4(1):1-3.

Rosman, K.J.R. and De Laeter, J.R. (1988) Cadmium mass fractionation in unequilibrated ordinary chondrites. *Earth and Planetary Science Letters.* 89:163-169.

Russ, G.P. (1972) Neutron Capture on Gd and Sm in the Luna 16, G-2 Soil. *Earth and Planetary Science Letters.* 13:384-386.

Russ, G.P. (1973) Apollo 16 neutron stratigraphy. *Earth and Planetary Science Letters.* 17:275-289.

Russ, G.P. (1974) Neutron stratigraphy in the lunar regolith, PhD thesis, California Institute of Technology, pp318.

Russ, G.P., Burnett, D.S., Lingenfelter, R.E. and Wasserburg, G.J. (1971) Neutron Capture on ^{149}Sm in Lunar Samples. *Earth and Planetary Science Letters.* 13:53-63.

Russ, G.P., Burnett, D.S. and Wasserburg, G.J. (1972) Lunar Neutron Stratigraphy. *Earth and Planetary Science Letters.* 15:172-186.

Russell, W.A., Papanastassiou, D.A. and Tombrello, T.A. (1978) Ca isotope fractionation on the Earth and other solar system materials. *Geochimica et Cosmochimica Acta.* 42:1075-1090.

Ryder, G. (Ed.) (1985) *Catalog of Apollo 15 Rocks, Part 1. 15015 - 15299,* NASA, Lyndon B. Johnson Space Center,, Houston, Texas.

Sands, D.G. and Rosman, K.J.R. (1997) Cd, Gd and Sm concentrations in BCR-1, BHVO-1, BIR-1, DNC-1, MAG-1, PCC-1 and W-2 by isotope dilution thermal ionisation mass spectrometry. *Geostandards Newsletter: The Journal of Geostandards and Geoanalysis.* 21(1):77-83.

Shima, M., Hidaka, H., Nakaya, D., Shinotsuka, K. and Ebihara, M. (1994) Precise determination of isotopic compositions for lanthanum, samarium, gadolinium, dysprosium, erbium, ytterbium and lutetium by thermal ionization mass spectrometry. *Bulletin National Science Museum, Tokyo.* 17(Ser. E):1-8.

Siekierski, S. and Sochacka, R.J. (1964) Reversed-phase partition chromatography with di(2-ethylhexyl) orthophosphoric acid as the stationary phase. Part II. Factors affecting the height of the plate. *Journal of Chromatography.* 10:385-395.

Smith, C.L. (1977) *The isotopic and elemental abundance of tellurium*, Masters thesis, Department of Physics, Western Australian Institute of Technology, Perth, Western Australia, pp. 289.

Sochacka, R.J. and Siekierski, S. (1964) Reversed-phase partition chromatography with di(2-ethylhexyl) orthophosphoric acid as the stationary phase. Part 1. Separation of rare earths. *Journal of Chromatography.* 16:376-384.

Strelow, F.W.E. (1960) An ion exchange selectivity scale of cations based on equilibrium distribution coefficients. *Analytical Chemistry.* 32(9):1185-1188.

Strelow, F.W.E., Rethemeyer, R. and Bothma, C.J.C. (1965) Ion exchange selectivity scales for cations in nitric acid and sulfuric acid media with a sulfonated polystyrene resin. *Analytical Chemistry.* 37(1):106-111.

Sullivan, R.W. (1988) Samarium-neodymium and rare-earth element liquid chromatography (HPLC) techniques at the Geochronology Laboratory. *Geological Survey of Canada.* 88(2):9-20.

Sun, S., Nesbitt, R. and Sharaskin, A. (1979) Geochemical characteristics of mid-ocean ridge basalts. *Earth and Planetary Science Letters.* 44:119-138.

Tanaka, S. and Inoue, T. (1979) 10 Be dating of North Pacific sediment cores up to 2.5 million years B.P. *Earth and Planetary Science Letters.* 45:181-187.

Taylor, S.R. (1975) *Lunar Science: A Post-Apollo View,* Pergamon Press Inc., New York.

Taylor, S.R. (1982) *Planetary Science: A Lunar Perspective*, Cambridge University Press.

Walker, R.M. (1975) Interaction of energetic nuclear particles in space with the lunar surface. *Annual Review of Earth and Planetary Science.* 3:99-128.

Wapstra, A.H. and Audi, G. (1985) The 1983 atomic mass evaluation (I) Atomic mass table. *Nuclear Physics.* A432:1-54.

Wasson, J.T., Chou, C.-L., Robinson, K.L. and Baedecker, P.A. (1975) Siderophiles and volatiles in Apollo 16 rocks and soils. *Geochimica et Cosmochimica Acta.* 39:1475-1485.

Webber, W.R. and Ormes, J.F. (1967) An upper limit on the quiet time solar neutron flux at energies >60 MeV. *Journal of Geophysical Research.* 72(13):3387.

Webster, R.K. (1960) Mass Spectrometric Isotope Dilution Analysis. In *Methods in Geochemistry*(Eds, Smales, A.A. and Wager, L.R.) Interscience, New York, 202-246.

Wedepohl, K.H. (1995) The composition of the continental crust. *Geochimica Cosmochimica Acta.* 59(7):1217-1232.

Winchester, J.W. (1963) Rare earth chromatography using bis (2-ethylhexyl) orthophosphoric acid. *Journal of Chromatography.* 10:502-506.

Woolum, D.S. and Burnett, D.S. (1974) In-situ measurement of the rate of ^{235}U fission induced by lunar neutrons. *Earth and Planetary Science Letters.* 21:153-163.

Woolum, D.S., Burnett, D.S., Furst, M. and Weiss, J.R. (1975) Measurements of the lunar neutron density profile. *The Moon.* 12:231-250.

Appendices

Appendix A - Units and abbreviations used in this thesis

1. Units

ng - nanogram

pg - picogram

μg - microgram

pg/g - picogram per gram

ppm - parts per million (10^6)

ppb - parts per billion (10^9)

2. Abbreviations

2-mla - methyl lactic acid

BP - boiling point

CV - column volume

GCR - galactic cosmic rays

GRM - geochemical reference materials

HDEHP - di(2-ethylhexyl)orthophosphoric acid

HDPE - high density polyethylene

HPLC - High Performance Liquid Chromatography

IDMS - Isotope dilution mass spectrometry

LOS - line-of-sight valve

LDPE - low density polyethylene

MP - melting point

PE - polyethylene

PFA - perfluoralkoxy

REE - rare earth elements

SCR - solar cosmic rays

SEM - scanning electron microscope

TIMS - thermal ionisation mass spectrometry

USGS - United States Geological Survey

Appendix B - Sample digestion procedures

The digestion procedures for all lunar and GRM concentration and composition measurements are described here in detail, complementing Chapter 2, Section 2.2.4.

Samples (about 100-200 mg) were weighed on an electronic balance, accurate to ±0.0002 g, in pre-cleaned 15 ml PFA Teflon beakers.

- 5g concentrated HF and 1 g concentrated HNO_3 were added to the sample, and left uncovered overnight in a clean airflow to allow the evaporation of SiF_6 at room temperature.
- Accurately weighed tracers enriched in $^{106 \text{ and } 111}Cd$, ^{152}Gd, and ^{147}Sm were added at this stage for the concentration measurements of the GRM only. Tracers were added at a later stage for the lunar sample concentration measurements.
- The PFA beaker is covered with a screw top, placed in a 1 litre polyethylene (PE) jar with the lid on, refluxed for 20 seconds in a microwave oven (650 W), left to cool for a few minutes, then opened and evaporated to dryness inside a closed container with a clean airflow (Figure 2-1).

Figure 2-1 Closed teflon pot with a clean air flow.

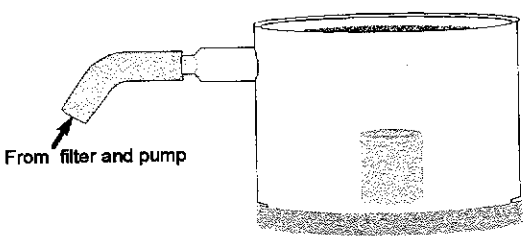

- 5g concentrated HF and 1 g concentrated HNO_3 was added to the sample. It was covered and refluxed for 15 seconds in a microwave oven, then evaporated to dryness, as before.
- 3g concentrated HCl and 1 g concentrated HNO_3 were added to the sample which was covered and refluxed twice for 20 seconds in

a microwave oven. It was left to cool for a few minutes before the second reflux, then evaporated to dryness.

- 5g concentrated HCl was added to the sample which was covered and refluxed for 30 seconds in a microwave oven, then evaporated to dryness.
- For a second time 5g concentrated HCl was added to the sample which was covered and refluxed for 30 seconds in a microwave oven. GRM and lunar samples, when 5% has been extracted, were then evaporated to dryness.
- For the concentration measurements of the lunar samples accurately weighed tracers enriched in $^{106 \text{ and } 111}Cd$, ^{152}Gd, and ^{147}Sm were added at this stage to the extracted 5% of the sample, before evaporation.

The sample was now ready for the six stage ion exchange separation process.

Appendix C - Cadmium separation chemistry

The reagents added to anion and cation exchange columns during cadmium separation are described here in detail, these details complement Chapter 2, Section 2.2.5.

1. Anion exchange, first column

The acid mix prepared for this procedure was one part of 6 M HF plus one part of 4 M HCl, giving an acid mix with a concentration of 3 M HF and 2 M HCl.

The 1.5 ml volume of resin, washed into the column in MQW, was cleaned to minimise contamination from any rare earths, silver, tin, indium or cadmium by adding in turn the reagents described next:

- 24 ml MQW
- 6 ml 3 M HCl
- 6 ml 9 M HCl (Added for the lunar samples only)
- 12 ml 3 M HF + 2 M HCl
- 6 ml 0.1 M HCl
- 12 ml 1 M HNO3
- 6 ml MQW
- 1.5 ml 9 M HCl (The height of the resin was corrected here)

The previously digested sample was added, a small amount at a time, dissolved in <1 ml 9 M HCl. If the sample was not fully dissolved in the 9 M HCl then low heat was applied and the sample cooled again before loading. The beaker and column were rinsed with a further 1 ml 9 M HCl. The REE were collected from the column during the first two stages, then evaporated and put aside for the rare earth element separation procedures:

- 12 ml 9 M HCl (6 ml 3 M HCl was used for the GRMs)
- 12 ml 3 M HCl (Not used for the GRMs)
- 12 ml 3 M HF + 2 M HCl (Sn and In was removed during this and the next stage)
- 24 ml 0.1 M HCl
- 9 ml 1 M HNO_3 (6 ml of HNO_3 was used for the GRMs)

The cadmium was collected at the last stage; evaporated to dryness, and passed to the second anion column described next (one anion column only was used for the GRMs).

2. Anion exchange, second column

This separation stage was used only for the lunar samples. The resin was washed into the column in MQW, then cleaned, with:

- 6 ml MQW
- 1.5 ml 3 M HCl
- 1.5 ml 9 M HCl
- 3 ml 3 M HF + 2 M HCl
- 1.5 ml 0.1 M HCl
- 3 ml 1 M HNO_3
- 1.5 ml MQW
- 0.4 ml 3 M HCl (The height of the resin was corrected here)

The sample from anion column one was added, dissolved in ¼ ml 3 M HCl and the beaker and column were rinsed with a further ¼ ml 3 M HCl. During the final stage any remaining tin ions were removed, then the cadmium:

- 6 ml 0.1 M HCl
- 2 ¼ ml 1 M HNO_3;

The cadmium was collected in the 1 M HNO_3 cut, evaporated to dryness and passed to the cation column.

3. Cation exchange

The cation resin was washed into the column in MQW and cleaned by adding in turn the following acids:

- 26 ml MQW
- 26 ml 3 M HCl
- 6.5 ml 0.5 M HCl
- 6.5 ml 3 M HCl
- 6.5 ml 0.5 M HCl (The height of the resin was checked here)

If the column was left overnight a further 6.5 ml of 3 M HCl and 6.5 ml 0.5 M HCl were added in the morning, in case any interfering ions had leached from the resin overnight.

The sample from the second anion column was added to the cation column dissolved in 1 ml 0.5 M HCl and the beaker and column were rinsed with a further 1 ml 0.5 M HCl.

Cadmium was eluted immediately with:

- 10 ml 0.5 M HCl

10 μL H_3PO_4 was added to the cadmium and the sample evaporated.

Appendix D - Rare earth separation chemistry

The four ion exchange stages used to separate the rare earth elements are described in detail below, complementing Chapter 2, Sections 2.4.2 to 2.4.4.

1. Anion exchange

Described in cadmium chemistry in Appendix D above.

2. Cation exchange, group separation of the REE

The acid mix prepared for this procedure was 3 parts 3M HNO_3 with 1 part 2.5 M HCl, resulting in a mix of 2.25 M HNO_3 with 0.6 M HCl.

The resin was cleaned, by adding in turn the following acids:

- 6 ml MQW
- 6 ml acid mix (9 ml for the GRMs)
- 9 ml 7 M HNO_3 (15 ml for the GRMs)
- 6 ml acid mix (The height of the resin was checked here. This stage was not used for the GRMs.)

The evaporated sample from the first anion column was added, a small amount at a time, dissolved in ½ ml of acid mix (the GRM samples were dissolved in 0.03 M HCl). The beaker and column were rinsed with a further ½ ml of acid mix (0.03 M HCl for the GRMs). Elements were washed off the column with:

- 8 ml acid mix (All elements except for the rare earths were eluted and reserved)
- 10 ml 7 M HNO_3 (Gd and Sm were collected between 0.5 ml and 10 ml)

The sample was evaporated and passed to the next ion exchange procedure.

The quantity of acid mix used for the dissolving and rinsing of the sample needed to be carefully measured so that less than 10 ml total was used (1 ml for dissolving the sample, and 8 ml for washing). The rare earth elements start leaving the column if more than 10 ml acid mix was added. The careful measurement of the acid mix was not followed for the GRMs.

3. Separation of gadolinium and samarium by HPLC

The 15 ml PFA beakers used to collect the eluent were cleaned with concentrated HF just before use.

Bubbles were easily trapped in this fine microcolumn so to prevent this the reservoir was first filled with MQW, the column was lifted slightly off the filter so that the water can flow down to the base of the column, then tightened again against the filter. The resin was placed in the water remaining in the reservoir so that it can flow down into the column. Enough resin was used to fill the column and the small cone at the base of the reservoir. A diagram of the column is in Figure 2-11 in Chapter 2.

- The resin was conditioned overnight with 10 ml 0.2 M methyl lactic acid, with pH 4.3.
- In the morning 1 ml methyl lactic acid was added to make sure that the column was flowing, and the resin was levelled to the bottom of the cone at the base of the reservoir.
- When the methyl lactic acid had moved into the resin 25 µl MQW was added to separate the methyl lactic acid from the HCl in which the sample was loaded.
- The sample was loaded in 10 µL 0.75 M HCl (prepared volumetrically).
- A further 10 µL 0.75 M HCl was used to rinse the beaker. If the beaker still contained some sample another 10 µL 0.75 M HCl was used.

- When the sample had moved into the resin another 25 µl MQW was added.
- When the water has moved into the resin methyl lactic acid was added in 50 µl drops, to prevent stirring up the resin. 12 ml methyl lactic acid was added to the reservoir.
- The pressure system was connected and started so that the column ran at 1.7 ml/hour.
- The gadolinium was collected between 1.9 and 3.1 ml.
- The samarium was collected between 4.1 and 8.5 ml.

During the separation of the GRMs (Sands and Rosman, 1997) any ammonium chloride evident after evaporation was decomposed by adding three drops of concentrated HNO_3 and 1 drop of concentrated HCl to the sample. If more ammonium chloride was present after evaporation this was repeated.

For the lunar samples the additional cleaning procedures and the extra ion exchange with Lanspec resin removes the ammonium chloride. Procedures were modified so that less HCl was present in the air when the REE were being separated, reducing the formation of ammonium chloride in the first place.

4. Separation of gadolinium and samarium with Lanspec resin.

This procedure was used for the separation of the lunar samples only. The Lanspec Resin was cleaned and conditioned using:

- 6 ml 6 M HCl
- 3 ml MQW
- 3 ml 0.3 M HCl

The evaporated samples of gadolinium and samarium collected from the microcolumn were placed on separate columns. A sample was dissolved in ½ ml 0.3 M HCl and loaded onto the resin, the beaker was then rinsed in a further ½ ml 0.3 M HCl.

The following procedure was used for the separation of gadolinium:

- 5.5 ml 0.3 M HCl (A total of exactly 6.5 ml, with the 1 ml for dissolution and rinsing included)
- 7.0 ml 0.4 M HCl
- 6.0 ml 0.5 M HCl (Gd was collected in the first 3.5 ml; and evaporated with 2 μL H_3PO_4)

The following procedure was used for the separation of samarium:

- 5.5 ml 0.3 M HCl (A total of exactly 6.5 ml, with the 1 ml for dissolution and rinsing included)
- 5.0 ml 0.4 M HCl (Sm was collected between 0.8-4.3 ml; and evaporated with 2 μL H_3PO_4)

Only 2 μL of phosphoric acid was used to concentrate the REE sample. The H_3PO_4 must be evaporated from the filament when loading the sample for the mass spectrometer, leading to the possibility of gadolinium or samarium oxides forming, so the minimum possible was used.

Appendix E - Type files and multi collector cup configurations

Type files, listing the ratios to be calculated, and the multi collector cup configurations which are attached to the Type files. These tables supplement Chapter 3.

1. Cadmium

Table 1-1 Type files used with GPJIF and the Daly detector to measure cadmium isotopes.

	Used for	Ratios measured	Pre- and post-scan masses
Type 5	IDMS	$^{106}Cd/^{112}Cd$ $^{111}Cd/^{112}Cd$ $^{113}Cd/^{112}Cd$ $^{114}Cd/^{112}Cd$	105, 115, 118
Type 6	neutron capture	$^{111}Cd/^{112}Cd$ $^{113}Cd/^{112}Cd$ $^{114}Cd/^{112}Cd$ $^{115}Cd/^{112}Cd$	105, 118
Type 9	neutron capture	$^{110}Cd/^{112}Cd$ $^{111}Cd/^{112}Cd$ $^{113}Cd/^{112}Cd$ $^{114}Cd/^{112}Cd$	103, 105, 118

Table 1-2 Cadmium isotopes measured by INTEG on the Faraday multi collector, showing Type file number, cup setting and the ratios calculated.

	Cup positions	Ratios measured
Type 42	CD(112AX)	$^{107}Cd/^{112}Cd$ $^{108}Cd/^{112}Cd$ $^{110}Cd/^{112}Cd$ $^{111}Cd/^{112}Cd$ $^{113}Cd/^{112}Cd$ $^{114}Cd/^{112}Cd$ $^{115}Cd/^{112}Cd$ $^{116}Cd/^{112}Cd$
Type 43	CD(111AX)	$^{106}Cd/^{112}Cd$ $^{107}Cd/^{112}Cd$ $^{108}Cd/^{112}Cd$ $^{110}Cd/^{112}Cd$ $^{111}Cd/^{112}Cd$ $^{113}Cd/^{112}Cd$ $^{114}Cd/^{112}Cd$ $^{116}Cd/^{112}Cd$

2. Gadolinium

Table 2-1 Type files used with GPJIF and the Daly detector to measure gadolinium isotopes.

	Used for	Ratios measured	Pre- and post-scan masses
Type 1	IDMS	$^{152}Gd/^{160}Gd$ $^{156}Gd/^{160}Gd$ $^{158}Gd/^{160}Gd$	149, 163
Type 7	neutron capture	$^{155}Gd/^{160}Gd$ $^{156}Gd/^{160}Gd$ $^{157}Gd/^{160}Gd$ $^{158}Gd/^{160}Gd$	149

Table 2-2 Gadolinium isotopes measured by INTEG on the Faraday multi collector, showing Type file number, cup setting and the ratios calculated.

	Cup positions	Ratios measured
Type 2	GD(AX156)	$^{150}Gd/^{160}Gd$ $^{152}Gd/^{160}Gd$ $^{154}Gd/^{160}Gd$ $^{155}Gd/^{160}Gd$ $^{156}Gd/^{160}Gd$ $^{157}Gd/^{160}Gd$ $^{158}Gd/^{160}Gd$ $^{163}Gd/^{160}Gd$

3. Samarium

Table 3-1 Type files used with GPJIF and the Daly detector to measure samarium isotopes.

	Used for	Ratios measured	Pre- and post-scan masses
Type 4	IDMS	$^{147}Sm/^{152}Sm$ $^{149}Sm/^{152}Sm$ $^{150}Sm/^{152}Sm$	157
Type 8	IDMS or neutron capture	$^{144}Sm/^{152}Sm$ $^{147}Sm/^{152}Sm$ $^{149}Sm/^{152}Sm$ $^{150}Sm/^{152}Sm$ $^{154}Sm/^{152}Sm$	157

Table 3-2 Samarium isotopes measured by INTEG on the Faraday multi collector, showing Type file number, cup setting and the ratios calculated.

	Cup positions	Ratios measured
Type 39	SM(149AX)	$^{144}Sm/^{152}Sm$ $^{147}Sm/^{152}Sm$ $^{148}Sm/^{152}Sm$ $^{149}Sm/^{152}Sm$ $^{150}Sm/^{152}Sm$ $^{154}Sm/^{152}Sm$ $^{157}Sm/^{152}Sm$
Type 38	SM(150AX)	$^{144}Sm/^{152}Sm$ $^{147}Sm/^{152}Sm$ $^{148}Sm/^{152}Sm$ $^{149}Sm/^{152}Sm$ $^{150}Sm/^{152}Sm$ $^{154}Sm/^{152}Sm$ $^{156}Sm/^{152}Sm$ $^{157}Sm/^{152}Sm$

Appendix F - Mass spectrometry procedures for elemental abundances

Concentration results are given in Chapter 5.

Tracer solutions added to the GRM samples are detailed. Also, for the concentration measurements on the GRMs and the lunar samples, the dates on which samples were prepared, the number of "runs", or sets of 10 measurements which were made, the average ion current for the most abundant isotope and whether the measurements were taken on the Faraday multi-collectors or on the Daly.

In the Tables below the number of "Runs" are listed. Each Run is a set of ten measurements on the mass spectrometer, the number outside the bracket is the number of Runs included in the reported abundance ratio, the numbers in brackets are the additional number of runs which were completed, but were rejected for the reasons stated below the Tables.

1. GRM samples

Results are in Chapter 5, Section 5.2.

1.1 Tracer solutions added to the GRM samples

Table 1-1 Details of the cadmium tracers added to the GRMs. Tracer concentration was 0.6349 ppm $^{106 \text{ and } 111}$Cd for BCR-1 and the first BHVO-1 sample, and 33.83 ppb $^{106 \text{ and } 111}$Cd for all the other samples.

Sample	$^{106 \text{ and } 111}$Cd tracer (ng) ±0.05 ng	Date
BCR-1	12.95±0.1	22/9/94
	12.83±0.1	22/9/94
BHVO-1	6.67±0.1	22/9/94
	7.3	9/11/94
	26.5	6/6/95
BIR-1	12.8	9/11/94
	12.4	9/11/94
	none	12/1/95
	9.5	8/5/95
DNC-1	30.3	6/2/95
	26.6	6/2/95
	8.9	8/5/95
	8.0	8/5/95
	13.7	6/6/95
MAG-1	15.0	9/1/95
	15.8	9/1/95
PCC-1	1.8	6/2/95
	14.7	27/2/95
	15.9	6/6/95
W-2	14.3	27/2/95
	14.1	27/2/95
	29.6	6/6/95

Table 1-2 Details of the gadolinium tracers added to the GRMs. Tracer concentration was 10.446 ppm ^{152}Gd for all samples except for BHVO-1 dated 6/6/95, BIR-1 dated 8/5/95, DNC-1 on 8/5/95 and PCC-1 and W-2 on 6/6/95, all of which had a 2.082 ppm ^{152}Gd tracer added.

Sample	^{152}Gd tracer (μg)	Date
BCR-1	1.298±0.003	22/9/94
	1.081±0.003	22/9/94
BHVO-1	1.087±0.003	22/9/94
	1.164±0.003	9/11/94
	0.858±0.002	6/6/95
BIR-1	1.120±0.003	9/11/94
	1.167±0.003	9/11/94
	1.043±0.003	12/1/95
	0.234±0.002	8/5/95
DNC-1	0.302±0.003	6/2/95
	0.325±0.003	6/2/95
	0.237±0.002	8/5/95
	0.239±0.002	8/5/95
MAG-1	1.077±0.003	9/1/95
	1.036±0.003	9/1/95
PCC-1	0.118±0.003	6/2/95
	0.108±0.003	27/2/95
	0.174±0.002	6/6/95
W-2	0.309±0.003	27/2/95
	0.315±0.003	27/2/95
	1.662±0.002	6/6/95

Table 1-3 Details of the samarium added to the GRMs. Tracer concentration was 11.643 ppm ^{147}Sm for all the samples except for BHVO-1 dated 6/6/95, BIR-1 dated 8/5/95, DNC-1 on 8/5/95 and PCC-1 and W-2 samples on 6/6/95, all of which had a 1.8138 ppm ^{147}Sm tracer added.

Sample	^{147}Sm tracer (μg)	Date
BCR-1	1.418±0.003	22/9/94
	1.112±0.003	22/9/94
BHVO-1	1.107±0.003	22/9/94
	1.395±0.003	9/11/94
	0.716±0.001	6/6/95
BIR-1	1.282±0.003	9/11/94
	1.342±0.003	9/11/94
	1.143±0.003	12/1/95
	0.241±0.001	8/5/95
DNC-1	0.307±0.003	6/2/95
	~0.3	6/2/95
	0.196±0.001	8/5/95
	0.191±0.001	8/5/95
MAG-1	1.078±0.003	9/1/95
	1.161±0.003	9/1/95
PCC-1	0.125±0.003	6/2/95
	0.128±0.003	27/2/95
	0.138±0.001	6/6/95
W-2	0.333±0.003	27/2/95
	0.290±0.003	27/2/95
	1.398±0.001	6/6/95

1.2 Cadmium

Table 1-4 Detailed mass spectrometry procedures for the cadmium concentration measurements of the GRMs.

Date	Sample	Runs included (and rejected)	Average ion current at mass 114 (A)	Daly or Faraday
22/9/94	**BCR-1**	11	$2x10^{-12}$	F
22/9/94		17(1)	$4x10^{-13}$	F
22/9/94	**BHVO-1**	10	$4x10^{-13}$	F
9/11/94		11	$5x10^{-14}$	F
6/6/95		15	$3x10^{-13}$	D
9/11/94	**BIR-1**	16	$1x10^{-13}$	F
9/11/94		10(1)	$2x10^{-13}$	F
12/1/95				
8/5/95		10	$4x10^{-14}$	D
6/2/95	**DNC-1**	7	$5x10^{-14}$	F
6/2/95		13	$2x10^{-13}$	D
8/5/95		7(1)	$3x10^{-15}$	D
8/5/95		5	$1x10^{-14}$	D
6/6/95		18	$3x10^{-12}$	F
9/1/95	**MAG-1**	10	$4x10^{-14}$	D
9/1/95		10	$4x10^{-14}$	D
6/2/95	**PCC-1**	2(1)	$5x10^{-17}$	D
27/2/95		9(1)	$6x10^{-14}$	D
6/6/95		9(1)	$7x10^{-14}$	D
27/2/95	**W-2**	19(2)	$9x10^{-13}$	F
27/2/95		9(1)	$3x10^{-14}$	D
6/6/95		14(1)	$8x10^{-13}$	F

Sets of 10 measurements on the mass spectrometer were rejected when a ratio varies more than 0.5% from the mean.

1.3 Gadolinium

Table 1-5 Detailed mass spectrometry procedures for the gadolinium concentration measurements of the GRMs.

Date	Sample	Runs included (and rejected)	Average ion current at mass 158 (A)	Daly or Faraday
22/9/94	**BCR-1**	10	$1x10^{-14}$	D
22/9/94		9	$2x10^{-13}$	F
22/9/94	**BHVO-1**	5	$5x10^{-15}$	D
9/11/94		7(2)	$3x10^{-13}$	F
6/6/95		8	$3x10^{-13}$	F
9/11/94	**BIR-1**	none		
9/11/94		13(5)	$4x10^{-12}$	F
12/1/95		9(1)	$2x10^{-13}$	D
8/5/95		10	$4x10^{-14}$	D
6/2/95	**DNC-1**	3(1)	$3x10^{-16}$	D
6/2/95		10	$2x10^{-15}$	D
8/5/95		7(3)	$6x10^{-15}$	D
8/5/95		10	$7x10^{-14}$	D
9/1/95	**MAG-1**	9(1)	$7x10^{-14}$	D
9/1/95		8(3)	$2x10^{-14}$	D
6/2/95	**PCC-1**	5(1)	$4x10^{-15}$	D
27/2/95		8(2)	$2x10^{-14}$	D
6/6/95		8(2)	$2x10^{-15}$	D
27/2/95	**W-2**	10	$4x10^{-14}$	D
27/2/95		7(1)	$9x10^{-14}$	D
6/6/95		11(1)	$8x10^{-13}$	F

Sets of 10 measurements on the mass spectrometer were rejected when a ratio varies more than 1% from the mean.

1.4 Samarium

Table 1-6 Detailed mass spectrometry procedures for the samarium concentration measurements of the GRMs.

Date	Sample	Runs included (and rejected)	Average ion current at mass 154 (A)	Daly or Faraday
22/9/94	**BCR-1**	10	$4x10^{-12}$	F
22/9/94		10	$1x10^{-13}$	D
22/9/94	**BHVO-1**	8	$2x10^{-12}$	D
9/11/94		9	$2x10^{-12}$	F
6/6/95		11	$8x10^{-14}$	D
		12	$2x10^{-12}$	F
9/11/94	**BIR-1**		none	
9/11/94		14	$8x10^{-12}$	F
12/1/95			none	
8/5/95		15	$7x10^{-13}$	F
6/2/95	**DNC-1**		none	
6/2/95		6	$6x10^{-15}$	
8/5/95		11(2)	$2x10^{-12}$	F
8/5/95		12(1)	$7x10^{-13}$	F
9/1/95	**MAG-1**	12	$5x10^{-13}$	F
9/1/95		9(1)	$2x10^{-13}$	D
6/2/95	**PCC-1**	8(2)	$6x10^{-14}$	D
27/2/95		10(1)	$4x10^{-13}$	D
6/6/95		9(1)	$4x10^{-14}$	D
27/2/95	**W-2**	4(3)	$1x10^{-15}$	D
27/2/95		9(1)	$5x10^{-14}$	D
6/6/95		16	$8x10^{-12}$	F

Sets of 10 measurements on the mass spectrometer were rejected when a ratio varies more than 1% from the mean. All the GRM samarium samples dated before May 1995 were measured on a single rhenium filament, the six samples dated May 1995 or later were measured on triple rhenium filaments.

2. Lunar samples

Results are given in Chapter 5, Section 5.3.

2.1 Cadmium

Table 2-1 Details of the procedures used in cadmium concentration measurements of the lunar samples.

Date	Sample	Runs included (and rejected)	Average ion current at mass 114 (A)	Daly or Faraday	Comments
9/4/97	**10017,341**	8	$6x10^{-14}$	F	In
21/3/97	**14163,848**	11	$4x10^{-15}$	D	In
15/7/97		4(1)	$2x10^{-14}$	D	In
9/4/97	**14310,615**	10	$3x10^{-14}$	D	In
9/4/97	**15041,188**	10	$4x10^{-15}$	D	In
9/4/97	**15059,240**	10	$2x10^{-13}$	F	In
16/1/97	**60501,105**	5	$2x10^{-15}$	D	In
15/7/97		5	$2x10^{-14}$	D	Sn
9/4/97	**65701,23**	10	$9x10^{-15}$	D	Sn
9/4/97	**72161,73**	10	$2x10^{-14}$	D	Sn
21/3/97	**74220,125**	11	$6x10^{-15}$	D	In
15/7/97		6	$2x10^{-15}$	D	In

All the lunar concentrations were calculated from the $^{111}Cd/^{112}Cd$ ratio only, as traces of indium, less than 0.2%, were detected at atomic mass 113.

2.2 Gadolinium

Table 2-2 Details of the procedures used in gadolinium concentration measurements of the lunar samples.

Date	Sample	Runs included (and rejected)	Average ion current at mass 158 (A)	Daly or Faraday
21/3/97	**14163,848**	(10)	$8x10^{-14}$	D
15/7/97		3	$4x10^{-16}$	D
16/1/97	**60501,105**	1	$1x10^{-14}$	F
15/7/97		9	$4x10^{-16}$	D
21/3/97	**74220,125**	4	$5x10^{-15}$	D
15/7/97		11	$1x10^{-14}$	D

The first concentration measurement of 14163,848 was highly contaminated with samarium, so was rejected. The analyser pressure was high (>1x10^{-8} mbar) for all gadolinium concentration measurement of all three lunar samples.

2.3 Samarium

Table 2-3 Details of the procedures used in samarium concentration measurements of the lunar samples.

Date	Sample	Runs included (and rejected)	Average ion current at mass 154 (A)	Daly or Faraday
21/3/97	**14163,848**	10	9x10^{-13}	F
15/7/97		10	5x10^{-13}	F
16/1/97	**60501,105**	3	1x10^{-13}	D
15/7/97		4(1)	3x10^{-15}	D
21/3/97	**74220,125**	12	6x10^{-14}	F
15/7/97		5	1x10^{-12}	F

The one run rejected in the second 60501,105 sample was a ratio 65% higher than the average. The analyser pressure was high (>1x10^{-8} mbar) for all samarium concentration measurement of all three lunar samples.

Appendix G - Mass spectrometry procedures for the composition measurements

Details of the mass spectrometry conditions and procedures used during the composition measurements of the terrestrial standards, BCR-1 and the lunar samples. The measurements are in Chapter 6.

In the Tables below the number of "Runs" are listed. Each Run is a set of ten measurements on the mass spectrometer, the number outside the bracket is the number of Runs included in the reported abundance ratio, the numbers in brackets are the additional number of runs which were completed, but were rejected for the reasons stated below the Tables.

Table 1 The weight of lunar samples used for composition measurement, after 5% has been removed for IDMS concentration measurements.

Date of digestion	Sample	Size of sample digested (mg) (±0.2 mg)	Size of sample removed for IDMS	Size of sample used for composition (±1.5 mg)
14/3/97 2/7/97	**14163,848**	200.8 235.8	5% 4%	191.2 226.2
16/1/97 2/7/97	**60501,105**	208.7 258.3	5% 4%	197.5 248.2
9/4/97	**65701,23**	195.8	4%	188.0
9/4/97	**72161,73**	198.7	5%	189.1
14/3/97 2/7/97	**74220,125**	210.1 207.6	4% 5%	201.0 198.0

1. Procedures for standard composition measurements

Composition measurements of the standards are in Chapter 6, Section 6.1.

1.1 Cadmium

Table 1-1 Details of conditions for the cadmium standard measurements on the mass spectrometer, all taken with ^{112}Cd in the axial cup of the multi-collector since August 1996.

Date	Sample size (ng)	Runs included (and rejected)	Average ion current at mass 114 (A)	Comments
8/8/96(1)	300	11	$4x10^{-12}$	Older Si gel
14/8/96(2)	28	11	$6X10^{-13}$	
23/8/96	17	11(10)	$7x10^{-13}$	
5/12/96	53	20(19)	$6X10^{-13}$	
12/2/97(1)	10	14(10)	$4x10^{-12}$	
12/2/97(2)	10	13(9)	$3x10^{-12}$	
15/2/97(1)	27	20(18)	$6x10^{-12}$	
26/5/97(1)	28	10(9)	$1.5x10^{-12}$	
26/5/97(2)	50	10(9)	$2x10^{-12}$	
14/6/97(2)	110	25(19)	$1\text{-}2.5x10^{-11}$	New Si gel
24/6/97(1)	15	12(10)	$2x10^{-12}$	
24/6/97(2)	15	11(9)	$8x10^{-12}$	
14/8/97	30	11(9)	$6x10^{-12}$	

Sets of 10 measurements on the mass spectrometer were rejected when the ratios vary by more than 0.1% from the mean.

1.2 Gadolinium

Table 1-2 Details of conditions for the gadolinium standard measurements on the mass spectrometer during 1996 and 1997.

Date	Sample size (μg)	Runs included (and rejected)	Average ion current at mass 158 (A)
20/3/96(1)	5	10	$2x10^{-11}$
20/3/96(2)	1	17	$1.6x10^{-11}$
20/3/96(3)	1	14(1)	$2x10^{-11}$
8/6/96	10	10	$2x10^{-11}$
12/6/96(1)	2.6	15	$1x10^{-11}$
12/6/96(2)	2.6	23(1)	$1.4x10^{-11}$
19/6/96	4	13(3)	$0.9x10^{-11}$
26/6/96	1	14(1)	$5x10^{-11}$
18/7/96	2	20	$1x10^{-11}$
1/8/96	2.5	17(4)	$3x10^{-11}$
12/9/96	1	7(2)	$0.5x10^{-11}$
20/9/96	1	15	$1x10^{-11}$
2/10/96	1.7	19	$1x10^{-11}$
15/10/96	5	12(3)	$1x10^{-11}$
11/2/97	2.5	18(2)	$1x10^{-11}$
8/5/97	2	17	$3x10^{-11}$
6/6/97	5	10	$1x10^{-11}$
21/8/97	2.5	13	$2x10^{-11}$

From October 1996 sample degassing in the mass spectrometer was increased to 30 minutes. Sets of 10 measurements on the mass spectrometer were rejected when the ratios vary by more than 0.2% from the mean.

1.3 Samarium

Table 1-3 Details of conditions for the samarium standard measurements on the mass spectrometer, all taken with ^{150}Sm in the axial cup of the multi-collector, since October 1996.

Date	Sample size (μg)	Runs included (and rejected)	Average ion current at mass 154 (A)
11/10/96	3	15(1)	$2x10^{-11}$
15/10/96	4	10	$3x10^{-11}$
30/10/96	4	19(1)	$3x10^{-11}$
18/11/96	4	19(1)	$1.6x10^{-11}$
5/12/96	1	19(1)	$1x10^{-11}$
17/12/96(1)	1	18(2)	$4x10^{-11}$
17/12/96(2)	1	18(2)	$3x10^{-11}$
24/12/96	1	15(1)	$0.6x10^{-11}$
12/2/97	2	12(2)	$2x10^{-11}$
27/2/97	2	18	$1x10^{-11}$
6/6/97	2	15	$2x10^{-11}$
7/8/97	1	10	$3x10^{-11}$

From October 1996 degassing of the sample was increased to 30 minutes. Sets of 10 measurements on the mass spectrometer were rejected when the ratios vary by more than 0.1% from the mean.

2. Procedures for BCR-1 composition measurements

Results are given in Chapter 6, Section 6.2.

2.1 Cadmium

Table 2-1 Details of the conditions for the measurement of cadmium in BCR-1.

Date	Sample size (g)	Runs included (and rejected)	Average ion current at mass 114 (A)
20/09/96	~0.3	25	$4x10^{-13}$
11/10/96(1)	0.2190	14	$4x10^{-13}$
11/10/96(2)	0.2266	13(1)	$9x10^{-13}$
3/4/97	0.2240	10(10)	$1x10^{-12}$
24/6/97(1)	0.1918	12(2)	$1x10^{-12}$
24/6/97(3)	0.0685	11(2)	$1x10^{-12}$

Sets of 10 measurements on the mass spectrometer were rejected when a ratio varies more than 0.1% from the mean.

2.2 Gadolinium

Table 2-2 Details of the conditions for the measurement of gadolinium in BCR-1.

Date	Sample size (g)	Runs included (and rejected)	Average ion current at mass 158 (A)
24/12/96	0.2508	22(1)	$0.4x10^{-11}$
27/2/97	0.2260	19(1)	$0.4x10^{-11}$

Sets of 10 measurements on the mass spectrometer were rejected when a ratio varies more than 0.4% from the mean.

2.3 Samarium

Table 2-3 Details of the conditions for the measurement of samarium in BCR-1.

Date	Sample size (g)	Runs included (and rejected)	Average ion current at mass 154 (A)
11/10/96	0.32	12(1)	1.8×10^{-11}
24/12/96	0.2508	17(3)	3×10^{-11}
24/12/96	0.2001	15(1)	0.068×10^{-11}
27/2/97	0.2260	23(2)	0.17×10^{-11}

Sets of 10 measurements on the mass spectrometer were rejected when a ratio varies more than 0.4% from the mean.

3. Lunar samples

Results are given in Chapter 6, Section 6.3.

Table 3-1 The weight of lunar samples used for composition measurements, after 5% had been removed for IDMS concentration measurements

Date	Sample	Size of sample digested (mg)	Sample removed for IDMS (%)	Sample size used for composition (mg) ±4%
14/3/97	**14163,848**	200.8	5	191.2
2/7/97	**14163,848**	235.8	4	226.2
16/1/97	**60501,105**	208.7	5	197.5
2/7/97	**60501,105**	258.3	4	248.2
2/7/97	**65701,23**	195.8	4	188.0
2/7/97	**72161,73**	198.7	5	189.1
14/3/97	**74220,125**	210.1	4	201.0
2/7/97	**74220,125**	207.6	5	198.0

3.1 Cadmium

Problems with the pressure in the mass spectrometer were experienced with two samples, 60501,105 dated 16/1/97 (1×10^{-8} mbar, 8×10^{-8} mbar) and the second sample of 74220,125 dated 2/7/97 (1×10^{-8}

mbar, $4x10^{-8}$ mbar). The first 74220,125 sample dated 14/3/97 ionised so poorly the data had to be rejected.

Table 3-2 Details of conditions for cadmium composition measurements of the lunar samples on the mass spectrometer.

Date	Sample	Runs included (and rejected)	Average ion current at mass 114 (A)	Daly or Faraday	Comments
14/3/97	**14163,848**	20 (14)	$1x10^{-12}$	Faraday	
2/7/97	**14163,848**	25	$1x10^{-11}$	Faraday	
16/1/97	**60501,105**	23 (2)	$9x10^{-15}$	Daly	
2/7/97	**60501,105**	10 (6)	$5x10^{-13}$	Faraday	
2/7/97	**65701,23**	22	$4x10^{-13}$	Faraday	new Sigel
2/7/97	**72161,73**	14	$3x10^{-13}$	Faraday	new Sigel
14/3/97	**74220,125**	8 3	$7x10^{-14}$ $1x10^{-14}$	Faraday Daly	rejected, poor ion beam
2/7/97	**74220,125**	25	$4x10^{-12}$	Faraday	

The multi collector cup configurations did not allow measurements of $^{106}Cd/^{112}Cd$.

3.2 Gadolinium

Sample 60501,105 dated 16/1/97 was rejected because of poor ionisation resulting from pressure problems in the mass spectrometer (analyser pressure $1.4x10^{-8}$, source pressure $1.7x10^{-7}$).

Sample 74220,125 dated 14/3/97 was measured successfully on the one day with both the Faraday and Daly detectors, so both sets of data have been included.

Rare earth chemistry problems were experienced with sample 74220,125, (2/7/97), during the separation of the rare earth group elements from the matrix sample and during the separation of the individual rare earths (a chloride precipitate formed blocking the columns). The sample was rinsed off the cation exchange resin and the chemistry was repeated. However, both the gadolinium and the samarium data had to be rejected. The gadolinium isotopes ^{157}Gd and

^{158}Gd were 25% greater and 12% lower respectively than standard gadolinium.

Table 3-3 Details of conditions for gadolinium composition measurements of the lunar samples on the mass spectrometer.

Date	Sample	Runs included (and rejected)	Average ion current at mass 158 (A)	Daly or Faraday	Comments
14/3/97	**14163,848**	5(1)	$4x10^{-13}$	Faraday	
2/7/97	**14163,848**	16(2)	$6x10^{-13}$	Faraday	
16/1/97	**60501,105**	13(13)	$8x10^{-15}$	Daly	rejected
2/7/97	**60501,105**	14(2)	$2x10^{-13}$	Faraday	
14/3/97	**74220,125**	9(1)	$1x10^{-13}$	Daly	one
14/3/97	**74220,125**	4	$2x10^{-12}$	Faraday	sample
2/7/97	**74220,125**	6	$4x10^{-15}$	Daly	rejected

3.3 Samarium

The 60501,105 sample dated 2/7/97 ionised so poorly that only 30 ratios could be measured, resulting in very poor precision.

The rare earth chemistry problems with sample 74220,125, dated 2/7/97, mentioned in Section 3.2 above, resulted in the samarium isotopes ^{149}Sm and ^{150}Sm being 45% greater and 72% greater respectively than standard samarium, so the data was rejected.

Table 3-4 Details of conditions for samarium composition measurements of the lunar samples on the mass spectrometer.

Date	Sample	Runs included (and rejected)	Average ion current at mass 152 (A)	Daly or Faraday	Comments
14/3/97	**14163,848**	25	$7x10^{-11}$	Faraday	
2/7/97	**14163,848**	20(5)	$7x10^{-12}$	Faraday	
16/1/97	**60501,105**	24(1)	$4x10^{-12}$	Faraday	
2/7/97	**60501,105**	3(1)	$2x10^{-12}$	Faraday	ionisation problems
14/3/97	**74220,125**	22(3)	$1x10^{-11}$	Faraday	
2/7/97	**74220,125**	10	$1x10^{-13}$	Faraday	rejected

Appendix H - Lunar rock samples

Photographs from NASA of the cutting and division of the three rocks, 10017,341, 14310,615 and 15059,240 are shown below.

1. Apollo 11

Figure 1-1 (a), (b), (c) and (d) Photographs of the subdivision of rock 10017,15 to produce 10017,341, from NASA-JSC (1978).

10017.280 5

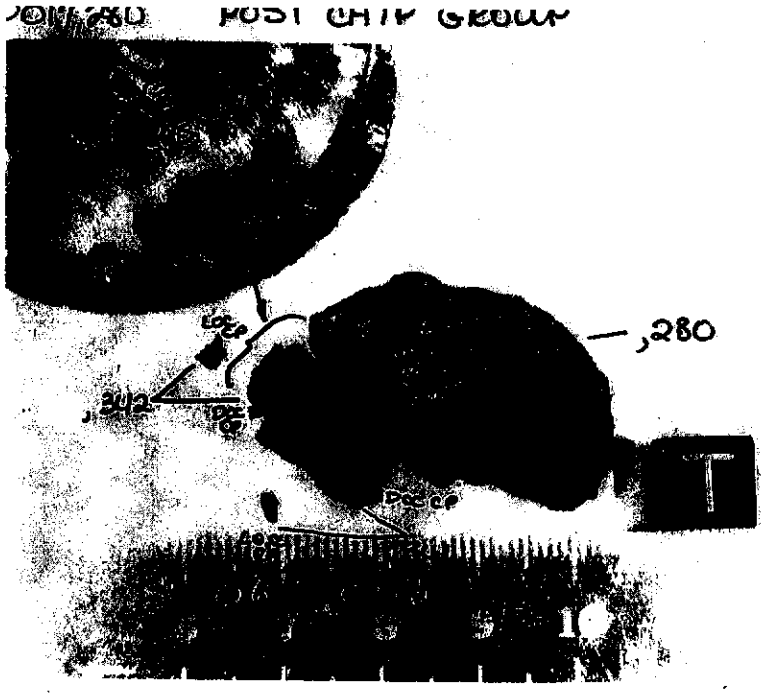

(a)

FORM F-6

PHOTOGRAPH PAGE

PARENT SAMPLE NO. 10017,280

PAGE _____ OF _____

10017,280

34

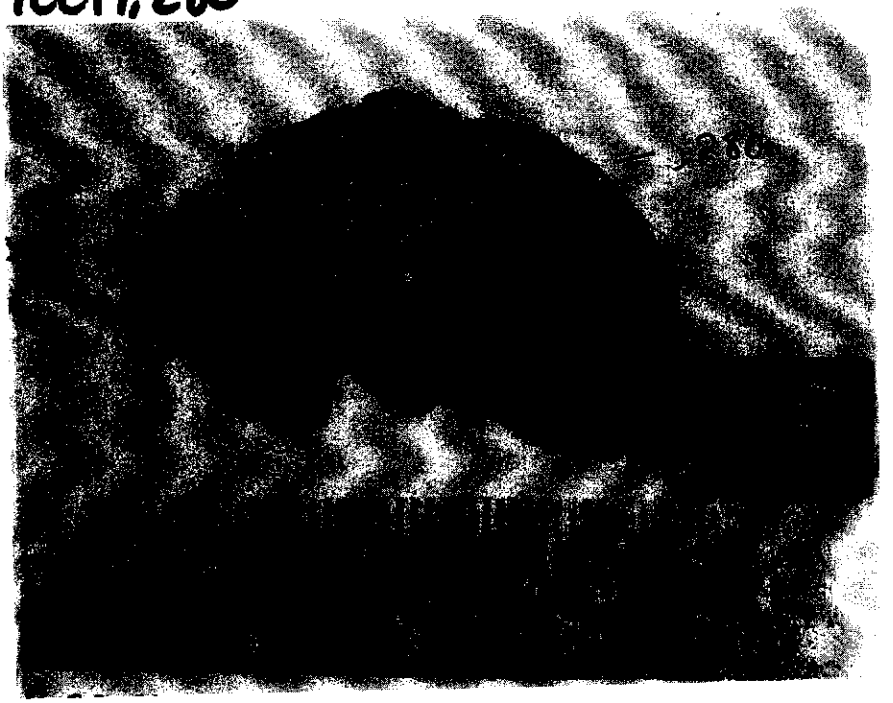

(b)

10017,280

4

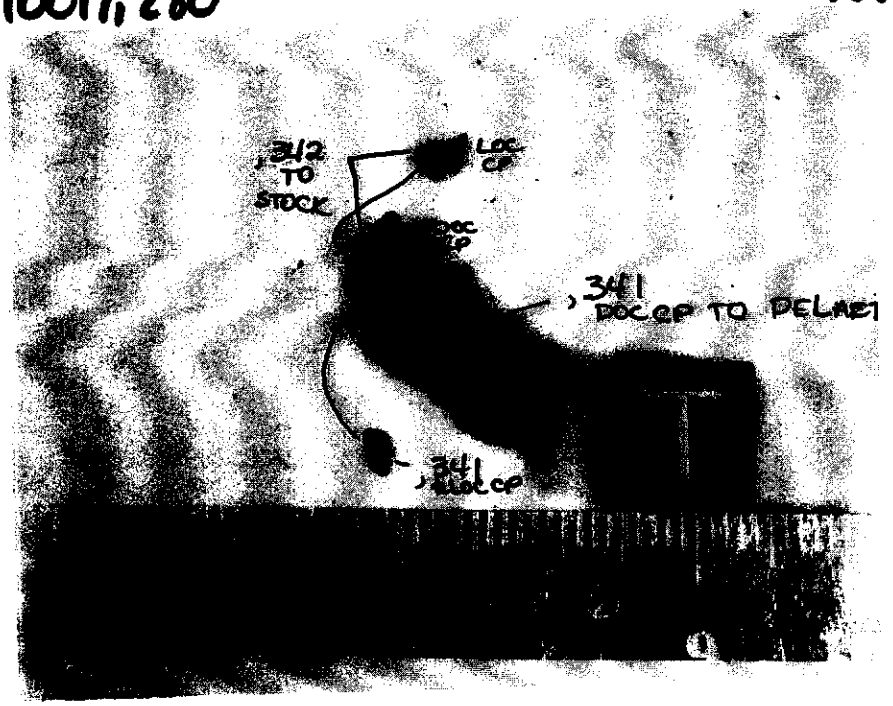

FORM F-6

PHOTOGRAPH PAGE

PARENT SAMPLE NO.
10017,280

PAGE _____ OF _____

10017,280 1

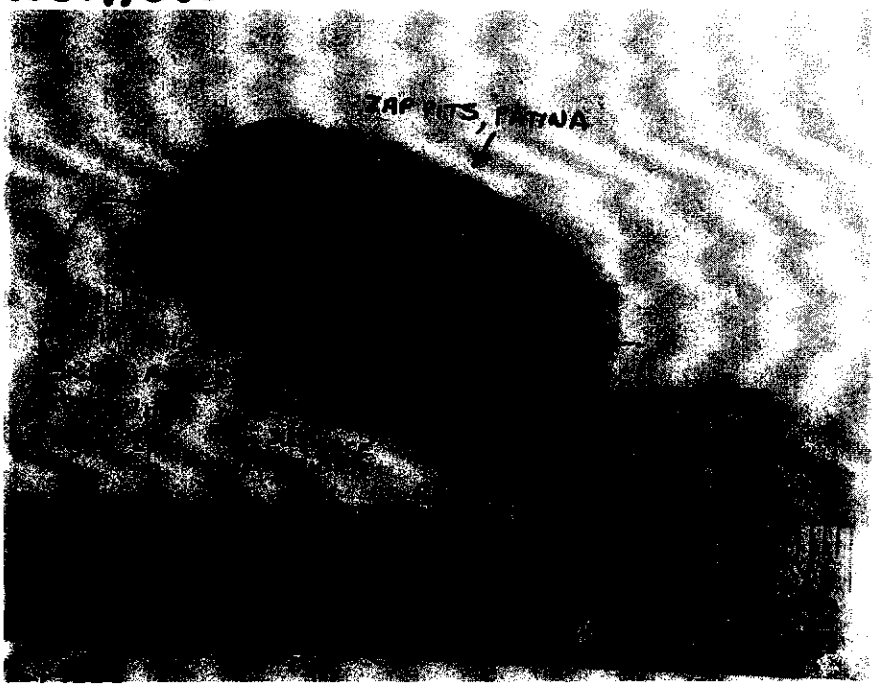

(c)

10017,280 2

FORM F-6

PHOTOGRAPH PAGE

PARENT SAMPLE NO. 10017,280

PAGE _____ OF _____

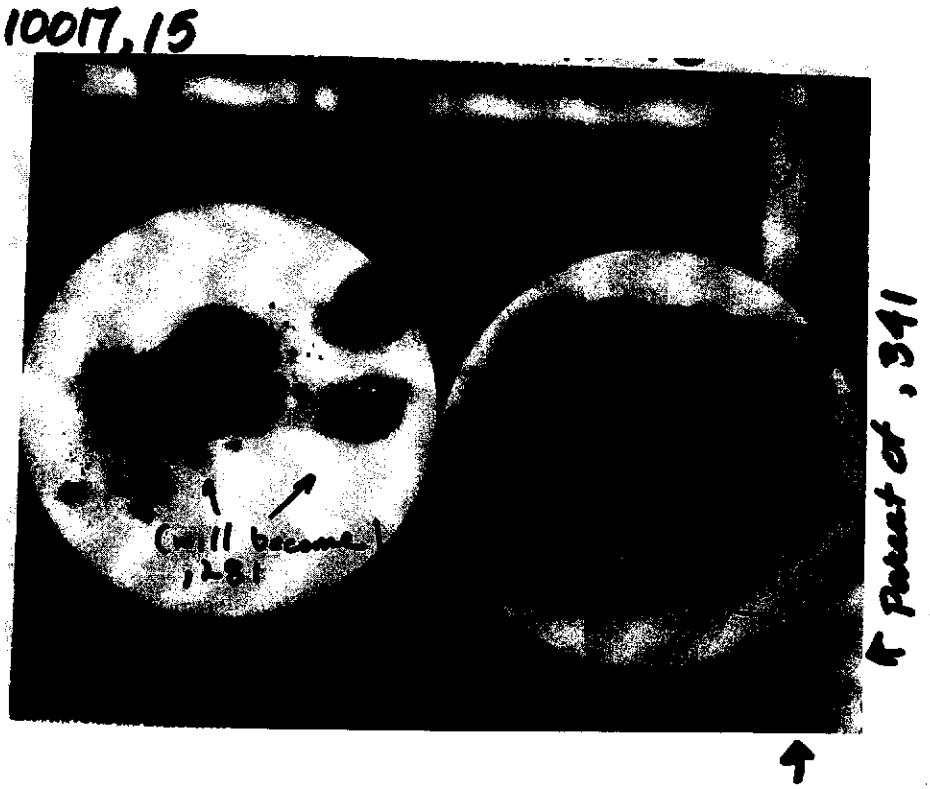

(d)

FORM F-6

PHOTOGRAPH PAGE

PARENT SAMPLE NO. 10017,15

PAGE _____ OF _____

2. Apollo 14

Figure 2-1 (a), (b), (c), (d), (e), (f) and (g), Photographs of the subdivision of rock 14310,35 to produce 14310,615, from NASA-JSC (1978).

14310,35

1

14310,35

2 (a)

14310,35 POST CHIP

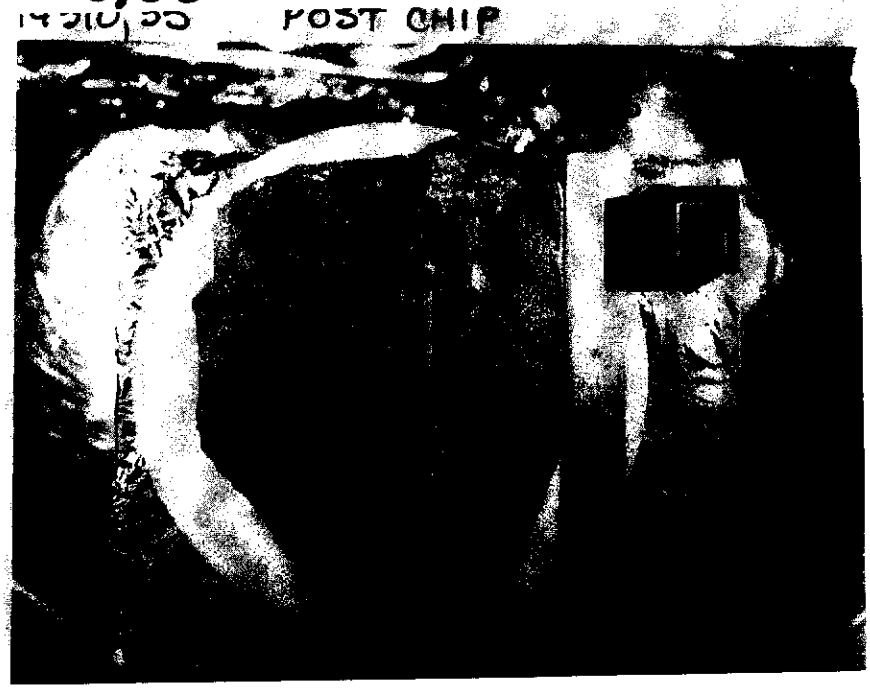

FORM F-6

PHOTOGRAPH PAGE

PARENT SAMPLE NO. 14310,35

PAGE _____ OF _____

14310,35 15

(b)

FORM F-6

PHOTOGRAPH PAGE

PARENT SAMPLE NO. 14310,35

PAGE _____ OF _____

14310,35 3

14310,35 4 (c)

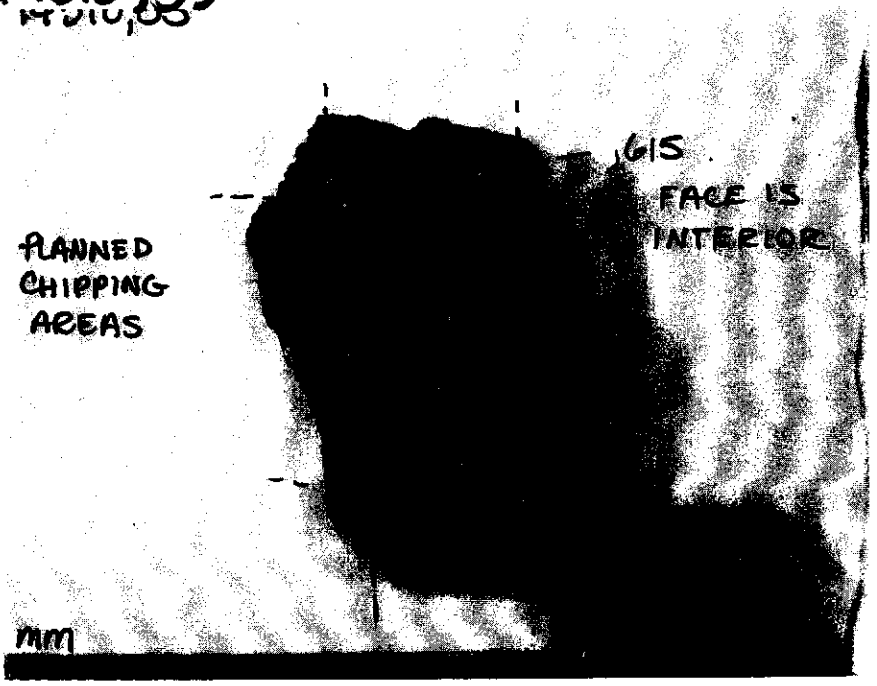

FORM F-6

PHOTOGRAPH PAGE

PARENT SAMPLE NO. 14310,35

PAGE _____ OF _____

14310,35

5

14310,35

6 (d)

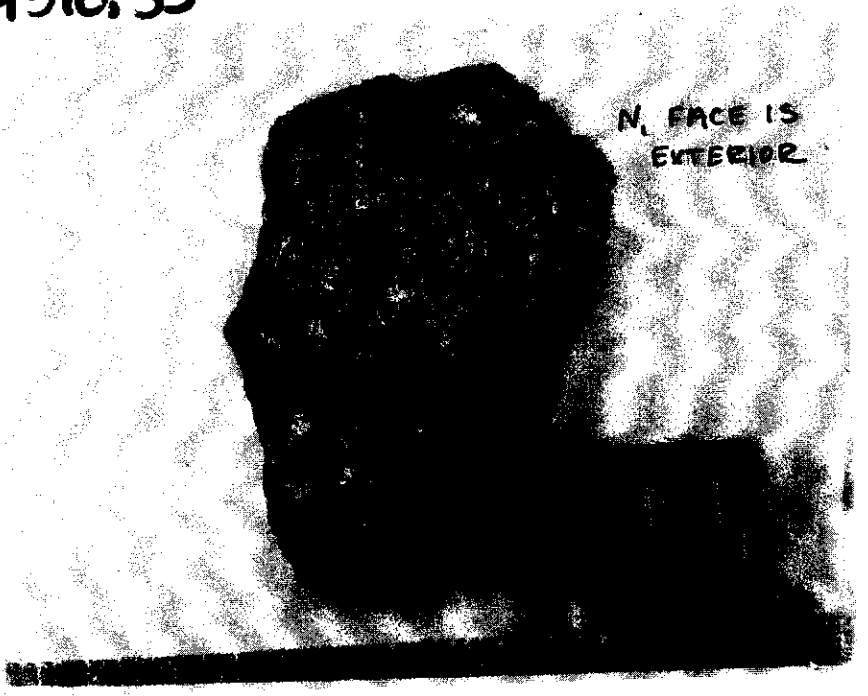

FORM F-6

PHOTOGRAPH PAGE

PARENT SAMPLE NO. 14310,35

PAGE _____ OF _____

14310,35

7

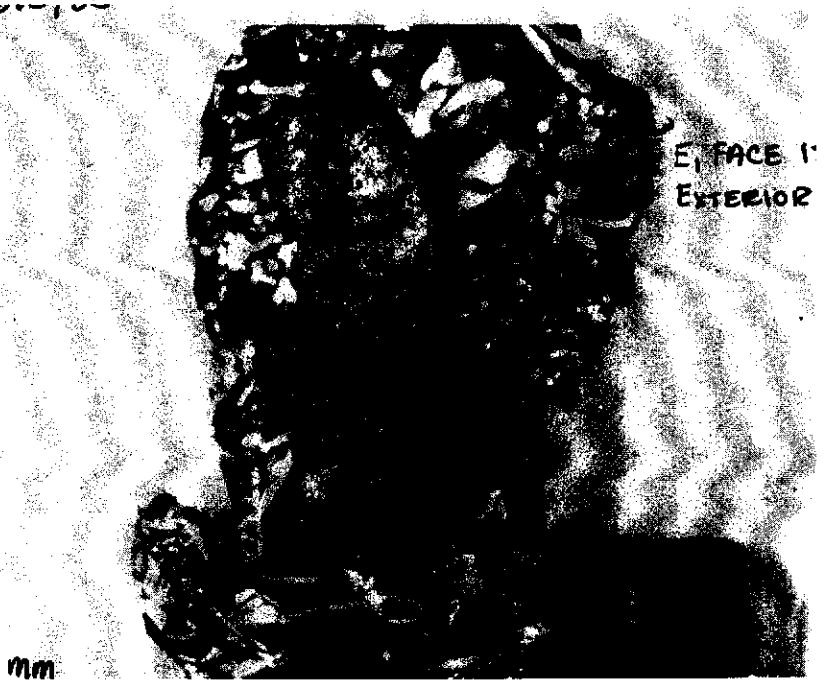

14310,35

8

(e)

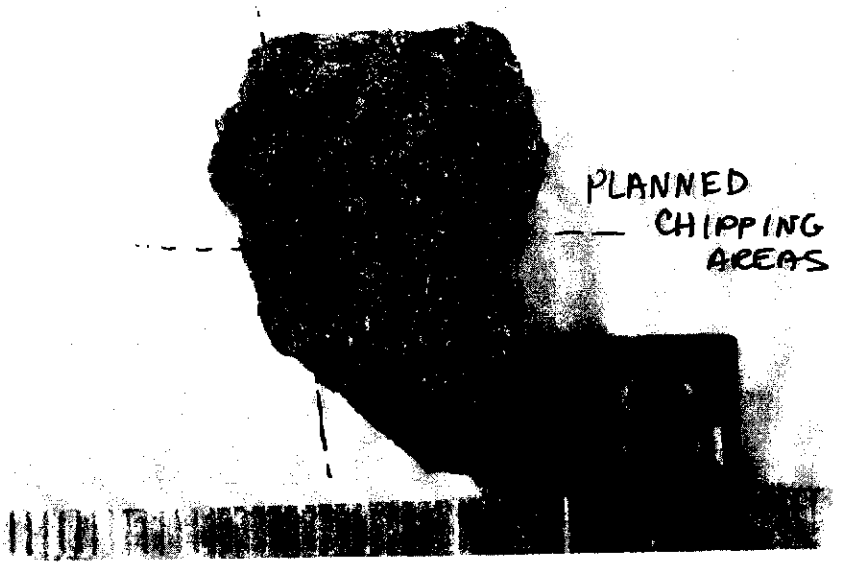

FORM F-6

PHOTOGRAPH PAGE

PARENT SAMPLE NO. 14310,35

PAGE _____ OF _____

14310,35 9

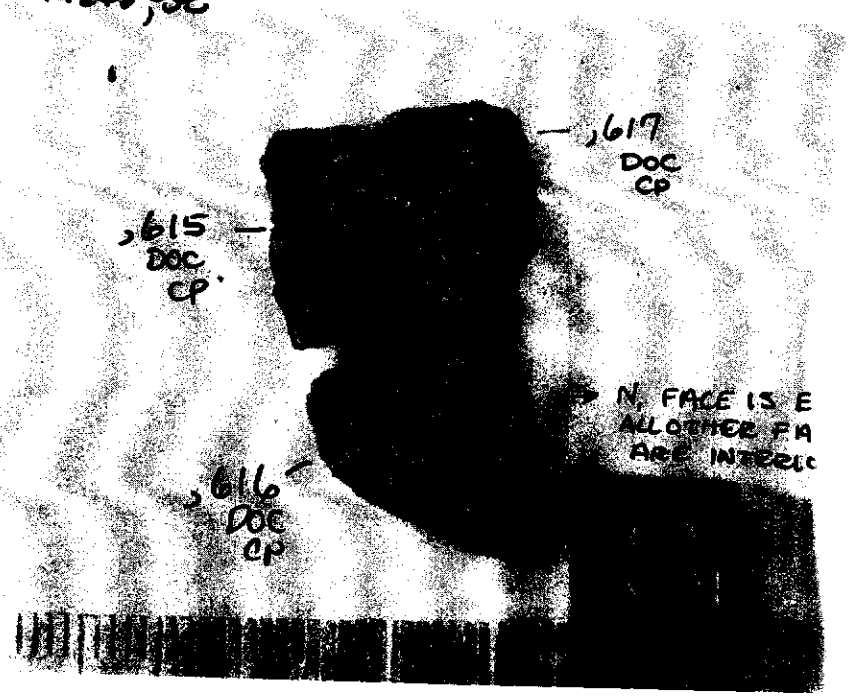

14310,35
14310,35

10 (f)

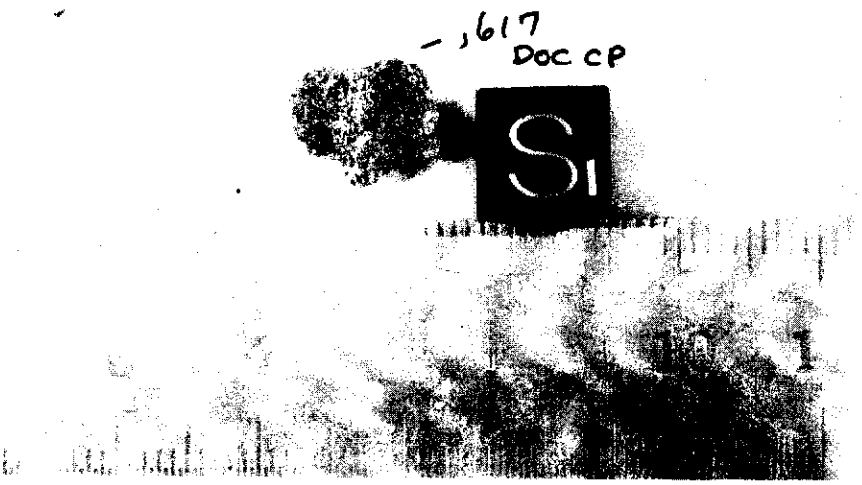

FORM F-6

PHOTOGRAPH PAGE

PARENT SAMPLE NO. 14310,35

PAGE _____ OF _____

14310,35

11

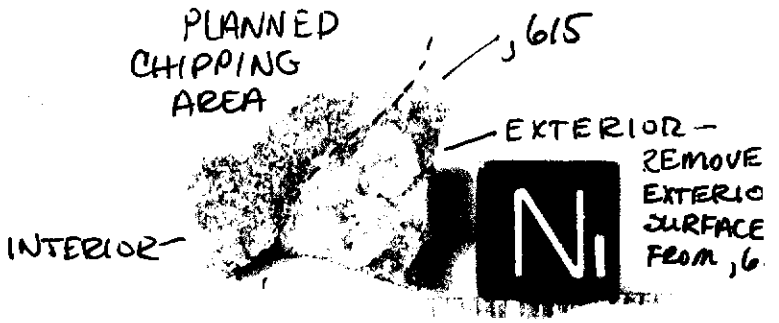

14310,35
14310,35

12 (g)

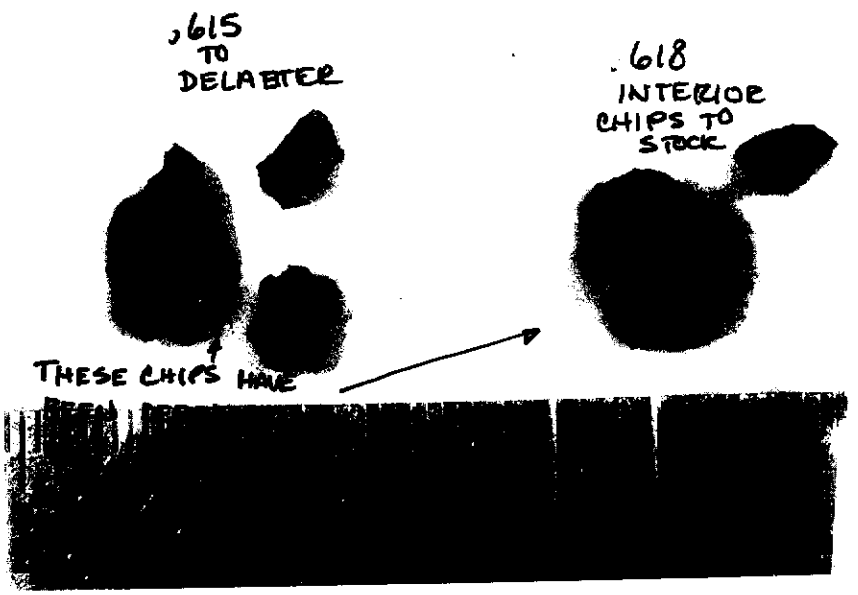

FORM F-6

PHOTOGRAPH PAGE

PARENT SAMPLE NO. 14310,35

PAGE _____ OF _____

3. Apollo 15

Figure 3-1 (a), (b), (c), (d), (e), (f), Photographs of the subdivision of rock 15059,0 to produce 15059,240, from NASA-JSC (1978).

15059,0 1

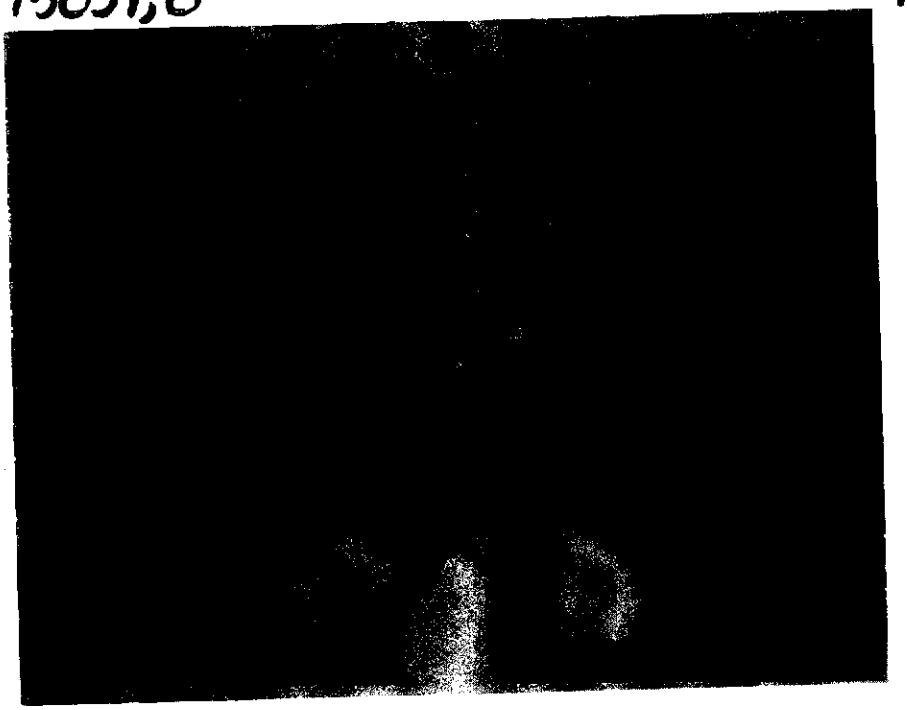

15059,0 3 (a)

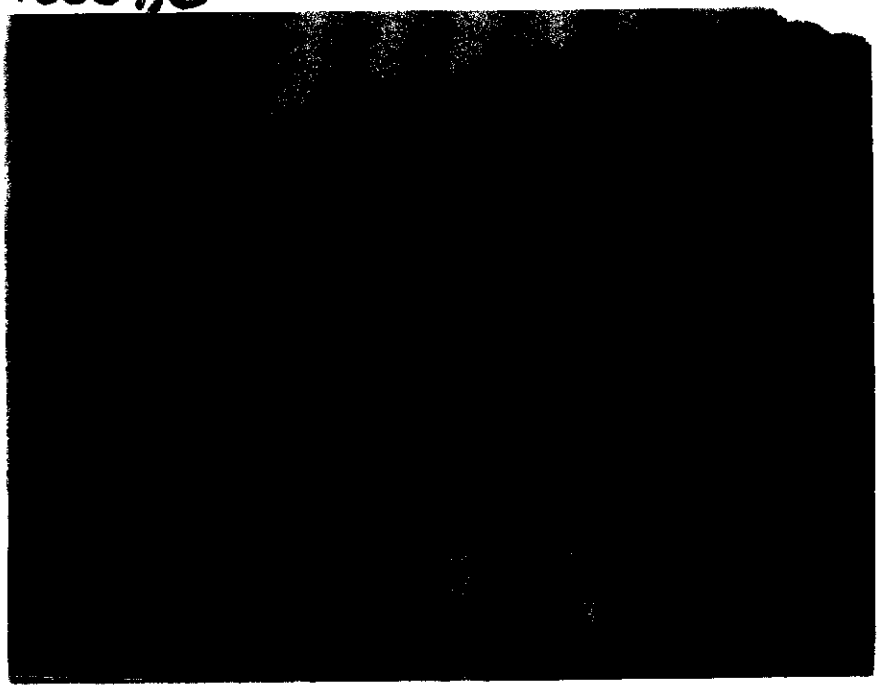

FORM F-6

PHOTOGRAPH PAGE

PARENT SAMPLE NO. 15059,0

PAGE _____ OF _____

15059,0 4

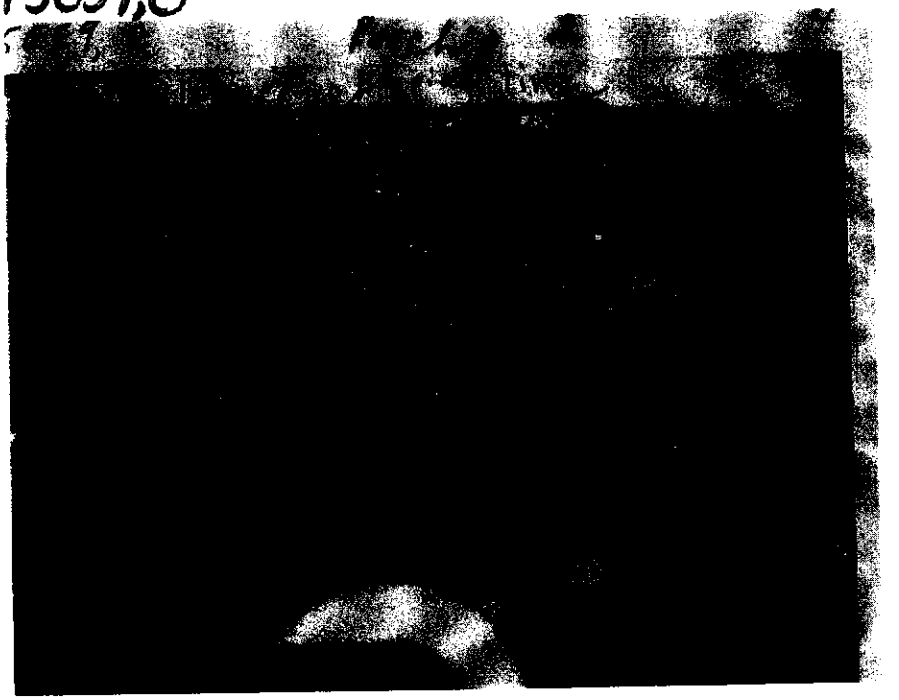

15059,0 5(b)

FORM F-6

PHOTOGRAPH PAGE

PARENT SAMPLE NO. 15059,0

PAGE _____ OF _____

15059,0 6

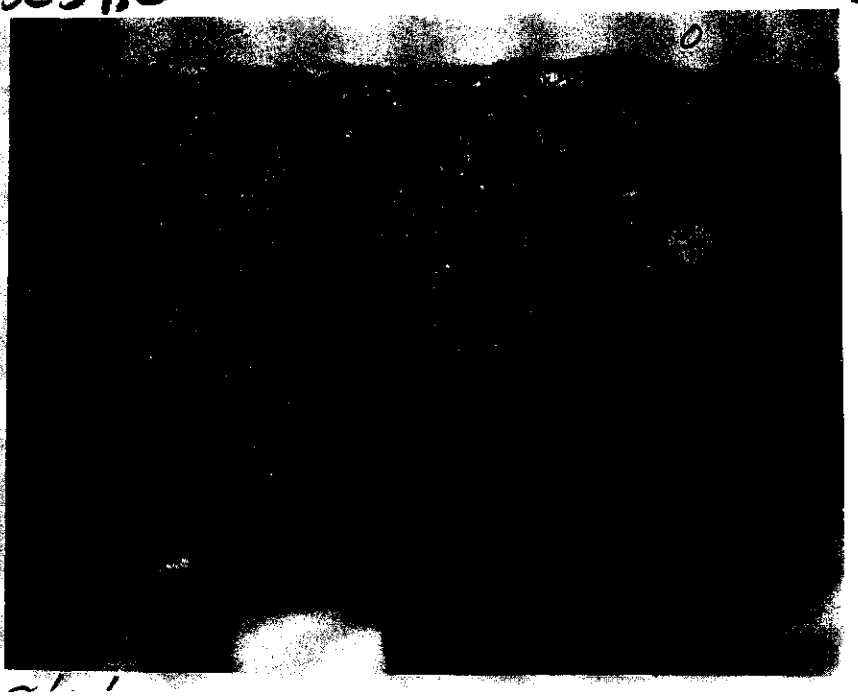

15059,0 8

,235 (c)

FORM F-6

PHOTOGRAPH PAGE

PARENT SAMPLE NO. 15059,0

PAGE _____ OF _____

15059,0 11

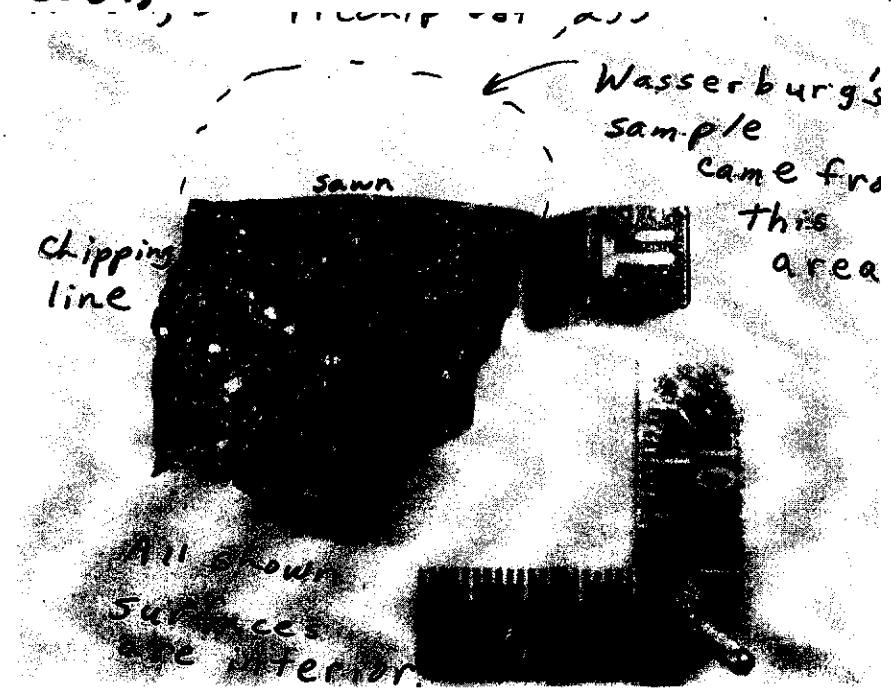

15059,0 12

(d)

FORM F-6

PHOTOGRAPH PAGE

PARENT SAMPLE NO. 15059,0

PAGE _____ OF _____

15059,0 13

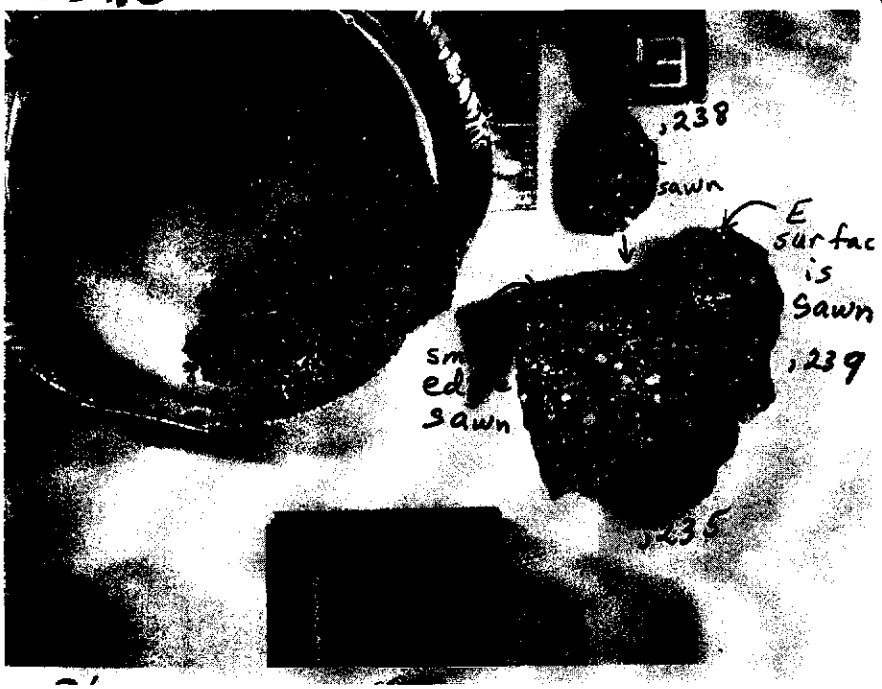

15059.0 14

(e)

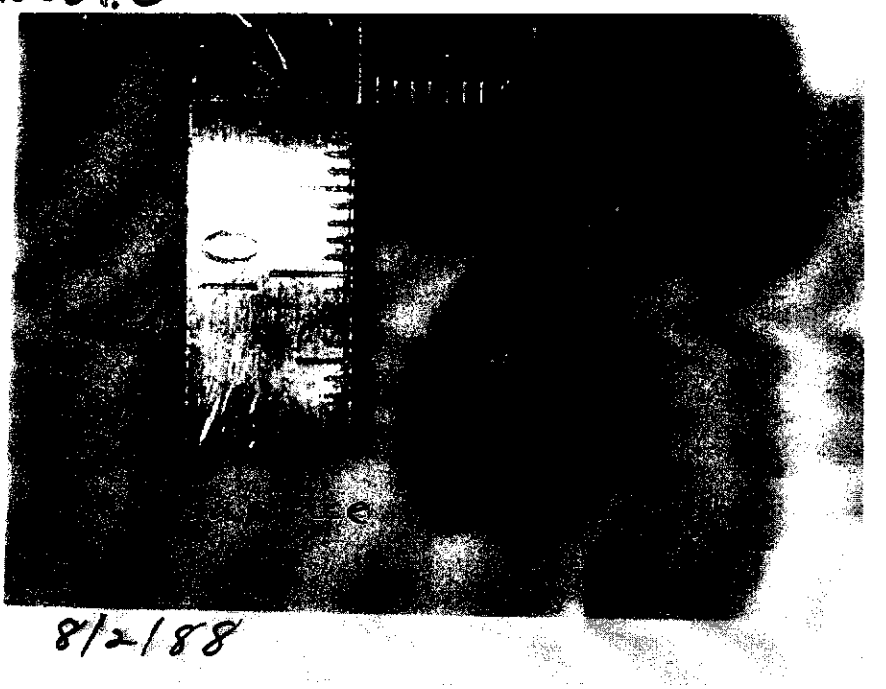

FORM F-6

PHOTOGRAPH PAGE

PARENT SAMPLE NO. 15059,0

PAGE _____ OF _____

15059,0 15

Post chip of ,238 1.

15059,0 16 (f)

FORM F-6

PHOTOGRAPH PAGE

PARENT SAMPLE NO. 15059,0

PAGE _____ OF _____

Appendix I

Published in 1997 in *Geostandards Newsletter: The Journal of Geostandards and Geoanalysis.* 21(1):77-83.

Cd, Gd and Sm Concentrations in BCR-1, BHVO-1, BIR-1, DNC-1, MAG-1, PCC-1 and W-2 by Isotope Dilution Thermal Ionisation Mass Spectrometry.

D.G. Sands and K.J.R. Rosman
Department of Applied Physics, Curtin University of Technology, Western Australia.

Note: For copyright reasons the content of Appendix I has not been reproduced

(Co-ordinator, ADT Project (Retrospective), Curtin University of Technology, 14.11.02)

Appendix J

Abstract for the 29th Lunar and Planetary Science Conference at Houston, Texas from 16-20th March, 1998.

Neutron capture on ^{113}Cd in lunar samples.

D.G. Sands, J. R. De Laeter and K. J. R. Rosman,
Curtin University of Technology, Perth, Western Australia.

Note: For copyright reasons the content of Appendix J has not been reproduced

(Co-ordinator, ADT Project (Retrospective), Curtin University of Technology, 14.11.02)

Appendix K

Abstract for the 13th National Congress of the Australian Institute of Physics, Fremantle, Western Australia. 27th September to 2nd October, 1998.

Neutron capture on ^{113}Cd in lunar samples.

D.G. Sands, J. R. De Laeter and K. J. R. Rosman,
Curtin University of Technology, Perth, Western Australia.

Note: For copyright reasons the content of Appendix K has not been reproduced.

(Co-ordinator, ADT Project (Retrospective), Curtin University of Technology, 14.11.02)